Mechanism and Kinetics of Ferrous Iron Oxidation and Ferric Iron Reduction in Simulated Natural Waters: Impact of light and pH

Chao Jiang

A thesis in fulfillment of the requirement for the degree of

Doctor of Philosophy

School of Civil and Environmental Engineering

Faculty of Engineering

January 2018

THE UNIVERSITY OF NEW SOUTH WALES
Thesis/Dissertation Sheet

Surname or Family name: Jiang

First name: Chao Other name/s:

Abbreviation for degree as given in the University calendar: PhD

School: School of Civil and Environmental Engineering Faculty: Faculty of Engineering

Title: Mechanism and kinetics of ferrous iron oxidation and ferric iron reduction in simulated natural waters: impact of light and pH

Abstract

The redox chemistry of iron in natural aquatic systems is of great interest due to its significance to the bioavailability of iron, a critical micronutrient to all living organisms. Natural organic matter (NOM) plays a significant role in iron redox transformations, mainly due to the interaction of redox-active organic moieties present in NOM with Fe(II) and Fe(III). In order to improve our understanding of iron redox transformations in natural waters, the oxidation and reduction kinetics of nanomolar concentrations of iron were investigated. Particular attention has been given to the role of quinone groups in iron redox transformations by comparing results obtained in Suwannee River fulvic acid (SRFA) and pure hydroquinone solutions. A kinetic modelling approach that facilitates the analysis and understanding of the mechanism of iron redox transformations under various conditions has been used extensively throughout this work.

The results show that hydroquinone-like moieties are intrinsically present in SRFA and reduce Fe(III) under acidic and circumneutral pH conditions. These hydroquinone-like moieties oxidize to form long-lived semiquinone-like moieties on irradiation that are capable of oxidizing Fe(II) under acidic and circumneutral pH conditions; they also act as Fe(III) reductant under circumneutral pH conditions. pH was shown to play a critical role in controlling the rate of iron redox transformations, mainly by affecting Fe(II) oxidation kinetics.

In the presence of light, ligand-to-metal charge transfer (LMCT) is the main Fe(III) reduction pathway under acidic and circumneutral pH conditions. It is further shown that while short-lived photo-generated peroxyl-like radicals play an important role in Fe(II) oxidation under acidic conditions, Fe(II) oxidation is mainly driven by dioxygen and/or semiquinone-like radicals under circumneutral pH conditions.

The presence of divalent calcium ions was shown to impact iron redox transformation kinetics in non-irradiated and irradiated SRFA solutions mainly due to changes in iron speciation as a result of the competition between iron and calcium for the binding sites on SRFA.

Overall, the results show that NOM affects iron availability, not only by providing organic ligands that enhance iron solubility, but also by facilitating redox transformations of iron by redox active groups that directly participate in iron redox transformations.

FOR OFFICE USE ONLY Date of completion of requirements for Award:

ORIGINALITY STATEMENT

'I hereby declare that this submission is my own work and to the best of my knowledge it contains no materials previously published or written by another person, or substantial proportions of material which have been accepted for the award of any other degree or diploma at UNSW or any other educational institution, except where due acknowledgement is made in the thesis. Any contribution made to the research by others, with whom I have worked at UNSW or elsewhere, is explicitly acknowledged in the thesis. I also declare that the intellectual content of this thesis is the product of my own work, except to the extent that assistance from others in the project's design and conception or in style, presentation and linguistic expression is acknowledged.'

Signed ……..

Date ……..

Abstract

The redox chemistry of iron in natural aquatic systems is of great interest due to its significance to the bioavailability of iron, a critical micronutrient to all living organisms. Natural organic matter (NOM) plays a significant role in iron redox transformations, mainly due to the interaction of redox-active organic moieties present in NOM with Fe(II) and Fe(III). In order to improve our understanding of iron redox transformations in natural waters, the oxidation and reduction kinetics of nanomolar concentrations of iron were investigated. Particular attention has been given to the role of quinone groups in iron redox transformations by comparing results obtained in Suwannee River fulvic acid (SRFA) and pure hydroquinone solutions. A kinetic modelling approach that facilitates the analysis and understanding of the mechanism of iron redox transformations under various conditions has been used extensively throughout this work.

The results show that hydroquinone-like moieties are intrinsically present in SRFA and reduce Fe(III) under acidic and circumneutral pH conditions. These hydroquinone-like moieties oxidize to form long-lived semiquinone-like moieties on irradiation that are capable of oxidizing Fe(II) under acidic and circumneutral pH conditions; they also act as Fe(III) reductant under circumneutral pH conditions. pH was shown to play a critical role in controlling the rate of iron redox transformations, mainly by affecting Fe(II) oxidation kinetics.

In the presence of light, ligand-to-metal charge transfer (LMCT) is the main Fe(III) reduction pathway under acidic and circumneutral pH conditions. It is further shown that while short-lived photo-generated peroxyl-like radicals play an important role in

Fe(II) oxidation under acidic conditions, Fe(II) oxidation is mainly driven by dioxygen and/or semiquinone-like radicals under circumneutral pH conditions.

The presence of divalent calcium ions was shown to impact iron redox transformation kinetics in non-irradiated and irradiated SRFA solutions mainly due to changes in iron speciation as a result of the competition between iron and calcium for the binding sites on SRFA.

Overall, the results show that NOM affects iron availability, not only by providing organic ligands that enhance iron solubility, but also by facilitating redox transformations of iron by redox active groups that directly participate in iron redox transformations.

Acknowledgements

I would like to express my special appreciation to my mentor and supervisor Professor David Waite for bringing me into the world of research, and providing me with constant support throughout my doctoral studies. I have been deeply inspired by his pursuit of knowledge and passion for research. I have gained ideas, advices, encouragement, and inspiration through every conversation and email with him, which are strong support for me to complete the four year's studies.

I would like to thank my co-supervisor, Dr. Shikha Garg for her guidance, and her time and effort on my study in the past four years. I have learned from her not only research skills and methods, but more importantly the positive attitude at work that have been essential to overcome many problems in the progress of my study. Without her supervision, I would not have been able to complete this thesis.

I am grateful for the opportunity to work and interact with experts and colleagues in Waite's group. I would like to thank Dr. Mark Bligh, Dr. An Ninh Pham, Dr. Xiu Yuan, Dr. Christopher Miller, Dr. Di He, and Dr. Andrew Kinsela for their assistance in my research project. I would also like to thank my fellow students including Guowei Xing, Huijie Yu, Kai Wang, Hongyan Rong, Yingying Sun, Wei Xiao, and Wangwang Tang for their company.

I would like to thank Dr. Gautam Chattopadhyay and Kelvin Ong for maintaining a safe and pleasant environment in the Water Quality Laboratories for me to conduct experimental work.

I would like to thank my parents for their endless love and support in the past three decades. Finally, I owe special thanks to my girlfriend, Dianfei Li, for her love, understanding and encouragement during the completion of this thesis.

This research was funded by Australian Federal Government through Australian Postgraduate Award (APAs), and by the School of Civil and Environmental Engineering, UNSW through Tuition Fee Scholarship (TFS) with a living allowance (August 2013 - Jun 2014). Facilities and resources from the School of Civil and Environmental Engineering, UNSW are also gratefully acknowledged.

Table of Contents

List of Figures

List of Tables

Chapter 1. Introduction

Iron, element 26 in the periodic table, is the fourth most abundant element and the second most abundant metal after aluminum in the earth's crust. Iron belongs to the first transition series, implying that it can exist in various oxidation states, from –II to +VI, with ferrous (Fe(II)) and ferric (Fe(III)) iron as the two principle oxidation states. Iron can act as an electron donor or accepter due to its ability to transit between different redox states, primarily Fe(II) and Fe(III). The redox properties of iron have drawn increasing interest from various researchers since it plays an important role in phytoplankton growth (Finden et al. 1984; Martin et al. 1990a; Martin et al. 1990b; Kuma and Matsunaga 1995; Coale et al. 1996; Hutchins et al. 2002), degradation of pollutants and natural organic matter (NOM) (Voelker and Sulzberger 1996; Fukushima and Tatsumi 2001; Southworth and Voelker 2003; Vione et al. 2004; Kochany and Lipczynska-Kochany 2007; Moonshine et al. 2008), and mineral dissolution (Blesa et al. 1984; Blesa et al. 1987; Cornell and Schindler 1987; Borghi et al. 1989; Stumm and Sulzberger 1992).

1.1. Scarcity of iron in natural waters

Although iron is abundant in the earth's crust, the concentration of iron in natural waters is extremely limited. This is mainly due to high insolubility of the thermodynamically stable Fe(III) in oxygenated natural waters. The solubility product (pK_s) for amorphous $Fe(OH)_3$(s) is 38.8 (Morel and Hering 1993), and the concentration of soluble Fe(III) at pH 7 is therefore calculated to be $10^{-9.5}$ M (25 °C, ionic strength = 0 M). Even though the solubility of Fe(III) is enhanced significantly in the presence of organic ligands that exist in natural waters, its solubility is merely 0.3-0.6 nM in surface seawater (Byrne and Kester 1976; Kuma et al. 1998; Liu and Millero 2002). Besides, at circumneutral pH, the much more soluble ferrous form, Fe(II) is prone to oxidation by a

range of oxidants, primarily dissolved oxygen (Rose and Waite 2002; Pham and Waite 2008b) and hydrogen peroxide when present at sufficiently high concentration (Millero and Sotolongo 1989; Remucal and Sedlak 2011). The oxidation of Fe(II) by these oxidants is pH dependent, with increasing oxidation rate at higher pH (Lee et al. 2016). Santana-Casiano et al. (2004) reported the apparent Fe(II) oxidation rate at pH 8 was 3,000 times greater than that measured at pH 6, and attributed this pH dependence to variation in the Fe(II) speciation with change in pH. Thus, the rapid oxidation rate of Fe(II) (half-life ~ few minutes) and the high insolubility of Fe(III) result in the scarcity of dissolved iron in natural waters.

1.2. Iron as a nutrient for phytoplankton

Iron is critical to all living organisms, from micro-organisms to human beings. For aquatic organisms, iron is one of their essential nutrients; as such iron deficiency is a general problem in marine biology (Crichton and Boelaert 2001). Iron is reported to participate in various cellular functions in organisms, namely photosynthesis (Menzel et al. 1963; Strzepek and Harrison 2004), nitrogen fixation (Murphy et al. 1976) and respiration (Sunda and Huntsman 1995). Recently, new evidence confirmed that iron can limit phosphorus acquisition, controlling the coupling between nitrogen and phosphorus cycles in the ocean (Browning et al. 2017).

A large body of literature has demonstrated that iron availability is associated with phytoplankton growth and affects the growth rate, efficiency of photosynthesis and nitrogen fixation, which causes change in the phytoplankton community structure and iron demand (Quigg et al. 2003; Hutchins and Boyd 2016). The link between soluble iron concentration and the growth rates of phytoplankton has been found for many decades and in various locations and conditions (Martin and Fitzwater 1988; Martin et

al. 1994; Coale et al. 1996; Morel et al. 2008). Morton and Lee (1974) reported that an increase in total dissolved iron resulted in the growth of blue-green algae, which are highly undesirable for causing surface scums and odors, as well as suppressing other algae and organisms (Morton and Lee 1974). The blooms of blue-green algae were attributed to its ability to produce strong iron chelators to facilitate rapid uptake of iron (Murphy et al. 1976). Also, reductive dissolution of iron via generation of various reductants (for e.g. superoxide) was also shown to be an effective pathway to increase the lability of iron in aqueous environment (Kustka et al. 2005; Rose and Waite 2006; Garg et al. 2007a).

1.3. Iron as environmental problem

Iron is associated with a number of environmental problems. As a nutrient for algae, iron exerts an indirect impact on the aqueous environment by causing algal blooms. The harmful algal blooms (HABs) in natural waters cause severe environmental problems, including threatening the balance of ecosystems by altering light and nutrient availability (Ginn et al. 2010), releasing toxic metabolic by-products (Arment and Carmichael 1996), and eventually threatening the health of human beings that rely on the water sources. However, the growth of algae does not always cause harm; it can be utilized to solve environmental problems if managed properly. A study carried out in the Southern Ocean reported that addition of iron encouraged diatom-dominated phytoplankton blooms, which captured significant amount of excess carbon in the atmosphere through photosynthesis (Smetacek et al. 2012). It was estimated that with addition of one atom of iron, 13,000 atoms of carbon can be stored in the deep ocean, of which at least half was deposited at a depth greater than 1,000 meters as the algae die (Smetacek et al. 2012). However, the side effects on ocean chemistry and marine

ecosystems have not been fully evaluated, which prevent the commercialization of this technology.

Iron cycles in natural waters are influenced by human activities. As an important iron input source, atmospheric iron inputs are influenced by anthropogenic activities. For instance, aerosols from combustion was modelled to contribute up to 70% and 85% of soluble iron to the surface ocean near Bermuda and Ireland (Sholkovitz et al. 2009). While it was predicted that changes in land use practices and climate may cause substantial reductions in future mineral aerosol loadings to the ocean, leading to a reduction in iron inputs via atmospheric aerosols (Mahowald and Luo 2003); however increased input of iron containing aerosols is expected from fossil fuel combustion (Chuang et al. 2005; Krishnamurthy et al. 2009). It was reported that combustion of fossil fuel resulted in an increase in aerosol iron as well as its solubility in Sargasso Sea from North America air masses (Sedwick et al. 2007) and in the East China Sea (Li et al. 2017). The complexity of iron inputs in aerosols can potentially influence the growth of phytoplankton due to its fertilizing effect, thereby creating other environmental problems such as influencing the capacity of the ocean to capture carbon dioxide.

Acid sulfate soil is another environmental problem associated with iron, mainly pyrite (FeS_2). Acid sulfate soil occurs in both inland (e.g. wetlands containing sulfidic sediment) (Glover et al. 2011) and coastal environments (e.g. costal flood plains) (Burton et al. 2006) in Australia. This phenomenon is mainly formed when sulfides containing soils are exposed to oxygen, releasing sulfuric acid and ferric hydroxide (Dent 1986). While this process can occur naturally during drought, it can also be driven by human activities such as mining and excavation operations (Lottermoser 2007), which expose pyrite to oxidation. Acid sulfate soil can cause severe

environmental consequences, such as fish kills (McCarthy et al. 2006), and declining water quality for agricultural use (Johnston et al. 2005).

Due to the critical role of iron availability and behavior in the above mentioned environmental problems, the redox transformations of iron are of interest to many researchers. For example, it is expected that the growth of algae can be predicted and controlled if the mechanism of iron redox transformations in various conditions are known.

1.4. The role of natural organic matter (NOM) in iron redox transformations

Natural organic matter (NOM) refers to the inherently complex mixture of organic molecules in multifunctional groups (Macalady and Walton-Day 2011). NOM is present in all natural waters and soils, mainly from the decay of a wide diversity of plant materials and microorganism (Stevenson 1994). Because of the multifunctional groups present in NOM, the study of NOM often involves large complexity and variabilities. One important aspect of NOM is its redox properties due to the redox-active functional groups such as quinone and phenol groups that are capable of accepting and donating electrons (Scott et al. 1998; Nurmi and Tratnyek 2002; Aeschbacher et al. 2010; Aeschbacher et al. 2012). The redox properties of NOM are critical in many environmental research areas such as metal redox property (Senesi 1990b), and pollution treatment (Aeschbacher et al. 2012). In addition, NOM is important in various environmental processes and applications including metal transport, contaminant degradation, water treatment processes and in soil fertility (Macalady and Walton-Day 2011).

NOM plays a significant role in the iron transformations in natural waters. First, NOM forms complex with iron, creating a stabilizing effect (Peiffer et al. 1999), which significantly enhances Fe solubility and alters its reactivity (Strathmann 2011). The solubility of Fe(III) in surface seawater was reported to be 0.3-0.6 nM in various locations (Byrne and Kester 1976; Kuma et al. 1998; Liu and Millero 2002), two orders of magnitude higher than the inorganic Fe(III) solubility reported in NaCl solutions (Liu and Millero 1999) due to iron binding by NOM. Metal binding by NOM is commonly attributed to the oxygen-containing functional groups such as carboxyl and phenolics (Tipping 2002). Fujii et al. (2014) further showed a strong correlation between aromatic carboxyl groups and NOM complexation capacity for Fe. In surface natural waters, organically complexed iron is the major form of dissolved iron (Nagai et al. 2007; Batchelli et al. 2010).

Secondly, the functional groups intrinsically present in NOM can play important roles in iron redox transformations. For instance, it was reported that aromatic moieties intrinsically present in NOM are capable of reducing Fe(III) to Fe(II) under anoxic condition (Chen et al. 2003; Garg et al. 2013a). Also, semiquione-like radicals have been reported to exist in aquatic NOM samples (Paul et al. 2006), and are proposed to be the dominant Fe(II) oxidant under acidic conditions (Garg et al. 2013a) in Suwannee River fulvic acid (SRFA; International Humic Substances Society) solution. It is widely accepted that quinones or quinone-like moieties are responsible for redox properties of NOMs (Macalady and Walton-Day 2011).

Finally, irradiation of NOM by sunlight produces reactive oxygen species (ROS), including superoxide ($O_2^{\bullet -}$), hydrogen peroxide (H_2O_2), singlet oxygen ($^1O_2$), and hydroxyl radicals ($OH^{\bullet}$). These are redox active species and can participate in iron

redox transformations either directly or indirectly (Voelker et al. 2000; Rose and Waite 2006). For example, $O_2^{\bullet-}$ directly reduces Fe(III) in alkaline conditions (Garg et al. 2011a), and/or oxidizes Fe(II) under acidic conditions. it also indirectly mediates the generation of Fe(II) oxidant in acidic conditions (Garg et al. 2013a).

1.5. Iron redox chemistry in natural waters

In natural waters, redox cycling of metals is largely affected by the presence of reactive oxygen species (ROS), including superoxide ($O_2^{\bullet-}$), hydrogen peroxide (H_2O_2) hydroxyl radical ($HO^{\bullet}$), and singlet oxygen ($^1O_2$) (Voelker et al. 2000; Rose and Waite 2006; Garg et al. 2011b). ROS can be generated both biotically and abiotically. The abiotic generation of ROS is mainly attributed to the photochemical reactions of NOM (Cooper et al. 1989), while there are increasing evidence suggesting that microbial activities could be an important source of ROS in natural waters (Rose et al. 2010; Vermilyea et al. 2010). Due to their abundancy and reactivity, ROS plays an important role in iron redox transformations. Reactions of ROS with iron are provided in eq.1.1-1.5 followed by discussion of current knowledge on these reactions.

$$Fe(II) + O_2^{\bullet-}/HO_2^{\bullet} \longrightarrow Fe(III) + H_2O_2 \quad (1.1)$$

$$Fe(III) + O_2^{\bullet-}/HO_2^{\bullet} \longrightarrow Fe(II) + O_2 \quad (1.2)$$

$$Fe(II) + H_2O_2 \longrightarrow Fe(III) + OH^{\bullet} \quad (1.3)$$

$$Fe(II) + OH^{\bullet} \longrightarrow Fe(III) + OH^{-} \quad (1.4)$$

$$Fe(II) + {}^1O_2 \longrightarrow Fe(III) + O_2^{-} \quad (1.5)$$

Superoxide can be generated both by the photolysis of NOM in natural surface waters (Voelker et al. 2000; Rose and Waite 2006) and by microorganisms (Diaz et al. 2013). An important aspect of its aqueous chemistry its reaction with trace metals, such as iron and copper. Superoxide exist in two forms, anionic form ($O_2^{\bullet -}$) and hydroperoxyl radical ($HO_2^{\bullet}$), with the proportion of each species dependent on pH (pK_a ~ 4.8). Superoxide can be Fe(II) oxidants and Fe(III) reductants as shown in eq.1.1 and eq.1.2. As a result of the speciation variation of superoxide at various pH, rate constants for reactions between $O_2^{\bullet -} / HO_2^{\bullet}$ and iron are also pH dependent. Rush and Bielski (1985) reported that rate constants for $O_2^{\bullet -} / HO_2^{\bullet}$ with Fe(II) and Fe(III) both increases with increase in pH, while Fe(III) oxidation rate by $O_2^{\bullet -} / HO_2^{\bullet}$ increases less dramatically than that of Fe(III) reduction.

The presence of H_2O_2 in natural waters is mainly attributed to photochemical processes mediated by NOM (Zika et al. 1985; Garg et al. 2011b). Rainwater, on the other hand, can also contribute significantly to the input of H_2O_2 in the order of around 40 µM compared with natural occurring H_2O_2 concentrations of typically several hundred nanomoles per liter (Miller et al. 2009). H_2O_2 is a relatively stable intermediate, and can also be a dominant Fe(II) oxidant if present in sufficient concentrations with the rate of Fe(II) oxidation by H_2O_2 potentially higher than the rate of Fe(II) oxidation by oxygen (Voelker and Sulzberger 1996; Miller et al. 2012). The reaction of Fe(II) with H_2O_2 is known as Fenton's reaction (eq.1.3), which generates Fe(III) and highly reactive and damaging hydroxyl radicals ($HO^{\bullet}$).

The hydroxyl radical ($HO^{\bullet}$) is the most reactive ROS and undergoes rapid and non-selective reaction with organic and inorganic compounds. The $HO^{\bullet}$ generated from Fenton's reaction can undergo further reaction with NOM and H_2O_2, generating other radicals that may be involved in further reactions with iron. For instance, Duesterberg et al. (2008) reported that $HO^{\bullet}$ reacts with Fe(II), H_2O_2, and other organic species by serving as a chain carrier. The concentration of $HO^{\bullet}$ is normally very low in natural waters and not likely to be a direct Fe(II) oxidant (eq.1.4).

Singlet oxygen ($^1O_2$), an electronically-excited state of O_2, is a highly reactive ROS. Due to the removal of the spin restriction, $^1O_2$ has a higher redox potential than the ground state oxygen ($^3O_2$). Thus, oxidation of Fe(II) by $^1O_2$ (eq.1.5) could be important if $^1O_2$ concentration is sufficiently high, such as in photolysed NOM solution where there is a source of $^1O_2$ (Latch and McNeill 2006; Garg et al. 2011a). However, $^1O_2$ is short lived in aqueous solution (lifetime ~ 4 μs), and therefore not likely to be direct Fe(II) oxidant.

1.6. The role of light in NOM-mediated iron redox transformations

Light plays a significant role in iron transformations mediated by NOM in natural waters. Under irradiated condition, Fe(III) may undergo reduction either directly via ligand-to-metal charge transfer (LMCT), and/or indirectly via interaction with photogenerated superoxide (SMIR). The former pathway is considered to be important under acidic conditions in photo active Fe(III) species (including organically complexed iron, and dissolved inorganic iron) (Faust and Zepp 1993; Sima and Makaiiova 1997), while the latter pathway is considered to be most important at circumneutral and

alkaline pH (Rose and Waite 2006; Garg et al. 2011a). The photochemically generated Fe(II) is considered as a main source of bioavailable iron in surface waters. The presence of light also influences the rate of Fe(II) oxidation in NOM containing natural waters due to the generation organic moieties capable of oxidizing Fe(II) (Garg et al. 2011a), including organic radicals and ROS especially under acidic conditions where the rate of Fe(II) oxidation by dioxygen is slow (Morel and Hering 1993).

1.7. Current knowledge on iron redox transformations in sunlit NOM

Over the last three decades, investigation of iron in natural waters has improved our understanding of the environmental functioning of iron, including its role in phytoplankton growth and its chemical speciation in surface waters. Our knowledge on iron redox transformations in the presence of NOM in sunlit natural waters is also improving, especially in terms of interaction of reactive oxygen species (ROS) with Fe, redox functional groups in NOM, and iron redox transformations. Based on the current knowledge on iron transformations, a schematic is presented showing important species and pathways of iron transformations (Figure 1.1).

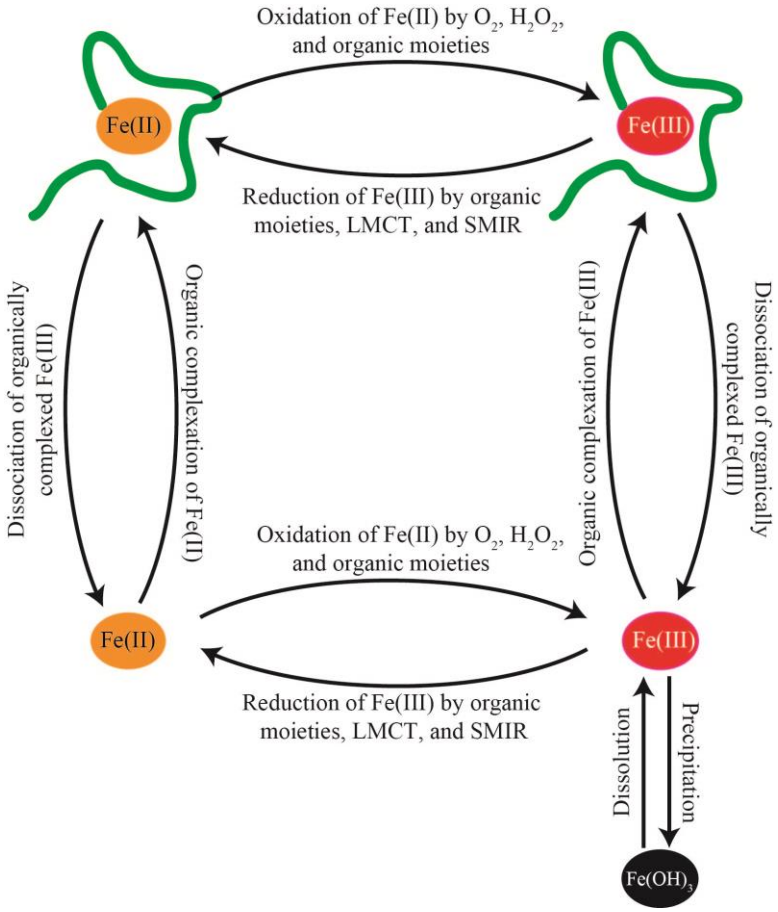

Figure 1.1: Schematic showing current knowledge on iron transformations in NOM.

There are three major pathways for Fe(III) reduction in natural waters. These include: direct reduction of Fe(III) by reducing moieties that exist intrinsically in NOM (Voelker and Sulzberger 1996; Garg et al. 2013a); reduction of Fe(III) by superoxide generated as a result of irradiation of NOM (SMIR) (Rose and Waite 2005); and reduction of Fe(III) via LMCT in photoactive Fe(III) species (Faust and Zepp 1993). A full iron cycle also consists of Fe(II) oxidation pathways. At circumneutral pH, Fe(II) is mainly oxidized by dioxygen (Santana-Casiano et al. 2005) and hydrogen peroxide (H_2O_2) if it exists in sufficiently high concentration (Miller et al. 2009). In addition to dioxygen and hydrogen peroxide, organic groups and/or ROS generated on photolysis of NOM may also play a role.

Recently, Garg et al. (2013a) showed that a long-lived Fe(II) oxidant (A^-) is generated via superoxide-mediated oxidation of reduced organic moieties (A^{2-}) intrinsically present in SRFA at pH 4 (Figure 1.2). The reduced organic species (A^{2-}) that is intrinsically present in SRFA is capable of reducing Fe(III) and can be oxidized partially to long-lived organic moieties (A^-) that is an Fe(II) oxidant. A steady state Fe(II) concentration is achieved as a result of the forward and backward reactions in eq.1.6 (Garg et al. 2013a).

$$A^{2-} + Fe(III) \rightleftharpoons A^- + Fe(II) \quad (1.6)$$

where A^{2-}, represents hydroquinone-like moieties that is intrinsically present in SRFA, and A^- represents semiquinone-like moieties that is capable of oxidizing Fe(II) (Garg et al. 2013a).

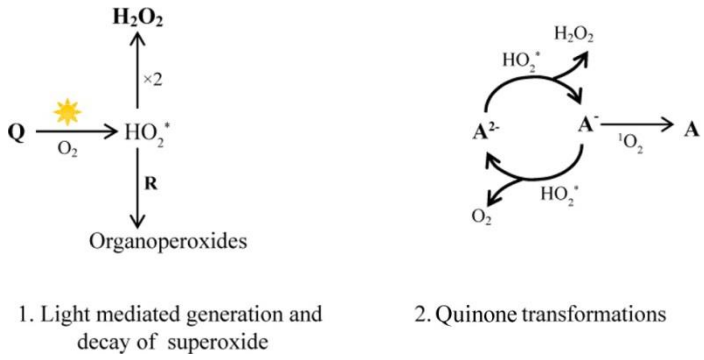

Figure 1.2: Reaction schematic showing the generation and decay of $HO_2^{\bullet}$, and its interaction with Fe(III) reductant (A^{2-}) and Fe(II) oxidant (A^-) (Garg et al. 2013a).

1.8. Knowledge gaps and objectives

Although the redox transformations of iron have been investigated in natural waters, there are still quite a few knowledge gaps. To better understand the redox

transformations of iron, the following questions are highlighted and are addressed in this thesis:

- Quinone moieties are considered to be important redox-active groups in NOM, and have been considered to be responsible for iron redox transformations in SRFA solutions under acidic conditions (Garg et al. 2013a). Is the mechanisms proposed by Garg et al. (2013a) in SRFA solutions applicable in pure hydroquinone solutions, and what are the similarities and differences between pure hydroquinone and SRFA solutions?

- The mechanism proposed in Garg et al. (2013a) successfully explains iron redox transformations in SRFA solutions at pH 4. Is the same mechanism applicable at other acidic pH? And what is the effect of pH on iron redox transformations occurring in SRFA solutions?

- LMCT and SMIR are two important pathways for light mediated iron redox transformations as proposed in various conditions though knowledge gaps still remain regarding the role of these two pathways under different conditions. A typical question would be, which pathway is more important at acidic/circumneutral pH and why?

- It is now recognized that iron redox transformations can be affected by a number of factors such as pH, light, and the presence of NOM. Are there any other factors that could affect iron redox transformations, such as ionic strength and the presence of divalent ions (e.g., Ca^{2+})?

- Investigation of iron redox transformations is largely impacted by pH with significant differences reported in mechanism and pathway controlling Fe

transformations at pH 4 (Garg et al. 2013a) and pH 8 (Garg et al. 2011a). While extensive insight regarding factors controlling iron redox transformations is available at pH 4 and 8, knowledge gaps remain regarding behavior (and controlling factors) at intermediate pH (i.e. pH 4-8). What are the main pathways controlling iron redox transformations in the intermediate pH range?

1.9. Layout of thesis

This thesis consists of eight chapters with each chapter focused on aspects of the questions mentioned above.

In chapter 2, general experimental methods and modelling approaches that have been used in this thesis are provided.

In chapter 3, iron redox transformations are examined in non-irradiated and previously irradiated SRFA solutions in the pH range of 3-5. The key pH dependent reactions are identified including the oxidation of Fe(II) by semiquinone-like radicals.

In chapter 4, iron redox transformations are examined in pure 1,4-hydroquinone solution and the results are compared with the results in SRFA solutions in Chapter 3. It is shown that semiquinone radicals are much more important in SRFA solutions than in pure hydroquinone solutions due to the rapid oxidation of semiquinone by oxygen in pure hydroquinone solutions. As a result, the cycling between Fe(II) and Fe(III) is found to be 10-20 times more rapid in SRFA solutions than that in pure hydroquinone solutions.

In chapter 5, iron redox transformations are investigated over the pH range of 3-5 under continuously irradiated conditions. The cycling of iron between the +(II) and +(III) oxidation states is more rapid at higher pH and under irradiated conditions. When Fe(III)

is irradiated in the presence of SRFA, LMCT is the dominant Fe(III) reduction pathway and photo-generated short-lived organic moieties similar to peroxyl radicals are found to be the main Fe(II) oxidant.

In chapter 6, the effect of the divalent ion Ca^{2+} on iron redox transformations is investigated in acidic conditions. The results show that the presence of Ca^{2+} increases the steady-state Fe(II) concentration by increasing the Fe(III) reduction rate and decreasing the Fe(II) oxidation rate. This is mainly due to change in Fe speciation as a result of formation of weakly complexed Fe(II) and Fe(III) species, thereby altering their reactivity.

In chapter 7, iron redox transformations are examined in the pH range 6.8-8.7 enabling extension of our current knowledge to a wider pH range. The results demonstrate that Fe(II) oxygenation rate increases with increasing pH with LMCT as the main Fe(III) reduction pathway under the experimental conditions where the iron: NOM ratio is low.

Chapters 3-6 in this thesis are based on published articles as shown below:

Chapter 4 Jiang, C., S. Garg and T. D. Waite (2015) 'Hydroquinone-mediated redox cycling of iron and concomitant oxidation of hydroquinone in oxic waters under acidic conditions: comparison with iron-natural organic matter interactions', Environmental Science and Technology, 49(24): 14076-14084.

Chapter 3 & 5 Garg, S., C. Jiang and T. D. Waite (2015) 'Mechanistic insights into iron redox transformations in the presence of natural organic matter: Impact of pH and light', Geochimica et Cosmochimica Acta, 165: 14-34.

Chapter 5 Garg, S., C. Jiang, C. J. Miller, A. L. Rose and T. D. Waite (2013) 'Iron redox transformations in continuously photolyzed acidic solutions containing natural

organic matter: Kinetic and mechanistic insights', Environmental Science and Technology, 47(16): 9190-9197.

Chapter 6 Jiang, C., S. Garg and T. D. Waite (2017) 'Iron redox transformations in the presence of natural organic matter: effect of calcium', Environmental Science and Technology, 51 (18): 10413-10422.

Chapter 2. General experimental methods and kinetic modelling approaches

2.1. General experimental methods

2.1.1. Reagents

All solutions were prepared using 18 MΩ.cm resistivity Milli-Q (MQ) water (TOC < 0.1 $mg.L^{-1}$) unless stated otherwise. All experiments were performed in air-saturated solutions at a temperature of 22 °C unless stated otherwise. All chemicals were analytical grade and were purchased from Sigma-Aldrich unless stated otherwise. All glass and plasticware were soaked in 3% HCl for at least 24 h prior to use. All stock solutions were stored at 4 °C in the dark when not in use.

All pH measurements were undertaken using a Hanna 210 pH meter with pH adjustments made using high purity HCl and NaOH. A maximum pH variation of ± 0.1 unit was allowed during experiments. Experiments at pH 3, 4 and 5 (Chapter 3-6) were performed in solutions containing 10^{-3}, 10^{-4}, and 10^{-5} M HCl respectively. Experiments at pH 8.3 (Chapter 7) were performed in 2 mM $NaHCO_3$ in equilibrium with CO_2 in the atmosphere. Experiments at pH 6.8, 7.8 and 8.7 (Chapter 7) were performed in 2 mM $NaHCO_3$ solution in equilibrium with synthetic air containing 15,000, 6,000, and 200 ppm CO_2 (HiQ® certified calibration standards; BOC) respectively. To allow equilibrium of CO_2 between the solution and the gas phase, sparging was performed for two hours prior to experiments and was also continued during the experiments. Organic buffers such as MES (2-(N-morpholino)ethanesulfonic acid hydrate) and HEPES (4-(2-hydroxyethyl)piperazine-1-ethanesulfonic acid) were not used in order to avoid interference with NOM in the system. All buffer solutions contained 10 mM NaCl. All buffer solutions were stored in containers covered with aluminum foil to avoid interference from the ambient light.

A 2.0 $g.L^{-1}$ stock solution of standard SRFA (International Humic Substances Society) was prepared in MQ water. The stock solution was stable over the duration of the study. Stock solutions of 0.1 M ferrozine (3-(2-pyridyl)-5,6-diphenyl-1,2,4-triazine-4′,4″-disulfonic acid sodium salt; abbreviated as FZ) and 20 mM desferrioxamine B (DFB) were prepared in MQ water. A mixture containing FZ (50 mM) and DFB (5 mM), which was prepared weekly by dilution of the 0.1 M FZ and 20 mM DFB stock solutions, was used for Fe(II) determination. A working 16 µM Fe(II) stock in 0.2 mM HCl was prepared weekly by 250-fold dilution with MQ water of a primary 4.0 mM Fe(II) stock solution in 0.2 M HCl. The working stock pH was 3.5, which was sufficiently low to prevent significant Fe(II) oxidation over a week. A 20 µM Fe(III) stock solution in 2 mM HCl was prepared every week by dilution of a primary 2 mM Fe(III) stock solution in 0.2 M HCl. The solution pH was sufficiently low to avoid polymerization or precipitation of iron. A working stock of 10 µM H_2O_2 prepared daily by dilution of 30% w/w H_2O_2 solution (reagent grade) was used for calibration of the H_2O_2 measurement. Stock solutions of 100 µM Amplex Red (AR; Invitrogen) mixed with 50 $kU.L^{-1}$ horseradish peroxidase (HRP) for H_2O_2 determination were prepared in MQ water and stored at -86 °C when not in use. A 3 $kU.mL^{-1}$ stock solution of superoxide dismutase (SOD from bovine erothrocytes containing Cu and Zn) was prepared in MQ water. A phosphate buffer was prepared by dissolving 10mM NaH_2PO_4 in MQ water and its pH was adjusted to 7.0. Stock solution of 50 mM DMSO (molecular biology grade) was prepared in MQ water. In Chapter 6, a stock solution of 1 M Ca^{2+} was prepared by dissolving $CaCl_2$ in 0.1 mM HCl. In Chapter 7, a stock solution of 0.1 M boric acid (reagent grade) with 1 µM Diethylenetriaminepentaacetic acid (DTPA) was prepared in MQ water and pH was adjusted to 12. MCLA CL reagent was prepared by dissolving 1 µM MCLA (6-(4-Methoxyphenyl)-2-methyl-3,7-

dihydroimidazo[1,2-a]pyrazin-3(7H)-one hydrochloride) in 50 mM sodium acetate in MQ water and pH was adjusted to 6.0 (Chapter 7).

2.1.2. Experimental setup

2.1.2.1. Photochemical experimental setup

Photochemistry experiments were performed in a 1 cm path length quartz cuvette (volume ~ 3.5 mL) in which concentrations of Fe(II), superoxide and/or H_2O_2 were monitored over time in irradiated solutions. A 150 W Xe lamp (ThermoOriel) equipped with AM0 and AM1 filters to simulate solar light was used as the light source and was positioned horizontally adjacent to the quartz cuvette. The spectral irradiance of the lamp and the absorbed photon irradiance (in $\mu Einstein.m^{-2}.s^{-1}$) of 10 $mg \cdot L^{-1}$ SRFA as function of wavelength are shown in Figure 2.1 below. Based on this, the quantum yield of superoxide and hydrogen peroxide generation were calculated to be 0.002% and 0.001% respectively for SRFA. The quantum yield of singlet oxygen was reported to be ~0.5% (Paul et al. 2004).

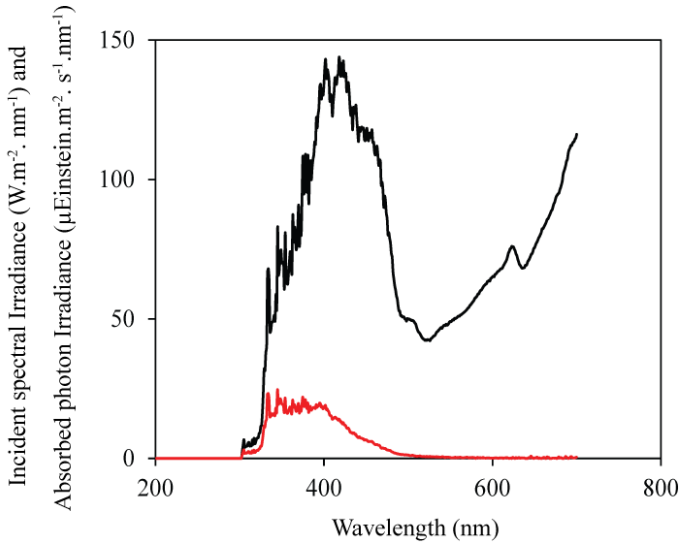

Figure 2.1: Incident spectral irradiance (black line) and the absorbed photon irradiance (red line) of the Xe lamp used for irradiation of 10 $mg.L^{-1}$ SRFA (Garg et al. 2013a).

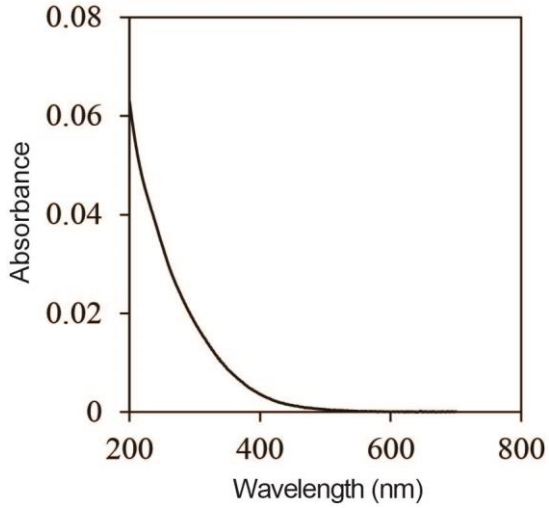

Figure 2.2: UV-visible absorption spectra of 10 mg.L^{-1} SRFA solution.

The UV-visible absorption spectra of SRFA solution (Figure 2.2) is considered invariant in the presence of iron (at the concentration range investigated here) and with pH variation. This is because the Fe concentration was low (≤ 100 nM) and insufficient to cause any effect on the absorption spectra. pH variation was considered to have little impact on the absorption spectrum, particularly in view of its much more significant effect on other factors such as the speciation of Fe and quinone moieties.

2.1.2.2. Experimental setup for various irradiation conditions

The Fe redox transformations were investigated in three irradiation conditions, namely non-irradiated, previously irradiated, and continuously irradiated conditions, which are expected to provide insights into the effects of different groups on Fe redox transformations. To study the effect of organic moieties intrinsically present in NOM on Fe redox transformations, experiments were performed in non-irradiated solutions. To study the effect of long-lived organic moieties generated on irradiation, experiments were performed in previously irradiated solutions; and experiments performed in continuously irradiated solutions were aimed to study the short-lived organic moieties

generated on irradiation. The experimental procedures for these three conditions in acidic conditions are provided below.

For experiments of Fe(II) oxidation and Fe(III) reduction in non-irradiated solutions, various concentrations of Fe(II)/Fe(III) were added to 30 mL of buffer solutions containing certain concentrations of SRFA/hydroquinone. 3 mL of sample were withdrawn and stored in a 1 cm quartz cuvette at different times after the addition of Fe with the concentrations of Fe(II) measured using a modified FZ method.

For experiments of Fe(II) oxidation and Fe(III) reduction in previously irradiated solutions, 3 mL of buffer solutions containing SRFA were irradiated in a 1 cm quartz cuvette for 10 min and various concentrations of Fe(II)/Fe(III) were added immediately after extinguishing the lamp. Subsequently, Fe(II) concentrations at different times after addition of Fe were measured using a modified FZ method.

For experiments of Fe(II) oxidation and Fe(III) reduction in continuously irradiated solutions, 3 mL of buffer solutions containing NOM and certain concentrations of Fe(II)/Fe(III) were irradiated in a 1 cm quartz cuvette for different duration, and the concentration of Fe(II) measured using a modified FZ method. It is noted that the lamp was turned on immediately after the addition of Fe into the solution and the concentration of Fe(II) measured immediately after the lamp was extinguished, to minimize the interference of the processes in non-irradiated solutions.

The experimental procedures at pH range 6.8-8.7 (Chapter 7) were performed in a slightly different manner, with major differences highlighted here. In the Fe(III) reduction experiments in non-irradiated and previously irradiated solution, FZ was mixed with SRFA solutions at a final concentration of 1mM FZ. The experiment was initiated by addition of 100 nM Fe(III) to the sample, which was immediately passed

through the 1 m path length type II liquid waveguide capillary cell (World Precision Instruments) for the measurement of Fe(II) concentration. The time between the addition of Fe(III) and a stable absorbance obtained by the spectrophotometer was ~ 1.5 min, therefore the Fe(II) concentration was recorded from 2 min onwards. For the Fe(III) reduction experiment in continuously irradiated solution, the lamp was turned on immediately after addition of 100nM Fe(III) in SRFA solutions containing 1mM FZ. The Fe(II) concentration was measured immediately after the lamp was extinguished.

2.1.2.3. Ca^{2+} addition experimental setup

In Chapter 6, to study the effect of calcium on the redox transformations of iron, an appropriate volume of calcium stock solution was added to the working SRFA solutions. No change in the pH of the SRFA solutions occurred on addition of calcium. The experimental setup used to study the effect of calcium addition on iron redox transformations under non-irradiated, previously irradiated and continuously irradiated conditions was similar to that used in the absence of Ca^{2+}.

The changes in the ionic strength of the solutions due to Ca^{2+} addition do not have any impact on Fe redox transformations since no impact of NaCl addition, when added to yield the same ionic strength as that in the presence of Ca^{2+}, was observed on Fe transformations. Note however that addition of Ca^{2+} may induce SRFA and Fe-SRFA aggregation due to bridging interactions that are unlikely to occur in the presence of NaCl. These effects of Ca^{2+} may induce variation in size and charge of SRFA and Fe-SRFA aggregates which, in turn, may impact the Fe binding capacity and strength of SRFA and, concomitantly, Fe redox transformations. Control experiments were performed in the absence of SRFA to ensure that trace quantities of organics or ROS present in our experimental matrix do not play a role in Fe redox transformations.

2.1.3. Removal of oxygen

Oxygen removal experiments in acidic environments (where pH was controlled by HCl addition) in Chapter 3-6 were carried out by sparging the buffer solution with argon gas (ultra-high purity grade, BOC) in a dreschel bottle for 4 hours prior to experiments. Oxygen removal experiments at pH 6.8, 7.3, 8.3 and 8.7 (where pH was controlled by CO_2 equilibrium with 2 mM $NaHCO_3$) in Chapter 7 were carried out by sparging 2 mM $NaHCO_3$ solution with argon gas containing 15,000, 6,000, 300 and 200ppm CO_2 (HiQ® certified calibration standards, BOC) in a dreschel bottle for 2 hours prior to experiments. The efficiency of oxygen removal was estimated to be ~ 95% based on the measurement of the rate of inorganic Fe(II) oxygenation in solution that was treated in a same manner. In all oxygen removal experiments, sparging was continued throughout the experiments to maintain sufficiently low oxygen level in the solution.

2.1.4. Measurement of Fe(II)

Concentrations of total Fe(II) under acidic conditions (Chapter 3-6) were determined spectrophotometrically using a modified FZ method (Garg et al. 2013a). In this method, FZ reacts rapidly with Fe(II) to form the $Fe(FZ)_3$ complex that absorbs strongly at 562 nm. Under acidic conditions, FZ facilitated Fe(III) reduction and hence, to avoid over prediction of Fe(II) concentration, DFB was also added to bind Fe(III) and prevent its reduction by FZ. For determination of Fe(II) concentration at acidic pH, 60 µL of 50 mM FZ and 5 mM DFB mixture was added to 3 mL of the sample and this solution was continuously circulated through a 1 m path length type II liquid waveguide capillary cell (World Precision Instruments). The absorbance of the solution was measured at 562 nm using an Ocean Optics fiber optic spectrophotometry system with correction for baseline drift by subtracting the absorbance at 690 nm (at which no components of the solution absorb significantly). Calibration of Fe(II) was performed immediately before

experiments by standard addition of Fe(II) to the buffer solution containing the FZ-DFB mix. A molar absorption coefficient of 27,000 $M^{-1}cm^{-1}$ was obtained for the $Fe(FZ)_3$ complex which is close to the published value of 27,900 $M^{-1}cm^{-1}$ (Stookey 1970). Since a small amount of Fe(III) was reduced by FZ even in the presence of DFB and hence increased absorbance at 562 nm, calibration of Fe(III) was also performed using standard addition of Fe(III) to the buffer solution containing the FZ-DFB mix. The concentration of Fe(II) in the sample was deduced using the equation:

$$[Fe(II)] = (A_{562} - \varepsilon_{Fe(III)}[Fe]_T) / (\varepsilon_{Fe(II)} - \varepsilon_{Fe(III)}) \quad (2.1)$$

where A_{562} represents sample absorbance at 562 nm wavelength, $\varepsilon_{Fe(II)}$ and $\varepsilon_{Fe(III)}$ represent molar absorption coefficient of $Fe(FZ)_3$ complex and $Fe(FZ)_3$ formed as a result of reduction of Fe(III) by FZ respectively, and $[Fe]_T$ represents the total Fe concentration. Fe(II) measurements were continued until the system had reached a quasi-steady state. The detection limit (defined as 3 times the standard deviation of the reagent blank) of the Fe(II) measurement method is ~ 2 nM.

Concentrations of total Fe(II) in the pH range 6.8-8.7 (Chapter 7) were measured in a similar manner. However, FZ facilitated Fe(III) reduction is negligible in this pH range thus DFB was not incorporated. For determination and calibration of Fe(II) concentration, 37 µL of 80 mM FZ (pH adjusted to sample pH) was added to 3 mL of the sample and this solution was continuously circulated through a 1 m path length type II liquid waveguide capillary cell (World Precision Instruments). The absorbance of the sample at 562 nm was measured using Ocean Optics spectrophotometry system using setting described above. The concentration of Fe(II) in the sample was determined using the equation:

$$[Fe(II)] = A_{562} / \varepsilon_{Fe(II)} \quad (2.2)$$

where A_{562} and $\varepsilon_{Fe(II)}$ represent sample absorbance at 562 nm wavelength and molar absorption coefficient of $Fe(FZ)_3$ complex.

2.1.5. Measurement of H_2O_2

For measurement of H_2O_2 production in acidic irradiated SRFA solutions (Chapter 3-6), 1 mL of sample that was irradiated in a 1 cm quartz cuvette for 1, 2, 5, and 10 min was mixed with 2 mL of 10 mM phosphate buffer (pH = 7.0) followed by addition of 60 µL of AR and HRP mixture and fluorescence was measured using a Cary Eclipse spectrophotometer (Agilent Technologies). Calibration was performed by standard addition of H_2O_2 to 1 mL of non-irradiated SRFA solution mixed with 2 mL of 10 mM phosphate buffer. The detection limit (defined as 3 times the standard deviation of the reagent blank) of the H_2O_2 measurement method is ~ 3 nM.

In the pH range 6.8-8.7 (Chapter 7), the AR and HRP mixture is active with regard to the measurement of H_2O_2 thus the phosphate buffer for pH adjustment was not incorporated. For measurement of H_2O_2 production in this pH range, 60 µL of AR and HRP mixture was added to a 1 cm quartz cuvette containing 3 mL of sample that was irradiated for 1, 2, 5, and 10 min and fluorescence was measured using a Cary Eclipse spectrophotometer (Agilent Technologies). Calibration was performed by standard addition of H_2O_2 to 3 mL of non-irradiated SRFA solution. Other experimental procedures for H_2O_2 measurement here are the same as the procedures at acidic pH.

2.1.6. Measurement of benzoquinone

In Chapter 4, the concentration of 1,4-benzoquinone formed on oxidation of 1,4-hydroquinone was determined by measuring its UV-absorbance at 247 nm using a 1 m

path length type II liquid waveguide capillary cell (World Precision Instruments) connected with broadband deuterium-halogen DH-2000 lamp (Ocean Optics) as the light source and a USB4000 spectrophotometer (Ocean Optics). A molar absorption coefficient of 1.8×10^4 M^{-1} cm^{-1} was obtained which is close to the reported value of 2.1×10^4 M^{-1} cm^{-1} (Wilcoxen et al. 2011).

2.1.7. Measurement of superoxide

For measurement of superoxide in Chapter 7, 3.5 mL of sample was circulated through a flow cell of a FeLume CL system (Waterville Analytical) by a peristaltic pump that delivered MCLA CL reagent at the same time. The mixing of sample solution and MCLA CL reagent yielded $O_2^{\bullet-}$ -specific-CL that was detected by the instrument's photomultiplier tube.

For calibration, superoxide stock solution was generated photochemically immediately prior to use by irradiating 3 mL of 0.1 M boric acid containing 1 µM DTPA, 12 µL absolute acetone (≥ 99.8 %) and 120 µL absolute ethanol (≥ 99.8 %) using a low-pressure mercury vapor pen-lamp (Pen-Ray) in a 1 cm quartz cuvette. The concentration of superoxide generated was determined by measuring the absorbance at 240 nm using a USB4000 spectrophotometer (Ocean Optics) coupled to a DH-2000 light source (Ocean Optics). Illumination by the pen-lamp was ceased immediately when the absorbance reached 0.06, 0.12, and 0.16, corresponding to 25, 50, and 75 µM $O_2^{\bullet-}$ (Bielski et al. 1985).

2.2. General modelling and statistical analysis approaches

Kinetic modelling was performed using the software package Kintecus (Ianni 2003) or KINTEK Explorer (Johnson et al. 2009). The sensitivity analysis of the kinetic model was performed by calculating normalized sensitivity coefficients (NSCs) and

undertaking principal component analysis as described by Vajda and co-workers (Vajda et al. 1985). The NSCs were calculated using Kintecus (Ianni 2003).

Statistical analysis was performed using single tailed student's t-test or one-way analysis of variance (ANOVA) at 5% significance level.

Chapter 3. Mechanistic insights into iron redox transformations in non-irradiated and previously irradiated Suwannee River fulvic acid solutions under acidic conditions

3.1. Introduction

Fe(III) reduction by NOM in the dark has been reported in various studies (Szilagyi 1971; Skogerboe and Wilson 1981; Voelker and Sulzberger 1996; Borman et al. 2010). While Voelker and Sulzberger (1996) attributed this Fe(III) reductant to be quinone-type structures, Garg and co-workers (2013a) more specifically suggested that this Fe(III) reductant is hydroquinone-like species, which is intrinsically present in SRFA solutions (Garg et al. 2013a). Furthermore, Garg and co-workers (Garg et al. 2013a) reported that long-lived (> 24 h) semiquinone-like moieties are generated on oxidation of hydroquinone-like moieties on irradiation which is capable of oxidizing Fe(II) at pH 4. This finding has strong implications in acidic sunlit environments where, if humic or fulvic-type NOM is present, steady state Fe(II) concentrations will be much lower than would be the case if Fe(II) oxidation were controlled by the presence of either oxygen or H_2O_2 only.

The objective of this chapter is to investigate the kinetics and mechanism of iron redox transformations in SRFA solutions in the pH range 3-5 with the goal of identifying the role of stable organic moieties in Fe redox transformations. Also, the mechanism of Fe redox transformations proposed by Garg and co-workers (Garg et al. 2013a) at pH 4 is extended to explain the Fe transformation rates in the pH range 3-5 with attention given to identifying the major pH dependent reactions involved in iron redox transformations. All experiments are performed under two conditions, namely: non-irradiated and previously irradiated (SRFA solutions that were irradiated for 10 min prior to Fe addition in the dark) solution. It is expected that the results of experiments performed under dark conditions will provide insight into the impact of organic radicals intrinsically present in SRFA on Fe redox transformations; while the results of experiments performed in the presence of previously irradiated SRFA solutions should

provide insight into the role of any long-lived organic moieties that may be formed on irradiation of SRFA in Fe(III) reduction and Fe(II) oxidation. While the acidic conditions used in these studies have been chosen, in part, to avoid complications associated with the precipitation of iron oxides and fast Fe(II) oxygenation, they do reflect conditions that are present in acid mine drainage waters, in coastal environments impacted by the presence of acid sulfate soils and in atmospheric aerosols. While we recognize that SRFA is but one example of a natural organic matter, it is well-characterized and frequently used in studies on Fe-NOM interactions, and, as such, is used in the work described here.

3.2. Experimental methods

Detailed description of reagents and experimental setup is provided in Chapter 2.

3.3. Results and discussion

3.3.1. Fe(III) reduction kinetics in non-irradiated SRFA solutions

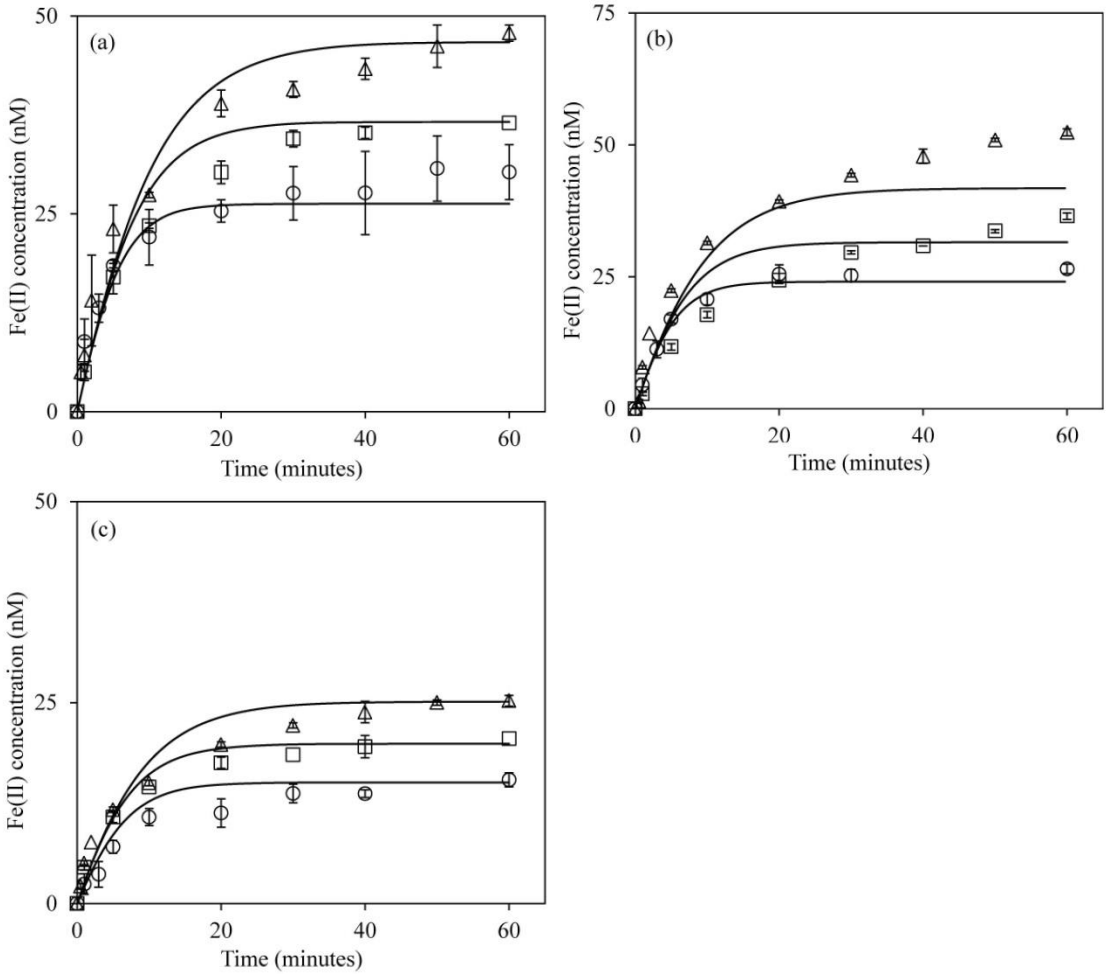

Figure 3.1: (a) Generation of Fe(II) during reduction of 100 nM Fe(III) in non-irradiated 10 mg.L^{-1} SRFA solutions at pH 3 (triangles), 3.5 (squares) and 4 (circles). (b) Generation of Fe(II) during reduction of 100 nM Fe(III) in non-irradiated 5 mg.L^{-1} SRFA solutions at pH 3 (triangles), 3.5 (squares) and 4 (circles). (c) Generation of Fe(II) during reduction of 50 nM Fe(III) in non-irradiated 5 mg.L^{-1} SRFA solutions at pH 3 (triangles), 3.5 (squares) and 4 (circles). Symbols represent experimental data (average of duplicate measurements); lines represent model values.

The concentrations of Fe(II) generated on reduction of Fe(III) when added to SRFA solutions in the dark over the pH range 3-5 are shown in Figure 3.1. As can be seen, the concentration of Fe(II) increased gradually however reached steady-state within 60 minutes, suggesting that Fe(II) oxidation is also important. Since negligible Fe(II) oxidation occurred in non-irradiated SRFA solutions for pH < 5 (at least over the time

scale of interest) (Figure 3.2), we further suggest that the Fe(II) oxidant at pH < 5 must have been formed as a result of the oxidation of reduced organic species by Fe(III).

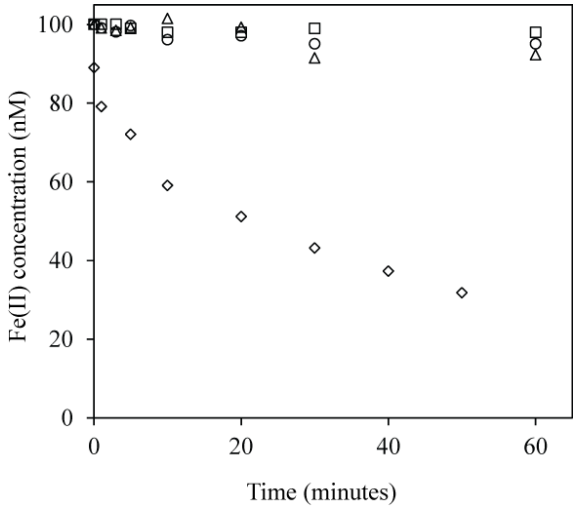

Figure 3.2: Fe(II) decay in presence of 10 mg.L^{-1} SRFA in the dark at pH 3 (circles) , 3.5 (squares), 4 (triangles), 5 (diamonds). Data represents average of duplicate measurement.

The concentration of Fe(II) generated decreased with increase in pH suggesting that either the rate of Fe(III) reduction decreased and/or the rate of Fe(II) oxidation increased with increase in pH. No Fe(II) generation was observed at pH 5 (data not shown) suggesting that either the Fe(III) reduction rate is very slow and/or Fe(II) oxidation is rapid at this pH.

As described by Garg et al. (2013a), the experimental data at pH 4 was well described by the simple reaction scheme shown in eq.3.1, with the ratio k_1/k_2 and A_0 calculated using the eq.3.2.

$$A^{2-} + \ Fe(III) \underset{k_2}{\overset{k_1}{\rightleftharpoons}} A^{-} + \ Fe(II) \tag{3.1}$$

$$\left(\frac{k_2}{k_1} - 1\right)\left[Fe(II)\right]_{ss}^2 + \left(Fe_0 + A_0\right)\left[Fe(II)\right]_{ss} - Fe_0A_0 = 0 \tag{3.2}$$

where Fe_0 and A_0 represent the initial concentrations of Fe(III) and A^{2-} respectively. The same reaction scheme describes the data obtained here for Fe(III) reduction in non-irradiated SRFA solutions in the pH range from 3-5 with the ratio k_1/k_2 decreasing with increase in pH assuming that the initial concentration of A^{2-} (35.4 μmoles.g^{-1} SRFA) remains constant with pH (see Table 3.1 for details). The concentration of A^{2-} determined here is reasonably consistent with the concentration (42 μmol.g^{-1}) of stable reduced groups determined in non-treated humic acid by Aeschbacher et al. (2010) and with the concentration of reduced groups (25.4 μmol.g^{-1}) in fulvic acid determined by Ratasuk and Nanny (2007). However the concentration of A^{2-} used here is much lower than the reported electron donating capacity of humic substances (Aeschbacher et al. 2012), which is mostly attributed to the presence of phenolic moieties, thereby suggesting that A^{2-} are distinct from phenolic moieties. It is to be noted here that A^{2-} and A^{-} represents free hydroquinone-like and semiquinone-like moieties respectively since the complexation of these groups by Fe is expected to be negligible given their low concentration compared to bulk organic matter (consisting of carboxylic groups and phenolic group) in SRFA.

Table 3.1: Calculated values of k_1/k_2, E_H^0 for A^-/A^{2-} redox couple and E_H for A^-/A^{2-} redox couple at equilibrium with Fe(III)/Fe(II) redox couple and TOF based on the measured $[Fe(II)]_{ss}$ generated on Fe(III) reduction in non-irradiated SRFA solutions in the dark.

pH	[SRFA] (mg.L^{-1})	$[Fe(III)]_0$ (nM)	$[Fe(II)]_{ss}$ (nM)	k_1/k_2	E_H^0 (V)	E_H (V)	TOF (h^{-1})
3	10.0	100	50.0	0.16	0.59	0.36	1.92
		50	27.2	0.11	0.60	0.36	2.01
	5.0	50	25.2	0.17	0.58	0.36	0.95

	2.5	25	13.0	0.19	0.59	0.36	0.46
3.5	10.0	100	36.5	0.07	0.60	0.34	2.54
		50	23.2	0.06	0.60	0.34	2.24
	5.0	50	19.5	0.08	0.60	0.33	1.21
	2.5	25	9.0	0.06	0.60	0.34	0.64
4.0	10.0	100	29.3	0.04	0.61	0.30	2.89
		50	19.5	0.04	0.60	0.29	2.57
	5.0	50	15.4	0.04	0.60	0.30	1.51
	2.5	25	7.5	0.04	0.61	0.30	0.71

The ratio k_1/k_2 calculated here also represents the equilibrium constant (K) for the reaction shown in eq.3.1. Based on the calculated equilibrium constant for this reaction, and the calculated reduction potential of the Fe(III)/Fe(II) redox couple in the experimental matrix, we can calculate the standard reduction potential (E^0_{H}) of the hydroquinone-like moieties. At equilibrium, the redox potential of Fe(III)/Fe(II) couple is defined by:

$$E_{\mathrm{H1}} = E^0_{\mathrm{H1}} - 0.059\log\frac{[\mathrm{Fe}^{2+}]}{[\mathrm{Fe}^{3+}]} \tag{3.3}$$

Given that hydroquinone-like moieties ($pK_a > 10$) exist mostly in the protonated form (H_2A) in the pH range investigated here while semiquinone-like groups most likely exist as HA ($pK_a \sim 4.1$), the redox potential of hydroquinone-like/semiquinone-like moieties redox couple is defined as

$$E_{\mathrm{H2}} = E^0_{\mathrm{H2}} - 0.059\log\frac{[\mathrm{H_2A}]}{[\mathrm{HA}][\mathrm{H}^+]} \tag{3.4}$$

At equilibrium,

$$E_{H1} = E_{H2} \quad (3.5)$$

Assuming that Fe(III) exist as Fe(III)-SRFA complex (stability constant ~ 10^{12}) (Rose and Waite 2003), and Fe(II) completely in inorganic form, we calculate the concentration of Fe^{3+} and Fe^{2+} at equilibrium at all the pH values investigated here.

For calculation of Fe^{3+} concentration, firstly the total inorganic Fe(III) concentration in equilibrium with the Fe(III)-SRFA complex was calculated and then Fe^{3+} fraction of the inorganic Fe(III) was calculated using the speciation data of inorganic Fe(III) reported earlier (Morel and Hering 1993). Since Fe^{2+} is the dominant Fe(II) specie in the pH range investigated, $[Fe^{2+}] = [Fe(II)]_{ss}$.

$$[H_2A]_{ss} = A_0 - [Fe(II)]_{ss} \quad (3.6)$$

$$[HA]_{ss} = \alpha_0 [Fe(II)]_{ss} = \frac{[H^+] \times Fe(II)_{ss}}{[H^+] + K_{HA}} \quad (3.7)$$

Substituting the concentration of Fe^{3+} , Fe^{2+} , H_2A , HA , H^+ at equilibrium and E^0_{h1} value (+ 0.77 V) , we calculate E^0_{H2} = 0.60 V (Table 3.1) at the pH values investigated here which is consistent with the standard reduction potential (E^0_H > +0.18 V) of reduced hydroquinone-like groups present in untreated humic acid determined by Aeschbacher et al. (2010). The standard reduction potential of the reductant determined here is also in accord with the reported E^0_H range (0.178 - 0.734 V) for various hydroquinones (Roginsky and Barsukova 2000).

It is to be noted here that the stability constant of Fe(III)-SRFA complex used here was determined at high pH and high ionic strength conditions and hence may be different under the low ionic strength and low pH condition employed here. The E^0_{H2} values

calculated here will vary with the changes in the stability constant of Fe(III)-SRFA complex with approximately 0.05 V change in the E^0_{H2} value with 10-fold change in the stability constant value; however we get same values for E^0_{H2} at all pHs irrespective of the stability constant value used.

The variation in E_{H2} with pH is shown in Figure 3.3 assuming that (i) HA has pK_a = 4 and (ii) pK_{a1} = 10 and pK_a =12 for H_2A. As shown, E_{H2} decreases with increase in pH suggesting that at a given E_H value more of the oxidized form will exist at higher pHs.

The similarity in the calculated value of standard reduction potential under various pH conditions supports the conclusion that the same Fe(III) reductant and Fe(II) oxidant exists under all pH conditions investigated here with the assumption that the pK_a values are consistent with quinone-type moieties.

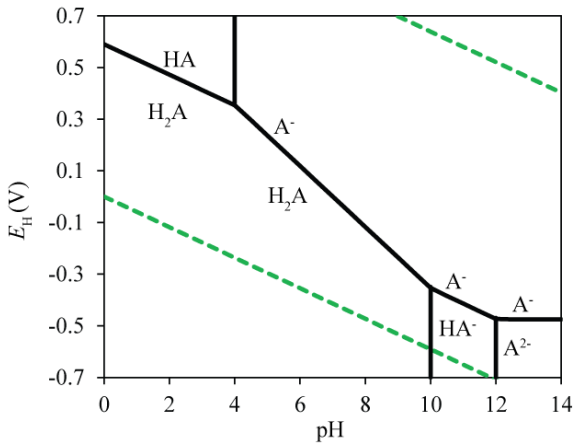

Figure 3.3: E_H-pH diagram of the HA/H_2A and associated redox couples. The dashed green lines show the stability limits of water in the solution.

3.3.2. Fe(III) reduction kinetics in previously irradiated SRFA solutions

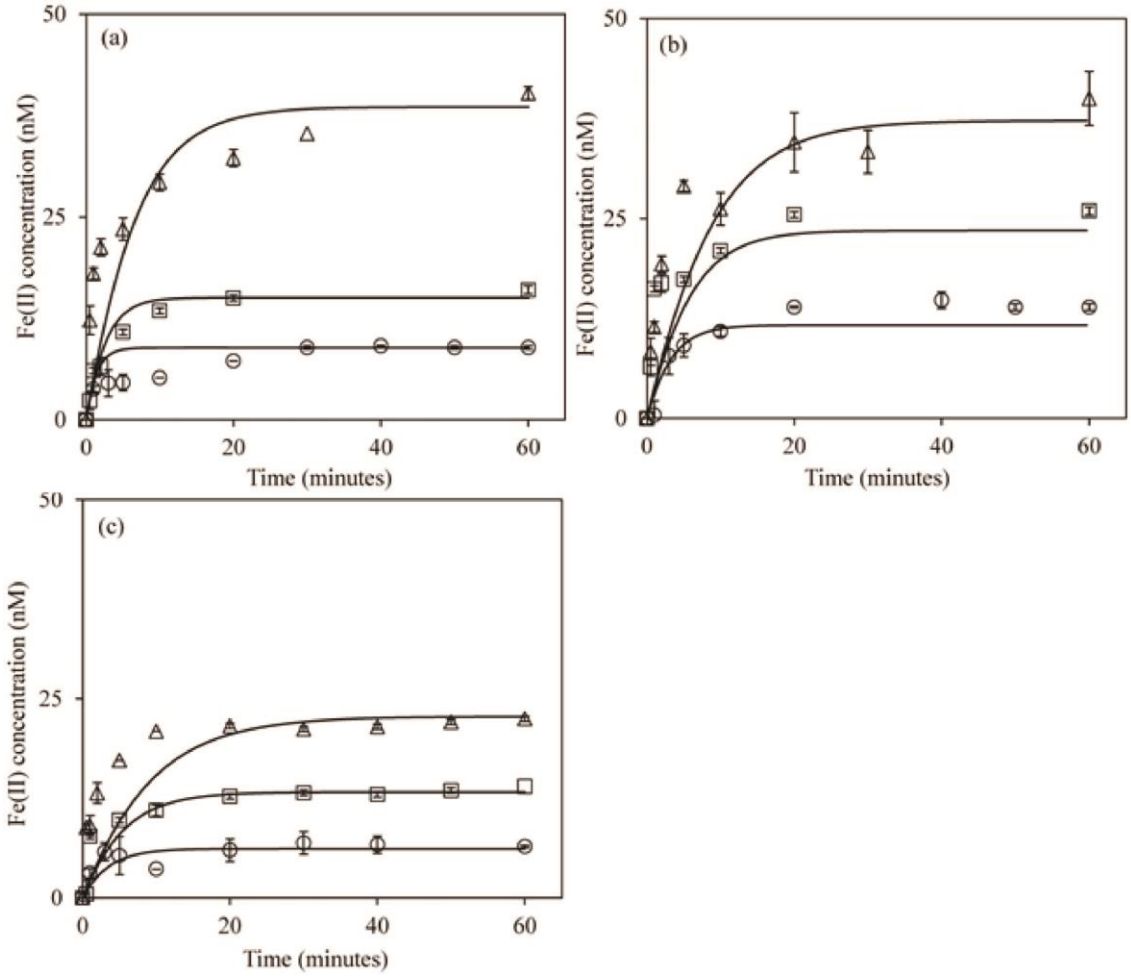

Figure 3.4: (a) Generation of Fe(II) during reduction of 100 nM Fe(III) in the dark in solutions containing 10 mg.L^{-1} SRFA that were irradiated for 10 min prior to addition of Fe(III) at pH 3 (triangles), 3.5 (squares) and 4 (circles). (b) Generation of Fe(II) during reduction of 100 nM Fe(III) in solutions containing 5 mg.L^{-1} SRFA that were irradiated for 10 min prior to addition of Fe(III) at pH 3 (triangles), 3.5 (squares) and 4 (circles). (c) Generation of Fe(II) during reduction of 50 nM Fe(III) in solutions containing 5 mg.L^{-1} SRFA that were irradiated for 10 min prior to addition of Fe(III) at pH 3 (triangles), 3.5 (squares) and 4 (circles). Symbols represent experimental data (average of duplicate measurements); lines represent model values.

As shown in Figure 3.4, the concentration of Fe(II) generated on addition of Fe(III) in the dark to SRFA solutions that were previously irradiated for 10 minutes, decreased with increase in pH. This is consistent with the observation in the non-irradiated solution (Figure 3.1) that the Fe(II) generation rate decreased with increase in pH. The steady-state Fe(II) concentration generated here is lower than that observed when Fe(III)

was added to non-irradiated SRFA solutions (Figure 3.1) and also decreased with increase in SRFA concentration (see Table 3.2). Both observations suggest that the Fe(II) oxidant concentration increased and/or Fe(III) reductant concentration decreased on irradiation of SRFA solutions which is in agreement with the pH 4 results reported earlier (Garg et al. 2013a).

Table 3.2: Calculated concentration of A^- ($A_0^{'}$) generated after 10 minutes of SRFA photolysis.

pH	[SRFA], $mg.L^{-1}$	Fe_T, nM	k_2/k_1[a]	$[Fe(II)]_{ss}$ on Fe(II) oxidation, nM	$A_0^{'}$, nM	$[Fe(II)]_{ss}$ on Fe(III) reduction, nM	$A_0^{'}$, nM	E_H[b]
3	10.0	100	5.8[c]	71.5	28.7	40.0	32.8	0.37
		50		31.8	37.8	-		0.37
	5	50		38.5	9.5	21.6	11.2	0.37
	2.5	25		-	-	11.2	4.2	0.36
3.5	10	100	14.8	58.5	46.8	16.1	75.4	0.36
		50		24.1	43.6	13.0	44.1	0.35
	5	50		34	16.7	14.0	12.6	0.35
	2.5	25		18.3	6.5	5.6	7.5	0.35
4.0	10	100	25.6	29.9	87.9	9	91.2	0.33
		50		10.4	79.5	4.5	95.6	0.33
	5	50		22.1	32.4	6.4	30.8	0.33
	2.5	25		10.0	17.5	3.0	16.7	0.32

[a]average of values shown in Table 3.1.

[b]Calculated redox potential of A^-/A^{2-} redox couple in equilibrium with Fe(III)/Fe(II) redox couple in previously irradiated SRFA solutions.

[c]average was calculated by ignoring the value of k_2/k_1 calculated for 10 $mg.L^{-1}$ SRFA and 50 nM Fe(III) since it was much higher than the value calculated under other conditions.

3.3.3. Fe(II) oxidation kinetics in previously irradiated SRFA solutions

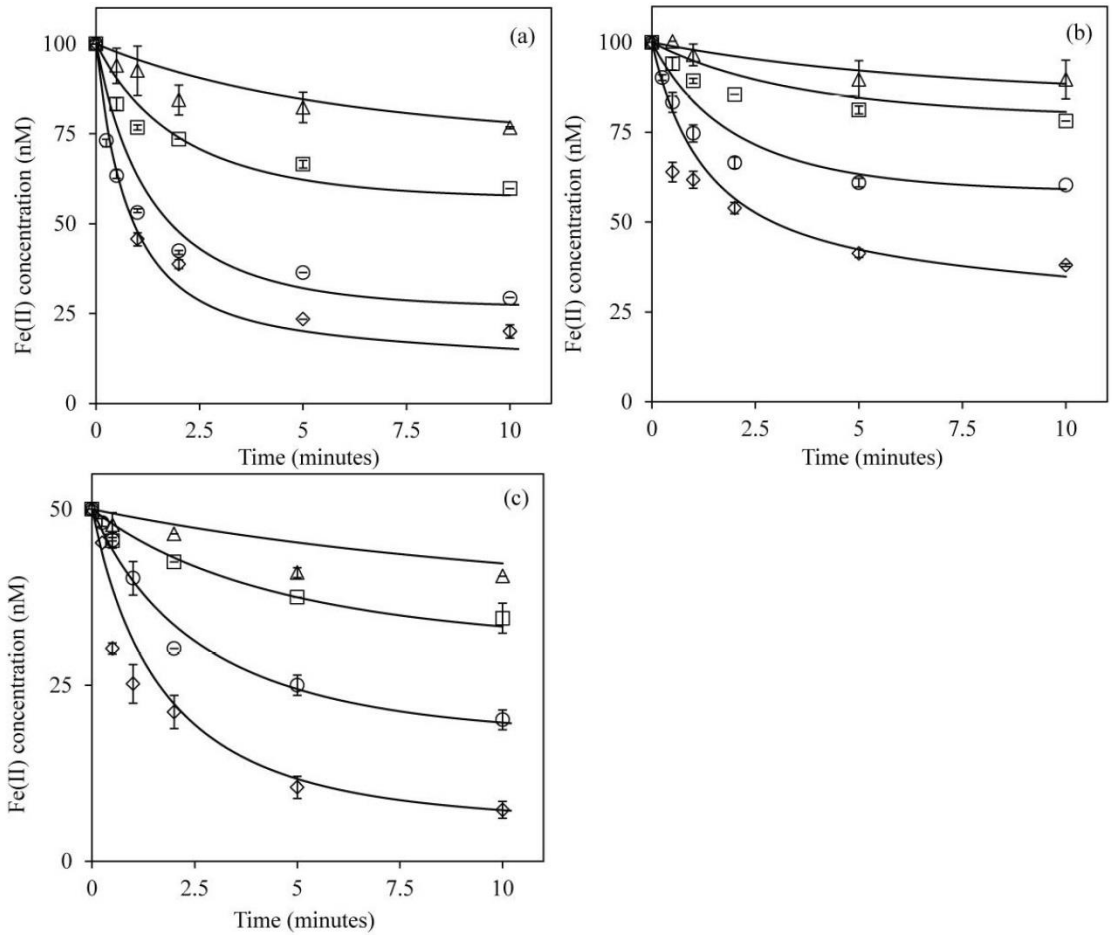

Figure 3.5: (a) Oxidation of 100 nM Fe(II) when added to solutions containing 10 $mg.L^{-1}$ SRFA that were irradiated for 10 min prior to addition of Fe(II) at pH 3 (triangles), 3.5 (squares) , 4 (circles) and 5 (diamonds). (b) Oxidation of 100 nM Fe(II) when added to solutions containing 5 $mg.L^{-1}$ SRFA that were irradiated for 10 min prior to addition of Fe(II) at pH 3 (triangles), 3.5 (squares), 4 (circles) and 5(diamonds). (c) Oxidation of 50 nM Fe(II) when added to solutions containing 5 $mg.L^{-1}$ SRFA that were irradiated for 10 min prior to addition of Fe(II) at pH 3 (triangles), 3.5 (squares), 4 (circles) and 5 (diamonds). Symbols represent experimental data (average of duplicate measurements); lines represent model values.

Fe(II) oxidizes rapidly when added to SRFA solutions that were irradiated for 10 min prior to addition of Fe(II) (Figure 3.5). As shown, the decay rate of Fe(II) increases with increase in pH which is in agreement with the results presented in Figure 3.1 and Figure 3.4. At a particular pH value, the steady state Fe(II) concentration remaining decreased with increase in SRFA concentration (Table 3.2) supporting the conclusion that the Fe(II) oxidant is formed as a result of SRFA photolysis.

The reaction scheme shown in eq.3.1 can readily explain the results obtained for both Fe(III) reduction and Fe(II) oxidation in previously irradiated SRFA solutions (Figure 3.4 and Figure 3.5) if A^{2-} is assumed to be partially oxidized to A^{-} on irradiation. The concentration of A^{-} formed after irradiation of SRFA for 10 min $\left(A_0^{'}\right)$ may be calculated from the relationship

$$A_0^{'} = \frac{\frac{k_1}{k_2}Fe_0A_0 + \left(Fe_0 - \frac{k_1}{k_2}A_0 - 2\frac{k_1}{k_2}Fe_0\right)\left[Fe(II)\right]_{ss} - \left(1-\frac{k_1}{k_2}\right)\left[Fe(II)\right]_{ss}^2}{\frac{k_1}{k_2}Fe_0 + \left(1-\frac{k_1}{k_2}\right)\left[Fe(II)\right]_{ss}} \tag{3.8}$$

when Fe(II) is added to the irradiated SRFA solutions, or from the relationship

$$A_0^{'} = \frac{\frac{k_1}{k_2}Fe_0A_0 - \frac{k_1}{k_2}\left(Fe_0 + A_0\right)\left[Fe(II)\right]_{ss} - \left(1-\frac{k_1}{k_2}\right)\left[Fe(II)\right]_{ss}^2}{\frac{k_1}{k_2}Fe_0 + \left(1-\frac{k_1}{k_2}\right)\left[Fe(II)\right]_{ss}} \tag{3.9}$$

when Fe(III) is added to the irradiated SRFA solutions (see Garg et al. (2013a) for more details on derivation of these equations).

Substituting the measured steady-state concentrations of Fe(II) when Fe(II) or Fe(III) were added to previously irradiated SRFA solutions (from Table 3.2) along with calculated values of k_2/k_1 and A_0 (from Table 3.1) permits calculation of $[A^{-}]$ formed for all SRFA concentrations investigated after 10 minutes of irradiation (see Table 3.2). As shown, the concentration of A^{-} formed at a given pH are consistent for all concentrations of SRFA and Fe investigated here, regardless of whether Fe was added as Fe(II) or Fe(III). The concentration of A^{-} formed was consistent for similar total Fe to SRFA ratios (1:100 assuming a molecular weight of 1000g for SRFA) ratios but

deviated somewhat at higher ratios of total Fe to SRFA concentration, with lower calculated [A^-] than observed at lower total Fe to SRFA concentration ratios. This result suggests that Fe(III) is more reducible at higher Fe to SRFA concentration ratios, possibly as a result of weaker Fe(III) binding as the proportion of metal to organic increases.

The concentration of A^- formed on SRFA irradiation increases with increase in pH (Table 3.2) thereby resulting in an increase in Fe(II) oxidation rate with increase in pH. The increased generation of A^- at higher pHs is consistent with the pH-dependence of the E_H of the A^-/A^{2-} redox couple (see Figure 3.3) with a greater concentration of the oxidized form (i.e. A^-) present at higher pHs. Also, it is possible that the deprotonated form of the semiquinone radical is more stabilized and longer-lived than the protonated form thereby resulting in higher overall semiquinone concentration at higher pHs. The E_H of the A^-/A^{2-} redox couple in equilibrium with the Fe(III)/Fe(II) redox couple in previously irradiated SRFA solutions (Table 3.2) is higher than that observed in non-irradiated solution (Table 3.1) which is consistent with increase in concentration of A^- on irradiation.

3.3.4. Role of H_2O_2

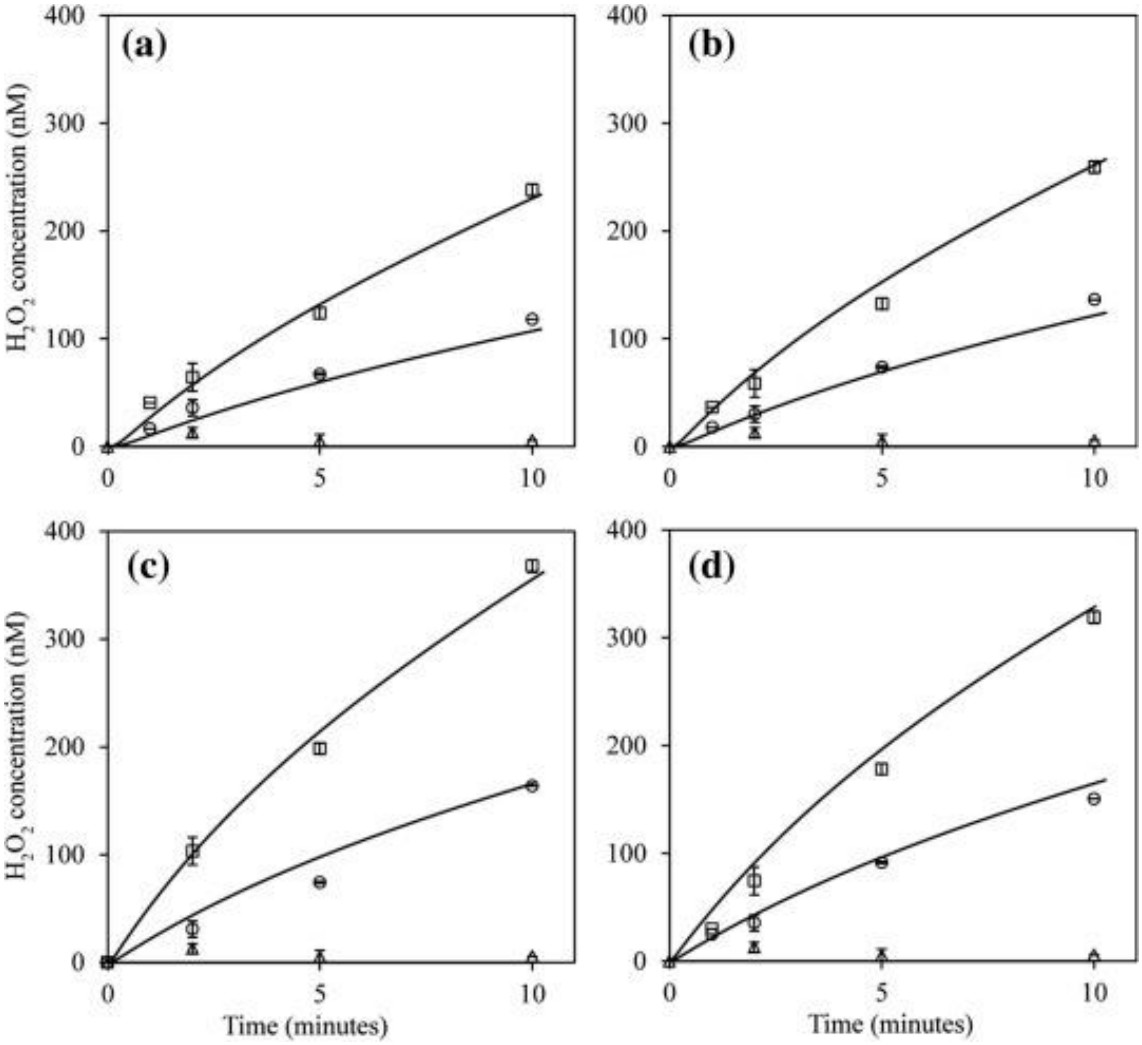

Figure 3.6: Generation of H_2O_2 in the dark (triangles) and on irradiation of 5mg.L^{-1} (circles) and 10 mg.L^{-1} (squares) SRFA at (a) pH 3 (b) pH 3.5 (c) pH 4 and (d) pH 5. Symbols represent experimental data (average of duplicate measurements); lines represent model values.

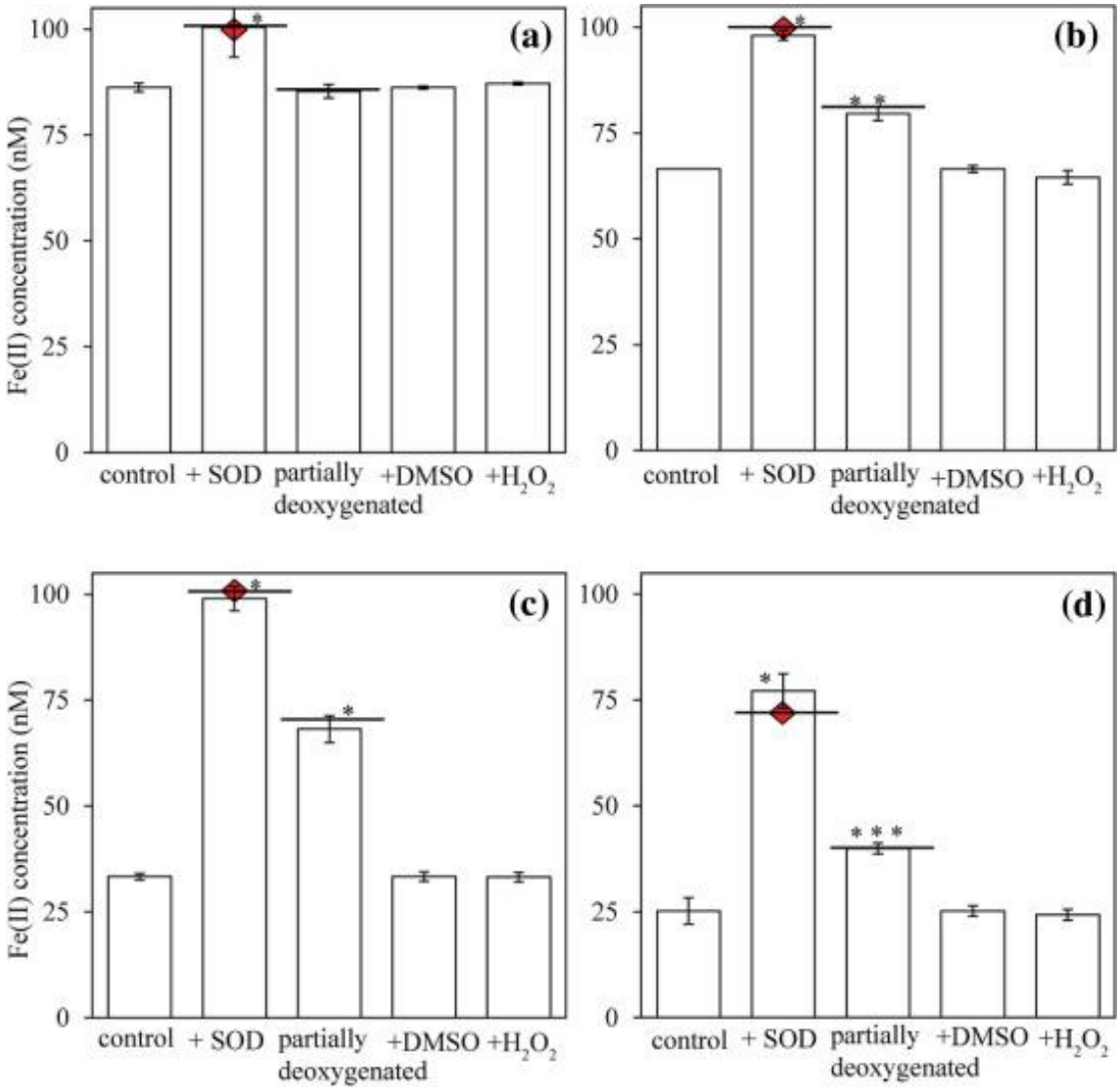

Figure 3.7: Effect of various treatments on Fe(II) concentration remaining after 10 minutes on addition of 100 nM Fe(II) to solutions containing 5 $mg.L^{-1}$ SRFA that had been irradiated for 10 minutes prior to adding Fe(II) at (a) pH 3 (b) pH 3.5 (c) pH 4 and (d) pH 5. Error bars represent the standard deviation from triplicate experiments. Red diamond point shows the Fe(II) concentration remaining measured for same initial Fe(II) and SRFA concentration in non-irradiated SRFA solutions. One asterisk shows that treatment was different than the control at 0.0001 significance level; two asterisk shows that treatment was different than the control at 0.0005 significance level; three asterisk shows that treatment was different than the control at 0.001 significance level.

No H_2O_2 generation occurs in the dark suggesting that ROS-mediated Fe redox transformations are not important under these conditions. Although significant concentrations of H_2O_2 were generated on irradiation of SRFA (Figure 3.6), no effect of H_2O_2 addition on Fe(II) oxidation was observed in previously irradiated (Figure 3.7)

SRFA solutions even when added at a concentration 10-fold higher than that generated in irradiated SRFA solutions. As such, it would appear reasonable to conclude that H_2O_2 plays a minimal role in the oxidation of Fe(II) under the experimental conditions investigated here.

3.3.5. Role of superoxide

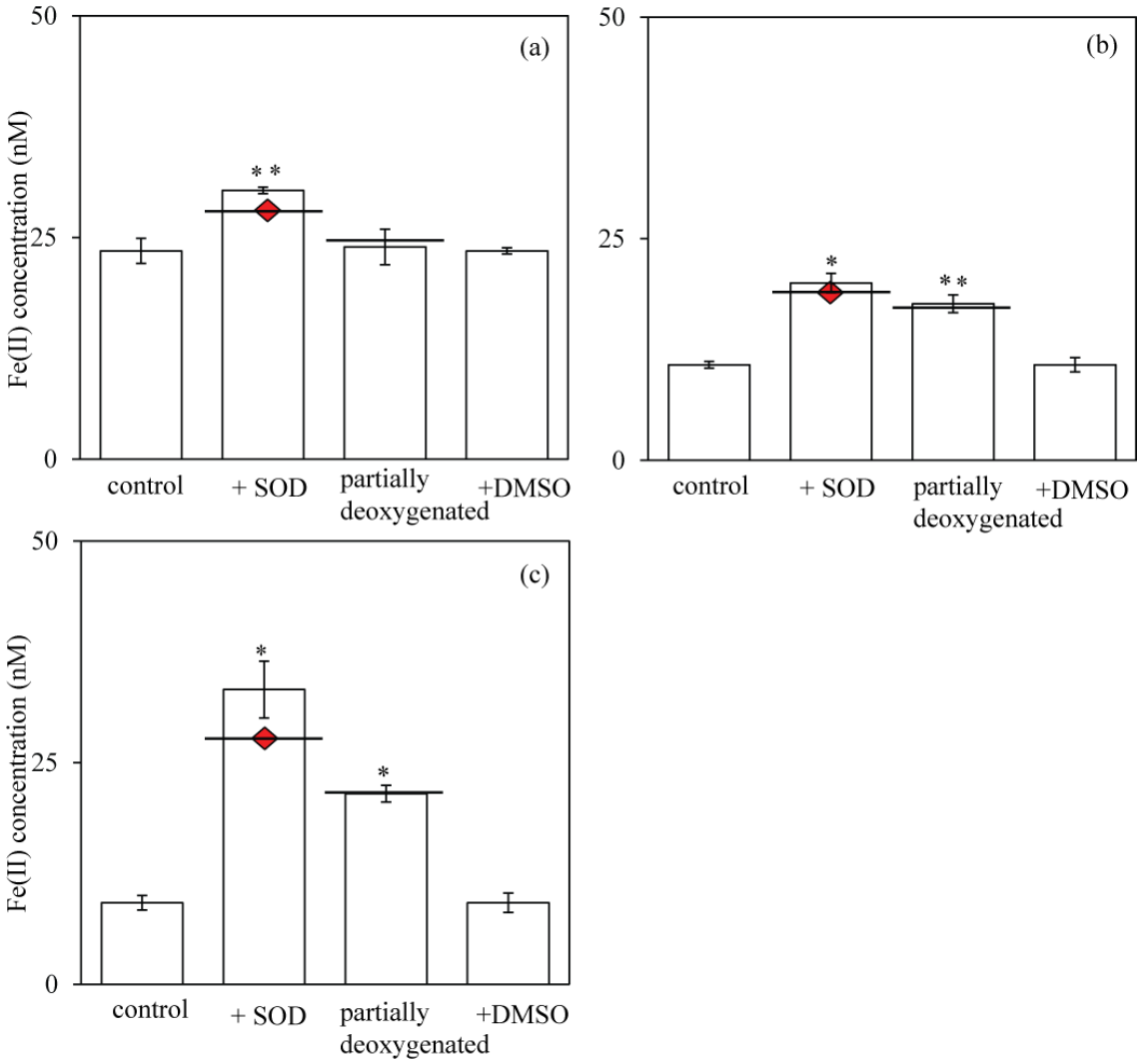

Figure 3.8: Effect of various treatments on Fe(II) concentration generated after 10 minutes on addition of 100 nM Fe(III) to solutions containing 5 $mg.L^{-1}$ SRFA that had been irradiated for 10 min prior to adding Fe(III) at (a) pH 3 (b) pH 3.5 and (c) pH 4. Error bars represent the standard deviation from triplicate experiments. Red diamond point shows the Fe(II) concentration generated for same initial Fe(III) and SRFA concentration in non-irradiated SRFA solutions. One asterisk shows that treatment was different than the control at 0.0001 significance level; two asterisk shows that treatment was different than the control at 0.0005 significance level.

As shown, addition of SOD, an enzyme which catalyzes decay of superoxide to H_2O_2 and O_2, caused a significant decrease in the rate of Fe(II) oxidation (Figure 3.7) as well as a marked increase in Fe(II) generation as a result of Fe(III) reduction (Figure 3.8) when added to previously irradiated SRFA solutions. The measured Fe(II) concentration (generated from Fe(III) reduction or remaining after Fe(II) oxidation) in the presence of SOD in previously irradiated SRFA solutions is the same as the measured Fe(II) concentration when Fe(III) or Fe(II) was added to non-irradiated SRFA solutions (shown by the red diamond point in the figure). This observation supports that superoxide is involved in oxidation of A^{2-} to A^{-} during irradiation. Addition of SOD catalyzes the decay of superoxide and hence prevents A^{-} generation as a result of A^{2-} oxidation by $HO_2^{\bullet}$ with the result that the Fe transformation rate is same as that observed in non-irradiated SRFA solutions.

3.3.6. Role of dioxygen

As shown above, superoxide played an important role in Fe redox transformations in both previously and continuously irradiated SRFA solutions with, according to the conceptual model, superoxide oxidizes A^{2-} to generate the Fe(II) oxidant (A^{-}). In order to further verify the role of superoxide, the rates of Fe(II) oxidation and Fe(III) reduction were measured when Fe(II) or Fe(III) were added to previously irradiated or continuously irradiated solutions of 5 $mg.L^{-1}$ SRFA that were partially deoxygenated prior to irradiation. Removal of dixoygen would be expected to result in a decrease in superoxide concentration since it is generated via dioxygen reduction. As shown, a decrease in O_2 concentration indeed resulted in a decrease in the Fe(II) oxidation rate at all pHs investigated in previously irradiated solutions (Figure 3.7), suggesting that O_2 is required for generation of the oxidant. Consistent with this observation, the concentration of Fe(II) generated on Fe(III) reduction increased in partially-

deoxygenated previously irradiated SRFA solutions (Figure 3.8) when compared to air-saturated solution, due to decreased generation of the Fe(II) oxidant in these solutions.

The effect of dioxygen removal was not significant at pH 3 in previously irradiated SRFA solutions ($p > 0.1$ using single tailed student's *t*-test) which suggests that either i) dioxygen is not involved in generation of the Fe(II) oxidant at this pH and/or ii) the Fe(II) oxidation rate at pH 3 in previously irradiated SRFA solutions is very slow. The second possibility is more consistent with the experimental data that shows similar Fe(II) generation rates at pH 3 in previously irradiated and non-irradiated SRFA solutions with these observations supporting the conclusion that very little of the long-lived Fe(II) oxidant is generated on SRFA irradiation at pH 3.

3.3.7. Kinetics and mechanism of Fe redox transformations

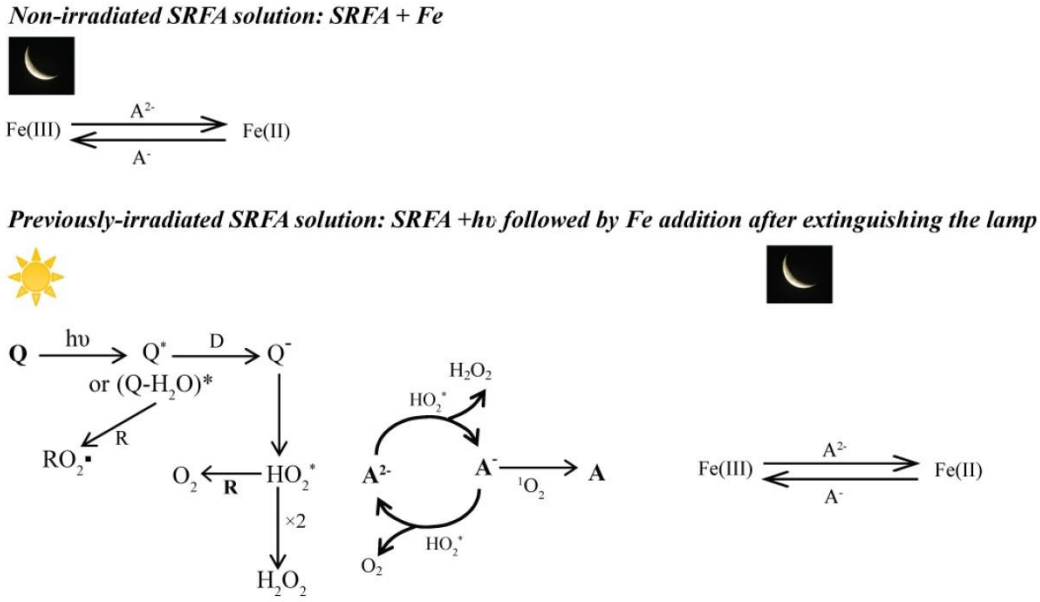

Figure 3.9: Reaction schemes showing Fe redox transformations in non-irradiated and previously irradiated SRFA solutions

The Fe redox transformation rates in non-irradiated and previously irradiated SRFA solutions in the pH range 3-5 can be explained based on reaction schematic shown in Figure 3.9 and is consistent with the mechanism proposed earlier at pH 4 (Garg et al.

2013a). A kinetic model is developed based on the mechanism presented with Table 3.3. Discussion on the kinetic model and determination of rate constants provided below.

Table 3.3: Kinetic model for generation of Fe(II) oxidant in non-irradiated and previously irradiated SRFA solutions.

No.	Reaction	Model Value	Published value	Reference
	Generation and Consumption of ROS ($^1O_2$, $HO_2^\bullet$, and H_2O_2 on irradiation)			
1	$SRFA + h\nu \longrightarrow SRFA^*$	Calculated		(Paul et al. 2004)
	$SRFA^* + {}^3O_2 \longrightarrow SRFA + {}^1O_2$	Φ~0.5%	Φ~0.5%	
2	$^1O_2 \xrightarrow{H_2O} {}^3O_2$	2.4×10^5 s^{-1}	2.4×10^5 s^{-1}	(Dalrymple et al. 2010)
3	$Q + h\nu \longrightarrow Q^-$	6×10^{-5} s^{-1a}	-	
4	$Q^- + {}^3O_2 \longrightarrow Q + HO_2^\bullet$	1×10^9 $M^{-1}s^{-1}$	1×10^9 $M^{-1}s^{-1}$	(Zhang et al. 2012)
5	$Q^- \longrightarrow Q$	5.8×10^3 s^{-1}	-	
6	$HO_2^\bullet + HO_2^\bullet \longrightarrow O_2 + H_2O_2$	$\frac{k_{HO_2^\bullet} + k_{O_2^{\bullet-}}\left(K_{HO_2^\bullet}/[H^+]\right)}{\left(1+\left(K_{HO_2^\bullet}/[H^+]\right)\right)^2}$ [b]	$\frac{k_{HO_2^\bullet} + k_{O_2^{\bullet-}}\left(K_{HO_2^\bullet}/[H^+]\right)}{\left(1+\left(K_{HO_2^\bullet}/[H^+]\right)\right)^2}$	(Bielski et al. 1985)
7	$R + h\nu \longrightarrow R^\bullet$	7.5×10^{-6} s^{-1c}	6×10^{-6} s^{-1}	(Garg et al. 2011b)

8	$R^{\bullet} + HO_2^{\bullet} \longrightarrow R^- + O_2 + H^+$	$\frac{k_1^{'} + k_2^{'}\left(K_{HO_2^{\bullet}}/[H^+]\right)}{\left(1+\left(K_{HO_2^{\bullet}}/[H^+]\right)\right)}$ [d]	-	
9	$R^{\bullet} + R^{\bullet} \longrightarrow R_2$	1×10^3 $M^{-1}s^{-1}$	1×10^3 $M^{-1}s^{-1}$	(Garg et al. 2011b)
	Transformation of hydroquinone-like and semiquinone-like moieties on irradiation			
10	$A^{2-} + HO_2^{\bullet} \xrightarrow{2H^+} A^- + H_2O_2$	k_{10}/k_{11}= -5.7 E_H^0 +2.5 [e]	~ 1×10^5 $M^{-1}s^{-1}$	(Roginsky and Barsukova 2000)
11	$A^- + HO_2^{\bullet} \longrightarrow A^{2-} + O_2$	2.5×10^5 $M^{-1}s^{-1}$	2.5×10^5 $M^{-1}s^{-1}$	(Garg et al. 2013a)
12	$A^- + {}^1O_2 \longrightarrow A + HO_2^{\bullet}$	1.5×10^8 $M^{-1}s^{-1}$	1.5×10^8 $M^{-1}s^{-1}$	(Garg et al. 2013a)
	Fe(II) oxidation and Fe(III) reduction reactions in the dark			
13	$Fe(III) + A^{2-} \longrightarrow Fe(II) + A^-$	3.5×10^3 $M^{-1}s^{-1}$ [f]	4×10^3 $M^{-1}s^{-1}$	(Garg et al. 2013a)
14	$Fe(II) + A^- \longrightarrow Fe(III) + A^{2-}$	$\frac{k_{HA} + k_{A^-}\left(K_{HA}/[H^+]\right)}{(1+K_{HA}/[H^+])}$ [g]	-	

[a] pseudo-first order rate constant based on $[Q]_T$ = 0.67 mmol.g^{-1} SRFA where Q represents electron accepting quinone moieties in humic and fulvic acids as reported earlier (Aeschbacher et al. 2010); varies slightly with pH

[b] See (Bielski et al. 1985) for definition of $k_{HO_2^{\bullet}}$ and $k_{O_2^{\bullet-}}$; $k_{HO_2^{\bullet}}$ = 8.3×10^5 $M^{-1}s^{-1}$, $k_{O_2^{\bullet-}}$ = 9.7×10^7 $M^{-1}s^{-1}$ and $K_{HO_2^{\bullet}}$ = $10^{-4.8}$

[c] pseudo-first order rate constant based on $[R]_T$ = 44 mmol.g^{-1} SRFA (Goldstone et al. 2002); R represents the bulk organic concentration in SRFA.

[d] See text for definition of $k_1^{'}$ and $k_2^{'}$; $k_1^{'}$ = 3.5×10^{4} $M^{-1}s^{-1}$, $k_2^{'}$ = 1.6×10^{5} $M^{-1}s^{-1}$ and $K_{HO_2^{\cdot}}$ = $10^{-4.8}$

[e] k_{10} and k_{11} in the range 1×10^{4} $M^{-1}s^{-1}$ - 1×10^{6} $M^{-1}s^{-1}$ will fit the data as long as the ratio k_{10}/k_{11} is as defined by E_H^0

[f] based on best-fit model results

[g] k_{14} was calculated using the ratio k_{13}/k_{14} shown earlier; k_{14} was then determined as function of $[H^+]$ assuming that variation in speciation of A^- changes k_{14} with pH; k_{HA} = 4.5×10^{3} $M^{-1}s^{-1}$, k_{A^-} = 1.5×10^{5} $M^{-1}s^{-1}$ and K_{HA} = 10^{-4}

3.3.7.1. Singlet oxygen generation and relaxation to triplet state

$^1O_2$ generation occurs on interaction of photo-excited SRFA with dioxygen (reaction 1; Table 3.3) and rapidly reaches steady-state due to relaxation to the triplet state of oxygen (reaction 2; Table 3.3). The rate constant for both of these reactions are as reported earlier (Paul et al. 2004; Dalrymple et al. 2010) and are not well constrained by the experimental data.

3.3.7.2. Superoxide formation during irradiation

Photoexcitation of quinone moieties (Q) followed by electron transfer from electron donor D results in formation of the O_2-reducing radical Q^-. The reaction shown in reaction 3 (Table 3.3) is an apparent reaction incorporating excitation of Q, relaxation of the excited molecule back to ground state, and reduction of the excited state by electron donor. The apparent rate constant for generation of Q^- was determined based on best-fit to the H_2O_2 generation data (Figure 3.6) assuming that the initial concentration of Q is identical to the reported electron accepting capacity (0.67 mmol.g^{-1} SRFA) of quinone moieties in humic and fulvic acids (Aeschbacher et al. 2010). The initial concentration of Q is not well constrained by the experimental data, with a similar fit obtained using varying concentrations with suitable adjustment of the rate constant for the reaction shown in reaction 3 (Table 3.3). The rate constant reported by Zhang and co-workers (2012) for the reaction shown in reaction 4 (Table 3.3) was used. The reaction shown in reaction 5 (Table 3.3) represents relaxation of Q^- to form a non-reactive product (NRP) with the rate constant for this reaction determined using the measured effect of dioxygen removal on H_2O_2 formation rate as described by Zhang and co-workers (2012). The H_2O_2 formation rate decreased by ~ 30% after 95% removal of dioxygen, which yields a ratio of 1.7×10^5 M for the rate constants for the reactions shown in reaction 4

and 5 (Table 3.3). Using the reported rate constant of 1×10^9 $M^{-1}.s^{-1}$ for the reaction shown in reaction 4, a value of 5.8×10^3 s^{-1} for the rate constant of reaction 5 (Table 3.3) can be obtained; however some uncertainty in this value (± 20%) should be recognized due to the difficulty in accurately measuring the dioxygen concentration.

3.3.7.3. Uncatalyzed disproportionation of superoxide

Superoxide undergoes uncatalyzed disproportionation to form H_2O_2 and O_2 (reaction 6; Table 3.3). The rate constant for this reaction reported by Bielski et al. (1985) was used here. In the pH range examined, superoxide exists in both the anionic form, $O_2^{\bullet -}$, and as the hydroperoxyl radical ($HO_2^{\bullet}$; pK_a ~ 4.8) with the proportion of each of these particular species present dependent on pH. As the reactivity of superoxide and the hydroperoxyl radical differ, the uncatalyzed disproportionation rate varies with pH with the uncatalyzed disproportionation rate constant described by the following equation:

$$k_{disp} = \alpha_0 \alpha_0 k_{HO_2^{\bullet}} + \alpha_0 \alpha_1 k_{O_2^{\bullet -}} \qquad (3.10)$$

where $\alpha_0 = \frac{[H^+]}{[H^+] + K_{HO_2^{\bullet}}}$, $\alpha_1 = 1 - \alpha_0$, $k_{HO_2^{\bullet}}$ = 8.3 × 10^5 $M^{-1}s^{-1}$, $k_{O_2^{\bullet -}}$ = 9.7 × 10^7 $M^{-1}s^{-1}$ and $K_{HO_2^{\bullet}}$ = $10^{-4.8}$.

3.3.7.4. Oxidative superoxide sink

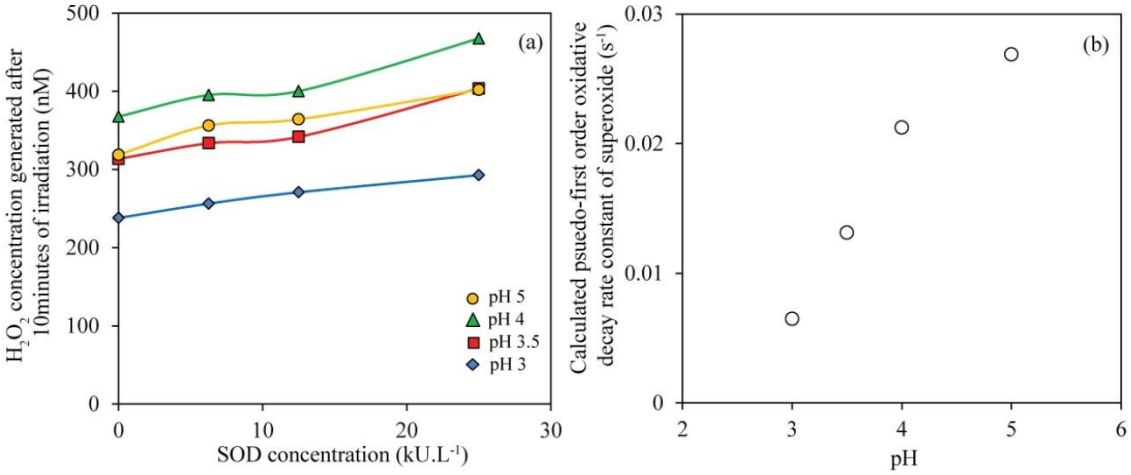

Figure 3.10: (a) Effect of SOD addition on concentration of H_2O_2 generated on irradiation of 10 mg.L^{-1} SRFA (b) Calculated pseudo-first order oxidative decay rate constant of superoxide based on the data shown in (a)

During irradiation, a substantial amount of $HO_2^{\bullet}$ decays via an oxidative pathway, as demonstrated by the increase in H_2O_2 production rates on addition of SOD (see Figure 3.10). As described earlier (Garg et al. 2011b), this occurs due to interaction of $HO_2^{\bullet}$ with organic radicals (depicted as $R^{\bullet}$) generated on irradiation of SRFA (reaction 8; Table 3.3). As shown in Figure 3.10, the contribution of this oxidative sink to superoxide decay increases with increase in pH thereby suggesting that the rate constant for the reaction of superoxide with $R^{\bullet}$ increases with increase in pH. The pH-dependence of the rate constant for oxidative decay of $HO_2^{\bullet}$ (reaction 8; Table 3.3) was modelled by variation in the speciation of superoxide by assuming that $O_2^{\bullet-}$ is more reactive than $HO_2^{\bullet}$ with the overall rate constant given by following equation:

$$k_{app} = \alpha_0 k_1^{'} + \alpha_1 k_2^{'} \qquad (3.11)$$

where k_{app} represents the overall rate constant for oxidation of superoxide by $R^{\bullet}$; $k_1^{'}$ = 3.5×10^4 $M^{-1}s^{-1}$ is the rate constant for oxidation of $HO_2^{\bullet}$ by $R^{\bullet}$, $k_2^{'}$ = 1.6×10^5 $M^{-1}s^{-1}$ is the rate constant for oxidation of $O_2^{\bullet-}$ by $R^{\bullet}$; $\alpha_0 = \frac{[H^+]}{[H^+]+K_{HO_2^{\bullet}}}$, and $K_{HO_2^{\bullet}}$ = $10^{-4.8}$.

The rate constant for generation rate of the radical $R^{\bullet}$ (reaction 7; Table 3.3) and its bimolecular decay rate constant (reaction 9; Table 3.3) was assumed to be pH-independent with values reported in the earlier work (Garg et al. 2011b) used here.

3.3.7.5. Stable Fe(II) oxidant generation

As discussed, superoxide oxidizes the reduced organic entity A^{2-} to form A^- (reaction 10; Table 3.3) which can undergo reaction with $HO_2^{\bullet}$ (reaction 11; Table 3.3) catalyzing its disproportionation in the dark; additionally, A^- can be oxidized by $^1O_2$ (reaction 12; Table 3.3). The concentration of A^- formed increased with increase in pH (see Table 3.2). Increased formation of A^- is consistent with the variation in redox potential of the A^-/A^{2-} couple which decreases with increase in pH (see Figure 3.3). The concentration of A^- generated as function of time can be derived as following:

The rate law for generation of A^- is given by:

$$\frac{d[A^-]}{dt} = k_{10}[A^{2-}][O_2^-] - k_{11}[A^-][O_2^-] \quad (3.12)$$

where k_{10} and k_{11} represents the rate constant for reactions 10 and 11 shown in Table 3.3 respectively.

$$\frac{d[A^-]}{dt} = k_{10}([A_0]-[A^-])[O_2^-] - k_{11}[A^-][O_2^-] \quad (3.13)$$

where A_0 represents the total initial concentration of A^{2-}.

Assuming superoxide reaches steady-state due to other reactions quickly such that

$$\frac{d[A^-]}{dt} = k_{10}[A_0 - A^-][O_2^-]_{ss} - k_{11}[A^-][O_2^-]_{ss} \quad (3.14)$$

Solving this rate law we get,

$$\left[A^-\right] = \frac{k_{10}A_0}{k_{10}+k_{11}}\left(1 - e^{-(k_6+k_7)[O_2^-]_{ss}t}\right) \quad (3.15)$$

and $\left[A^-\right]_{ss} = \frac{k_{10}A_0}{k_{10}+k_{11}}$ (3.16)

Thus, the concentration of A^- generated varies with the rate constant ratio k_{10}/k_{11}. Since the concentration of A^- generated varies with pH (see Table 3.2), k_{10}/k_{11} would also be expected to vary with pH. This variation in the value of the ratio of the rate constants with pH can be due to changes in either (i) superoxide reactivity or (ii) E_H of the A^-/A^{2-} redox couple with pH (Figure 3.3). The rate constant for reaction 10 (Table 3.3) was determined based on best-fit to the calculated A^- concentration after 10 minutes of SRFA photolysis (Table 3.2) and is very well correlated with the E_H of the A^-/A^{2-} redox couple. The rate constant for reaction 11 (Table 3.3) was assumed to be independent of pH and equal to 2.5×10^5 $M^{-1}s^{-1}$ as reported earlier at pH 4 (Garg et al. 2013a). The rate constant for reaction 12 (Table 3.3) was used as reported earlier with the determined value based on the measured effect of $^1O_2$ concentration on A^- generation (Garg et al. 2013a) and hence is well constrained by the experimental data.

The total initial concentration of A^{2-} was used as calculated using eq.3.2 based on the measured steady-state concentration of Fe(II) generated on Fe(III) reduction in SRFA solutions in the dark (Table 3.1).

3.3.7.6. Fe redox transformations in the dark and previously irradiated SRFA solutions

As shown in Table 3.1, the ratio of the rate constants for reduction of Fe(III) by hydroquinone-like moieties (k_1) and oxidation of Fe(II) by semiquinone-like moieties (k_2) in non- irradiated SRFA increases with increase in pH. The variation in the ratio k_1/k_2 with pH possibly occurs due to variation in Fe(III) or hydroquinone-semiquinone-like moieties speciation and/or due to variation in E_H of the A^-/A^{2-} redox couple. Since, E_H decreases with increase in pH, we expect that the rate of reduction of Fe(III) should increase and/or rate of Fe(II) oxidation decrease with increase in pH which is not in agreement with the experimental observations here. This suggests that speciation plays an important role in controlling the kinetics of Fe redox transformations. At the low pH and low Fe concentrations employed here, Fe(III) is expected to exist as an Fe(III)-SRFA complex with A^{2-} present mostly in protonated form (i.e. H_2A; $pK_{a1} \sim 10$ and $pK_{a2} \sim 12$ for hydroquinone). Although the deprotonated form of hydroquinone is more kinetically active than H_2A (Yuan et al. 2013), the concentration of these deprotonated forms at these acidic pH would appear to be too small (at least 6 fold less than H_2A) to contribute to the kinetics of hydroquinone-mediated Fe(III) reduction. Although some pH-dependence in Fe(III)-SRFA speciation may occur at low pH (as is evident for Fe complexes with synthetic ligands such as EDTA), little information on this possibility is available from the literature; as such, Fe(III)-SRFA speciation is assumed to be invariant with pH and, as a result, the rate constant for the reduction of Fe(III) by the hydroquinone (reaction 13; Table 3.3) considered to be pH-independent. This assumption is further supported by the observation that the initial Fe(III) reduction rate under non-irradiated conditions is similar at the various pH considered here. The speciation of Fe(II), which is expected to be present in mostly inorganic form, would

not be expected to change over the pH range investigated. Hence, it appears that the speciation of A^- ($pK_a \sim 4$ for semiquinone) is important in controlling the oxidation rate of Fe(II). Since the rate of oxidation increases with increase in pH, we further suggest that A^- oxidizes Fe(II) faster than HA. The oxidation rate constant of Fe(II) by semiquinone-like moieties (reaction 14; Table 3.3) was modelled according to the following equation:

$$k_2 = \alpha_0 k_{HA} + \alpha_1 k_{A^-} \quad (3.17)$$

where k_{HA} and k_{A^-} represents the rate constants for oxidation of Fe(II) by HA and A^- respectively; $\alpha_0 = \frac{[H^+]}{[H^+] + K_{HA}}$ and $\alpha_1 = 1 - \alpha_0$; $k_{HA} = 4.5 \times 10^3$ $M^{-1}s^{-1}$, $k_{A^-} = 1.5 \times 10^5$ $M^{-1}s^{-1}$ and $K_{HA} = 10^{-4}$.

3.4. Conclusions

In this chapter, Fe redox transformation rates in non-irradiated and previously irradiated SRFA solutions are investigated in the pH range 3-5. Consistent with the previous study at pH 4 (Garg et al. 2013a), quinone moieties present in SRFA are responsible for the Fe redox transformations in the pH range 3-5. In particular, the following key conclusions may be drawn.

(1) Under dark conditions, hydroquinone groups intrinsically present in the natural organic material (SRFA) investigated here induce the reduction of Fe(III) to Fe(II) species. The resultant semiquinone groups formed in this initial redox process are capable of re-oxidizing Fe(II) to Fe(III) such that a dynamic equilibrium between hydroquinone/semiquinone and Fe(III)/Fe(II) redox pairs is established. Results reported here indicate that the hydroquinone/semiquinone redox pairs exhibit the same

standard reduction potential (E_H^0 ~ 0.60 V) at each pH considered (3, 3.5 and 4) with this redox pair reasonably represented as:

$$HA + H^+ + e^- \rightleftharpoons H_2A \qquad E_H^0 = 0.60\ V \tag{3.18}$$

(2) Photolysis of this natural organic matter results in generation of superoxide which, in turn, induces oxidation of hydroquinone moieties present to semiquinone moieties that appear to be long-lived in the dark and in the absence of one-electron reductants. These relatively stable semiquinone moieties are effective oxidants of Fe(II) with added Fe(II) rapidly oxidized to Fe(III). The concentration of semiquinone moieties formed on photolysis increases with increase in pH with the altered proportion of hydroquinone and semiquinone moieties on photolysis effectively resulting in an increase in standard reduction potential for SRFA from 0.30 V under dark conditions to 0.33 V following 10 minutes of photolysis at pH 4. The pH-dependence of this redox pair under irradiated conditions is the same as that observed under dark conditions with the E_H value decreasing with increase in pH.

Overall, the work in this chapter extends the current knowledge of Fe redox transformations to a wider pH range, and the mechanism and important species are found to be consistent in acidic pH. The findings in non-irradiated and previously irradiated conditions here provide an important basis for the investigation of Fe redox transformations under continuously irradiated conditions, which will be specially focused on in Chapter 5.

Chapter 4. Hydroquinone-mediated redox cycling of iron and concomitant oxidation of hydroquinone in oxic waters under acidic conditions: comparison with iron-natural organic matter interactions

4.1. Introduction

The redox properties of natural organic matter (NOM) have been associated with quinone moieties with the presence of these moieties in NOM confirmed by NMR (Thorn et al. 1992), fluorescence spectroscopy (Cory and McKnight 2005; Fimmen et al. 2007), and electrochemical methods (Aeschbacher et al. 2010). These quinone moieties are implicated in a wide-range of redox active processes including generation of reactive oxygen species (ROS) (Garg et al. 2011b), degradation of organic contaminants and, potentially, mediating redox transformations of metals such as iron (Uchimiya and Stone 2006) and copper (Yuan et al. 2013).

As discussed in Chapter 3, hydroquinone-like moieties in SRFA are shown to be an important Fe(III) reductant in the pH range 3-5. In this chapter, we investigate the kinetics and mechanism of iron redox transformations in pure hydroquinone solution in the pH range 3-5 in air-saturated and partially-deoxygenated solution with the goal of identifying the similarities and differences between this simple quinone and the quinone moieties present in SRFA. Despite the similarities that might be expected between the redox behavior of pure quinones and SRFA, major differences are also likely. For example, SRFA consists of an extended network of potentially conjugated aromatic structures leading to the possibility of stabilization of radicals (Senesi 1990a, 1990b). Such an effect will not occur with a simple hydroquinone. Furthermore, in the hydroquinone solution, iron will be present in inorganic form while in SRFA solutions, iron (especially Fe(III)) will be complexed by SRFA. The effect of these differences in SRFA and hydroquinone properties on Fe redox transformations is discussed within the context of the experimental results obtained here. Although there are many different hydroquinones, we focus here on the simplest, 1,4-hydroquinone (pK_{a1} = 10.2; pK_{a2} = 12.0) and its oxidized forms (semiquinone radical (pK_a = 4.1) and 1,4-benzoquinone)

because no direct binding of iron by this organic compound is expected. Note that 1,4 hydroquinone is not a representative of quinones in general but is being used as an example of a simple quinone. Under acidic conditions, oxygenation of both Fe(II) and hydroquinone are expected to be negligible; as such, it is possible to investigate the Fe(III)-mediated oxidation of hydroquinone as well as hydroquinone-mediated Fe(III) redox transformations.

4.2. Experimental methods

Detailed description of reagents and experimental setup is provided in Chapter 2.

4.3. Results and discussion

4.3.1. Fe(II) generation on Fe(III) reduction by hydroquinone

When Fe(III) was added to air-saturated hydroquinone solution at pH 4, the Fe(II) concentration increased as a result of Fe(III) reduction by hydroquinone (Figure 4.1a). The Fe(II) concentration increased rapidly initially, however the Fe(II) generation rate slowed down over time. Because the generation rate of Fe(II) decreases over time with the Fe(II) concentration approaching steady-state (especially at higher concentrations of H_2Q), it appears that back-oxidation of Fe(II), formed as a result of Fe(III) reduction, also occurs. Because negligible Fe(II) oxidation occurs by reaction with dioxygen at pH 4 (at least over the time scale of interest; see Figure 4.2), this observation further suggests that one or more of the quinone moieties (presumably semiquinone or benzoquinone) are able to oxidize Fe(II). Because no Fe(II) oxidation is observed in solutions containing benzoquinone at concentrations comparable to those used and/or measured here (data not shown), the Fe(II) oxidant is most likely the semiquinone radical ($Q^{\bullet -}$) which is formed as a result of oxidation of hydroquinone by Fe(III) (eq.4.1).

$$H_2Q + Fe(III) \underset{k_{-1}}{\overset{k_1}{\rightleftharpoons}} Q^{\bullet -} + Fe(II) \qquad (4.1)$$

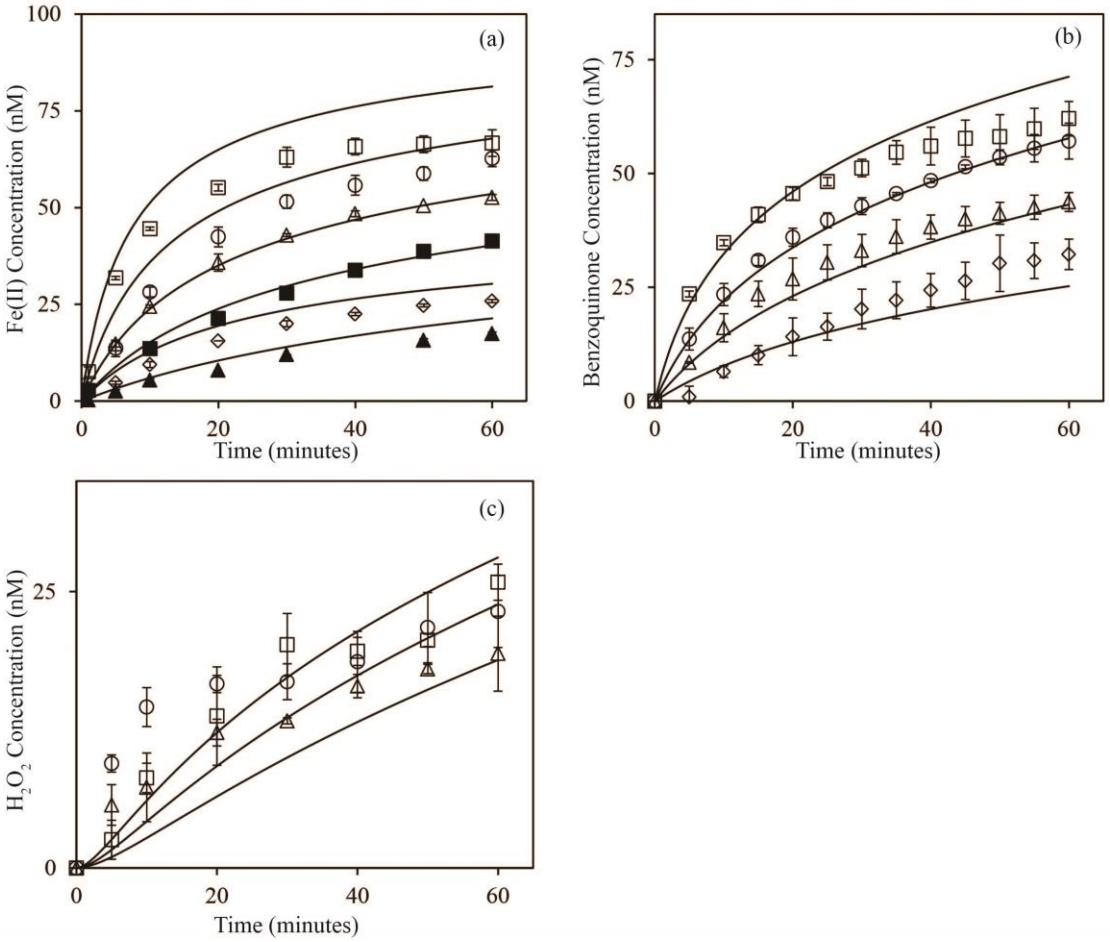

Figure 4.1: (a) Generation of Fe(II) as a result of reduction of 100nM Fe(III) in air-saturated solution containing 100 nM (closed triangles), 250 nM (closed squares), 500 nM (open triangles), 1 µM (open circles), and 2 µM (open squares) hydroquinone. Open diamonds show Fe(II) generated on reduction of 50nM Fe(III) by 500 nM hydroquinone in air-saturated solution at pH 4. (b) Generation of benzoquinone as a result of reduction of Fe(III) in air-saturated pH 4 solution containing 500 nM (triangles), 1 µM (circles), and 2 µM (squares) hydroquinone with 100nM Fe(III), and 50 nM Fe(III) with 500 nM hydroquinone (diamonds) at pH 4. (c) Generation of H_2O_2 in air-saturated pH 4 solution containing 500 nM (triangles), 1 µM (circles) and 2 µM (squares) hydroquinone and 100 nM Fe(III). Symbols are experimental data (average of duplicate measurements); lines are model predicted values.

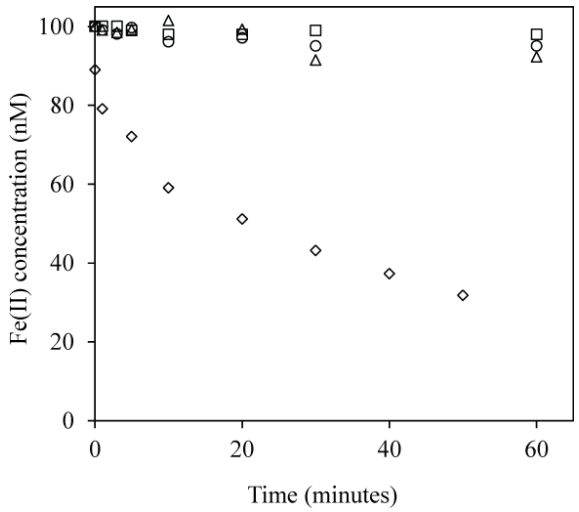

Figure 4.2: Fe(II) decay in the dark at pH 3 (circles) , 4 (squares), 4.5 (triangles), 5 (diamonds) in air-saturated solution. Data represents average of duplicate measurements.

4.3.2. Benzoquinone formation on Fe(III) reduction by hydroquinone

As shown in Figure 4.1b, the concentration of benzoquinone increased over time in air-saturated solutions containing Fe(III) and H_2Q at pH 4. An increase in Fe(III) concentration results in an increase in the concentration of Q generated, suggesting that benzoquinone formation is due to the presence of Fe(III). No benzoquinone generation is observed in hydroquinone solution in the absence of Fe(III) (data not shown), in accord with the recognition that autoxidation of H_2Q is spin-restricted and very slow under acidic conditions (Roginsky and Barsukova 2000). The presence of Fe(III) overcomes the spin restriction and catalyzes the oxidation of H_2Q as shown in previous studies on the trace-metal-mediated oxidation of hydroquinone (Miller et al. 1990; Uchimiya and Stone 2006; Yuan et al. 2013). Although nearly complete oxidation of H_2Q was observed in presence of Cu(II) under circumneutral pH condition (Yuan et al. 2013), only a small fraction of H_2Q was oxidized under acidic conditions investigated here, which is consistent with the rate law for the metal-catalyzed oxidation of hydroquinone being proportional to $[H^+]^{-1}$, indicating that, rather than the protonated

form H_2Q, the monoanion HQ^- is the important species in this redox reaction (Song and Buettner 2010).

Table 4.1: Concentration of Fe(II), benzoquinone, and H_2O_2 formed in air-saturated solution containing H_2Q and Fe(III) after 60 minutes

	Initial concentration		Concentration at 60 minutes		
pH	HQ (nM)	Fe(III) (nM)	Fe(II) (nM)	Benzoquinone (nM)	H_2O_2 (nM)
3	500	50	29.1±6.2	27.8±3.0	n.d.*
	500	100	56.5±11.6	27.4±3.7	13.0±1.1
	1000	100	71.8±0.8	48.8±0.6	17.7±2.0
	2000	100	83.2±2.1	67.4±0	n.d.*
4	500	50	25.8±0.4	35.2±3.3	n.d.*
	500	100	52.6±0.7	43.7±2.1	19.4±3.4
	1000	100	62.7±2.1	57.1±3.9	23.2±3.3
	2000	100	66.7±3.4	62.1±3.8	25.9±1.6
4.5	500	50	17.1±2.6	25.0±0	n.d.*
	500	100	38.1±2.9	44.2±1.2	22.4±1.1
	1000	100	50.8±3.1	51.7±0.5	25.1±2.4
	2000	100	52.8±1.6	59.4±5.1	n.d.*
5	500	50	7.03±1.5	19.1±2.5	n.d.*
	500	100	26.9±1.2	33.2±5.2	28.0±4.4
	1000	100	25.9±1.9	52.1±12.9	44.0±2.4
	2000	100	41.3±0.4	54.1±5.4	n.d.*

The stoichiometry of Q formation to Fe(II) formation at pH 4 is approximately 1:1 (see Table 4.1), which suggests that either (i) there exists additional oxidant of $Q^{\bullet-}$ apart from Fe(III) (eq.4.2) or $Q^{\bullet-}$ via disproportionation reaction (eq.4.3) or (ii) there are additional sink(s) of Fe(II) apart from $Q^{\bullet-}$ and Q (as indicated in eq.4.1 and 4.2). Given that no oxidation of Fe(II) was observed by dioxygen (which is the only expected sink of Fe(II) apart from quinone species in our experimental matrix), this suggests that Q formation occur via reaction sequence, whereby $Q^{\bullet-}$ formed in the reaction shown in eq.4.1 is oxidized by dioxygen to form Q (eq.4.4). This mechanism of Q formation is further supported by the observation that partial deoxygenation (~ 90%) of the solution results in complete inhibition of Q generation (Figure 4.3).

$$Q^{\bullet-} + Fe(III) \underset{k_{-2}}{\overset{k_2}{\rightleftharpoons}} Fe(II) + Q \tag{4.2}$$

$$Q^{\bullet-} + Q^{\bullet-} + 2H^+ \underset{k_{-3}}{\overset{k_3}{\rightleftharpoons}} Q + H_2Q \tag{4.3}$$

$$Q^{\bullet-} + O_2 \underset{k_{-4}}{\overset{k_4}{\rightleftharpoons}} Q + HO_2^{\bullet} \tag{4.4}$$

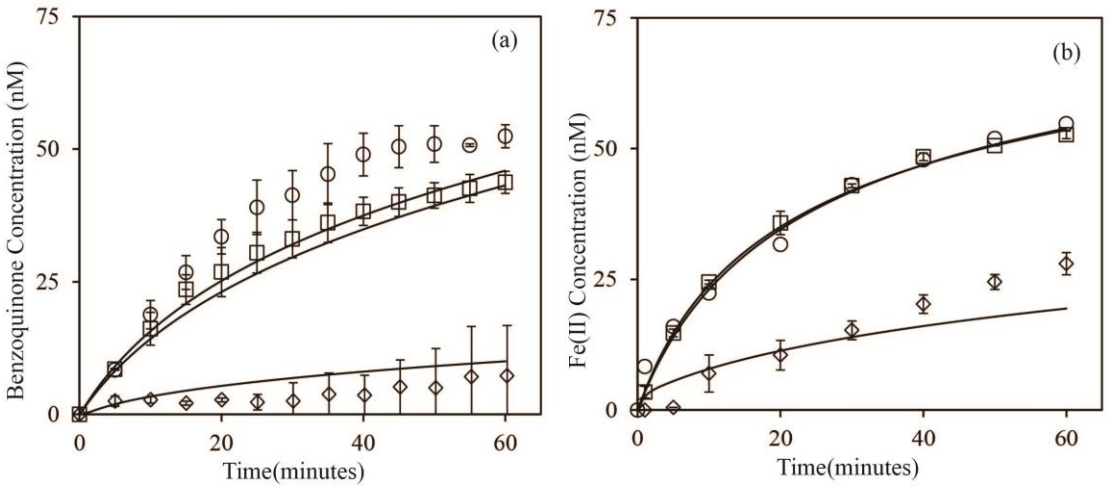

Figure 4.3: (a) Generation of benzoquinone in solutions containing 100 nM Fe(III) and 500 nM hydroquinone in air-saturated solution (squares), partially deoxygenated solution (diamonds) and in air-saturated solution containing 25 $kU.L^{-1}$ SOD (circles) at pH 4. (b) Generation of Fe(II) in solutions containing 100 nM Fe(III) and 500 nM

hydroquinone in air-saturated solution (squares), partially deoxygenated solution (diamonds) and in air-saturated solution containing 25 $kU.L^{-1}$ SOD (circles) at pH 4. Symbols are experimental data (average of duplicate measurements); lines are model predicted values.

A lack of Q generation in partially-deoxygenated solution further supports that Q formation via $Q^{\bullet-}$ oxidation by Fe(III) (eq.4.2) or $Q^{\bullet-}$ disproportionation (eq.4.3) is negligible at least over the time scale, concentration, and pH of our experiments. Although, oxidation of $Q^{\bullet-}$ by Fe(III) is reported to occur under circumneutral pH conditions (Yamazaki and Ohnishi 1966), it may not occur at comparable rates under acidic conditions, given that the redox potential of the $Q^{\bullet-} / H_2Q$ redox couple and the $Q / Q^{\bullet-}$ redox couple increases with decrease in pH (see Figure 4.4), making $Q^{\bullet-}$ a better oxidant than reductant at lower pHs. The disproportionation of semiquinone radicals is most likely unimportant as a result of both the limited generation of $Q^{\bullet-}$ and its rapid removal by dioxygen and Fe(II).

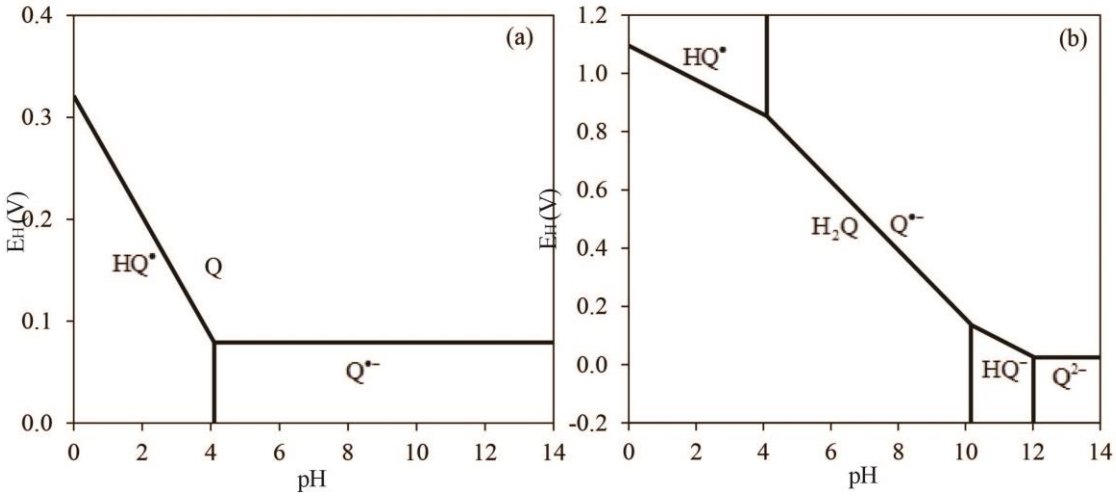

Figure 4.4: E_H-pH diagram for (a) quinone/semiquinone redox couple and (b) semiquinone/hydroquinone redox couple.

Direct two electron oxidation of H_2Q by Fe(III) resulting in formation of Q is also expected to be negligible because the formation of Q by such a pathway should be

dioxygen independent and should result in Fe(II) and Q formation in 2:1 stoichiometry, neither of which are consistent with our observation.

4.3.3. Generation of H_2O_2 on Fe(III) reduction by hydroquinone

As shown in Figure 4.1c, H_2O_2 is generated on addition of Fe(III) to air-saturated H_2Q solutions at pH 4 with the concentration of H_2O_2 generated increasing slightly with an increase in H_2Q concentration. H_2O_2 generation in these solutions occurs due to disproportionation of the superoxide (eq.4.5) formed upon the oxidation of $Q^{\bullet-}$ by O_2 (eq.4.4). Because the stoichiometry of Q to H_2O_2 generation is slightly less than 2:1 (Table 4.1), it appears that a small amount of $HO_2^{\bullet}$ decays via a pathway that does not result in H_2O_2 production. While the nature of this loss pathway is not clear from our experimental results, possibilities include reduction of semiquinone (eq.4.6), Fe(III) (eq.4.7), or benzoquinone (eq.4.4) by superoxide.

$$HO_2^{\bullet} + HO_2^{\bullet} \xrightarrow{k_{disp}} O_2 + H_2O_2 \tag{4.5}$$

$$Q^{\bullet-} + HO_2^{\bullet} \xrightarrow{H^+} H_2Q + O_2 \tag{4.6}$$

$$Fe(III) + HO_2^{\bullet} \underset{k_{-7}}{\overset{k_7}{\rightleftharpoons}} Fe(II) + O_2 \tag{4.7}$$

4.3.4. Role of dioxygen

Both Fe(II) and Q formation during H_2Q oxidation by Fe(III) at pH 4 is significantly ($p < 0.001$ using single-tailed students *t*-test) reduced in partially-deoxygenated (~ 90%) solutions (Figure 4.3). This effect of dioxygen removal on Q formation provides confirmation that Q is indeed formed via the oxygenation of $Q^{\bullet-}$, and the decrease in rate and extent of Fe(II) formation presumably arises as a result of an increase in steady-state concentration of $Q^{\bullet-}$ and concomitant increase in the rate of Fe(II) oxidation by

$Q^{\bullet-}$ upon decrease in dioxygen concentration. The overall effect of removal of dioxygen is more pronounced on Q than Fe(II) formation, with the stoichiometric generation of Fe(II) to benzoquinone generation increasing from 1:1 in air-saturated solution to ~ 4:1 in partially-deoxygenated solution. No H_2O_2 generation was observed in partially deoxygenated solution (data not shown) supporting the conclusion that H_2O_2 formation occurs principally via dioxygen reduction through the formation of superoxide.

4.3.5. Role of superoxide

The role of superoxide in Fe(II) and Q generation was examined by adding SOD, which catalyzes the disproportion of superoxide to O_2 and H_2O_2. As shown in Figure 4.3, SOD has no significant effect (p > 0.1 using single-tailed students t-test) on either Fe(II) generation or Q generation in air-saturated solution at pH 4, indicating that superoxide-mediated H_2Q oxidation (Roginsky and Barsukova 2000) and superoxide-mediated Fe redox transformations (Rush and Bielski 1985) are unimportant under acidic conditions. The latter result is in contrast with the findings of earlier work, in which inorganic Fe(III) reduction and Fe(II) oxidation by superoxide occurred rapidly under acidic conditions (Rush and Bielski 1985). As confirmed later, the lack of effect of SOD addition on Fe(II) generation observed here is due to the fact that the forward Fe(III) reduction by $HO_2^{\bullet}$ (eq.4.7) balances the backward Fe(II) oxidation by $HO_2^{\bullet}$ (eq.4.8), thereby resulting in zero-net Fe(II) generation by $HO_2^{\bullet}$ but catalytic disproportionation of $HO_2^{\bullet}$. We will also show that even though $HO_2^{\bullet}$ can reduce $Q^{\bullet-}$ and Q, these are important reactions with respect to the fate of $HO_2^{\bullet}$, but they play a minor role in controlling fate of $Q^{\bullet-}$ and Q with the result that SOD addition has minimal effect on Q generation.

$$Fe(II) + HO_2^{\bullet} \xrightarrow{H^+} Fe(III) + H_2O_2 \qquad (4.8)$$

4.3.6. Effect of pH

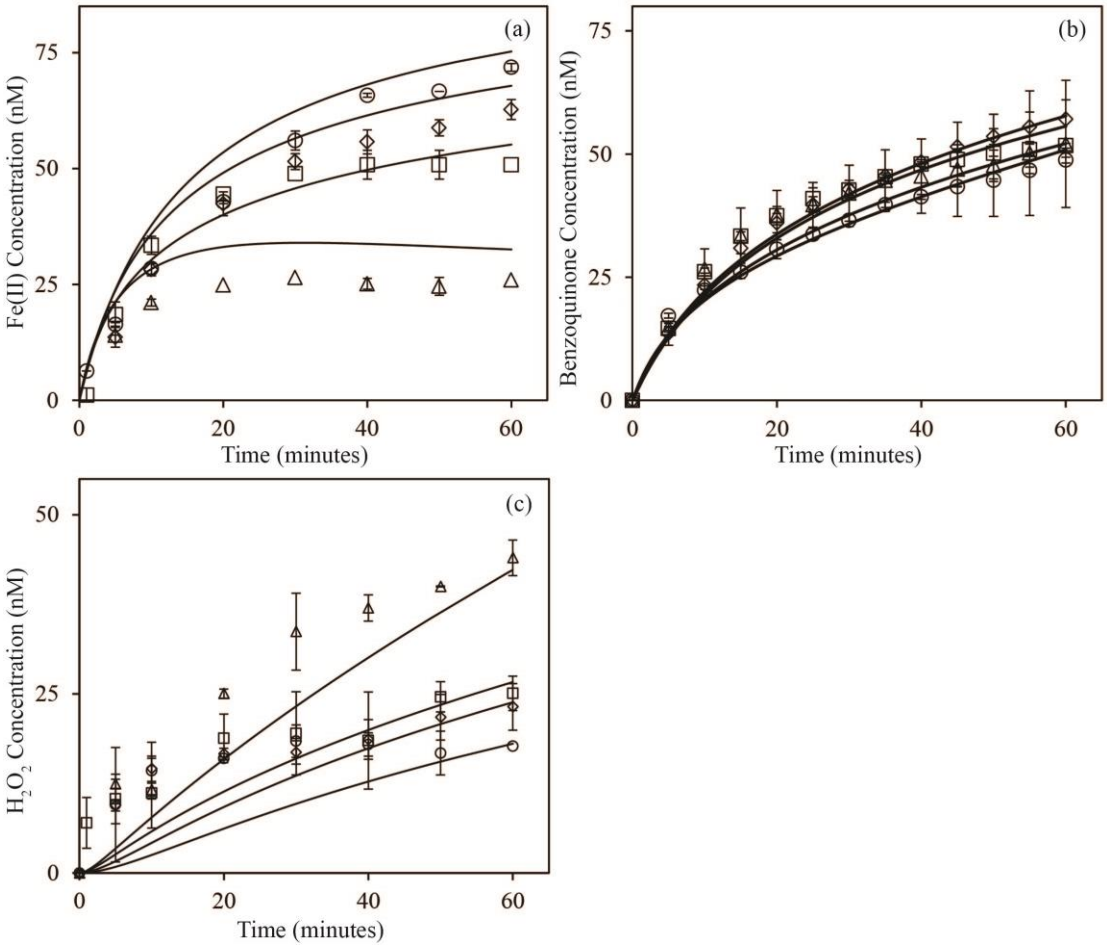

Figure 4.5: Generation of (a) Fe(II), (b) benzoquinone, and (c) H_2O_2 as a result of 100 nM Fe(III) reduction at pH 3 (circles), pH 4 (diamonds), pH 4.5 (squares), and pH 5 (triangles) in presence of 1 µM hydroquinone solution in air-saturated solution. Symbols are experimental data (average of duplicate measurements); lines are model predicted values.

As shown in Figure 4.5a, an increase in pH results in a decrease in the concentration of Fe(II) generated on Fe(III) reduction by H_2Q, with Fe(II) concentration generated after 60 minutes being two fold higher at pH 4 than at pH 5. This suggests that the Fe(III) reduction rate decreases and Fe(II) oxidation rate increases with an increase in pH. Benzoquinone generation decreases slightly with increase in pH (Figure 4.5b) which is consistent with the observed effect of pH on Fe(II) generation (Figure 4.5a). With an

increase in pH, the overall extent of Fe(II) and $Q^{\bullet-}$ generation via the reactions shown in eq.4.1 decreases, which further results in decreased Q generation via oxidation of $Q^{\bullet-}$. H_2O_2 generation increases slightly with increase in pH in the pH range 3-5; however the difference in H_2O_2 generation rate at pH 4 and 5 is not significant ($p > 0.1$ using single-tailed students *t*-test; Figure 4.5c).

The stoichiometry for Fe(II) to Q generation is slightly higher than 1:1, and the stoichiometry for Q to H_2O_2 generation is slightly less than 2:1 at pH 3 (see Table 4.1), which is similar to that observed at pH 4. The stoichiometry for Fe(II) to Q generation is approximately 1:1, and the stoichiometry for Q to H_2O_2 generation is slightly less than 2:1 at pH 4.5 (Table 4.1), which is the same as that observed at pH 4. The same effect of dioxygen removal and SOD addition on Fe(II) and Q generation is observed at pH 3, 4 and 4.5 (Figure 4.6 and Figure 4.7), thereby supporting the conclusion that same reactions occur at these pHs.

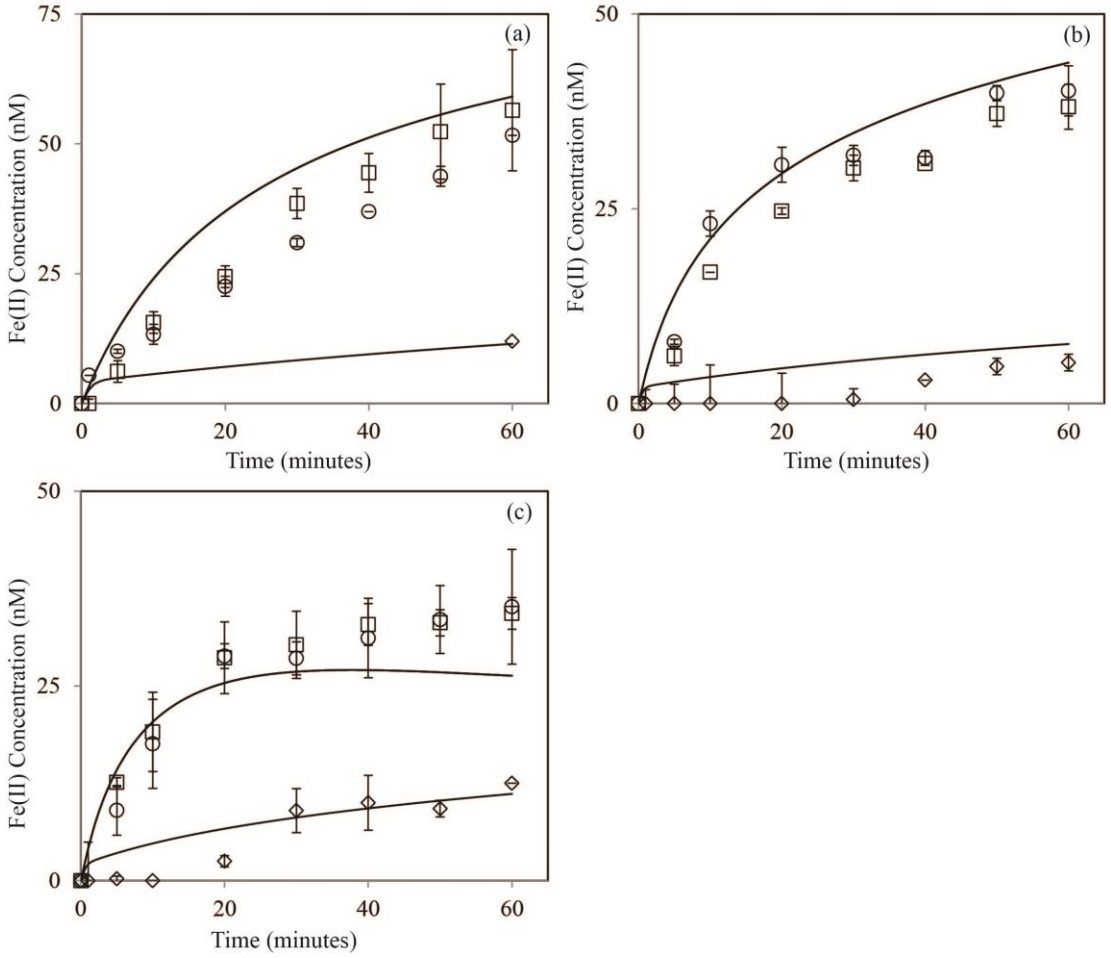

Figure 4.6: Generation of Fe(II) in solutions containing 100 nM Fe(III) and 500 nM hydroquinone in air-saturated solution (squares), partially-deoxygenated solution (diamonds) and in air-saturated solution containing 25 $kU.L^{-1}$ SOD (circles) at (a) pH 3 , (b) pH 4.5 and (c) pH 5. Symbols are experimental data (average of duplicate measurements); lines are model predicted values.

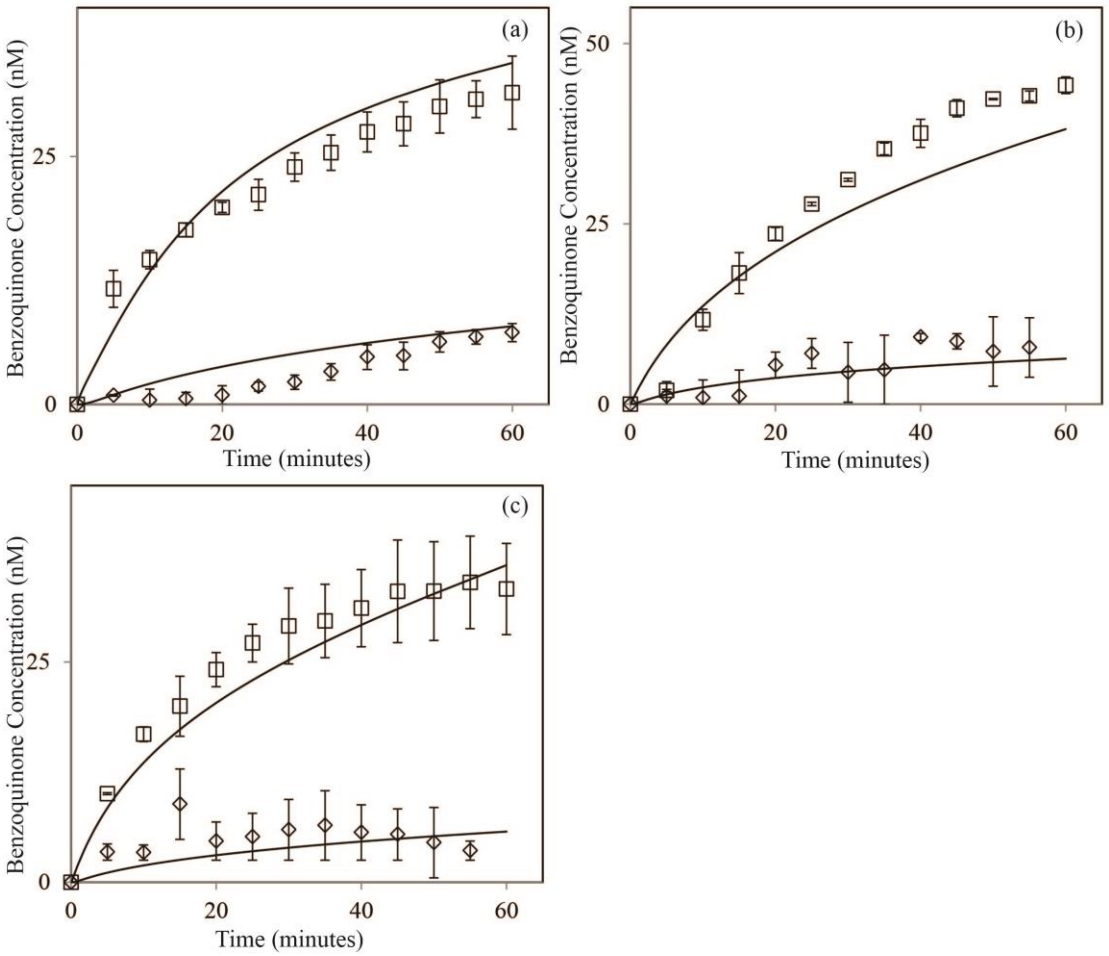

Figure 4.7: Generation of benzoquinone in solutions containing 100 nM Fe(III) and 500 nM hydroquinone in air-saturated solution (squares) and partially-deoxygenated solution (diamonds) at (a) pH 3 , (b) pH 4.5 and (c) pH 5. Symbols are experimental data (average of duplicate measurements); lines are model predicted values.

Because the oxygenation of Fe(II) is important at pH 5 (see Figure 4.2), the stoichiometry of Fe(II) to Q generation is less than 1:1 and the stoichiometry of Q to H_2O_2 generation is less than 2:1 at this pH. The oxygenation of Fe(II) in addition to its oxidation by the semiquinone radical results in a net decrease in Fe(II) generation and increase in H_2O_2 generation. Although the oxygenation of Fe(II) occurs, Fe(II) oxidation by $Q^{\bullet -}$ is still the main pathway for Fe(II) oxidation at pH 5 because the partial removal of dioxygen results in decreased Fe(II) generation (Figure 4.7c).

4.3.7. Thermodynamic considerations relating to the reduction of Fe(III) by H_2Q

4.3.7.1. Speciation calculation assuming equilibrium between Q/H_2Q and Fe(III)/Fe(II) redox couple

Global thermodynamics calculations assuming equilibrium between the Fe(III)/Fe(II) redox couple and the Q/ H_2Q redox couple results in the predicted concentrations and stoichiometry of Fe(II) and Q that are inconsistent with the measured concentrations of these parameters, with this result providing further support for our conclusion that direct two-electron oxidation of H_2Q by Fe(III) or the sequential two-electron oxidation of H_2Q by Fe(III) does not occur to an appreciable extent at the pH and time-scale employed in this study. A detailed thermodynamics calculation is provided below.

For the redox reaction,

$$\mathrm{Fe(III)} + \frac{1}{2}\mathrm{H_2Q} \rightleftharpoons \frac{1}{2}\mathrm{Q} + \mathrm{Fe(II)} \qquad (4.9)$$

The concentration of Fe(II) and Q at equilibrium can be calculated using chemical thermodynamics as shown below for pH 3.

At pH 3, $Fe(OH)^{2+}$ is the dominant Fe(III) specie, and H_2Q is the dominant hydroquinone specie. Thus, the half-redox reactions and redox potentials are:

$$\mathrm{Fe(OH)^{2+}} + e^- + \mathrm{H^+} \rightleftharpoons \mathrm{Fe^{2+}} + \mathrm{H_2O} \qquad \mathrm{pe_1^0} = 15.2 \qquad (4.10)$$

$$\frac{1}{2}\mathrm{Q} + e^- + \mathrm{H^+} \rightleftharpoons \frac{1}{2}\mathrm{H_2Q} \qquad \mathrm{pe_2^0} = 4.83 \qquad (4.11)$$

$$\mathrm{pe_1} = \mathrm{pe_1^0} - \log\frac{[\mathrm{Fe^{2+}}]}{[\mathrm{Fe(OH)^{2+}}][\mathrm{H^+}]} = \mathrm{pe_1^0} - \log\frac{\alpha_{\mathrm{Fe^{2+}}}[\mathrm{Fe(II)}]_\mathrm{T}}{\alpha_{\mathrm{Fe(OH)^{2+}}}(\mathrm{Fe_0}\text{-}[\mathrm{Fe(II)}]_\mathrm{T})[\mathrm{H^+}]} \qquad (4.12)$$

$$pe_2 = pe_2^0 - \log \frac{[H_2Q]^{\frac{1}{2}}}{[Q]^{\frac{1}{2}}[H^+]} = pe_2^0 - \log \frac{([H_2Q_0]-[Q])^{\frac{1}{2}}}{[Q]^{\frac{1}{2}}[H^+]} \quad (4.13)$$

where H_2Q_0 and Fe_0 represents the initial concentration of H_2Q and Fe(III) respectively. Since, Fe(III) and H_2Q reaction occur in stoichiometric ratio of 2:1, $[Fe(II)]_T = 2 \times [Q]$

$$\text{Thus, } pe_2 = pe_2^0 - \log \frac{([H_2Q_0]-0.5[Fe(II)]_T)^{\frac{1}{2}}}{[0.5Fe(II)]_T^{\frac{1}{2}}[H^+]} \quad (4.14)$$

At equilibrium $pe_1 = pe_2$. Thus equating eq.4.12 and eq.4.14 and solving we get Fe(II) concentration at equilibrium (see Table 4.2).

Table 4.2: Calculated equilibrium concentration of Fe(II) and Q assuming equilibrium between Q/H_2Q and Fe(III)/Fe(II) redox couple in air-saturated solution

	Initial Concentration		Concentration at Equilibrium	
pH	H_2Q_0 (nM)	$Fe(III)_0$ (nM)	Calculated Fe(II) (nM)	Calculated Q (nM)
3	500	50	50	25
	500	100	100	50
	1000	100	100	50
4	500	50	50	25
	500	100	100	50
	1000	100	100	50
4.5	500	50	50	25
	500	50	50	25
	1000	100	100	50

5	500	50	50	25
	500	100	100	50
	1000	100	100	50

As shown, the calculated concentration of Fe(II) and Q at equilibrium are significantly different than the measured values (see Table 4.1) and hence suggests that Fe(III)/Fe(II) redox couple is not in equilibrium with Q/H_2Q redox couple, thereby supporting that direct 2 electron oxidation of H_2Q by Fe(III) is not possible.

As expected, the calculated ΔG value using measured Fe(II) and Q concentration is very high (Table 4.3), supporting that this is not at equilibrium.

Table 4.3: Calculated ΔG value assuming equilibrium between Q/H_2Q and Fe(III)/Fe(II) redox couple for initial Fe(III) and H_2Q concentration of 100 nM and 500 nM respectively

pH	Calculated ΔG (KJ)
3	-61.26
4	-59.59
4.5	-59.04
5	-58.18

4.3.7.2. ΔG calculation assuming equilibrium between $HQ^{\bullet}/H_2Q$ and Fe(III)/Fe(II) redox couple and equilibrium between $Q/HQ^{\bullet}$ and $O_2 / HO_2^{\bullet}$ redox couples

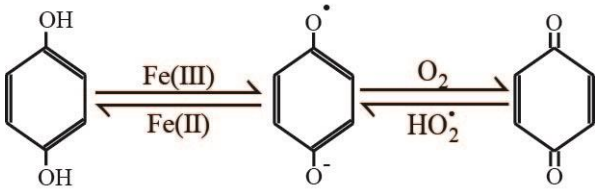

Figure 4.8: Reaction schematic showing equilibrium between various quinone species in the presence of Fe in air-saturated solution.

Thermodynamic calculations performed assuming i) equilibrium between the Fe(III)/Fe(II) and the $H_2Q / Q^{\bullet -}$ redox couples, and ii) equilibrium between the $Q^{\bullet -} / Q$ and $O_2 / HO_2^{\bullet}$ redox couples results in ΔG close to zero (Table 4.4), supporting the conclusion that quasi-equilibrium between these four redox couples exists (see detailed calculation below) as depicted in the reaction schematic shown in Figure 4.8. This observation further suggests that the ratio of the rate constant for the forward reaction (i.e. k_1) and the backward reaction (i.e. k_{-1}) is related to the ΔE_H^0 for the reactions shown in eq.4.1 calculated using the reported redox potential (E_H^0) for the Fe(III)/Fe(II) and $Q^{\bullet -}/H_2Q$ redox couples. Similarly, the ratio of the forward and backward rate constants for the reactions shown in eq.4.4 (i.e. k_4/k_{-4}) is calculated using E_H^0 for the $Q / Q^{\bullet -}$ and E_H^0 for $O_2 / HO_2^{\bullet}$ redox couples. These calculated values of the equilibrium constants for these reactions are shown in Table 4.5 and are used as thermodynamic constraints in the kinetic modelling of our experimental results as described in the following section.

At pH 3, $Fe(OH)^{2+}$ is the dominant Fe(III) specie, and $HQ^{\bullet}$ is the dominant semiquinone specie. Thus, the half-redox reactions and redox potentials are:

$$Fe(OH)^{2+} + e^- + H^+ \rightleftharpoons Fe^{2+} + H_2O \qquad pe_1^0 = 15.2 \qquad (4.15)$$

$$HQ^\bullet + e^- + H^+ \rightleftharpoons H_2Q \qquad pe_2^0 = 18.5 \qquad (4.16)$$

The energy (ΔG) required for the above reaction can be calculated using reported redox potentials for Fe(III)/Fe(II) and $HQ^\bullet / H_2Q$ redox couples at all pHs examined. The calculation of ΔG at pH 3 is shown below as an example.

$$pe_1 = pe_1^0 - \log\frac{[Fe^{2+}]}{[Fe(OH)^{2+}][H^+]} = pe_1^0 - \log\frac{\alpha_{Fe^{2+}}[Fe(II)]_T}{\alpha_{Fe(OH)^{2+}}[Fe(III)]_T[H^+]}$$
$$= 15.2 - \log\frac{1\times 56.5\times 10^{-9}}{0.75\times 43.5\times 10^{-9}\times 10^{-3}} \qquad (4.17)$$

$$pe_2 = pe_2^0 - \log\frac{[H_2Q]}{[HQ^\bullet][H^+]} = 18.5 - \log\frac{\left(4.57\times 10^{-7}\right)}{[HQ^\bullet]\times 10^{-3}} \qquad (4.18)$$

Assuming, equilibrium exists between $Q/HQ^\bullet$ and $O_2 / HO_2^\bullet$ redox couples, we write the reaction in terms of dominant species at pH 3.

$$Q + e^- + H^+ \longrightarrow HQ^\bullet \qquad pe_3^0 = 5.42 \qquad (4.19)$$

$$O_2 + e^- + H^+ \longrightarrow HO_2^\bullet \qquad pe_4^0 = 1.76 \qquad (4.20)$$

$$pe_3 = pe_3^0 - \log\frac{[HQ^\bullet]}{[Q][H^+]} = 5.42 - \log\frac{[HQ^\bullet]}{27.4\times 10^{-9}\times 10^{-3}} \qquad (4.21)$$

$$pe_4 = pe_4^0 - \log\frac{[HO_2^\bullet]}{[O_2][H^+]} = 1.76 - \log\frac{[HO_2^\bullet]}{2.4\times 10^{-4}\times 10^{-3}} \qquad (4.22)$$

$$[HO_2^\bullet] = \alpha_0\sqrt{\frac{P_{H_2O_2}}{k_{disp}}} \qquad (4.23)$$

where $\alpha_0 = \frac{[H^+]}{[H^+] + K_{HO_2^\bullet}}$, $K_{HO_2^\bullet}$ = $10^{-4.8}$, $P_{H_2O_2}$ = measured H_2O_2 generation rate and k_{disp} is rate constant for superoxide disproportionation. At pH 3,

$[HO_2^\bullet] = 1.6\times10^{-10}$ M

At equilibrium $pe_3 = pe_4$ and substituting $[HO_2^\bullet] = 1.6\times10^{-10}$, we get $[HQ^\bullet] = 8.3\times10^{-11}$ M.

Therefore, $pe_2 = 11.7$ and the energy ΔG required for reaction is:

$$\Delta G = 2.3nRT(pe_2\text{-}pe_1) = 2.3\times1\times8.314\times298\times(11.7-11.9) = -1.0\text{KJ} \quad (4.24)$$

Results of calculated ΔG in a same manner at all pHs are provided in Table 4.4 below.

Table 4.4: Calculated ΔG for the reaction of Fe(III) and H_2Q assuming equilibrium between $HQ^\bullet/H_2Q$ and Fe(III)/Fe(II) redox couple and equilibrium between $Q/HQ^\bullet$ and $O_2 / HO_2^\bullet$ redox couples in air-saturated solution.

	Initial Concentration		ΔG (kJ)
pH	H_2Q_0 (nM)	$Fe(III)_0$ (nM)	
3	500	100	-1
	1000	100	0.8
4	500	100	0.5
	1000	100	0.7
4.5	500	100	0.3
	1000	100	0.3
5	500	100	0.2
	1000	100	-0.4

Because the calculated ΔG ~ 0, Fe(III)/Fe(II) redox couple is in equilibrium with $HQ^{\bullet}$ / H_2Q redox couples at all pHs examined.

4.3.7.3. Calculation of equilibrium constant for the reaction of Fe(III) and H_2Q

$$H_2Q + Fe(III) \underset{k_{-1}}{\overset{k_1}{\rightleftharpoons}} Q^{\bullet -} + Fe(II) \qquad (4.25)$$

The equilibrium constant $K_{H_2Q\text{-}Fe(III)}$ of the above reaction was calculated thermodynamically using the reported redox potentials for Fe(III)/Fe(II) and $Q^{\bullet -}/H_2Q$ redox couples at all pHs examined. The calculation of $K_{H_2Q\text{-}Fe(III)}$ using thermodynamic constraints at pH 3 is shown below and the calculated value of $K_{H_2Q\text{-}Fe(III)}$ at other pHs is shown in Table 4.5.

At pH 3, $Fe(OH)^{2+}$ is the dominant Fe(III) specie, and $HQ^{\bullet}$ is the dominant semiquinone specie. Thus, the dominant half-redox reactions are of the form:

$$Fe(OH)^{2+} + e^- + H^+ \rightleftharpoons Fe^{2+} + H_2O \qquad pe^0 = 15.2 \qquad (4.26)$$

$$HQ^{\bullet} + e^- + H^+ \rightleftharpoons H_2Q \qquad pe^0 = 18.5 \qquad (4.27)$$

With the overall redox reaction given by:

$$Fe(OH)^{2+} + H_2Q \rightleftharpoons Fe^{2+} + HQ^{\bullet} + H_2O \qquad pe^0 = -3.3 \qquad (4.28)$$

$$\text{Therefore, } K = \frac{[Fe^{2+}][HQ^{\bullet}]}{[Fe(OH)^{2+}][H_2Q]} = 10^{-3.3} \qquad (4.29)$$

Since, in the kinetic model, total concentration (rather than concentration of Fe^{2+}, $Fe(OH)^{2+}$, $HQ^{\bullet}$) is used, calculated *K* value is expressed in terms of total concentration of the involved species,

$$K = \frac{\alpha_{Fe^{2+}}[Fe(II)]_T \alpha_{HQ^{\bullet}}[Q^{\bullet -}]_T}{\alpha_{Fe(OH)^{2+}}[Fe(III)]_T \alpha_{H_2Q}[H_2Q]_T} = 10^{-3.3} \quad (4.30)$$

$$K_{H_2Q\text{-}Fe(III)} = \frac{[Fe(II)]_T[Q^{\bullet -}]_T}{[Fe(III)]_T[H_2Q]_T} = \frac{\alpha_{Fe(OH)^{2+}}\alpha_{H_2Q}10^{-3.3}}{\alpha_{Fe^{2+}}\alpha_{HQ^{\bullet}}} \quad (4.31)$$

Since, $\alpha_{Fe^{2+}}$ = α_{H_2Q} = 1; $\alpha_{HQ^{\bullet}}$ = 0.93; $\alpha_{Fe(OH)^{2+}}$ = 0.75, we calculate the equilibrium constant $K_{H_2Q\text{-}Fe(III)}$ in terms of total concentration at pH 3 to be $10^{-3.39}$ which is used in the kinetic model to constrain the rate constant k_{-1}.

4.3.7.4. Calculation of equilibrium constant for the reaction of $Q^{\bullet -}$ and O_2

$$Q^{\bullet -} + O_2 \underset{k_{-4}}{\overset{k_4}{\rightleftharpoons}} Q + HO_2^{\bullet} \quad (4.32)$$

Similar with above calculation for equilibrium constant of Fe(III) and H_2Q, the equilibrium constant $K_{Q^{\bullet -}\text{-}O_2}$ of $Q^{\bullet -}$ and O_2 can be calculated thermodynamically using the reported redox potentials for $Q/Q^{\bullet -}$ and $O_2/HO_2^{\bullet}$. The calculation of $K_{Q^{\bullet -}\text{-}O_2}$ using thermodynamic constraints at pH 3 is shown below and the calculated value of $K_{Q^{\bullet -}\text{-}O_2}$ at all pHs is shown in Table 4.5.

At pH 3, $HQ^{\bullet}$ is the dominant $Q^{\bullet -}$ specie, and $HO_2^{\bullet}$ is the dominant superoxide specie. Thus, the dominant half-redox reactions are:

$$O_2 + H^+ + e^- \rightleftharpoons HO_2^{\bullet} \qquad pe^0 = 1.76 \quad (4.33)$$

$$HQ^{\bullet} \rightleftharpoons Q + e^- + H^+ \qquad pe^0 = -5.42 \quad (4.34)$$

With the overall redox reaction given by:

$$HQ^{\bullet} + O_2 \rightleftharpoons HO_2^{\bullet} + Q \qquad pe^0 = -3.65 \qquad (4.35)$$

Therefore,

$$K = \frac{[HO_2^{\bullet}][Q]}{[HQ^{\bullet}][O_2]} = 10^{-3.65} \qquad (4.36)$$

Since the model predicted *K* is in terms of total concentration of the involved species,

$$K_{Q^{\bullet-}\text{-}O_2} = \frac{[O_2^{-}]_T[Q]_T}{[Q^{\bullet-}]_T[O_2]_T} = \frac{\alpha_{HQ^{\bullet}}\alpha_{O_2}}{\alpha_{HO_2}\alpha_{Q}} 10^{-3.65} \qquad (4.37)$$

Since α_{Q} = α_{O_2} =1; α_{HO_2} = 0.98; $\alpha_{HQ^{\bullet}}$ = 0.93, we calculate the equilibrium constant, $K_{Q^{\bullet-}\text{-}O_2}$, in terms of total concentration at pH 3 to be $10^{-3.57}$ which is used in the kinetic model to constrain the ratio of rate constants k_2 and k_{-2}.

Table 4.5: Calculated equilibrium constant for Fe(III) and H_2Q reaction ($K_{H_2Q\text{-}Fe(III)}$) and $Q^{\bullet-}$ and dioxygen interaction ($K_{Q^{\bullet-}\text{-}O_2}$)

pH	Calculated $K_{H_2Q\text{-}Fe(III)}$	Calculated $K_{Q^{\bullet-}\text{-}O_2}$
3	$10^{-3.39}$	$10^{-3.68}$
4	$10^{-3.42}$	$10^{-3.84}$
4.5	$10^{-3.85}$	$10^{-4.03}$
5	$10^{-3.88}$	$10^{-4.20}$

4.3.8. Kinetics and mechanism of Fe(III) and hydroquinone interaction

The kinetic model showing the proposed Fe(III) and hydroquinone interactions is shown in Table 4.6. The rate constant for the reduction of Fe(III) by hydroquinone (k_1; reaction

1; Table 4.1) was determined on the basis of the best fit to the measured rate and the extent of Fe(II) generation and was found to be pH-independent. The pH-dependent rate constants for oxidation of Fe(II) by semiquinone (k_{-1}; reaction 1; Table 4.6) and the rate constants for the oxidation of semiquinone radicals by dioxygen (k_4; reaction 4; Table 4.6) were determined on the basis of the best fit to the measured rate and extent of Fe(II) and Q generation and with the thermodynamic constraint that $k_{-1} = k_1 / K_{\mathrm{H_2Q\text{-}Fe(III)}}$ imposed (as mentioned in section 4.3.7).

Table 4.6: Kinetic model for hydroquinone-mediated reduction of Fe(III) in the pH range 3-5 with important reactions highlighted.

No.	Reaction	Rate constant ($M^{-1}S^{-1}$)					Reference
			pH 3	pH 4	pH 4.5	pH 5	-
1	$H_2Q + Fe(III) \underset{k_{-1}}{\overset{k_1}{\rightleftharpoons}} Q^{\bullet-} + Fe(II)$			$k_1 = 1\times10^3$			Chapter 3
		k_{-1}	2.4×10^6	4×10^6	7×10^6	9×10^6	-
2	$Q^{\bullet-} + Fe(III) \underset{k_{-2}}{\overset{k_2}{\rightleftharpoons}} Fe(II) + Q$			$k_2 \leq 1\times10^5$			Yamazaki and Ohnishi (1966)
				$k_{-2} \leq 1\times10^3$			Yuan et al. (2013)
3	$Q^{\bullet-} + Q^{\bullet-} + 2H^+ \underset{k_{-3}}{\overset{k_3}{\rightleftharpoons}} Q + H_2Q$			$k_3 \leq 1\times10^{10}$			Yamazaki and Ohnishi (1966); Yuan et al. (2013)
				$k_{-3} \leq 8\times10^7$			Yamazaki and Ohnishi (1966); Yuan et al. (2013)
4	$Q^{\bullet-} + O_2 \underset{k_{-4}}{\overset{k_4}{\rightleftharpoons}} Q + HO_2^{\bullet}$	k_4	5×10^2	7×10^2	9×10^2	1×10^3	Yamazaki and Ohnishi (1996); Meisel (1975)
		k_{-4}	1.8×10^6	4×10^6	8×10^6	1.9×10^7	Meisel (1975)
5	$HO_2^{\bullet} + HO_2^{\bullet} \xrightarrow{k_{disp}} O_2 + H_2O_2$	k_{disp}	2×10^6	1.1×10^7	2×10^7	2.5×10^7	Bielski et al. (1985)
6	$Q^{\bullet-} + HO_2^{\bullet} \xrightarrow{k_6} H_2Q + O_2$			$k_6 = 5\times10^8$			-
7	$Fe(III) + HO_2^{\bullet} \underset{k_{-7}}{\overset{k_7}{\rightleftharpoons}} Fe(II) + O_2$	k_7	5×10^5	9×10^5	1.4×10^6	2.5×10^6	Rush and Bielski (1985)
		k_{-7}	-	-	-	1.3	-
8	$Fe(II) + HO_2^{\bullet} \xrightarrow{k_8} Fe(III) + H_2O_2$	k_8	1.3×10^6	2.4×10^6	4.1×10^6	6.6×10^6	Rush and Bielski (1985)

As discussed, the oxidation of $Q^{\bullet-}$ by Fe(III) (reaction 2; Table 4.6) is unimportant in the conditions of our experiments due to decrease in reduction capacity of $Q^{\bullet-}$ that occurs at lower pHs, as indicated by increased redox potential of $Q/Q^{\bullet-}$ couple under acidic conditions (see Figure 4.4). Furthermore, under acidic conditions, the redox potential of the $Q^{\bullet-}/H_2Q$ couple increases, making $Q^{\bullet-}$ a better oxidant than reductant under acidic conditions (Figure 4.4). Similarly, the oxidation of Fe(II) by Q (reaction 2; Table 4.6), which is reported to occur with other trace metals such as Cu under circumneutral pH conditions (Yuan et al. 2013; Yuan et al. 2014), and the resultant catalysis of comproportionation reaction is also determined to be unimportant at the time scale and pH investigated here due to the limited generation of Q. Our kinetic modelling further shows that the inclusion of this reaction using rate constants of $\leq 1 \times 10^5\ M^{-1}s^{-1}$ and $\leq 1 \times 10^3\ M^{-1}s^{-1}$ for k_2 and k_{-2} respectively, does not affect the model output. The value of k_{-2} used here is 10-fold higher than the reported value (Yuan et al. 2013), supporting the premise that the oxidation of Fe(II) by Q is unimportant due to the limited generation of Q. Although the value of k_2 ($1 \times 10^5\ M^{-1}s^{-1}$) used here is lower than the value reported for the Fe(III) cytochrome-semiquinone reaction at pH 7 (Yamazaki and Ohnishi 1966), it is possibly due to variation in the redox potential and speciation of $Q^{\bullet-}$ with change in pH. The semiquinone radical is mostly present in the deprotonated form at pH 7, and it exists in both deprotonated ($Q^{\bullet-}$) and protonated ($HQ^{\bullet}$) forms under acidic conditions. Because $HQ^{\bullet}$ is expected to be less reactive than $Q^{\bullet-}$ (Yuan et al. 2013), the rate constant of Fe(III)-semiquinone reaction decreases under acidic conditions. Furthermore, as discussed, variation in the redox potential of $Q^{\bullet-}$ with change in pH is also expected to affect its reactivity as reductant, with

resultant decrease in the rate of oxidation of $Q^{\bullet-}$ by Fe(III). Although this reaction was determined to be unimportant at the time scales of our experiments, it may play an important role in Q generation in the complete absence of dioxygen on longer time-scales.

Disproportionation of the semiquinone radical (reaction 3; Table 4.6) is also unimportant in the experimental system investigated here as a result of the low steady-state concentrations of the semiquinone radical present. The comproportionation reaction between H_2Q and Q (reaction 3; Table 4.6) is also not important in the system investigated here as a result of the extremely low concentrations of the doubly deprotonated hydroquinone species (Q^{2-}) (the reported active species towards comproportionation reaction (Yamazaki and Ohnishi 1966; Rich and Bendall 1980; Roginsky et al. 1999) with concentrations of ~ 10^{-13} - 10^{-15} M in the pH 5-3 solutions used in these studies. Furthermore, the concentration of Q is also very small (~ 10^{-8} M) supporting the conclusion that the comproportionation reaction is unimportant in our system. The results of our kinetic modelling further show that the inclusion of the comproportionation reaction and the semiquinone disproportionation reaction does not have any effect on the model output, even when the rate constants for these reactions are > 1×10^{10} $M^{-1}s^{-1}$ and $\leq 8 \times 10^{7}$ $M^{-1}s^{-1}$ respectively.

The pH-dependent rate constant for superoxide disproportionation (k_{disp}; reaction 5; Table 4.6) reported by Bielski and co-workers (Bielski et al. 1985) was used here. The reduction of $Q^{\bullet-}$ and Q by superoxide (reactions 6 and 4 respectively; Table 4.6) were included in the model to account for superoxide loss via pathways other than the disproportionation reaction, with the rate constants for these reactions determined on the basis of the best fit to the H_2O_2 concentration data and the effect of SOD addition on

Fe(II) generation. However, the rate constant for oxidation of superoxide by semiquinone (reaction 6; Table 4.6) is not well-constrained by our kinetic model due to its minor role in controlling the Fe(II) and Q generation rates. Although the reaction of Q with superoxide (reaction 4; Table 4.6) plays a minor role in affecting the model output, the rate constant for this reaction (k_{-4}) is well-constrained by the relationship $k_{-4} = k_4 / K_{Q^{\bullet-}\text{-}O_2}$ (see section 4.3.7). We have also included $HO_2^{\bullet}$-mediated Fe(II) oxidation and Fe(III) reduction (reactions 7 and 8; Table 4.6) with rate constants similar to the values reported by Rush and Bielski (1985); however, these reactions do not play an important role in Fe(II) generation in the pH range 3-5, as confirmed by the model-predicted effect of SOD addition (Figures 4.3 and 4.6).

The rate of Fe(II) oxidation by dioxygen (reaction 7; Table 4.6) is extremely slow at pH < 5 (see Figure 4.2) and therefore neglected. However, at pH 5, oxygenation of Fe(II) becomes important ($t_{1/2}$ < 1 h) and is therefore included in the kinetic model. The rate constant for this reaction (k_{-7}) at pH 5 was determined on the basis of the best fit to the H_2O_2 generation data and Fe(II) oxygenation rate observed in pH 5 solution; however, the value at other pHs investigated here could not be determined.

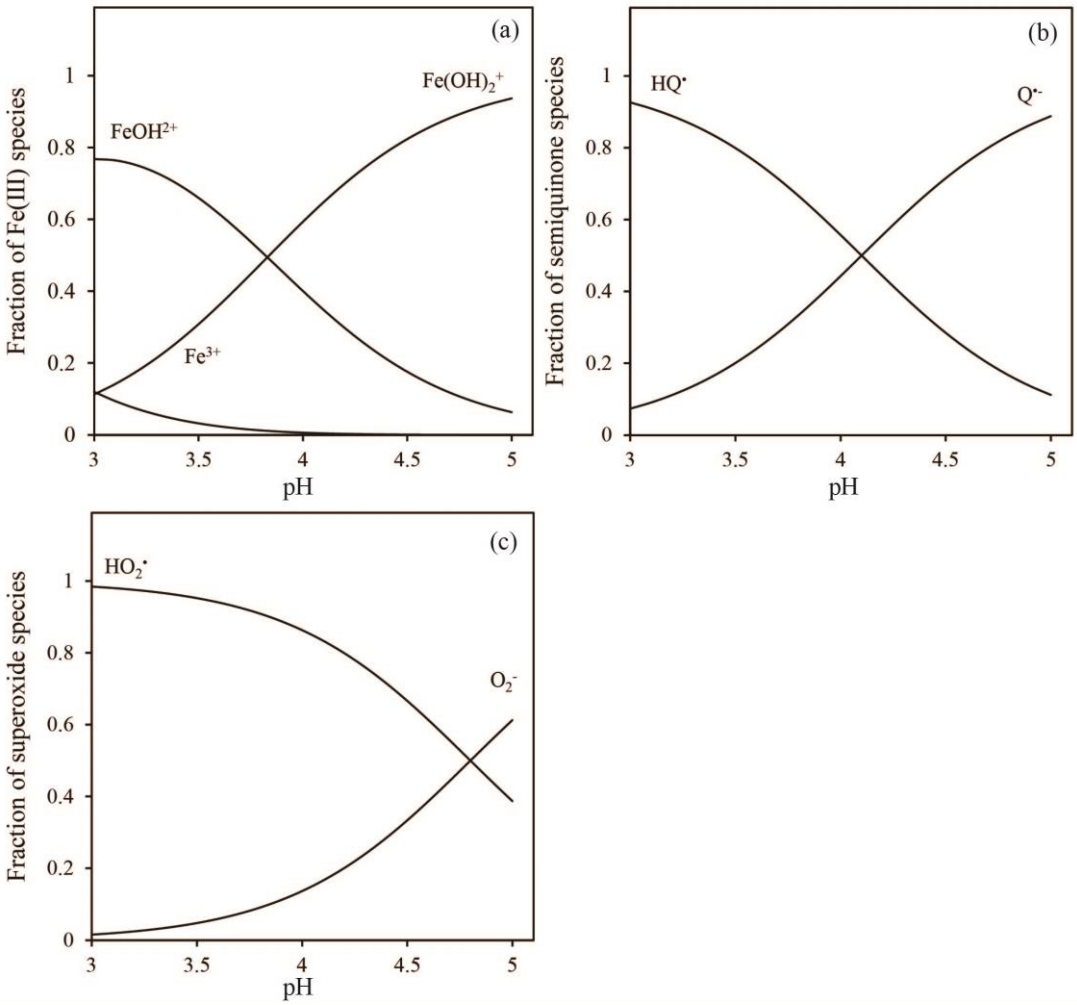

Figure 4.9: Variation in speciation of (a) Fe(III), (b) $Q^{\bullet -}$ and (c) superoxide with change in pH.

As shown in Table 4.6, the rate constant for some reactions are pH-dependent due to changes in the speciation of the entities involved in these reactions. Although the speciation of Fe(III) varies in the pH range investigated here (see Figure 4.9), the rate constant for the Fe(III) and H_2Q reaction (reaction 1; Table 4.6) based on our experimental data is similar under all conditions examined. This result suggests that the reactivity of $FeOH^{2+}$ and $Fe(OH)_2^+$ (the two dominant Fe(III) species in our experimental matrix) are similar, thereby resulting in the same Fe(III) reduction rate under all pH conditions investigated here. This is consistent with earlier studies of Fe(III) reduction by superoxide, which reported that all Fe(III) species have similar

reactivity towards superoxide, with the experimentally determined rate constant for reduction of $FeSO_4^+$ and $FeOH^{2+}$ by $O_2^{\bullet-}$ being similar (1.5×10^8 $M^{-1}s^{-1}$) (Rush and Bielski 1985). The rate constant for the oxidation of Fe(II) by $Q^{\bullet-}$ is pH-dependent (k_{-1}; Table 4.6) becasue the form of the semiquinone radical (with pK_a= 4.1) changes over the pH range investigated. As reported earlier (Yuan et al. 2013), the deprotonated form, $Q^{\bullet-}$, is a more active oxidant than $HQ^{\bullet}$ and therefore oxidizes Fe(II) more rapidly than the protonated form, with resultant decrease in the concentration of Fe(II) and Q formed at higher pHs. As shown in eq.4.9, the overall rate constant of Fe(II) oxidation is a function of the fraction of the protonated and deprotonated species at each pH , i.e.

$$k_{-1} = \alpha_0 k_{-1}^{HQ} + \alpha_1 k_{-1}^{Q^{\bullet-}} \tag{4.38}$$

where $\alpha_0 = \dfrac{[H^+]}{[H^+]+K_{HQ}}$; $\alpha_1 = 1-\alpha_0$; K_{HQ} = $10^{-4.1}$; k_{-1}^{HQ} = 2 × 10^6 $M^{-1}s^{-1}$, and $k_{-1}^{Q^{\bullet-}}$ = 1 × 10^7 $M^{-1}s^{-1}$.

The rate constant for oxygenation of the semiquinone radical (reaction 4; Table 4.6) also increases with an increase in pH due to the higher reactivity of $Q^{\bullet-}$ than $HQ^{\bullet}$. The variation in this rate constant with pH is also modelled as a function of the speciation of the semiquinone radical and is given by the following equation:

$$k_4 = \alpha_0 k_4^{HQ} + \alpha_1 k_4^{Q^{\bullet-}} \tag{4.39}$$

where $\alpha_0 = \dfrac{[H^+]}{[H^+]+K_{HQ}}$; $\alpha_1 = 1-\alpha_0$; K_{HQ} = $10^{-4.1}$; k_4^{HQ} = 4.6 × 10^2 $M^{-1}s^{-1}$, and $k_4^{Q^{\bullet-}}$ = 1.0 × 10^3 $M^{-1}s^{-1}$. The model-predicted rate constant for the semiquinone oxygenation

reaction is slightly lower than that reported under alkaline conditions (for example, Yuan et al. (2013) report a value of 1.0×10^4 $M^{-1}s^{-1}$ at pH 8.0).

The pH-dependence of the rate constant for superoxide disproportionation (reaction 5; Table 4.6) is modelled as a function of the speciation of superoxide as described earlier (Bielski et al. 1985); i.e.

$$k_{disp} = \alpha_0 \alpha_0 k_{HO_2^\bullet} + \alpha_0 \alpha_1 k_{O_2^{\bullet-}} \quad (4.40)$$

where $\alpha_0 = \frac{[H^+]}{[H^+] + K_{HO_2^\bullet}}$, $\alpha_1 = 1 - \alpha_0$, $k_{HO_2^\bullet} = 8.3 \times 10^5$ $M^{-1}s^{-1}$, $k_{O_2^{\bullet-}} = 9.7 \times 10^7$ $M^{-1}s^{-1}$, and $K_{HO_2^\bullet} = 10^{-4.8}$.

As reported earlier (Rush and Bielski 1985), the rate constant of Fe(III) reduction by $HO_2^\bullet$ is very low ($< 1 \times 10^3$ $M^{-1}s^{-1}$), with most of the Fe(III) reduction by superoxide attributed to its reaction with $O_2^{\bullet-}$. Thus, the rate constant for Fe(III) reduction by superoxide (reaction 7; Table 4.6) determined on the basis of the best fit to our experimental results is shown to vary with pH due to the change in concentration of $O_2^{\bullet-}$; i.e.

$$k_7 = \alpha_1 k_7^{O_2^{\bullet-}} \quad (4.41)$$

where $\alpha_1 = \frac{K_{HO_2^\bullet}}{[H^+] + K_{HO_2^\bullet}}$; k_7 represents the overall rate constant for reduction of Fe(III) by superoxide, $k_7^{O_2^{\bullet-}} = 1.5 \times 10^7$ $M^{-1}s^{-1}$ and $K_{HO_2^\bullet} = 10^{-4.8}$. The value of $k_7^{O_2^{\bullet-}}$ determined here is 1-fold lower than the reported value of 1.5×10^8 $M^{-1}s^{-1}$ (Rush and Bielski 1985)

under strongly acidic conditions (< pH 2) by very high concentration of Fe(III) (~ 100 μM).

The rate constant for Fe(II) oxidation by superoxide (reaction 8; Table 4.6) varies with pH due to the difference in reactivity of $O_2^{\bullet-}$ and $HO_2^{\bullet}$ as reported earlier (Rush and Bielski 1985); i.e.

$$k_8 = \alpha_0 k_8^{HO_2^{\bullet}} + \alpha_1 k_8^{O_2^{\bullet-}} \quad (4.42)$$

where $\alpha_0 = \frac{[H^+]}{[H^+] + K_{HO_2^{\bullet}}}$ and $\alpha_1 = 1 - \alpha_0$; k_8 represents the overall rate constant for oxidation of Fe(II) by superoxide; $k_8^{HO_2^{\bullet}} = 1.2 \times 10^6$ $M^{-1}s^{-1}$, $k_8^{O_2^{\bullet-}} = 1.0 \times 10^7$ $M^{-1}s^{-1}$ and $K_{HO_2^{\bullet}} = 10^{-4.8}$.

As shown in Figures 4.1, 4.3 and 4.5-4.7, the model provides a good description of the experimental results obtained here, with the kinetic model predicting the effect of dioxygen removal, SOD addition, and pH reasonably well. Because Fe continually cycles between the +III and +II oxidation states in the presence of H_2Q, the Fe turnover frequency (TOF) at steady-state can be deduced from the kinetic model developed here using the expressions:

$$\text{TOF} = \frac{\text{Fe(III) reduction rate}}{\text{Total Fe concentration}} \quad (4.43)$$

and

$$\text{Fe(III) reduction rate} = k_1[\text{Fe(III)}]_{ss}[H_2Q]_{ss} = k_1(Fe_0 - [\text{Fe(II)}]_{ss})(Q_0 - [Q]_{ss}) \quad (4.44)$$

where k_1 = 1×10^3 $M^{-1}s^{-1}$ and Fe_0 and Q_0 represent the initial Fe(III) and H_2Q concentrations, respectively. The $[Fe(II)]_{ss}$ and $[Q]_{ss}$ values were determined from the kinetic model.

The calculated TOF increases with increase in pH as a result of the higher rates of Fe(II) oxidation at higher pHs with values of 0.73, 1.23, 2.22 and 4.41 h^{-1} deduced for 2 µM H_2Q solutions at pH 3, 4, 4.5 and 5 respectively.

4.4. Conclusions

Our results show that hydroquinone reduces Fe(III) resulting in formation of Fe(II) and semiquinone radicals. The semiquinone radicals so formed subsequently oxidize Fe(II) to Fe(III). The oxidation rate of Fe(II) by semiquinone radicals increases with an increase in pH due to the speciation change of semiquinone radicals, with its deprotonated form ($Q^{\bullet-}$) oxidizing Fe(II) more rapidly than the protonated form ($HQ^{\bullet}$). The rapid redox cycling of Fe between the +III and +II oxidation states in the presence of H_2Q is accompanied by generation of benzoquinone and reactive oxygen species (particularly $HO_2^{\bullet}$ and H_2O_2), with O_2 playing an important role in these redox transformations.

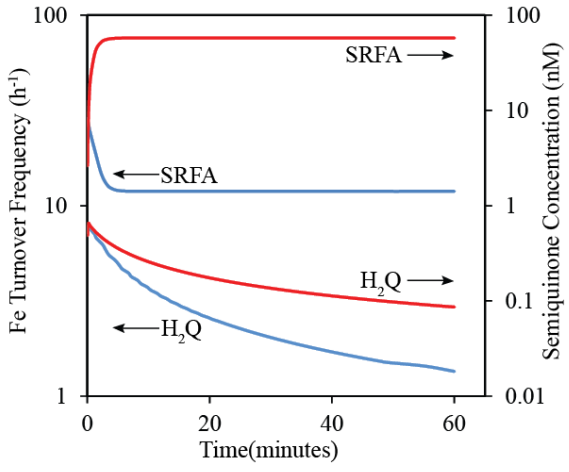

Figure 4.10: Comparison of turnover frequency and semiquinone concentration in air-saturated solution containing SRFA and 1,4-hydroquinone in presence of 100 nM Fe(III) and 2 μM hydroquinone at pH 4.

As noted earlier, quinone moieties are recognized to be responsible, to a large extent, for the redox behavior of natural organic matter (NOM). Indeed, the results presented here showing the interplay between iron and quinone species bear many similarities, as well as some striking differences, to the results of the interaction of Fe(II) and Fe(III) with SRFA in Chapter 3. Of particular note, as shown in Figure 4.10, is the 100- to 1000-fold lower estimated steady-state concentration of the semiquinone radical in solutions of 1,4-hydroquinone compared to those in SRFA solutions containing comparable concentrations of hydroquinone-like moieties. The substantially higher steady-state concentration of the semiquinone in SRFA is most likely a consequence of the ability of the unpaired electron on the semiquinone radical in this large molecule to be stabilized by both delocalization over an array of conjugated aromatic carbons and the presence of electron-donating alkyl groups. The increased stability of semiquinone radicals in SRFA solutions compared to that in pure hydroquinone solution make it a substantially more effective Fe(II) oxidant than is the case in the simpler quinone, with the result that quinone moieties present in SRFA are expected to play a much more important role in Fe redox transformations compared to that of pure hydroquinone solutions. This is reflected in the differences in Fe TOF shown in Figure 4.10, with Fe cycling between the +III and +II oxidation states in SRFA at 10-100 times the rate observed in pure 1,4-hydroquinone solution. Although notable differences are observed between simple hydroquinone and quinone moieties found in SRFA, it is possible that more complex quinone compounds, particularly those with alkyl substitution or those with the potential for a high degree of electron delocalization, may behave in a manner similar to NOM.

We therefore conclude that, while quinone moieties are recognized to be principally responsible for the redox properties of NOM, care should be taken in extrapolating the results observed in pure quinone solutions to the natural aquatic environment. In particular, the unique stability of the semiquinone radical in the highly conjugated and substituted environment of NOM will have strong implications to the rate and extent of metal redox transformations as well as reactive oxygen species generation in natural aquatic systems, with the latter of relevance to both the oxidative degradation of the NOM itself and any other organic compounds associated with it.

Chapter 5. Mechanistic insights into light-mediated iron redox transformations in the SRFA solution under acidic conditions

5.1. Introduction

In Chapter 3, Fe redox transformations in non-irradiated and previously irradiated SRFA solutions were studied in the pH range 3-5, with Fe(III) reduction under these conditions occurring via interaction with hydroquinone-like moieties and semiquinone-like moieties are the main Fe(II) oxidant. In this chapter, Fe redox transformations under irradiated conditions in SRFA solutions in the pH range 3-5 are investigated. In addition to the generation of long-lived organic Fe(II) oxidant (A^-) as described in Chapter 3, other Fe(II) oxidants may also be generated on photolysis of SRFA including reactive oxygen species (ROS: $O_2^{\bullet-}/HO_2^{\bullet}$) (Bielski et al. 1985), hydroxyl radical (Buxton et al. 1988), and $^1O_2$ (Garg et al. 2011a), short-lived oxidizing organic radicals (peroxyl radicals (Khaikin et al. 1996)), excited triplets and organo-peroxides (Chevallier et al. 2004). However the role of these short-lived ROS and organic moieties in Fe transformations under conditions typically encountered in nature is not well-known. Photolysis of NOM can also facilitate Fe(III) reduction via two main pathways: i) reduction of Fe(III) by photochemically-produced superoxide/hydroperoxyl radical ($O_2^-/HO_2^{\bullet}$), i.e. superoxide-mediated iron reduction (SMIR) (Rose and Waite 2005; Rose and Waite 2006; Garg et al. 2007b); and ii) ligand-to-metal charge transfer (LMCT) in photoactive Fe(III) species (Faust and Zepp 1993; Sima and Makaiiova 1997). While SMIR was shown to play a dominant role in Fe(III) reduction at pH 8 (Garg et al. 2011a), its role under acidic conditions is expected to be minor given the short lifetime of superoxide under acidic conditions (Bielski et al. 1985). The importance of LMCT or short-lived organic intermediates in Fe(III) reduction, although suggested previously (Borer et al. 2009), has not been well elucidated under acidic conditions.

The objective of this chapter is to investigate the importance of LMCT and short-lived organic species in Fe redox transformations. Special attention is given to the effect of pH on iron redox transformations in the pH range 3-5. Results on Fe redox transformations, together with the effects of various chemical manipulations on iron transformation kinetics are used to refine a mechanistically-based kinetic model of key processes underlying iron and reactive intermediate transformations under various conditions investigated here.

All experiments were performed in continuously irradiated SRFA solutions (SRFA solutions that were irradiated in the presence Fe). Investigation of Fe redox transformations under continuously irradiated conditions as well as non-irradiated and previously irradiated conditions as investigated in Chapter 3 is required to properly understand (and, potentially predict) the diurnal changes that would be expected to occur in Fe speciation in natural surface waters.

5.2. Experimental methods

Detailed description of reagents and experimental setup is provided in Chapter 2.

5.3. Results and discussion

5.3.1. Fe(III) reduction kinetics in continuously irradiated SRFA solutions

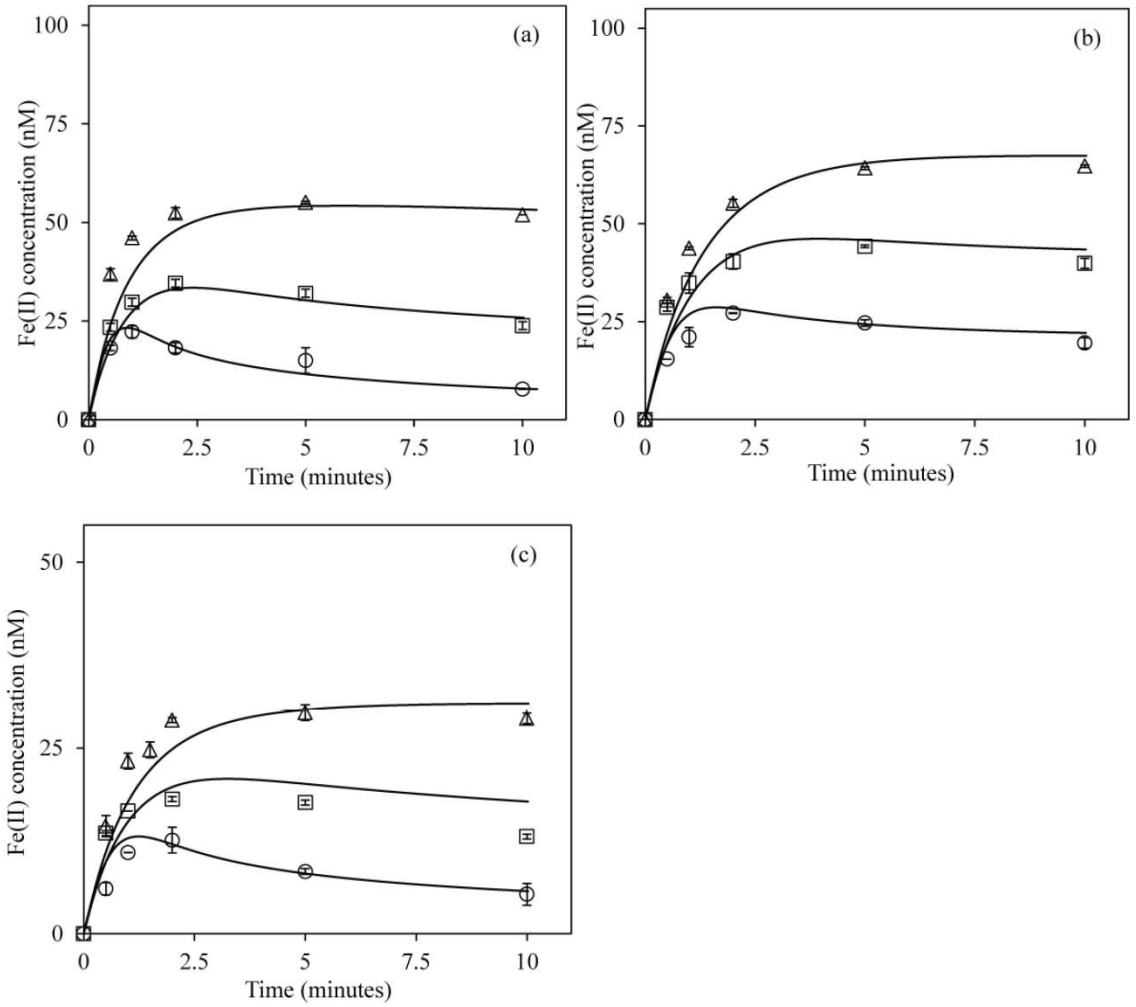

Figure 5.1: (a) Generation of Fe(II) during photochemical reduction of 100 nM Fe(III) in presence of 10 mgL^{-1} irradiated SRFA solutions at pH 3 (triangles) ; 3.5 (squares) and 4 (circles). (b) Generation of Fe(II) on photochemical reduction of 100 nM Fe(III) in presence of 5 mgL^{-1} irradiated SRFA solutions at pH 3 (triangles) , 3.5 (squares) and 4 (circles). (c) Generation of Fe(II) on photochemical reduction of 50 nM Fe(III) in presence of 5 mgL^{-1} irradiated SRFA solutions at pH 3 (triangles) ; 3.5 (squares) and 4 (circles). Symbols represent experimental data (average of duplicate measurements); lines represent model values.

As shown in Figure 5.1, Fe(II) is generated on reduction of Fe(III) in the presence of continuously irradiated SRFA solutions. The Fe(II) concentration generated reaches a peak value within 2 minutes of irradiation and then decreases slowly over time. The peak concentration of Fe(II) generated on Fe(III) reduction decreases and the decay rate of Fe(II) after the peak concentration is attained increases with increase in pH

suggesting that the rate of forward Fe(III) reduction decreases and/or backward Fe(II) oxidation increases with increase in pH. This is consistent with the pH dependence of Fe redox transformations in non-irradiated (Figure 3.1) and previously irradiated (Figure 3.4) SRFA solutions as in Chapter 3. No Fe(II) generation was observed at pH 5 (data not shown) suggesting that the Fe(III) reduction rate is slow and/or Fe(II) oxidation rate is very fast at this pH.

At a particular pH value, the peak concentration of Fe(II) generated increases with increase in Fe(III) concentration however the peak concentration is affected minimally by increase in SRFA concentration. This observed lack of effect may be due to the change in both forward reduction rate of Fe(III) as well backward oxidation rate of any Fe(II) generated with change in SRFA concentration. The decay rate of Fe(II) after the peak value is achieved increases with increase in SRFA concentration which is consistent with the earlier observation regarding Fe(II) oxidation in previously irradiated SRFA solutions (Figure 3.5; Chapter 3).

The initial rate of light-mediated Fe(III) reduction is much faster than that observed in the dark (where Fe(III) is reduced due to the presence of hydroquinone-like moieties intrinsically present in SRFA) which suggests that other processes such as SMIR and LMCT are important under irradiated conditions. The importance of these processes is discussed in detail in later sections.

5.3.2. Fe(II) oxidation in continuously irradiated SRFA solutions

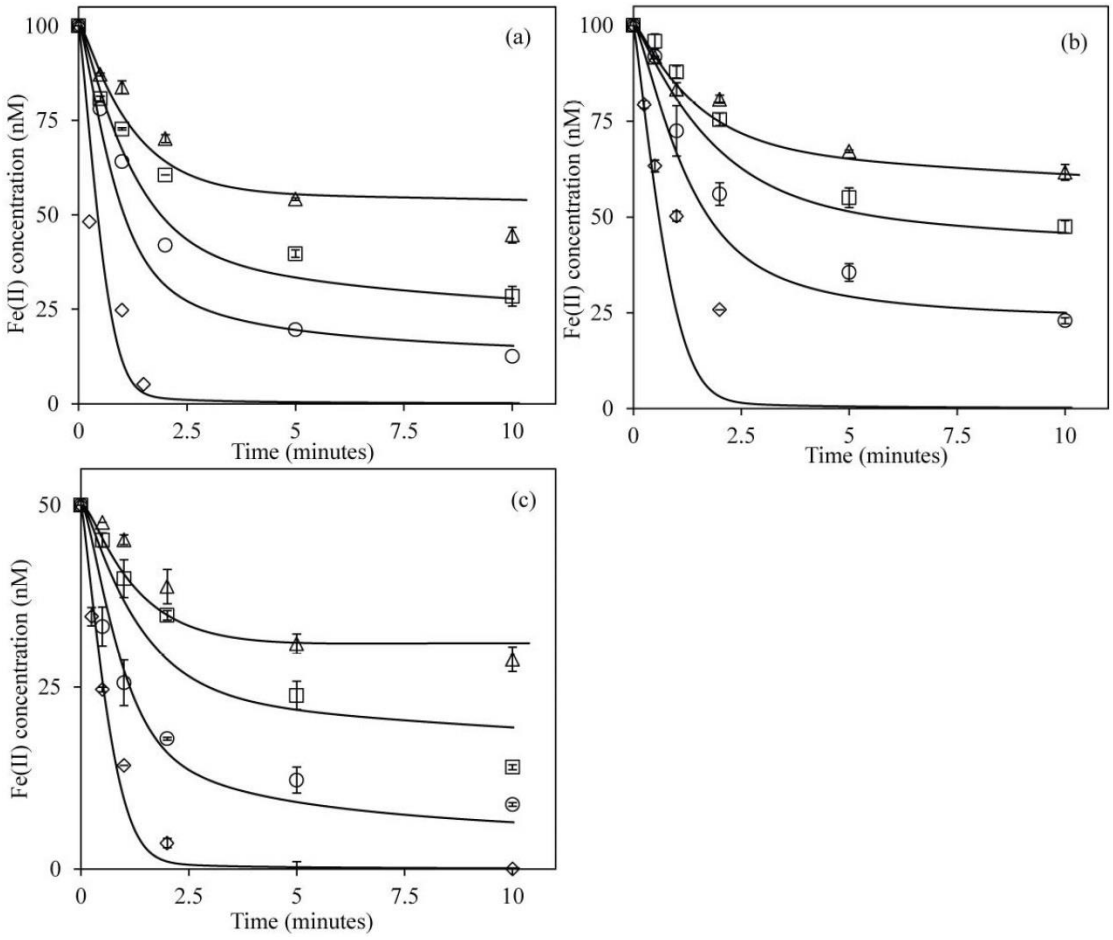

Figure 5.2: Photochemical oxidation of (a) 100 nM Fe(II) in presence of 10 mgL^{-1} SRFA at pH 3 (triangles) ; 3.5 (squares), 4 (circles) and 5 (diamonds). (b) Oxidation of 100 nM Fe(II) in presence of 5 mgL^{-1} SRFA at pH 3 (triangles), 3.5 (squares) , 4 (circles) and 5 (diamonds). (c) Oxidation of 50 nM Fe(III) in presence of 5 mgL^{-1} SRFA at pH 3 (triangles), 3.5 (squares) , 4 (circles) and 5 (diamonds). Symbols represent experimental data (average of duplicate measurements); lines represent model values.

When Fe(II) was added to SRFA solutions and subsequently irradiated, the Fe(II) decay rate increases with increase in pH (Figure 5.2) which is in agreement the observation in previously irradiated solutions (Figure 3.4 and Figure 3.5; Chapter 3), as well as the data shown in Figure 5.1. For a given pH, the Fe(II) decay rate increases with increase in initial SRFA concentration which is also consistent with the data shown in Figure 3.4, Figure 3.5 (Chapter 3) and in Figure 5.1 and supports the conclusion that irradiation of SRFA results in generation of an Fe(II) oxidant. The Fe(II) oxidation rate decreases

over time, which suggests that either the Fe(II) oxidant concentration decreases over time and/or the back reduction of Fe(III) becomes important when significant amounts of Fe(III) are generated. The overall Fe(II) decay rate observed here is faster than that observed in previously irradiated SRFA (Figure 3.5; Chapter 3) suggesting that i) additional short-lived Fe(II) oxidants are generated under continuously irradiated conditions, and ii) these oxidants decay rapidly when the lamp is extinguished and hence do not contribute to Fe(II) oxidation in the dark.

Thus, in summary, hydroquinone-like moieties (that are intrinsically present in SRFA) and semiquinone-like groups (that are formed on oxidation of native hydroquinone group) appear to be the main Fe(III) reductants and Fe(II) oxidants in the dark but, under irradiated conditions, additional pathways for Fe(II) oxidation and Fe(III) reduction exist. The entities responsible for these additional pathways are short-lived and hence become inactive once the lamp is extinguished. Possible additional pathways for Fe(III) reduction include LMCT and SMIR, while possible additional pathways for Fe(II) oxidation include ROS-mediated oxidation and oxidation by short-lived organic species such as peroxyl radicals which are generated via hydroxylation of organic moieties and known to oxidize Fe(II) (Khaikin et al. 1996). It is also possible that reactive semiquinone radicals (distinct from those playing a role in Fe(II) oxidation in previously irradiated SRFA solutions), which rapidly oxidize on reaction with dioxygen, are involved in Fe(II) oxidation but, as shown later, this option is unlikely. Results from other experiments undertaken to assist in identifying the nature and mechanism of generation of various Fe(III) reductants and Fe(II) oxidants that are produced on irradiation of SRFA in the pH range 3-5 are presented below.

5.3.3. Role of superoxide

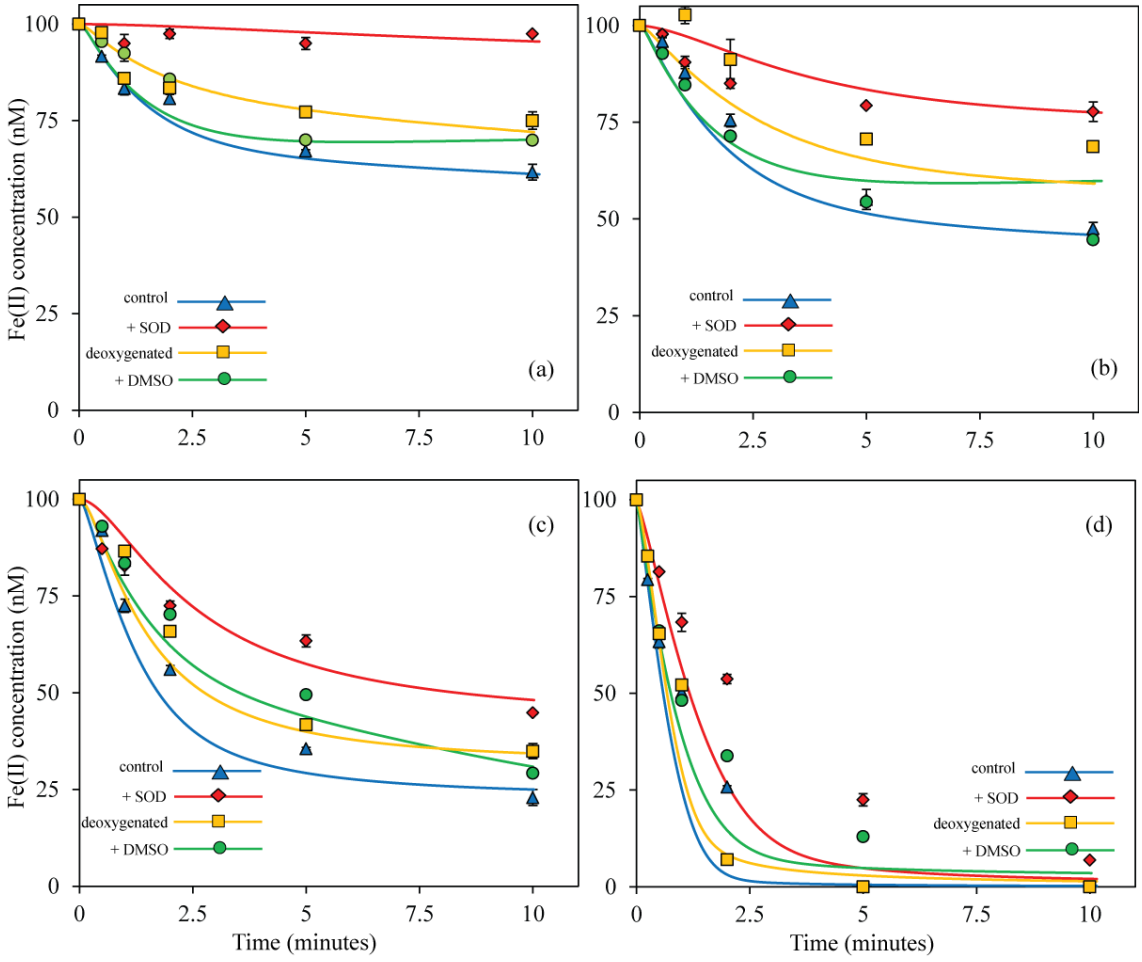

Figure 5.3: Effect of various treatments on Fe(II) concentration remaining after addition of 100 nM Fe(II) to irradiated 5 mg.L^{-1} SRFA solutions at (a) pH 3 b) pH 3.5 (c) pH 4 and (d) pH 5. Error bars represent the standard deviation from duplicate experiments. The effect of SOD addition was modelled by increasing the superoxide disproportionation rate constant to diffusion-limited value. For modelling, no effect of dioxygen removal was assumed on peroxyl radical generation rate since the rate-limiting step in peroxyl radical generation is formation of hydroxylating intermediates. Model results in the presence of DMSO were obtained by neglecting oxidation of Fe(II) by peroxyl radicals.

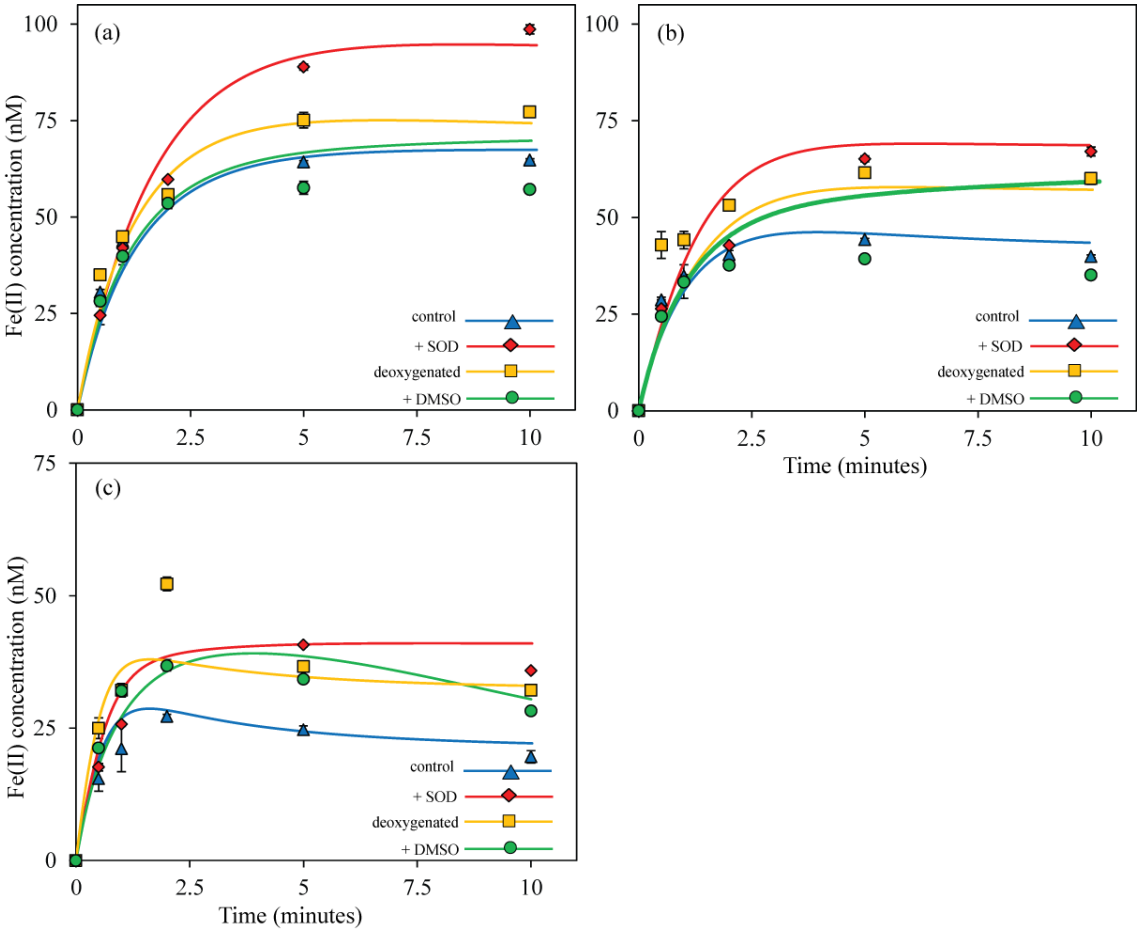

Figure 5.4: Effect of various treatments on Fe(II) concentration formed on addition of 100 nM Fe(III) to irradiated 5 mg.L^{-1} SRFA solutions at (a) pH 3 b) pH 3.5 and (c) pH 4. Error bars represent the standard deviation from duplicate experiments. The effect of SOD addition was modelled by increasing the $O_2^{\bullet-}$ disproportionation rate constant to diffusion-limited value. For modelling, no effect of dioxygen removal was assumed on peroxyl radical generation rate since the rate-limiting step in peroxyl radical generation is formation of hydroxylating intermediates. Model results in the presence of DMSO were obtained by neglecting oxidation of Fe(II) by peroxyl radicals.

In continuously irradiated SRFA solutions, addition of SOD resulted in a decrease in the Fe(II) oxidation rate (Figure 5.3) and an increase in the Fe(III) reduction rate (Figure 5.4) supporting involvement of superoxide in Fe redox transformations either directly or indirectly at all the pH values investigated here. Fe(II) oxidation is completely inhibited at pH 3 with concomitant reduction of all added Fe(III) in the presence of SOD with this result confirming that Fe(III) reduction by hydroquinone-like moieties that are intrinsically present is not important at pH 3 (at least on the time scale used here). If any

Fe(III) reduction had occurred by this pathway then back-oxidation of Fe(II) by semiquinone-like moieties would also occur with steady-state Fe(II) concentration lower than the total Fe concentration; a result which is not consistent with the observation. Furthermore, direct reduction by superoxide is also not important at pH 3 because addition of SOD should inhibit this process. Thus, it appears that at pH 3, Fe(III) reduction occurs principally via LMCT under continuously irradiated conditions. Furthermore, since addition of SOD completely inhibits Fe(II) oxidation at pH 3, we suggest that either semiquinone-like moieties, which are generated on superoxide-mediated oxidation of hydroquinone, or superoxide is the main Fe(II) oxidant at pH 3. At other pHs, addition of SOD inhibited Fe(II) oxidation with concomitant increase in Fe(II) generated on Fe(III) reduction in continuously irradiated SRFA solutions though the decrease in rate of Fe(II) oxidation was not more than 30%. This observation suggests that other Fe(II) oxidants must be generated via non-$HO_2^{\bullet}$ mediated pathways with these oxidants inducing Fe(II) oxidation even when SOD is absent.

Since SOD addition increased the Fe(III) reduction rate in continuously-irradiated SRFA solutions, SMIR can be disregard as the main pathway for Fe(III) reduction under acidic conditions. This is reasonable given that $HO_2^{\bullet}$ is very short-lived under these conditions (Bielski et al. 1985).

5.3.4. Role of dioxygen

In order to further verify the role of superoxide, the rates of Fe(II) oxidation and Fe(III) reduction were measured when Fe(II) or Fe(III) were added to continuously irradiated solutions of 5 $mg.L^{-1}$ SRFA that were partially deoxygenated prior to irradiation. Because superoxide is generated by the reduction of dioxygen, it is expected that partially removal of dioxygen have similar effect as the addition of SOD. As shown in

Figure 5.3 and Figure 5.4, a 0decrease in O_2 concentration resulted in a decrease in the Fe(II) oxidation rate and an increase in Fe(III) reduction rate at all pHs investigated. This observation can be ascribed to decreased generation of the Fe(II) oxidant in the deoxygenated solutions, which suggests that O_2 is required for the generation of the Fe(II) oxidant. This is consistent with the observation in the presence of SOD, suggesting that superoxide is either directly and/or indirectly (via generation of A^-) is involved in Fe(II) oxidation, which is inhibited in the absence of dioxygen.

5.3.5. Effect of DMSO

As discussed above, a short-lived Fe(II) oxidant appears to be generated in continuously irradiated SRFA solutions. Although the exact identity of this Fe(II) oxidant is not known, peroxyl radicals are a possibility since these radicals are formed primarily via hydroxylation of organic moieties (von Sonntag and Schuchmann 1991). Another possibility is that reactive short-lived semiquinone radicals (distinct from the long-lived semiquinones playing a key role in Fe(II) oxidation in previously irradiated SRFA solutions), are formed on light-mediated reduction of quinone moieties via formation of a hydroxylating intermediate (e.g. a quinone-water exciplex), with these short-lived semiquinones capable of oxidizing Fe(II) but which rapidly decay on reaction with dioxygen in the absence of Fe(II). This possibility seems unlikely however since removal of dioxygen should increase the concentration of these short-lived semiquinone radicals, thereby resulting in faster Fe(II) oxidation rates; a deduction which is not consistent with the observations (Figure 5.3 and Figure 5.4). The importance of these short-lived radicals in Fe redox transformations is investigated using DMSO which acts as the scavenger for hydroxyl radicals or hydroxylating intermediates. No interaction between DMSO and Fe (either as Fe(II) or Fe(III); data not shown) was observed in the

absence of SRFA confirming that any effect of DMSO addition on Fe redox transformations was due to interaction between DMSO and SRFA.

In comparison, in irradiated SRFA solutions, addition of DMSO inhibited Fe(II) oxidation (Figure 5.3) while increasing the concentration of Fe(II) generated on Fe(III) reduction (Figure 5.4) in irradiated SRFA solutions for pH > 3.5. This observation supports the involvement of peroxyl radicals in Fe(II) oxidation in irradiated SRFA solutions of pH > 3.5. The lack of a measureable effect of DMSO addition on Fe(II) oxidation and Fe(III) reduction at pH 3 and 3.5 suggests that peroxyl radicals are not involved in Fe(II) oxidation at pH 3 and 3.5 which is consistent with the earlier observations regarding the effect of SOD (Figure 5.3 and Figure 5.4) suggesting that Fe(II) oxidation at pH 3 mostly occurs via interaction with superoxide and/or semiquinone-like moieties. Although, some (~ 20%) oxidation of Fe(II) was observed in the presence of SOD at pH 3.5 (Figure 5.3), it is possible that low concentration of semiquinone-like moieties and/or superoxide exist even in the presence of SOD and contribute to the observed Fe(II) oxidation at this pH.

5.3.6. Kinetics and mechanism of Fe redox transformations

Based on the discussion presented above, Fe(III) reduction under irradiated conditions mainly occur via LMCT while Fe(II) oxidation occurs, for the most part, via interaction with superoxide and a short-lived radical which, while its precise identity is unclear, is generated via a pathway involving hydroxyl radicals or a hydroxylating intermediate. Schematics of these key processes that are involved in Fe transformations are shown in Figure 5.5 and a kinetic model consistent with these schematics is shown in Table 5.1. Key reactions (reaction 1-14; Table 3.3) in non-irradiated and previously irradiated solutions have been described as in Chapter 3. A brief summary of other reactions in

continuously irradiated solutions together with justification of the rate constants used and pH dependence of these rate constants is provided below.

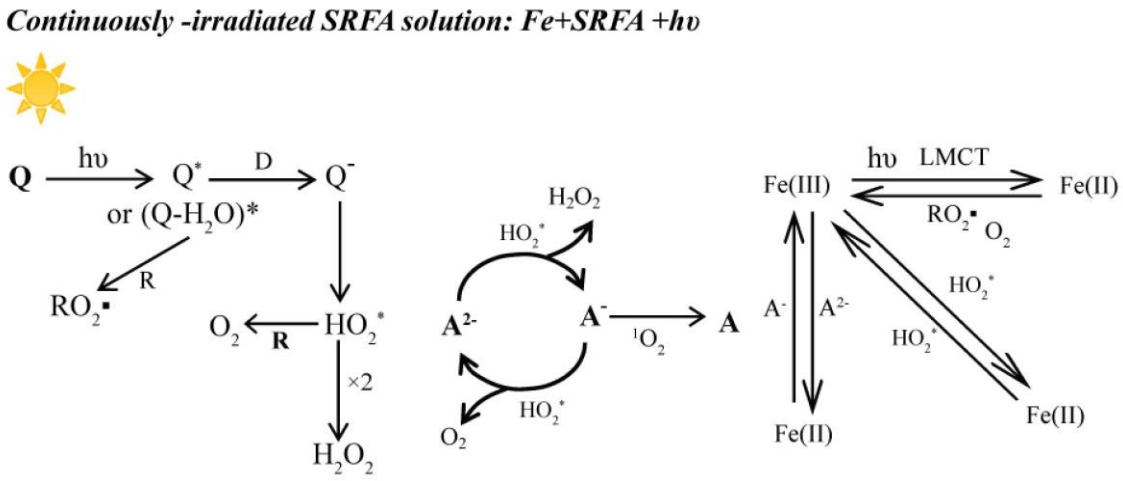

Figure 5.5: Reaction schematic showing Fe redox transformations as well as generation of various ROS and redox-active organic radicals from SRFA under continuously irradiated conditions at pH 3-5.

Table 5.1: Kinetic model for generation of Fe(II) oxidant on photolysis of SRFA solutions.

No.	Reaction	Model Value	Published value	Reference
	Generation and Consumption of ROS ($^1O_2$, $HO_2^\bullet$, and H_2O_2 on irradiation)			
1	$SRFA + h\nu \longrightarrow SRFA^*$	Calculated		(Paul et al. 2004)
	$SRFA^* + {}^3O_2 \longrightarrow SRFA + {}^1O_2$	$\Phi \sim 0.5\%$	$\Phi \sim 0.5\%$	
2	$^1O_2 \xrightarrow{H_2O} {}^3O_2$	2.4×10^5 s^{-1}	2.4×10^5 s^{-1}	(Dalrymple et al. 2010)
3	$Q + h\nu \longrightarrow Q^-$	6×10^{-5} s^{-1}[a]	-	
4	$Q^- + {}^3O_2 \longrightarrow Q + HO_2^\bullet$	1×10^9 $M^{-1}s^{-1}$	1×10^9 $M^{-1}s^{-1}$	(Zhang et al. 2012)
5	$Q^- \longrightarrow Q$	5.8×10^3 s^{-1}	-	
6	$HO_2^\bullet + HO_2^\bullet \longrightarrow O_2 + H_2O_2$	$\frac{k_{HO_2^\bullet} + k_{O_2^{\bullet-}}\left(K_{HO_2^\bullet}/[H^+]\right)}{\left(1+\left(K_{HO_2^\bullet}/[H^+]\right)\right)^2}$ [b]	$\frac{k_{HO_2^\bullet} + k_{O_2^{\bullet-}}\left(K_{HO_2^\bullet}/[H^+]\right)}{\left(1+\left(K_{HO_2^\bullet}/[H^+]\right)\right)^2}$	(Bielski et al. 1985)
7	$R + h\nu \longrightarrow R^\bullet$	7.5×10^{-6} s^{-1}[c]	6×10^{-6} s^{-1}	(Garg et al. 2011b)

8	$R^{\bullet} + HO_2^{\bullet} \longrightarrow R^{-} + O_2 + H^{+}$	$\frac{k_1^{'} + k_2^{'}\left(K_{HO_2^{\bullet}}/[H^{+}]\right)}{\left(1+\left(K_{HO_2^{\bullet}}/[H^{+}]\right)\right)}$ [d]	-	
9	$R^{\bullet} + R^{\bullet} \longrightarrow R_2$	1×10^3 $M^{-1}s^{-1}$	1×10^3 $M^{-1}s^{-1}$	(Garg et al. 2011b)
	Transformation of hydroquinone-like and semiquinone-like moieties on irradiation			
10	$A^{2-} + HO_2^{\bullet} \xrightarrow{2H^{+}} A^{-} + H_2O_2$	k_{10}/k_{11}= -5.7 E_H^0 +2.5 [e]	~ 1×10^5 $M^{-1}s^{-1}$	(Roginsky and Barsukova 2000)
11	$A^{-} + HO_2^{\bullet} \longrightarrow A^{2-} + O_2$	2.5×10^5 $M^{-1}s^{-1}$	2.5×10^5 $M^{-1}s^{-1}$	(Garg et al. 2013a)
12	$A^{-} + {}^1O_2 \longrightarrow A + HO_2^{\bullet}$	1.5×10^8 $M^{-1}s^{-1}$	1.5×10^8 $M^{-1}s^{-1}$	(Garg et al. 2013a)
	Fe redox transformations under non-irradiated condition			
13	$Fe(III)+A^{2-} \longrightarrow Fe(II)+A^{-}$	3.5×10^3 $M^{-1}s^{-1}$ [f]	4×10^3 $M^{-1}s^{-1}$	(Garg et al. 2013a)
14	$Fe(II)+A^{-} \longrightarrow Fe(III)+A^{2-}$	$\frac{k_{HA} + k_{A^-}\left(K_{HA}/[H^{+}]\right)}{(1+K_{HA}/[H^{+}])}$ [g]	-	
	Generation of short-lived Fe(II) oxidant on irradiation			
15	$R + h\nu \xrightarrow{O_2, OH^{\bullet}} RO_2^{\bullet}$	1.8-3 × 10^{-6} s^{-1} [f]	-	

16	$RO_2^{\bullet} + RO_2^{\bullet} \longrightarrow RO_4R$	1×10^4 $M^{-1}s^{-1}$	10^5-10^6 $M^{-1}s^{-1}$	(Neta et al. 1990)
17	$RO_2^{\bullet} \longrightarrow R^{\bullet+} + HO_2^{\bullet}$	1×10^{-3} s^{-1}	< 3 s^{-1}	(Neta et al. 1990)
	Fe redox transformations under irradiated condition			
18	$Fe(II)+RO_2^{\bullet} \longrightarrow Fe(III)+RO_2H$	1×10^7 $M^{-1}s^{-1}$	10^5- 10^7 $M^{-1}s^{-1}$	(Khaikin et al. 1996)
19	$Fe(III) \xrightarrow{h\upsilon} Fe(II)$	1×10^{-2} s^{-1}[f]	-	
20	$Fe(II) + HO_2^{\bullet} \longrightarrow Fe(III) + H_2O_2$	$\frac{k_{19}^{HO_2^{\bullet}} + k_{19}^{O_2^{\bullet-}}\left(K_{HO_2^{\bullet}}/[H^+]\right)}{(1+K_{HO_2^{\bullet}}/[H^+])}$ [h]	$\frac{k_{19}^{HO_2^{\bullet}} + k_{19}^{O_2^{\bullet-}}\left(K_{HO_2^{\bullet}}/[H^+]\right)}{(1+K_{HO_2^{\bullet}}/[H^+])}$	(Rush and Bielski 1985)
21	$Fe(III) + HO_2^{\bullet} \longrightarrow Fe(II) + O_2$	1×10^5 s^{-1}	1×10^5 s^{-1}[i]	(Garg et al. 2011a)

[a] pseudo-first order rate constant based on $[Q]_T$ = 0.67 mmol.g^{-1} SRFA where Q represents electron accepting quinone moieties in humic and fulvic acids as reported earlier (Aeschbacher et al. 2010); varies slightly with pH

[b] See (Bielski et al. 1985) for definition of $k_{HO_2^{\bullet}}$ and $k_{O_2^{\bullet-}}$; $k_{HO_2^{\bullet}}$ = 8.3×10^5 $M^{-1}s^{-1}$, $k_{O_2^{\bullet-}}$ = 9.7×10^7 $M^{-1}s^{-1}$ and $K_{HO_2^{\bullet}}$ = $10^{-4.8}$

[c] pseudo-first order rate constant based on $[R]_T$ = 44 mmol.g^{-1} SRFA (Goldstone et al. 2002); R represents the bulk organic concentration in SRFA.

[d] See text for definition of $k_1^{'}$ and $k_2^{'}$; $k_1^{'}$ = 3.5×10^4 $M^{-1}s^{-1}$, $k_2^{'}$ = 1.6×10^5 $M^{-1}s^{-1}$ and $K_{HO_2^{\bullet}}$ = $10^{-4.8}$

[e] k_{10} and k_{11} in the range 1×10^4 $M^{-1}s^{-1}$ - 1×10^6 $M^{-1}s^{-1}$ will fit the data as long as the ratio k_{10}/k_{11} is as defined by E_H^0

[f] based on best-fit model results

[g] k_{14} was calculated using the ratio k_{13}/k_{14} shown in Chapter 3; k_{14} was then determined as function of $[H^+]$ assuming that variation in speciation of A^- changes k_{18} with pH; k_{HA} = 4.5×10^3 $M^{-1}s^{-1}$, k_{A^-} = 1.5×10^5 $M^{-1}s^{-1}$ and K_{HA} = 10^{-4}

[h] k_{20} was determined as function of $[H^+]$ assuming that variation in speciation of superoxide changes k_{19} with pH; $k_{20}^{HO_2^\bullet} = 1.2\times10^6\ M^{-1}s^{-1}$, $k_{20}^{O_2^{\bullet-}} = 1.0\times10^7\ M^{-1}s^{-1}$ and $K_{HO_2^\bullet} = 10^{-4.8}$

[i] reported value at pH 8

5.3.6.1. Generation of short-lived Fe(II) oxidant ($RO_2^{\bullet}$)

As shown in reaction 15 (Table 5.1), generation of $RO_2^{\bullet}$ occurs on photolysis of SRFA via interaction between hydroxylating intermediates and dioxygen. Based on the experimental data, the contribution of $RO_2^{\bullet}$-like radicals to Fe(II) oxidation increases with increase in pH (as indicated by the more pronounced effect of DMSO at higher pHs; see Figure 5.4) which suggests that either the $RO_2^{\bullet}$ generation rate varies with pH and/or the rate constant for oxidation of Fe(II) by peroxyl radicals increases with increase in pH. The oxidation rate constant of Fe(II) by peroxyl radicals (reaction 18; Table 5.1) is assumed to be pH independent since oxidation of Fe^{2+} by peroxyl radicals takes place by an inner-sphere mechanism controlled by the rate of dissociative interchange of the water ligand (Khaikin et al. 1996)- a process which is expected to be pH-independent. Thus, the variation in rate of Fe(II) oxidation by peroxyl radicals with change in pH was assumed to be due to a change in the concentration of peroxyl radicals generated on SRFA photolysis (reaction 15; Table 5.1). The increased generation of peroxyl radicals with pH possibly occurs due to increased generation of hydroxylating intermediates though the exact reason is not known. However, this possibility appears most consistent with the experimental observations. The rate constant for bimolecular (reaction 16; Table 5.1) and unimolecular decay (reaction 17; Table 5.1) of peroxyl radicals were assumed to be pH-independent, however these rate constants are not well constrained by the experimental results with various values possible with suitable adjustments to peroxyl radical generation rate (reaction 15; Table 5.1).

5.3.6.2. LMCT mediated Fe(III) reduction

A rate constant of 1×10^{-2} s^{-1} was determined for LMCT-mediated Fe(III) reduction (reaction 19; Table 5.1) based on best fit to the experimental data (Figure 5.1 and Figure 5.2) and is well constrained by the data. The best-fit rate constant is pH-independent in accord with the presumed negligible change in speciation of the Fe(III)-SRFA complex over the pH range investigated.

5.3.6.3. Superoxide mediated oxidation of Fe(II) in continuously irradiated SRFA solutions

Fe(II) may also be oxidized by superoxide (reaction 20; Table 5.1) with the rate constant for this reaction varying with pH due to the difference in reactivity of $O_2^{\bullet-}$ and $HO_2^{\bullet}$ as described earlier (Rush and Bielski 1985).

$$k_{20}^{app} = \alpha_0 k_{20}^{HO_2^{\bullet}} + \alpha_1 k_{20}^{O_2^{\bullet-}} \quad (5.1)$$

where $\alpha_0 = \frac{[H^+]}{[H^+] + K_{HA}}$ and $\alpha_1 = 1 - \alpha_0$; k_{20}^{app} represents the overall oxidation rate of Fe(II) by superoxide; $k_{20}^{HO_2^{\bullet}} = 1.2 \times 10^6$ $M^{-1}s^{-1}$, $k_{20}^{O_2^{\bullet-}} = 1.0 \times 10^7$ $M^{-1}s^{-1}$ and $K_{HO_2^{\bullet}} = 10^{-4.8}$.

5.3.6.4. SMIR mediated Fe(III) reduction

Although the experimental results show that SMIR is not important at low pH, a small portion of Fe(III) can be reduced via SMIR (reaction 21; Table 5.1) and thus is included in the model. The rate constant for reduction of the Fe(IIII)SRFA complex was assumed to be pH independent and was assumed to be same as that reported at pH 8 (Garg et al. 2011a). This rate constant is not well constrained by the experimental given that SMIR is unimportant under the conditions investigated here.

5.3.6.5. Diel variation in Fe redox transformations

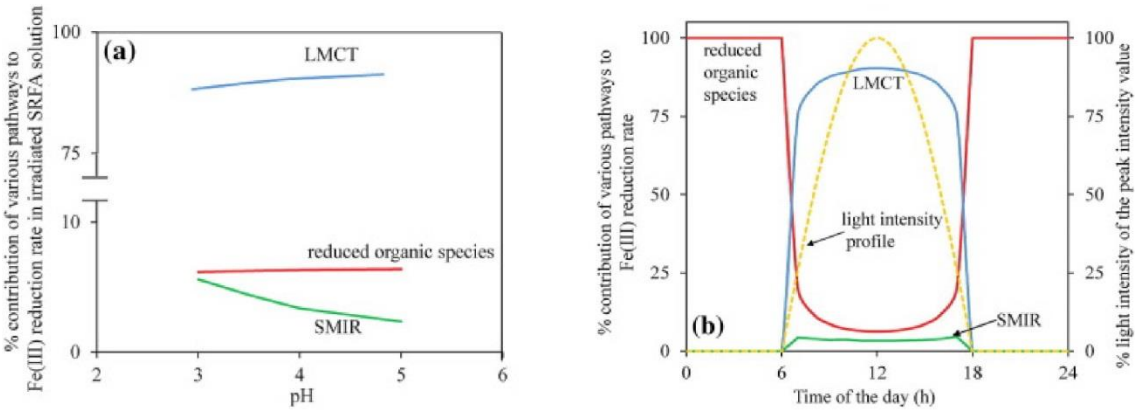

Figure 5.6: Contribution of various pathways to Fe(III) reduction as function of (a) pH and (b) time of the day. The solid points (circles) and solid lines represent the data measured/predicted based on kinetic model developed in this chapter. Panel (b) shows the contribution of various Fe(III) reduction pathways at pH 4 subject to a sinusoidal variation in sunlight intensity.

Using the kinetic model developed here, the contribution of various pathways involved in Fe(III) reduction to overall Fe(III) reduction rates can also be determined. While LMCT, reaction with reduced organic species and SMIR all contribute to photochemical Fe(III) reduction in the presence of SRFA under acidic conditions, LMCT contribution dominates accounting for more than 75% of the Fe(III) reduction observed for all pH conditions investigated here (see Figure 5.6). Although SMIR play a minor role under acidic conditions, its contribution will increase under alkaline conditions since superoxide is longer-lived at higher pHs. Indeed, the earlier work by Garg and co-workers (Garg et al. 2011a) at pH 8 showed that SMIR play a much more important role in photo generation of Fe(II) than LMCT. As expected, diel variation in the proportional contribution of the various Fe(III) reduction pathways is evident with LMCT being the most important pathway during the daytime while reaction with reduced organic species is important in the dark (Figure 5.6).

Finally, it is worth noting that iron continually cycles between +2 and +3 oxidation states under both dark and light conditions with the rate of cycling (or turnover

frequency) considerably higher under continuously irradiated conditions than either non-irradiated or previously irradiated conditions. The turnover frequency (TOF) can be deduced from the experimental data obtained and the kinetic model developed here. Utilizing the knowledge of the Fe(III) reduction rates, the TOF can be defined as:

$$\text{TOF} = \frac{\text{Fe(III) reduction rate}}{\text{Total Fe concentration}} \tag{5.2}$$

Note that, provided the system is at steady state, Fe(III) reduction rate should be equal to the Fe(II) oxidation rate.

Under non-irradiated conditions,

$$\text{Fe(III) reduction rate} = k_1[\text{Fe(III)}]_{ss}[A^{2-}]_{ss} = k_1(\text{Fe}_0\text{-}[\text{Fe(III)}]_{ss})(A_0\text{-}[\text{Fe(II)}]_{ss}) \tag{5.3}$$

Where k_1 = 3.5 × 10^3 $M^{-1}s^{-1}$, Fe_0 and A_0 represent the initial Fe(III) and A^{2-} concentration respectively. The $[Fe(II)]_{ss}$ values are shown in Table 3.1.

Under irradiated conditions,

$$\text{Fe(III) reduction rate} = k_{LMCT}[\text{Fe(III)}]_{ss} = k_{LMCT}(\text{Fe}_0\text{-}[\text{Fe(II)}]_{ss}) \tag{5.4}$$

Where k_{LMCT} = 1 × 10^{-2} s^{-1}, Fe_0 represent the initial Fe(III) and $[Fe(II)]_{ss}$ was determined from Figure 5.1.

The calculated turnover frequencies under non-irradiated conditions are shown in Table 3.1. As shown the turnover frequency increases with increase in pH due to faster Fe(II) oxidation kinetics at higher pH values. Slightly higher turnover frequencies were obtained under previously irradiated conditions than non-irradiated conditions in

view of the increased concentration of oxidant (A^{-1}) with values of 2.1, 2.7 and 3.0 h^{-1} deduced for 10 $mg.L^{-1}$ SRFA solutions at pH 3, 3.5 and 4 respectively. The turnover frequency in continuously irradiated solution also increases with increase in pH and, as noted above, is much higher than that observed under dark conditions with TOFs of 17.3, 27.4 and 33.2 h^{-1} at pH 3, 3.5 and 4 respectively in 10 $mg.L^{-1}$ irradiated SRFA solutions.

5.4. Conclusions

A quite different set of processes contribute to Fe transformations on continuous photolysis compared to those occurring in the dark (with or without pre-photolysis). In particular, short-lived radicals (most likely peroxyl radicals) drive Fe(II) oxidation in the light while LMCT processes appear to dominate Fe(III) reduction at the low pHs examined here. In all cases, Fe species undergo continual cycling between Fe(II) and Fe(III) oxidation states. Fe transformations are considerably more dynamic in the light than in the dark with Fe(II)-Fe(III) turnover frequencies in the presence of 10 $mg.L^{-1}$ SRFA of 17.3, 27.4 and 33.2 h^{-1} at pH 3, 3.5 and 4 on continuous photolysis compared to turnover frequencies of 1.9, 2.5 and 2.9 h^{-1} at pH 3, 3.5 and 4 in the dark.

Overall, the results in this chapter provide insight into the mechanism(s) for generation of various organic and reactive oxygen species involved in Fe redox transformations in the presence of SRFA. This chapter also demonstrates the relative importance of various pathways for photochemical Fe(III) reduction and Fe(II) oxidation in sunlit waters under acidic conditions typical of acid mine drainage, acid sulfate soils and atmospheric aerosols.

Chapter 6. Iron redox transformations in the presence of natural organic matter under acidic conditions: effect of calcium

6.1. Introduction

We have investigated the effect of pH, NOM and light on iron redox transformations in Chapter 3 and 5 and, in this Chapter, extend our examination to the effect of the presence of calcium on these critical processes. The concentration of calcium varies widely in natural waters ranging from 0.4 mM in river water (Livingstone 1963) to 10.3 mM in seawater (Wilson 1975). Although calcium is redox-inert, there are several reports of this element playing a role in redox transformations of metals such as iron and copper (Garg et al. 2007a; Fujii et al. 2008; Stewart et al. 2011; Fujii et al. 2015). The presence of calcium may affect iron redox transformations by competing with iron for the complexation sites on NOM thereby affecting the speciation of iron (Fujii et al. 2008). Fujii and co-workers have reported that the presence of divalent metals (Me) such as Ca and Mg affect the kinetics of complexation of Fe(III) by a variety of organic ligands including fulvic acids, citrate and ethylenediaminetetraacetic acid (EDTA) (Fujii et al. 2008). The presence of Me at concentrations comparable to EDTA retarded the rate of Fe(III)EDTA complex formation significantly; however, in the presence of fulvic acids, the impact of Me is observed only when their concentration is at least 10-fold higher than the fulvic acid concentration (Fujii et al. 2008). The impact of Ca on the complexation of Fe may also alter the Fe(II) oxidation kinetics. As described by Pham and Waite (Pham and Waite 2008a), the second order rate constant for oxidation of organically-complexed Fe(II) is affected by the stability constant of the Fe(III)L and Fe(II)L complexes with an increase in the $K_{\mathrm{Fe(III)L}} / K_{\mathrm{Fe(II)L}}$ value resulting in an increase in the Fe(II) oxidation rate constant. Thus, the change in the stability constant of the Fe-SRFA complex on Ca addition may also impact the Fe(II) oxidation rate. In addition to affecting the Fe(II) oxidation kinetics, these divalent metals are also reported to impact the photochemical reduction rate of organically complexed Fe(III), especially in the

presence of EDTA (Fujii et al. 2015). The photochemical reduction of Fe(III)EDTA is promoted via adjunctive association of Me (including Ca and Mg) with Fe(III)EDTA forming a more photolabile ternary-complex of the form Fe(III)EDTA-Me (Fujii et al. 2015). However, the impact of Ca addition on the rate of Fe(III) reduction has previously been reported to be minor in the presence of fulvic acids (Fujii et al. 2015). The addition of Ca also increased the rate of superoxide-mediated reduction of Fe(III) complexed to organic ligands such as EDTA and 3,4-dihydroxybenzoic acid under circumneutral pH conditions (Garg et al. 2007a).

Interaction of calcium with hydroquinone-like and semiquinone-like moieties present in SRFA may also influence iron transformations (Hering and Morel 1988; Hong and Elimelech 1997; Jezierski et al. 2000; Jerzykiewicz et al. 2002) given their important role in Fe redox transformations in SRFA solutions. As reported earlier, the reduction of Fe(III) by organic moieties such as catechol, catechin or sinapic acid are affected by their interaction with Ca and Mg (Santana-Casiano et al. 2010; Santana-Casiano et al. 2014). These divalent metal ions are reported to stabilize semiquinone radicals within humic structures by creating bridging interactions and by inducing intramolecular aggregation (Yates and von Wandruszka 1999; Palmer and von Wandruszka 2001; Bakajová and Von 2011). Calcium ions have also been reported to have an effect on the redox reactions of quinoid compounds as a result of alteration in both the acid-base properties of hydroquinone moieties and the redox potential of quinone/semiquinone or semiquinone/hydroquinone redox couples due to stabilization of semiquinone radicals (Eaton 1964; Lebedev et al. 2003; Alegría et al. 2004).

In this chapter, the effect of calcium addition on iron redox transformations in SRFA solutions is investigated under acidic conditions. As described in Chapter 3 and 5, the impact of Ca addition on Fe redox transformations is investigated under three

conditions: non-irradiated, previously irradiated (i.e. SRFA solutions that were irradiated for 10 minutes prior to Fe addition in the dark) and continuously irradiated Fe-containing SRFA solutions. As described in Chapter 3 and 5, the results of experiments performed under dark conditions provide insight into the impact of stable organic moieties naturally present in SRFA on Fe redox transformations. The results of experiments performed in the presence of previously irradiated SRFA and continuously irradiated SRFA solutions describes the role of any photo-generated long- and short-lived organic moieties, respectively, in Fe redox transformations.

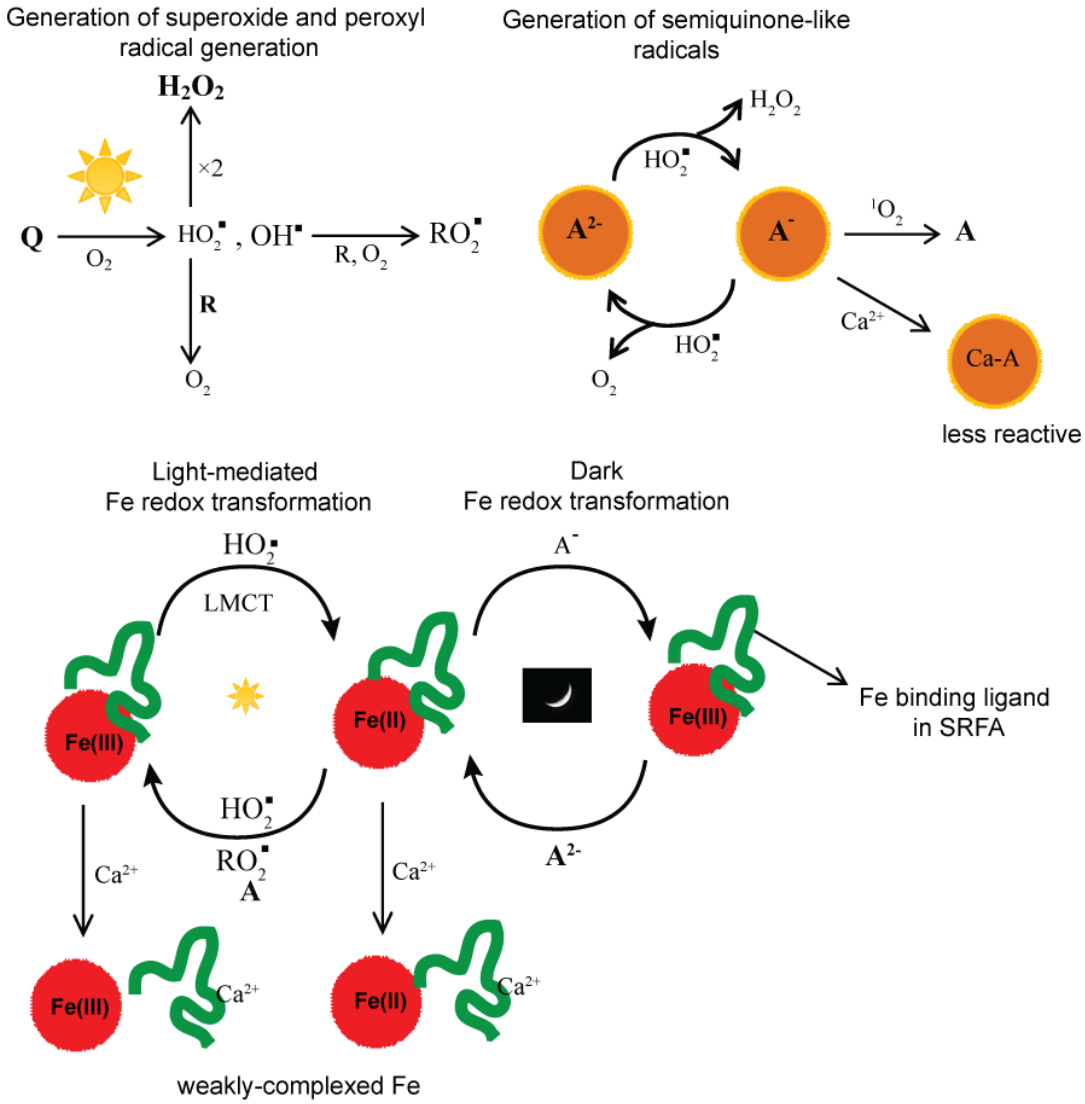

Figure 6.1: Reaction schematic showing redox transformations of Fe under various conditions.

A reaction schematic is shown in (Figure 6.1) highlighting important mechanism controlling Fe redox transformations in the absence Ca in acidic conditions based on the observations in Chapter 4 and 5. On the basis of knowledge available in the existing literature, schematics of the various processes via which Ca can interact with Fe and/or organic moieties present in SRFA are also presented in (Figure 6.1). These processes in detail in accordance with our experimental results are discussed in the following sections.

6.2. Experimental methods

Detailed description of reagents and experimental setup is provided in Chapter 2.

6.3. Results and discussion

6.3.1. Fe redox transformations in non-irradiated SRFA solutions in the presence of Ca^{2+} in the pH range of 3-5

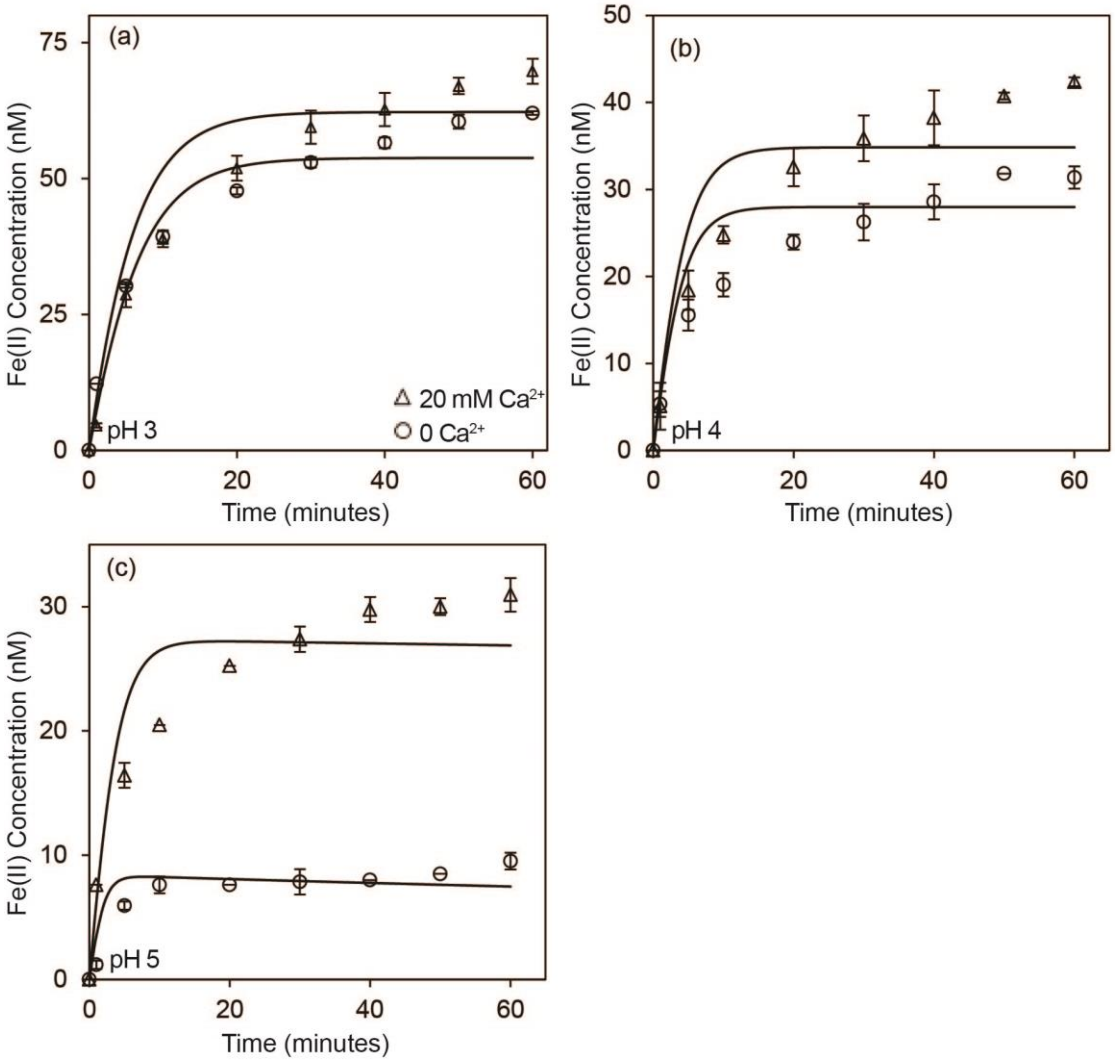

Figure 6.2: Generation of Fe(II) as a result of reduction of 100 nM Fe(III) in 10 $mg.L^{-1}$ SRFA solutions containing 0 (circles) and 20 mM (triangles) Ca^{2+} in the dark at pH 3 (panel a), pH 4 (panel b) and pH 5 (panel c). Symbols represent the average of duplicate measurements; lines represent model values.

As shown in Figure 6.2, Fe(II) concentration increased as a result of reduction of Fe(III) by reducing moieties (A^{2-}) present in SRFA in the pH range of 3-5 with the concentration of Fe(II) generated increasing in the presence of 20 mM Ca^{2+}. Thus, it was concluded that the addition of Ca^{2+} either increases the Fe(III) reduction rate and/or

decreases the Fe(II) oxidation rate. Comparing the Fe(II) generation rate in the absence and presence of Ca^{2+}, the % increase in the Fe(II) generation rate in the presence of Ca^{2+} increases from 12.3% to 173.3% with an increase in pH from 3 to 5 (Figure 6.2), which is consistent with the observed increase in Fe(II) oxidation rate with increasing pH in Chapter 3. The Fe(III) reduction rate by SRFA in acidic solution was shown to be independent of pH in Chapter 3. The Fe(III) reduction rate (as determined from the measured initial Fe(II) generation rate; Figure 6.2) is also independent of pH in the presence of Ca^{2+} with very similar Fe(III) reduction rates ($p > 0.05$) observed in the pH range of 3-5 (Table 6.1). The observed pH-dependence of the impact of Ca^{2+} thus supports the conclusion that the effect of Ca^{2+} addition on the Fe(II) oxidation rate is more substantive than the effect of Ca^{2+} addition on Fe(III) reduction rate in non-irradiated SRFA solutions. The decrease in Fe(II) oxidation rate may occur as a result of a decrease in the reactivity of the species involved (i.e. Fe(II) and semiquinone-like radicals) due to their interaction with Ca^{2+}. The interaction of Ca^{2+} with Fe(II) species appears consistent with the measured Fe(II) oxidation rates in non-irradiated SRFA solutions (where oxidation is mostly governed by dioxygen) which shows that the Fe(II) oxidation rate decreases in the presence of Ca^{2+} (Figure 6.3).

Table 6.1: The initial rate of Fe (III) reduction in non-irradiated SRFA solutions containing 20 mM Ca^{2+} in the pH range 3-5.

pH	3	4	5
Initial rate of Fe(III) reduction ($nM.min^{-1}$)	4.6 ± 0.4	5.1 ± 2.7	7.6 ± 1.4

Even though the impact of Ca^{2+} addition on Fe(II) oxidation rate is small (~ 16%, $p < 0.05$) at pH 4, it is more apparent (46%, $p < 0.05$) at pH 5 where Fe(II) oxygenation

occurs at a much faster rate. It is possible that Fe(II) speciation may change in the presence of Ca^{2+} with less and/or weaker Fe(II)SRFA complexes formed as a result of competition between Fe and Ca^{2+} for the binding sites on SRFA. In addition, the binding affinity of SRFA for Fe may also decrease due to a decrease in the negative charge on the SRFA molecules and/or increase in size (hence reduced surface area) of NOM aggregates due to bridging interactions in the presence of Ca^{2+}. The formation of less/weaker Fe(II) and Fe(III) complexes result in a decrease in the Fe(II) oxidation rate since binding of Fe(II)/Fe(III) by SRFA is known to increase the Fe(II) oxidation rate (Emmenegger et al. 1998).

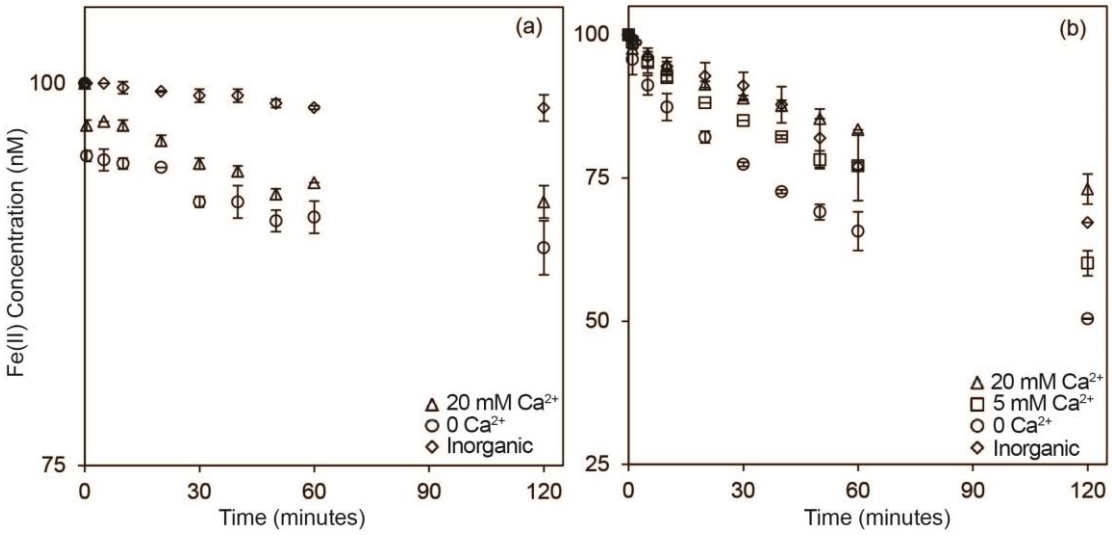

Figure 6.3: Concentration of Fe(II) remaining as a result of oxidation of 100 nM Fe(II) in 0 $mg.L^{-1}$ SRFA solutions (diamonds), 10 $mg.L^{-1}$ SRFA solutions (circles), and 10 $mg.L^{-1}$ SRFA solutions containing 5mM Ca^{2+} (squares), 20 mM Ca^{2+} (triangles) at pH 4 (panel a) and pH 5 (panel b).

There is no direct evidence to support or reject the possibility that the Ca^{2+} interaction with semiquinone-like radicals, previously shown to be involved in Fe(II) oxidation, plays a role as well. In the pH range investigated here, semiquinone radicals exist both as neutral and negatively charged species with the negatively-charged semiquinone radicals capable of forming complexes with Ca^{2+} (Fujii et al. 2015). This possibility is

further investigated below by measuring the effect of Ca^{2+} addition on Fe redox transformations in previously irradiated and continuously irradiated solutions.

6.3.2. Fe redox transformations in previously irradiated SRFA solutions in the presence of Ca^{2+} in the pH range of 3-5

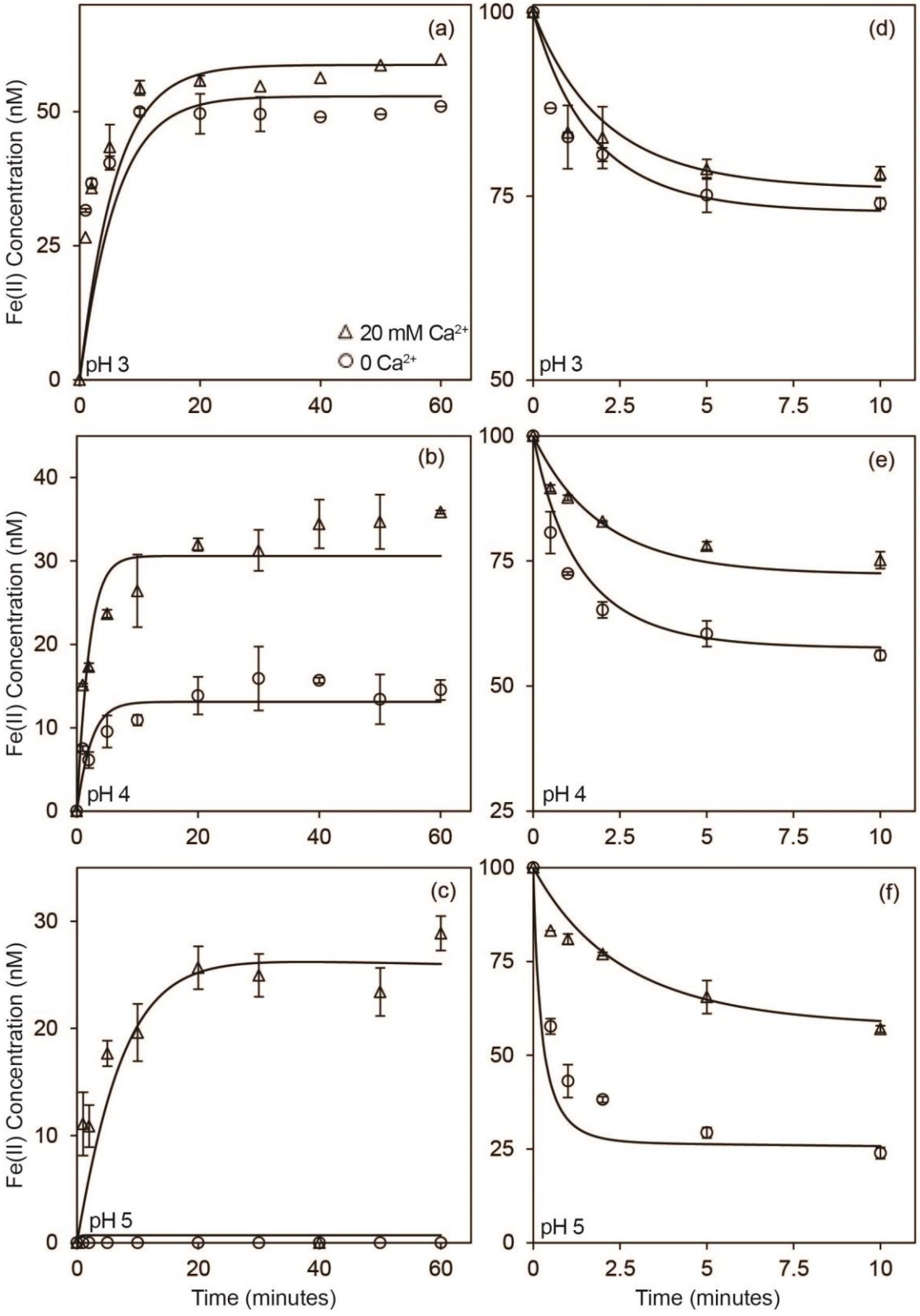

Figure 6.4: Generation of Fe(II) as a result of reduction of 100 nM Fe(III) when added to previously irradiated 10 $mg.L^{-1}$ SRFA solutions containing 0 (circles), and 20 mM (triangles) Ca^{2+} at pH 3 (panel a), pH 4 (panel b) and pH 5 (panel c). Concentration of

Fe(II) remaining as result of oxidation of 100 nM Fe(II) when added to previously irradiated 10 mg.L^{-1} SRFA solutions containing 0 (circles), and 20 mM (triangles) Ca^{2+} at pH 3 (panel d), pH 4 (panel e) and pH 5 (panel f).

When Fe(III) was added to previously irradiated SRFA solutions in the dark, the Fe(II) concentration increased over time (Figure 6.4) though the extent of increase was less than the Fe(II) concentrations generated in non-irradiated SRFA solutions (Figure 6.2). Concomitantly, the Fe(II) oxidation rate in previously irradiated SRFA solutions (Figure 6.4) is much higher than that observed in non-irradiated SRFA solutions (Figure 6.3). As discussed in Chapter 3, this is due to partial oxidation of hydroquinone-like moieties to form semiquinone-like moieties during irradiation thereby resulting in an overall decrease in the Fe(III) reduction rate and an increase in the Fe(II) oxidation rate (Figure 6.1). Note that the role of any photo-generated H_2O_2 in Fe(II) oxidation in previously irradiated SRFA solutions was minor under the experimental conditions investigated here since no increase in Fe(II) oxidation rate was observed, even with the addition of 2 µM H_2O_2 as shown in the previous work (Garg et al. 2013a). The effect of Ca^{2+} addition in previously irradiated SRFA solutions is consistent with that observed in non-irradiated SRFA solutions (Figure 6.1) with the presence of Ca^{2+} resulting in an increase in Fe(II) generation rate ($p < 0.05$) on Fe(III) reduction and a decrease in Fe(II) oxidation rate ($p < 0.05$) (Figure 6.4). The impact of Ca^{2+} addition increases with increase in Ca^{2+} concentration but saturates at 20 mM Ca^{2+} for the Fe concentration range of 50-150 nM investigated here (Figure 6.5).

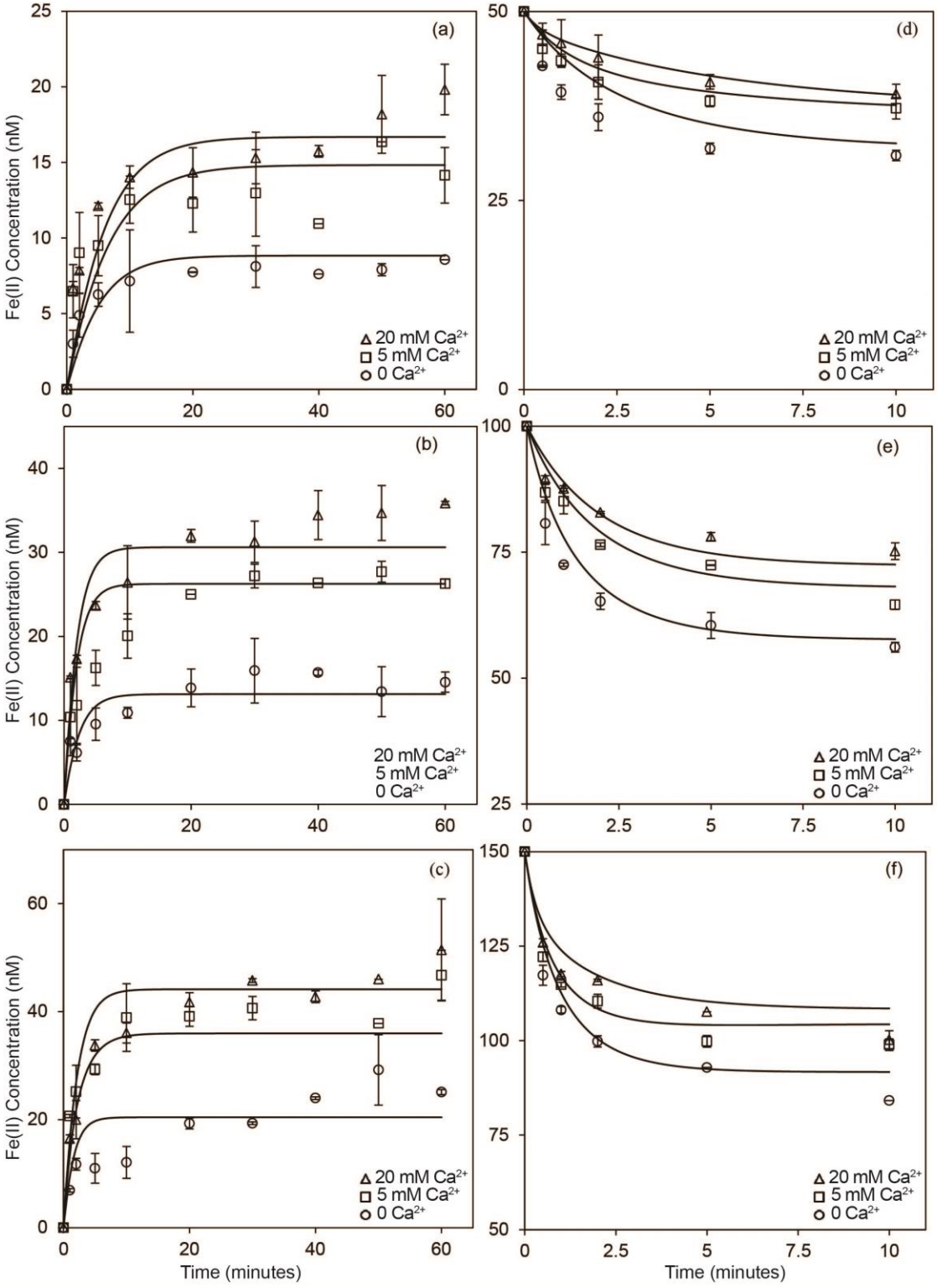

Figure 6.5: Concentration of Fe(II) generated as a result of reduction of Fe(III) in solution containing 0 (circles), 5 mM (squares), and 20 mM (triangles) Ca^{2+} and 50 nM Fe(III) + 5 $mg.L^{-1}$ SRFA (panel a), 100 nM Fe(III) + 10 $mg.L^{-1}$ SRFA (panel b) and 150 nM Fe(III) + 15 $mg.L^{-1}$ SRFA (panel c) in previously irradiated solution at pH 4. Concentration of Fe(II) remaining as result of oxidation of Fe(II) in solution containing 0 (circles), 5 mM (squares), and 20 mM (triangles) Ca^{2+} and 50 nM Fe(II) + 5 $mg.L^{-1}$ SRFA (panel d), 100 nM Fe(II) + 10 $mg.L^{-1}$ SRFA (panel e) and 150 nM Fe(II) + 15

mg.L^{-1} SRFA (panel f) in previously irradiated solution at pH 4. Symbols represent the average of duplicate measurements; lines represent model values.

As shown in Figure 6.1, the generation of A^- (Fe(II) oxidant) during irradiation occurs via the superoxide-mediated oxidation of A^{2-} that are intrinsically present in SRFA. No impact of Ca^{2+} addition occurs on the mechanism controlling the generation of A^- and consequent Fe redox transformations in previously irradiated solution since addition of SOD completely inhibited Fe(II) oxidation with a consequent increase in the concentration of Fe(II) generated on Fe(III) reduction in previously irradiated SRFA solutions containing 20 mM Ca^{2+} at pH 4 (Figure 6.6), which is same as the effect of SOD addition observed in the absence of Ca^{2+} (Figure 3.8; Chapter 3). As discussed in Chapter 3, SOD catalyzes the decay of superoxide, thereby preventing oxidation of A^{2-} to A^-. Furthermore, our results support the conclusion that the concentration of A^- generated on irradiation of SRFA is not affected by Ca^{2+} addition. As shown in Figure 6.7, the Fe(II) generation and Fe(II) decay rates observed in Ca^{2+} containing previously irradiated SRFA solutions are the same irrespective of whether Ca^{2+} was added prior to or after irradiation, thereby supporting that the observed impact of Ca^{2+} addition is not due to changes in A^- concentration but due to changes in the reactivity of A^- and/or a result of modification in the speciation of Fe with more easily reducible and more weakly bound Fe species formed in the presence of Ca^{2+}. Note that the change in the reactivity of hydroquinone-like moieties, involved in Fe(III) reduction, due to interaction with Ca^{2+} is not considered here as the protonated form of hydroquinone (the dominant species under the pH conditions investigated here) cannot complex Ca^{2+}.

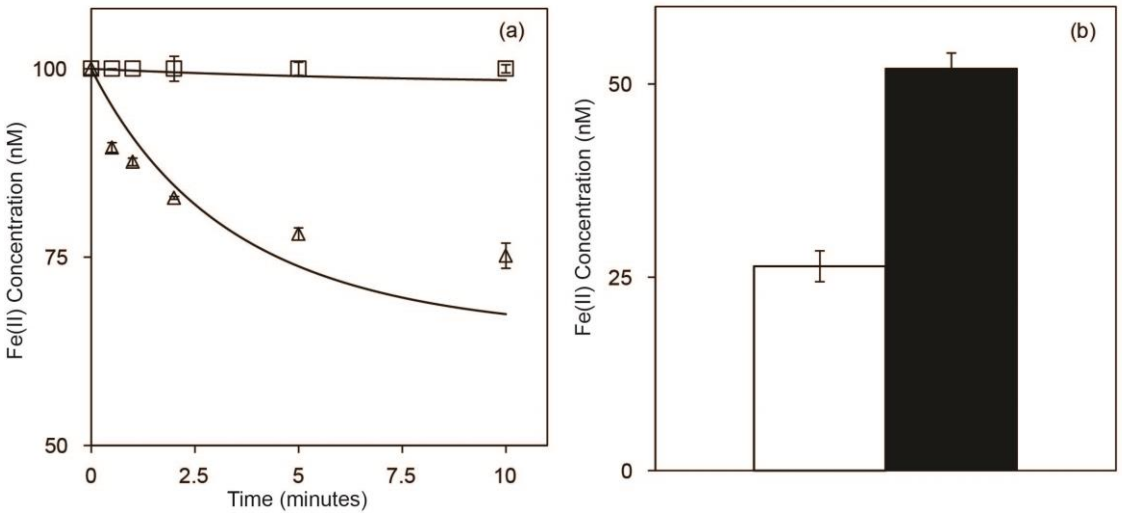

Figure 6.6: (a) Concentration of Fe(II) remaining as a result of oxidation of 100 nM Fe(II) in previously irradiated 10 mg.L^{-1} SRFA solutions containing 20 mM Ca^{2+} in the presence (squares) and absence (triangles) of 25 kU.L^{-1} SOD at pH 4. Symbols represent the average of duplicate measurements; lines represent model values. (b) Concentration of Fe(II) generated after 10 minutes as a result of reduction of 100 nM Fe(III) in previously irradiated 10 mg.L^{-1} SRFA solutions containing 20 mM Ca^{2+} in the presence (closed) and absence (open) of 25 kU.L^{-1} SOD at pH 4.

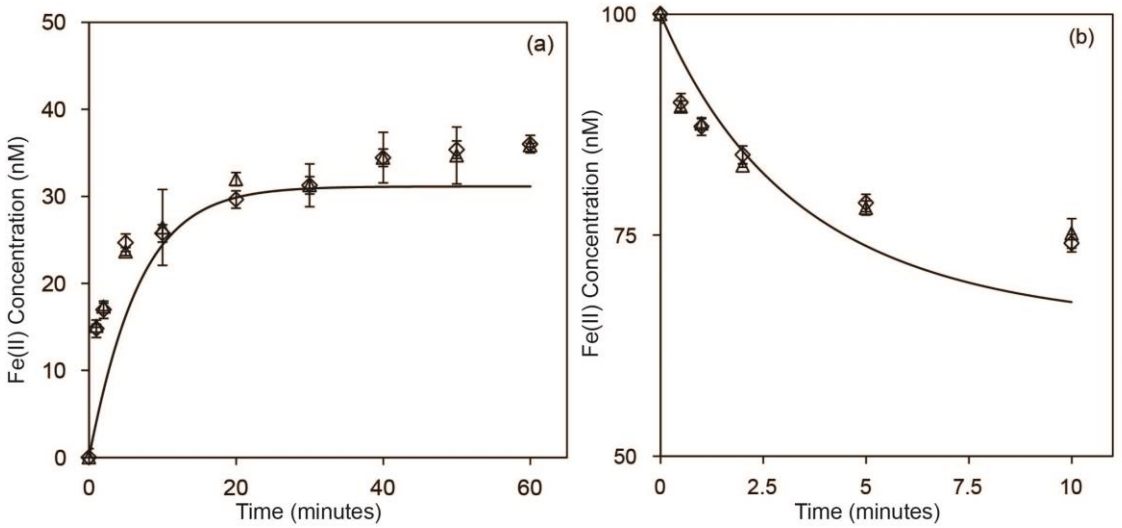

Figure 6.7: (a) Generation of Fe(II) as a result of reduction of 100 nM Fe(III) in previously irradiated 10 mg.L^{-1} SRFA solution with addition of 20 mM Ca^{2+} before (diamonds) and after (triangles) irradiation at pH 4. (b) Decrease in Fe(II) concentration as a result of oxidation of 100 nM Fe(II) in previously irradiated 10 mg.L^{-1} SRFA solutions with addition of 20 mM Ca^{2+} before (diamonds) and after (triangles) irradiation at pH 4. Symbols represent the average of duplicate measurements; lines represent model values.

As observed in non-irradiated SRFA solutions (Figure 6.2), the impact of Ca^{2+} addition (when compared to the rates observed in the absence of Ca^{2+}) on Fe redox

transformations in previously irradiated SRFA solutions increases with an increase in pH (Figure 6.4). As shown, only a small (< 10%) effect of Ca^{2+} addition on Fe(II) oxidation and Fe(III) reduction kinetics in previously irradiated SRFA solutions at pH 3 is observed but Ca^{2+} addition significantly ($p < 0.05$) decreased the rate and extent of Fe(II) oxidation and increased the rate and extent of Fe(III) reduction in previously irradiated SRFA solutions at pH 5 with the effect of Ca^{2+} addition at pH 5 (> 200%) more pronounced than observed at pH 4 (~ 110%; Figure 6.4). This pH dependence of the Ca^{2+} effect is consistent with the measured pH dependence of the Fe(II) oxidation rate. Thus, it appears that the impact of Ca^{2+} addition on Fe redox transformations in previously irradiated SRFA solutions is due to a decrease in the Fe(II) oxidation rate with this occuring as a result of the change in speciation of semquinone-like radicals and/or Fe(II) due to their interaction with Ca^{2+} as was determined to be the case in non-irradiated SRFA solutions. Note that Ca^{2+} addition may imapct Fe(III) reduction rates as well though its overall impact on Fe(II) oxidation rates is much more prominent.

6.3.3. Fe(III) reduction in continuously irradiated SRFA solutions in the presence of Ca^{2+} in the pH range of 3-5

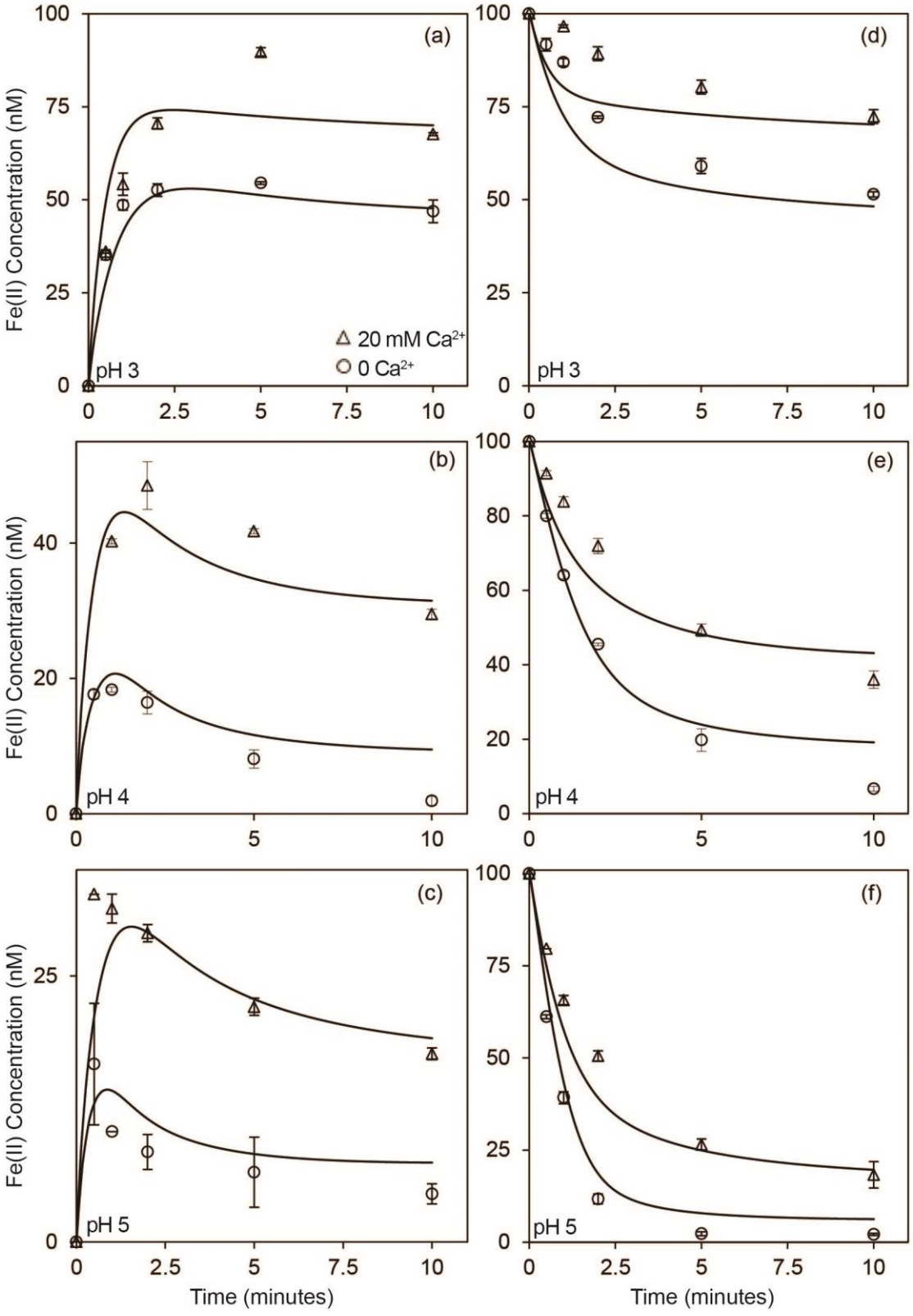

Figure 6.8: Generation of Fe(II) as a result of reduction of 100 nM Fe(III) when added to continuously irradiated 10 $mg.L^{-1}$ SRFA solution containing 0 (circles), and 20 mM

(triangles) Ca^{2+} at pH 3 (panel a), pH 4 (panel b) and pH 5 (panel c). Concentration of Fe(II) remaining as result of oxidation of 100 nM Fe(II) when added to continuously irradiated 10 $mg.L^{-1}$ SRFA solution containing 0 (circles), and 20 mM (triangles) Ca^{2+} at pH 3 (panel d), pH 4 (panel e) and pH 5 (panel f).

As shown in Figure 6.8, the concentration of Fe(II) generated on Fe(III) reduction in continuously irradiated SRFA solutions increases in the presence of 20 mM Ca^{2+} ($p < 0.05$). Concomitantly, the rate of oxidation of Fe(II) in continuously irradiated SRFA solutions decreases in the presence of 20 mM Ca^{2+} ($p < 0.05$) (Figure 6.8). These observations are consistent with the results in Figure 6.2 and Figure 6.4, showing that the presence of Ca^{2+} increases the concentration of Fe(II) generated via Fe(III) reduction and decreases the Fe(II) oxidation rate in non-irradiated and previously irradiated SRFA solutions. Furthermore, as observed in previously irradiated SRFA solutions, the impact of Ca^{2+} addition increases with an increase in Ca^{2+} concentration but saturates at 20 mM Ca^{2+} in continuously irradiated SRFA solutions as well (Figure 6.9).

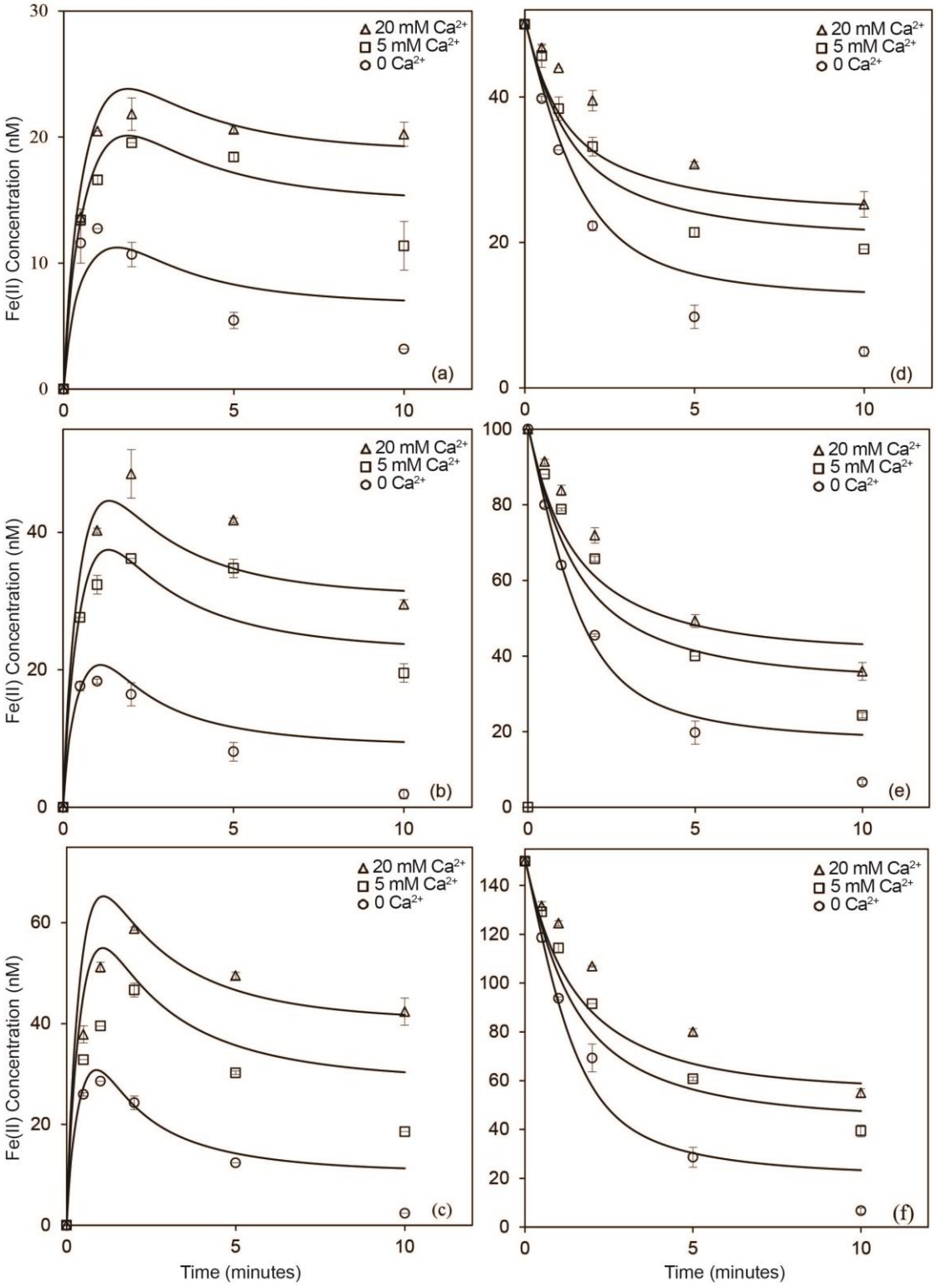

Figure 6.9: Concentration of Fe(II) generated as a result of reduction of Fe(III) in solution containing 0 (circles), 5 mM (squares), and 20 mM (triangles) Ca^{2+} and 50 nM Fe(III) + 5 $mg.L^{-1}$ SRFA (panel a), 100 nM Fe(III) + 10 $mg.L^{-1}$ SRFA (panel b) and 150 nM Fe(III) + 15 $mg.L^{-1}$ SRFA (panel c) in continuously irradiated solution at pH 4. Concentration of Fe(II) remaining as result of oxidation of Fe(II) in solution containing 0 (circles), 5 mM (squares), and 20 mM (triangles) Ca^{2+} and 50 nM Fe(II) + 5 $mg.L^{-1}$

SRFA (panel d), 100 nM Fe(II) + 10 mg.L^{-1} SRFA (panel e) and 150 nM Fe(II) + 15 mg.L^{-1} SRFA (panel f) in continuously irradiated solution at pH 4. Symbols represent the average of duplicate measurements; lines represent model values.

As reported earlier (Garg et al. 2013b), under continuously irradiated conditions, Fe(II) oxidation occurs for the most part as a result of the generation of superoxide (via reduction of dioxygen) and peroxyl-like radicals ($RO_2^{\bullet}$) (via hydroxylation of SRFA) as indicated in Figure 6.1. Our results show that the same mechanism drives Fe(II) oxidation in the presence of Ca^{2+} in continuously irradiated SRFA solutions with SOD and DMSO addition (data not shown) increasing Fe(III) reduction and decreasing Fe(II) oxidation rate, respectively, as previously observed in the absence of Ca^{2+} (Garg et al. 2013b). Addition of SOD catalyzes the decay of superoxide to dioxygen and H_2O_2 and hence prevents the oxidation of Fe(II) by superoxide. Note that Fe(II) oxidation by H_2O_2 and O_2 (the decay products of superoxide) is very slow under the experimental conditions investigated here. Addition of DMSO scavenges any hydroxylating intermediate formed and hence prevents formation of peroxyl-like radicals involved in Fe(II) oxidation.

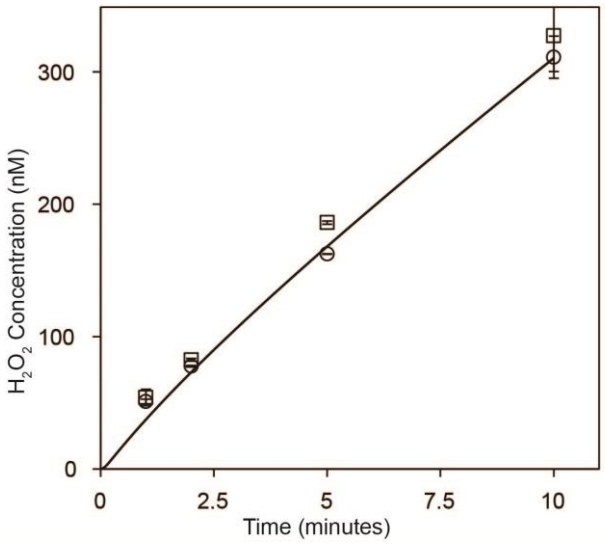

Figure 6.10: Generation of hydrogen peroxide (H_2O_2) as a result of irradiation of 10 $mg.L^{-1}$ SRFA in the presence (squares) and absence (circles) of 20 mM Ca^{2+} at pH 4. Symbols represent the average of duplicate measurements; lines represent model values.

Our results further support the conclusion that the addition of Ca^{2+} does not impact the rate of generation of superoxide on irradiation of SRFA with the same concentration of H_2O_2 (which is a stable end product of superoxide disproportionation) generated in continuously irradiated SRFA solutions in the presence and absence of Ca^{2+} (Figure 6.10). While there is no direct experimental evidence to support the conclusion that peroxyl-like radical generation is not affected by Ca^{2+} addition (note that it is difficult to measure these radicals in our system due to their low concentration and short lifetime), any decrease in peroxyl radical generation rate in Ca^{2+} containing solutions is unlikely to explain the observed decrease in Fe(II) oxidation rates in the presence of Ca^{2+} since this decrease in Fe(II) oxidation rates is much more significant than that observed in the absence of peroxyl radicals (~ 30%; determined by measuring Fe(II) oxidation rates in the presence of DMSO) as illustrated in our earlier work (Figure 5.3; Chapter 5). Thus, it appears that the observed impact of Ca^{2+} is not due to changes in the mechanism and/or concentration of the species controlling Fe redox transformations but due to changes in the reactivity of the Fe species involved.

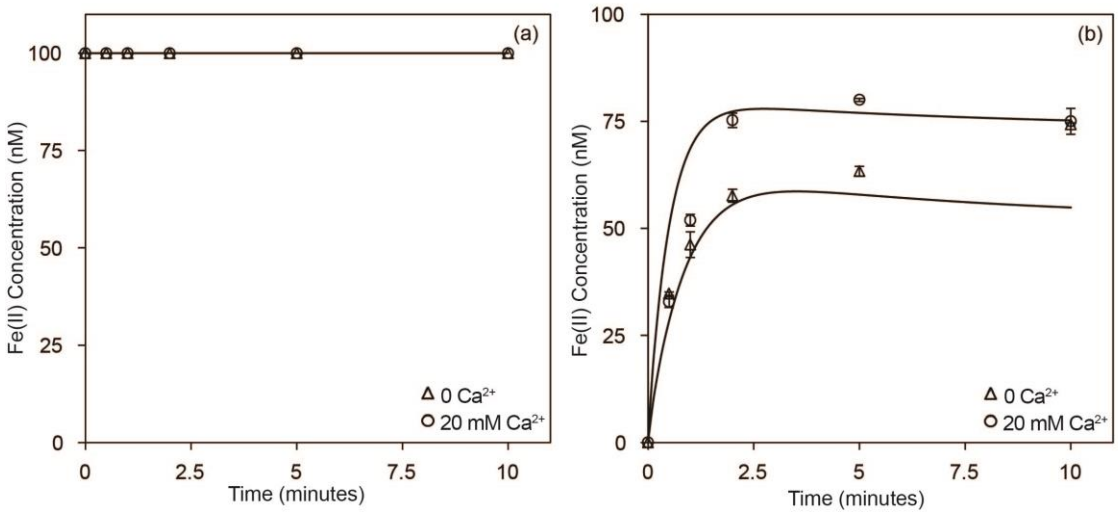

Figure 6.11: (a) Concentration of Fe(II) remaining as a result of 100 nM Fe(II) oxidation in the presence (circles) and absence (triangles) of 20 mM of Ca^{2+} in the presence of 25 $kU.L^{-1}$ SOD in continuously-irradiated SRFA solutions at pH 3. (b) Generation of Fe(II) as a result of 100 nM Fe(III) reduction in the presence (circles) and absence (triangles) of 20 mM of Ca^{2+} in the presence of 25 $kU.L^{-1}$ SOD in continuously-irradiated SRFA solutions at pH 3. Symbols represent the average of duplicate measurements; lines represent model values.

The measured impact of Ca^{2+} addition (100 ± 20%; % change in the Fe transformation rate measured in the absence and presence of Ca^{2+}) is statistically invariant in the pH range investigated ($p > 0.05$) which suggests that iron redox transformations in the presence of Ca^{2+} in continuously irradiated SRFA solutions are, for the most part, independent of pH. This observation is in contrast to the impact of pH on the effect of Ca^{2+} addition on Fe redox transformation rates in non-irradiated and previously irradiated SRFA solutions (Figure 6.2 and Figure 6.4) however, it is consistent with the hypothesis that the nature of the Fe(III)-SRFA complex is relatively invariant over the pH range investigated here. The measured Fe(III) reduction rates at pH 3 in the presence of Ca^{2+} (Figure 6.11) provides more support to the hypothesis that it is the Fe(III) reduction rate (and not Fe(II) oxidation rate) that is impacted much more significantly with Ca^{2+} addition in continuously irradiated solution. As shown in Figure 6.11, at pH 3 in the presence of SOD, Fe(II) oxidation is completely inhibited and thus the measured

Fe(II) generation rate is the same as the Fe(III) reduction rate (a rate which increases in the presence of Ca^{2+}). Since ligand-to-metal charge transfer is the main pathway of Fe(III) reduction in continuously irradiated solution, the effect of Ca^{2+} on iron reduction most likely occurs through its interaction with the Fe(III)-SRFA complex. It is possible that the Fe(III) speciation changes on addition of Ca^{2+} with Fe(III) existing as a weaker Fe(III)-SRFA complex with this weaker complex much more photolabile than the complex formed in the absence of Ca^{2+}. The formation of a weakly bound Fe(III)-SRFA complex is also consistent with the observed decrease in Fe(II) oxidation kinetics in Ca^{2+} containing non-irradiated SRFA solutions since binding of Fe(III) by organic ligands is known to increase the oxidation rate of Fe(II) (Pham and Waite 2008a). Note that the fraction of SRFA bound Fe(III) can be confirm not to decrease in the presence of Ca^{2+} since the LMCT-mediated reduction rate of inorganic Fe(III) is substantially lower than that of the SRFA-complexed Fe(III) at pH 4 (Fiure 6.12). This observation thus supports the conclusion that it is the binding strength rather than the extent of Fe(III) binding by SRFA that is affected by the presence of Ca^{2+}.

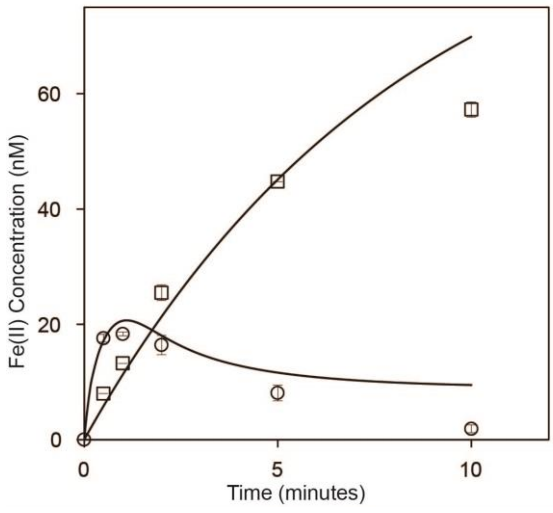

Figure 6.12: Concentration of Fe(II) generated as a result of reduction of 100 nM Fe(III) in continuously irradiated solution in the presence (circles) and absence (squares) of 10 $mg.L^{-1}$ SRFA. Symbols represent the average of duplicate measurements; lines represent model values.

It is worth to note that, even though the impact of Ca^{2+} addition is much more pronounced on the Fe(III) reduction rate in continuously irradiated SRFA solutions, the presence of Ca^{2+} may also impact the rate of oxidation of Fe(II) by superoxide and peroxyl radicals due to changes in Fe(II) speciation as was determined to be the case in non-irradiated and previously irradiated SRFA solutions.

6.3.4. Reaction mechanism accounting for the effect of Ca^{2+} on Fe redox transformations in non-irradiated, previously irradiated and continuously irradiated SRFA solutions

As discussed in Chapter 3, Fe redox transformations in non-irradiated and previously irradiated SRFA solutions are considered to be controlled by the interaction of Fe(III) with hydroquinone-like moieties that are intrinsically present in SRFA resulting in formation of semiquinone-like moieties which subsequently oxidize Fe(II) to Fe(III) (eq.6.1).

$$A^{2-} + \text{Fe(III)} \underset{k_2}{\overset{k_1}{\rightleftharpoons}} A^{-} + \text{Fe(II)} \qquad (6.1)$$

In contrast, Fe redox transformations in continuously irradiated SRFA solutions occur via LMCT reduction of Fe(III) while peroxyl-like radical and superoxide oxidize Fe(II) as observed in Chapter 5. On the basis of our experimental results and the discussion presented above, it can be concluded that the presence of Ca^{2+}

(1) does not affect the mechanism controlling Fe redox transformations in non-irradiated, previously irradiated and continuously irradiated SRFA solutions.

(2) does not affect the generation rate of the various species (including ROS as well as organic moieties involved in Fe redox transformations) formed on irradiation of SRFA.

(3) impacts the Fe(III) reduction rate and/or Fe(II) oxidation rate by interacting with the species involved in these reactions, thereby altering their reactivity.

(4) increases the Fe(III) reduction rate in continuously irradiated SRFA solutions while decreasing the Fe(II) oxidation rates in non-irradiated and previously irradiated SRFA solutions.

(5) impacts the binding strength of SRFA bound Fe(III) but has no impact on the binding extent of Fe(III) by SRFA.

While the conclusions listed above are strongly supported by our experimental results, the exact manner via which calcium affects the Fe(III) reduction rates and/or Fe(II) oxidation rates is unclear from the results presented. The increase in Fe(III) reduction rate in continuously irradiated SRFA solutions containing Ca^{2+} most likely occurs via formation of a more photolabile weakly bound Fe(III)-SRFA complex. The decrease in the Fe(II) oxidation rate in non-irradiated solution that is observed in the presence of Ca^{2+} most likely occurs as a result of a decrease in the strength of binding of Fe (both Fe(III) and Fe(II) by SRFA and/or decrease in the fraction of organically bound Fe(II) as confirmed by the measured Fe(II) oxidation rates in non-irradiated SRFA solutions (where oxidation occurs due to interaction with dioxygen).

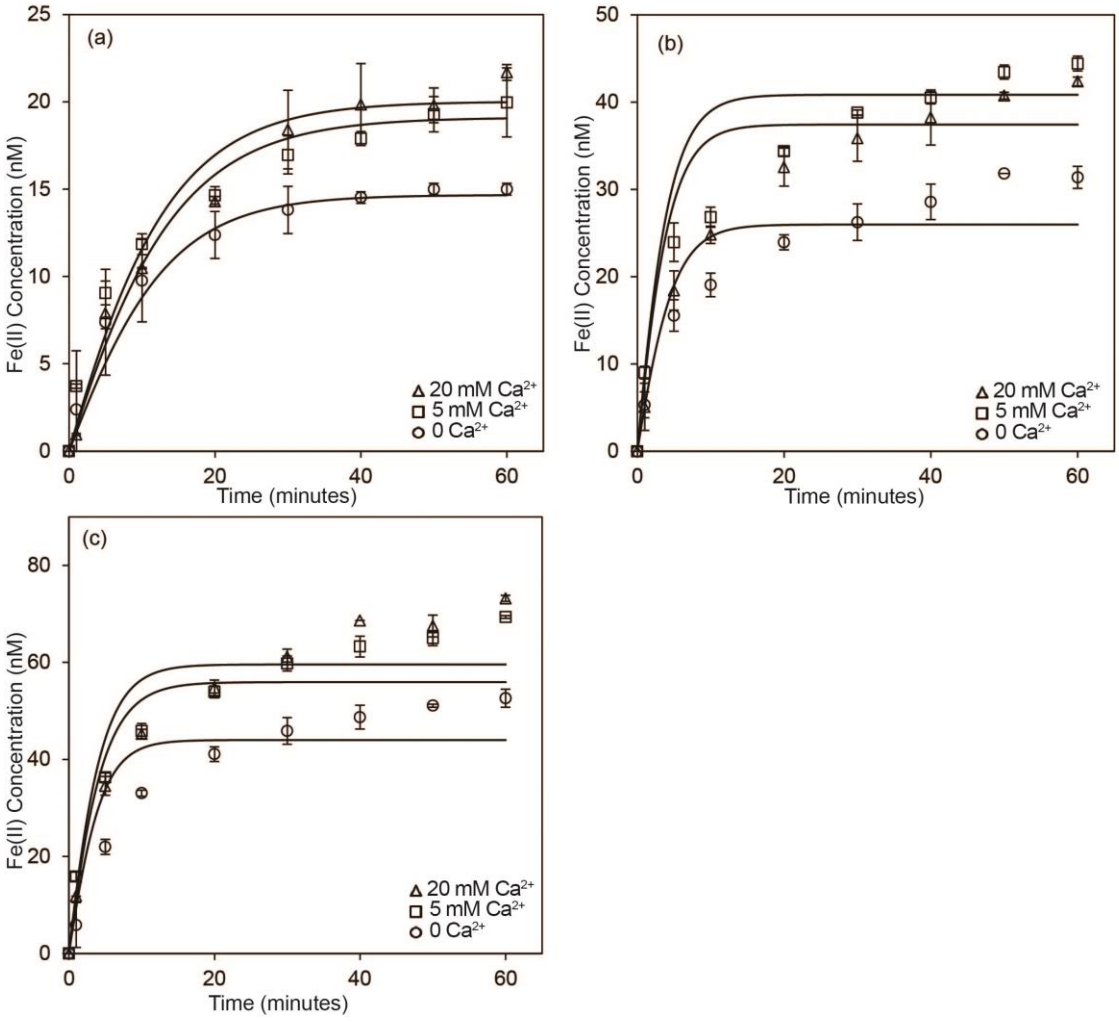

Figure 6.13: Generation of Fe(II) as a result of reduction of Fe(III) in solution containing 0 (circles), 5 mM (squares), and 20 mM (triangles) Ca^{2+} and 50 nM Fe(III) + 5 $mg.L^{-1}$ SRFA (panel a), 100 nM Fe(III) + 10 $mg.L^{-1}$ SRFA (panel b) and 150 nM Fe(III) + 15$mg.L^{-1}$ SRFA (panel c) in non-irradiated solution at pH 4. Symbols represent the average of duplicate measurements; lines represent model values.

The impact of Ca^{2+} addition on Fe redox transformations has been modelled by including formation of (i) weakly complexed Fe(III) ($Fe(III)L'$) and (ii) weakly complexed Fe(II) ($Fe(II)L'$) to the mathematical model developed in Chapter 5 to explain the nature of Fe transformations in acidic SRFA solutions. To simplify the modelling, it has been assumed that all added Fe exists as strongly bound Fe complexes (i.e. Fe(III)L and Fe(II)L) in the absence of Ca^{2+} and as weakly bound Fe complexes (i.e. $Fe(III)L'$ and $Fe(II)L'$) in the presence of 20 mM Ca^{2+}. The fraction of strongly and

weakly bound Fe in the presence of 5 mM Ca^{2+} was determined on the basis of the best-fit to Fe redox transformation rates observed in the presence of 5 mM Ca^{2+} (Figure 6.5, Figure 6.9, and Figure 6.13).

The conditional stability constants of Fe (including both Fe(II) and Fe(III)) binding by SRFA in the presence of Ca^{2+} are lower than the stability constants for Fe binding by SRFA in the absence of Ca^{2+} with this effect possibly due to consumption of a portion of the strong binding sites by Ca^{2+}. This decrease in the binding strength of SRFA in the presence of Ca^{2+} may also occur due to decrease in the negative charge of SRFA and/or increase in the size of NOM aggregates in the presence of Ca^{2+}. While our experimental results can be rationalized in this way, further work is required to determine the exact mechanism(s) via which Ca impacts Fe binding by SRFA.

Table 6.2: Kinetic model to explain the impact of Ca^{2+} addition on SRFA-mediated iron redox transformations.

No	Reaction	Rate constant	Ref
Generation and consumption of singlet oxygen, superoxide and H_2O_2 on irradiation			
1	$SRFA + h\nu \longrightarrow SRFA^*$	Calculated	-
	$SRFA^* + {}^3O_2 \longrightarrow SRFA + {}^1O_2$	$\Phi \sim 0.5\%$	(Paul et al. 2004)
2	${}^1O_2 \xrightarrow{H_2O} {}^3O_2$	$2.4\times10^5\ s^{-1}$	(Dalrymple et al. 2010)
3	$Q + h\nu \xrightarrow{k_f} Q^- \xrightarrow{k_d} NRP$	$k_f = 1.5\times10^{-4}$ [a]; $k_d = 5.8\times10^3 s^{-1}$	(Garg et al. 2013a)
4	$Q^- + {}^3O_2 \xrightarrow{H^+} Q + HO_2^\bullet$	$\sim 1\times10^9\ M^{-1}s^{-1}$	(Zhang et al. 2012)
5	$HO_2^\bullet + HO_2^\bullet \longrightarrow O_2 + H_2O_2$	$\frac{k_{HO_2^\bullet} + k_{O_2^{\bullet-}}\left(K_{HO_2^\bullet}/[H^+]\right)}{\left(1+\left(K_{HO_2^\bullet}/[H^+]\right)\right)^2}$ [b]	(Bielski et al. 1985)

6	$R + h\nu \longrightarrow R^{\bullet}$	7.2×10^{-6} s^{-1}[c]	(Garg et al. 2011b)
7	$R^{\bullet} + HO_2^{\bullet} \longrightarrow R^{-} + O_2 + H^{+}$	$\frac{k_7^{HO_2^{\bullet}} + k_2^{O_2^{\bullet-}} \left(K_{HO_2^{\bullet}} / [H^+] \right)}{\left(1 + \left(K_{HO_2^{\bullet}} / [H^+] \right) \right)}$ [d]	(von Sonntag et al. 1997)
8	$R^{\bullet} + R^{\bullet} \longrightarrow R_2$	1×10^{3} $M^{-1}s^{-1}$	(Garg et al. 2011b)
	Transformation of hydroquinone and semiquinone-like moieties on irradiation		
9	$A^{2-} + HO_2^{\bullet} \xrightarrow{H^+} A^{-} + H_2O_2$	$k_9 / k_{10} = -5.7E_H + 2.5$	(Garg et al. 2015)
10	$A^{-} + HO_2^{\bullet} \longrightarrow A^{2-} + O_2 + H^{+}$	1.5×10^{6} $M^{-1}s^{-1}$[e]	(Garg et al. 2011b)
11	$A^{-} + {}^1O_2 \xrightarrow{H^+} A + HO_2^{\bullet}$	1.5×10^{8} $M^{-1}s^{-1}$[e]	(Garg et al. 2013a)
	Generation of short-lived Fe(II) oxidant on irradiation		
12	$R \xrightarrow{h\nu} RO_2^{\bullet}$	5×10^{-7} s^{-1}	(Garg et al. 2015)
13	$RO_2^{\bullet} + RO_2^{\bullet} \longrightarrow RO_4R$	1×10^{6} $M^{-1}s^{-1}$	(Garg et al. 2015)
14	$RO_2^{\bullet} \longrightarrow R^{\bullet+} + HO_2^{\bullet}$	1×10^{-2} $M^{-1}s^{-1}$	(Garg et al. 2015)
	Fe redox transformations under irradiated condition		
15	$Fe(III)L \xrightarrow{h\nu} Fe(II)' + L_{ox}$	7.5×10^{-3} s^{-1}	(Garg et al. 2013b)
16	$Fe(III)L' \xrightarrow{h\nu} Fe(II)' + L_{ox}$	1.5×10^{-2} s^{-1}	This work
17	$Fe(III)L + HO_2^{\bullet} \longrightarrow Fe(II)L + O_2$	2×10^{5} $M^{-1}s^{-1}$	(Rush and Bielski 1985; Garg et al. 2011a)
18	$Fe(III)L' + HO_2^{\bullet} \longrightarrow Fe(II)L' + O_2$	$2\times10^{5} \sim 4\times10^{5}$ $M^{-1}s^{-1}$	This work
19	$Fe(II)L + RO_2^{\bullet} \longrightarrow Fe(III)L + RO_2^{-}$	1×10^{7} $M^{-1}s^{-1}$	(Khaikin et al. 1996)
20	$Fe(II)L' + RO_2^{\bullet} \longrightarrow Fe(III)L' + RO_2^{-}$	$5\times10^{6} \sim 1\times10^{7}$ $M^{-1}s^{-1}$	This work

21	$Fe(II)L+HO_2^{\bullet} \longrightarrow Fe(III)L+H_2O_2$	$\frac{k_{21}^{HO_2^{\bullet}} + k_{21}^{O_2^{\bullet-}}(K_{HO_2^{\bullet}}/[H^+])}{1+(K_{HO_2^{\bullet}}/[H^+])}$ f	(Rush and Bielski 1985)
22	$Fe(II)L'+HO_2^{\bullet} \longrightarrow Fe(III)L'+H_2O_2$	$0.5\ k_{21} \sim k_{21}$	This work
	Fe redox transformations under non-irradiated condition		
23	$Fe(III)L+A^{2-} \longrightarrow Fe(II)L+A^{-}$	$3.0 \times 10^3\ M^{-1}s^{-1}$ g	(Garg et al. 2015)
24	$Fe(III)L'+A^{2-} \longrightarrow Fe(II)L'+A^{-}$	$6.0 \times 10^3\ M^{-1}s^{-1}$	This work
25	$Fe(II)L+A^{-} \longrightarrow Fe(III)L+A^{2-}$	$\frac{k_{HA} + k_{A^-}(K_{HA}/[H^+])}{(1+K_{HA}/[H^+])}$ e,h	(Garg et al. 2015)
26	$Fe(II)L'+A^{-} \longrightarrow Fe(III)L'+A^{2-}$	$\sim 0.61\, k_{26}$	This work
27	$Fe(II)L+O_2 \longrightarrow Fe(III)L+HO_2^{\bullet}$	$0.5\ M^{-1}s^{-1}$ i	This work
28	$Fe(II)L'+O_2 \longrightarrow Fe(III)L'+HO_2^{\bullet}$	$0.25\ M^{-1}s^{-1}$ i	This work

[a] pseudo-first order rate constant based on $[Q]_T$ = 0.67 mmol.g^{-1} SRFA where Q represents the redox-active chromophere responsible for superoxide generation. The concentration of Q is assumed to be the same as the concentration of electron accepting moieties in SRFA as reported earlier.(Aeschbacher et al. 2010)

[b] $k_{HO_2^{\bullet}}$ = 8.0 × 10^5 M^{-1}s^{-1}, $k_{O_2^{\bullet-}}$ = 9.7 × 10^7 M^{-1}s^{-1}, and $K_{HO_2^{\bullet}}$ = 10$^{-4.8}$.

[c] pseudo-first order rate constant based on $[R]_T$ = 43 mmol.g^{-1} SRFA(Goldstone et al. 2002); R represents the bulk carbon concentration in SRFA as reported earlier (Goldstone et al. 2002).

[d] $k_7^{HO_2^{\bullet}}$ = 3.5 × 10^4 M^{-1}s^{-1}, $k_7^{O_2^{\bullet-}}$ = 1.6 × 10^5 M^{-1}s^{-1}, and $K_{HO_2^{\bullet}}$ = 10$^{-4.8}$.

[e] rate constant is based on total A^- concentration including both forms i.e. HA and A^-; initial total A^- concentrations in previously irradiated SRFA solutions were calculated to be 3.2, 4.9, 6.5 μmoles.g^{-1} SRFA at pH 3, 4 and 5 respectively based on the measured steady-state Fe(II) concentrations in these solutions as described in our earlier work.[1]

[f] $k_{21}^{HO_2^{\bullet}}$ = 1.2 × 10^6 M^{-1}s^{-1}, $k_{21}^{O_2^{\bullet-}}$ = 1.0 × 10^7 M^{-1}s^{-1}, and $K_{HO_2^{\bullet}}$ = 10$^{-4.8}$.

[g] based on $[A]_T$ =35.4 μmol.g^{-1} SRFA (Garg et al. 2013a).

[h] k_{HA} = 2.4 × 10^4 M^{-1}s^{-1}, k_{A^-} = 1.4 × 10^5 M^{-1}s^{-1}, K_{HA} = 10^{-4}.

[i] rate constant at pH 5.

The mathematical model developed here is presented in Table 6.2 with detailed description of the reactions provided in Chapter 3 and 5. As shown in Table 6.2, the weakly bound Fe(III) complex formed in the presence of Ca^{2+} is more photolabile as well as slightly easily reducible by hydroquinone-like moieties and superoxide as

compared to strongly bound Fe(III) complexes. Similarly, the weakly bound Fe(II) complexes oxidize at much slower rate by dioxygen and semiquinone-like moieties. Although the reactivity of weakly bound Fe(II) complexes towards superoxide and peroxyl-like radicals is assumed to be same as the strongly bound Fe(II)L specie, even a 2-fold lower value of the rate constants for these reactions produces the same model output.

As shown in all Figures, the mathematical model describes the general trend of our experimental results over a range of conditions, including the impact of pH and light, very well. Although the model describes the observed initial Fe(III) reduction rates and the steady-state Fe(II) concentrations formed on Fe(III) reduction in non-irradiated SRFA solutions very well, there is some discrepancy between the measured and model-predicted Fe(II) concentrations in the intermediate time period though this discrepancy is well within the variability in experimental data expected at such low Fe concentrations.

While there is no direct evidence to reject the possibility that Ca^{2+} interaction with semiquinone-like radicals influences Fe redox transformations, this pathway appears to be relatively unimportant since the impact of Ca^{2+} on Fe redox transformations can be explained without invoking this possibility. In conclusion, it appears that the impact of Ca^{2+} addition on Fe redox transformations is mainly due to its influence on Fe speciation.

Using our mathematical model, the effect of Ca^{2+} on the turnover frequency (TOF) of iron can be determined using eq.6.2:

$$\text{TOF} = \frac{\text{Fe(III) reduction rate}}{\text{Total Fe concentration}} = \frac{\text{Fe(II) oxidation rate}}{\text{Total Fe concentration}} \qquad (6.2)$$

The iron turnover frequency slightly decreases with increase in Ca^{2+} concentration (TOF = 1.6 h^{-1} in the absence of Ca^{2+} and 1.2 h^{-1} in the presence of 20 mM Ca^{2+} at pH 4) in previously irradiated SRFA solutions due to a decrease in the Fe(II) oxidation rate in the presence of Ca^{2+}. In contrast, the TOF increases from 30.3 h^{-1} in the absence of Ca^{2+} to 38.0 h^{-1} in the presence of 20 mM Ca^{2+} in continuously irradiated SRFA solutions due to the increased Fe(III) reduction rate in Ca^{2+} containing irradiated SRFA solutions. These results suggest that the presence of Ca^{2+} renders Fe redox transformations less dynamic in the dark and more dynamic under irradiated conditions.

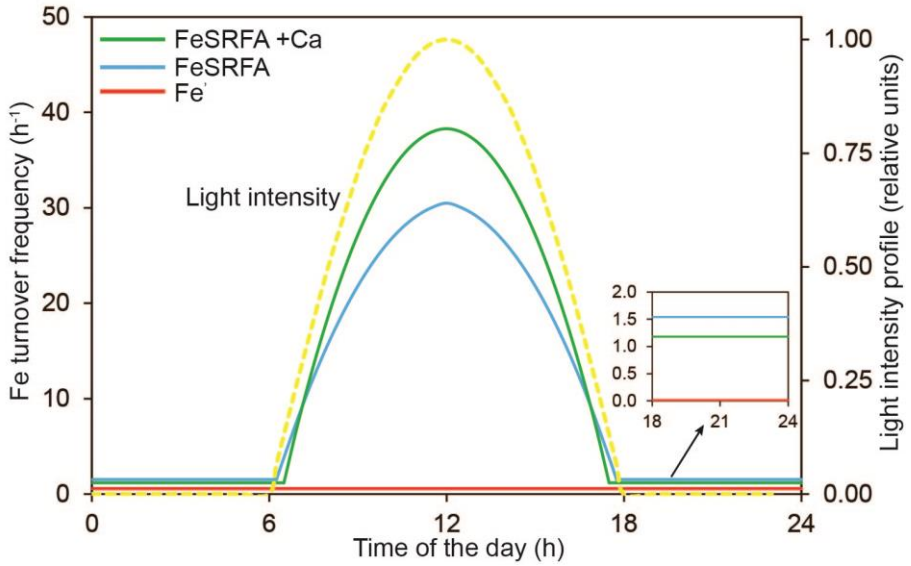

Figure 6.14: Diurnal cycling of cycling rate of Fe in the presence and absence of Ca^{2+} in SRFA solutions at pH 4. Inset shows the Fe turnover frequency during the dark period at pH 4 under various conditions.

6.4. Conclusions

Our results show that Ca^{2+} has a significant effect on Fe redox transformations mediated by SRFA under acidic conditions. The effect of Ca^{2+} addition on Fe redox transformations can be attributed principally to a change in Fe speciation as a result of interaction between Ca and SRFA binding sites. The Fe(III) reduction rates increase due to formation of a more photolabile weakly complexed Fe(III) species while the Fe(II)

oxidation rates decrease due to formation of weaker Fe(II) and Fe(III) complexes in the presence of Ca^{2+}. The impact of Ca^{2+} addition is more pronounced under irradiated conditions than in non-irradiated SRFA solutions. The Fe(II)-Fe(III) turnover frequency increased by as much as 25% in the presence of Ca^{2+} under irradiation but decreased by approximately 25% in the presence of Ca^{2+} in the dark at pH 4. As shown in Figure 6.14, the kinetic model developed in this work can be used to ascertain the likely effect of the presence of Ca^{2+} on Fe cycling rate over the full diurnal cycle. As shown, significant diel variation in the rate of Fe cycling occurs, even in acidic waters, since the time scales of Fe(III) reduction and Fe(II) oxidation are similar. Even though the Fe cycling rate decreases after sunset due to cessation of light-mediated Fe transformations, the cycling rate is still much higher than that expected in humic and fulvic acid free acidic waters where Fe(II) oxidation is controlled by dioxygen only (Figure 6.14). As shown, the cycling rate of Fe in the absence of SRFA is essentially the same under dark and irradiated conditions since the turnover frequency is controlled by the rate of Fe(II) oxidation. Overall, the impact of Ca^{2+} on binding of Fe by SRFA and associated Fe redox transformations can have significant implications to Fe availability in Ca^{2+} containing natural waters.

Chapter 7. Mechanistic insights into iron redox transformations in the presence of SRFA in the circumneutral pH range

7.1. Introduction

As discussed, the availability of iron is governed by a number of factors, including light, pH, divalent calcium ions, and the presence of natural organic matter (NOM). We have studied iron redox transformations in sunlit water containing SRFA in acidic environments (pH 3-5) in Chapter 3-6. Several important findings are: 1) Fe(III) is reduced by hydroquinone-like moieties that exists intrinsically in SRFA solutions, which is the dominant Fe(III) reduction pathway in non-irradiated solution; 2) ligand-to-metal charge transfer (LMCT) is the dominant Fe(III) reduction pathway in irradiated solution; 3) while oxygenation of Fe(II) is slow at acidic pH, irradiation of NOM generates important Fe(II) oxidants including long-lived semiquinone-like radicals and short-lived moieties similar to peroxyl radicals; 4) the presence of Ca^{2+} affects iron redox transformations by decreasing Fe(II) oxidation rate and increasing Fe(III) reduction rate; 5) the pH dependence of iron transformations in acidic pH is primarily controlled by the varying Fe(II) oxidation rate, while Fe(III) reduction rate by various pathways are relatively pH independent due to the invariant nature of the Fe(III)-SRFA complexes in the pH range 3-5.

In this Chapter, we extend our examination of Fe redox transformations in SRFA solutions to circumneutral pH conditions (6.8-8.7). The key objective of this study is to fill the knowledge gap in our understanding of iron redox transformations under these conditions. Also, we aim to determine the pH dependence of iron redox transformations, with special interest in the mechanisms, species, and pathways controlling the pH dependence of these transformations. The pathways mediating iron redox transformations under circumneutral condition are expected to be significantly different to those in acidic environments (Garg et al. 2011a). Under circumneutral pH conditions, Fe(II) oxidation by dioxygen occurs rapidly with an apparent rate constant of 0.036 s^{-1}

in oxygen-saturated solutions (equivalent to $t_{1/2}$ ~ 19 s) for organically complexed Fe(II). Furthermore, while superoxide was shown to play no role in Fe(III) reduction under acidic conditions, superoxide-mediated iron reduction (SMIR) was considered to be the main Fe(III) reduction pathway in irradiated NOM solutions based on the similarity of Fe(II) generation and $O_2^{\bullet-}$ generation profile as well as the observation that the presence of superoxide dismutase (SOD) decreased Fe(II) generation, although the role of LMCT in Fe(III) reduction was not entirely excluded (Garg et al. 2011a). It is worth noting that even though SMIR was reported to be the dominant photochemical Fe(III) reduction pathway at circumneutral pH (Rose and Waite 2005; Rose and Waite 2006), there are other studies suggesting that Fe(III) reduction via LMCT is more likely to be an important Fe(II) source for strongly bound Fe(III) complexes at circumneutral pH (Barbeau et al. 2003). Due to the difference in the experimental conditions used in various studies, we thus hypothesize that both LMCT and SMIR could potentially be important Fe(III) photochemical reduction pathways with their relative importance likely to depend on conditions such as iron: NOM ratio, ionic strength, and pH.

7.2. Experimental methods

Detailed description of the reagents and experimental setup is provided in Chapter 2 with additional remarks provided below.

One difficulty in studying iron transformations at this pH range is the predominant role of oxygenation of Fe(II) that is likely to conceal other iron transformation pathways. To avoid the influence of rapid Fe(II) oxidation by oxygen, 1 mM FZ was introduced in the experiments in which Fe(III) reduction pathways were investigated with this approach similar to the 'FZ trapping' technique that was used in other studies (Pullin and Cabaniss 2003; Garg et al. 2011a). FZ complexes Fe(II) rapidly to form $Fe(FZ)_3$ that is

resistant to oxygenation. Furthermore, the presence of 1 mM FZ outcompetes Fe(II) oxidation completely as confirmed by the observation that no decrease in Fe(II) concentration occurs within 1 h in the presence 1 mM FZ at all pH studied. In addition, the presence of FZ does not have any influence on Fe(III) reduction pathway(s), as the Fe(III) reduction kinetics is invariant in the presence of 0.5, 1, and 2 mM FZ (p > 0.05 ,calculated using one-way ANOVA). It should be acknowledged that $Fe(FZ)_3$, representing Fe(II) trapped by FZ, does not undergo further redox reactions, which allows the investigation of Fe(III) reduction kinetics alone. To prevent Fe(III) precipitation, the ratio of iron: SRFA concentrations was maintained at 0.056 % w/w. This ratio is also consistent with our previous studies at acidic pH (Chapter 3, 5 and 6) allowing the exploration of iron transformations at these different pH ranges.

7.3. Results and discussion

7.3.1. Fe(III) reduction kinetics in non-irradiated SRFA solutions

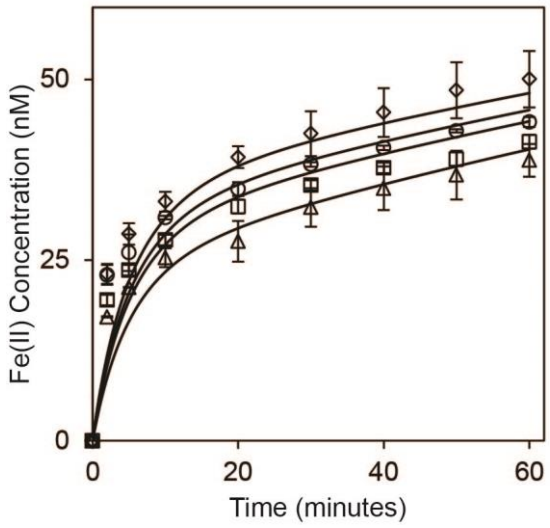

Figure 7.1: Generation of Fe(II) as a result of 100 nM Fe(III) reduction in non-irradiated 10 $mg.L^{-1}$ SRFA solutions containing 1 mM FZ at pH 6.8 (diamonds), 7.3 (squares), 8.3 (circles), and 8.7 (triangles). Symbols represent the average of duplicate measurements; lines represent model values.

As shown in Figure 7.1, Fe(II) concentration increased as a result of reduction of Fe(III). The reduction rate of Fe(III) is rapid in the first 10 min, and slows down in the later stages. This observation is similar to the results of previous studies under acidic conditions in Chapter 3 where Fe(II) generation due to Fe(III) reduction was rapid initially before reaching a steady state, however there are differences in the experimental conditions. In acidic conditions, the steady state concentration of Fe(II) was considered to be a result of a balance between Fe(III) reduction by hydroquinone-like moieties, A^{2-} (eq.7.1) and Fe(II) oxidation by semiquinone-like moieties, A^{-} (eq.7.2). In this study, FZ acts as a scavenger for Fe(II), preventing Fe(II) oxidation by dioxygen (eq.7.3) and other oxidants (e.g. A^{-}) (eq.7.2). Also, the Fe(II) generation rate in the later stages in Figure 7.1 does not reach a steady state, excluding the possibility of the depletion of a single Fe(III) reductant in this solution. However, the Fe(II) generation profile as shown in Figure 7.1 is more likely a result of a rapid Fe(III) reduction followed by a relatively slow Fe(III) reduction. We thus presume that the initial rapid Fe(III) reduction in the first 10 min is due to the depletion of a stronger Fe(III) reductant (R_s; eq.7.4); and a relatively weaker Fe(III) reductant (R_w; eq.7.5), present in SRFA solutions, is responsible for the slower Fe(III) reduction in the later stages.

$$A^{2-} + \text{Fe(III)} \xrightarrow{k_1} A^{-} + \text{Fe(II)} \tag{7.1}$$

$$A^{-} + \text{Fe(II)} \xrightarrow{k_2} A^{2-} + \text{Fe(III)} \tag{7.2}$$

$$\text{Fe(II)} + O_2 \xrightarrow{k_3} \text{Fe(III)} + O_2^{\bullet -} \tag{7.3}$$

$$R_s + \text{Fe(III)} \xrightarrow{k_4} R_s^{-} + \text{Fe(II)} \tag{7.4}$$

$$R_w + Fe(III) \xrightarrow{k_5} R_w^- + Fe(II) \quad (7.5)$$

By neglecting the role of the relatively weaker Fe(III) reductant in the initial 10 min, the rate of Fe(II) generation over time due to the strong Fe(III) reductant (eq.7.4) can be deduced and, as shown below, can be described by the second-order rate equation:

$$\frac{d[Fe(II)]}{dt} = k_4[R_s][Fe(III)] \quad (7.6)$$

and the relationship between Fe(II) concentration and time can be obtained as in eq.7.7,

$$[Fe(II)]_t = \frac{Fe_0 e^{k_4(R_{s0}-Fe_0)t+\ln R_{s0}-\ln Fe_0} - R_{s0}}{e^{k_4(R_{s0}-Fe_0)t+\ln R_{s0}-\ln Fe_0} - 1} \quad (7.7)$$

where Fe_0 and R_{s0} represent the initial concentration of Fe(III) and R_s respectively, and $[Fe(II)]_t$ represents Fe(II) concentration at time *t*. The concentration of R_{s0} and rate constant k_4 can be obtained based on best-fit of this function (eq.7.7) to the measured Fe(II) concentration at different time t using GraphPad Prism (Table 7.1). The small variation in k_4 at different pH values suggests that Fe(III) reduction in non-irradiated SRFA solutions is pH independent, consistent with the observation in Chapter 3 at acidic pH. This pH independency suggests that either the reactivity and/or speciation of Fe(III)-SRFA complex is invariant in the pH range 6.8-8.7.

Table 7.1: Initial concentration of strong Fe(III) reductant (R_s), and the rate constant calculated based on the rapid Fe(III) reduction results in 0-10 min using GraphPad Prism

	Non-irradiated solution		Previously irradiated solution	
pH	Initial concentration of strong Fe(III) reductant (nM)	Rate constant ($\times 10^6$ $M^{-1}s^{-1}$)	Initial concentration of strong Fe(III) reductant (nM)	Rate constant ($\times 10^6$ $M^{-1}s^{-1}$)

6.8	32.4 ± 1.3	6.8 ± 1.1	47.7 ± 2.2	7.5 ± 1.4
7.3	36.9 ± 1.4	6.8 ± 1.4	51.6 ± 3.6	8.7 ± 2.7
8.3	29.4 ± 1.7	8.1 ± 2.2	41.5 ± 0.3	7.9 ± 0.3
8.7	24.6 ± 1.3	6.1 ± 1.2	32.9 ± 2.3	4.8 ± 1.1

In later stages (20-60 min), the pseudo first-order rate constant for the reduction of Fe(III) by the relatively weak reductant (R_w; eq.7.5) is calculated to be (1.8 ± 0.29) × 10^{-3} min^{-1} (Table 7.2), suggesting that the concentration of R_w is in sufficiently large excess and k_5 is also invariant with pH. Hydroquinone-like moieties, reported to be the Fe(III) reductant under acidic conditions in Chapter 3, is likely to be the Fe(III) reductant at the pH investigated here. Although the other reductant could be a different group of hydroquinone-like moieties, we hypothesize that semiquinone-like moieties as the other Fe(III) reductant, which is most consistent with the observation in this chapter with this possibility justified in later sections. Although the semiquinone-like moieties are considered to be absent in non-irradiated SRFA solutions under acidic conditions (see discussion in Chapter 3), its concentration in fulvic acids has been reported to increase as pH increases (Paul et al. 2006). The presence of semiquinone-like moieties at the pH used in this study is most likely due to the autoxidation of hydroquinone by oxygen, while this process is inhibited in acidic conditions due to spin-restriction (Roginsky and Barsukova 2000).

Table 7.2: Pseudo first-order rate constant (min^{-1}) for Fe(III) reduction by the weak Fe(III) reductant (R_w), calculated based on experimental results in 20-60 min

pH	Non-irradiated solution	Previously irradiated solution

6.8	2.2×10^{-3}	3.4×10^{-3}
7.3	1.7×10^{-3}	2.8×10^{-3}
8.3	1.5×10^{-3}	1.2×10^{-3}
8.7	1.8×10^{-3}	9.0×10^{-4}

7.3.2. Fe(III) reduction kinetics in previously irradiated SRFA solutions

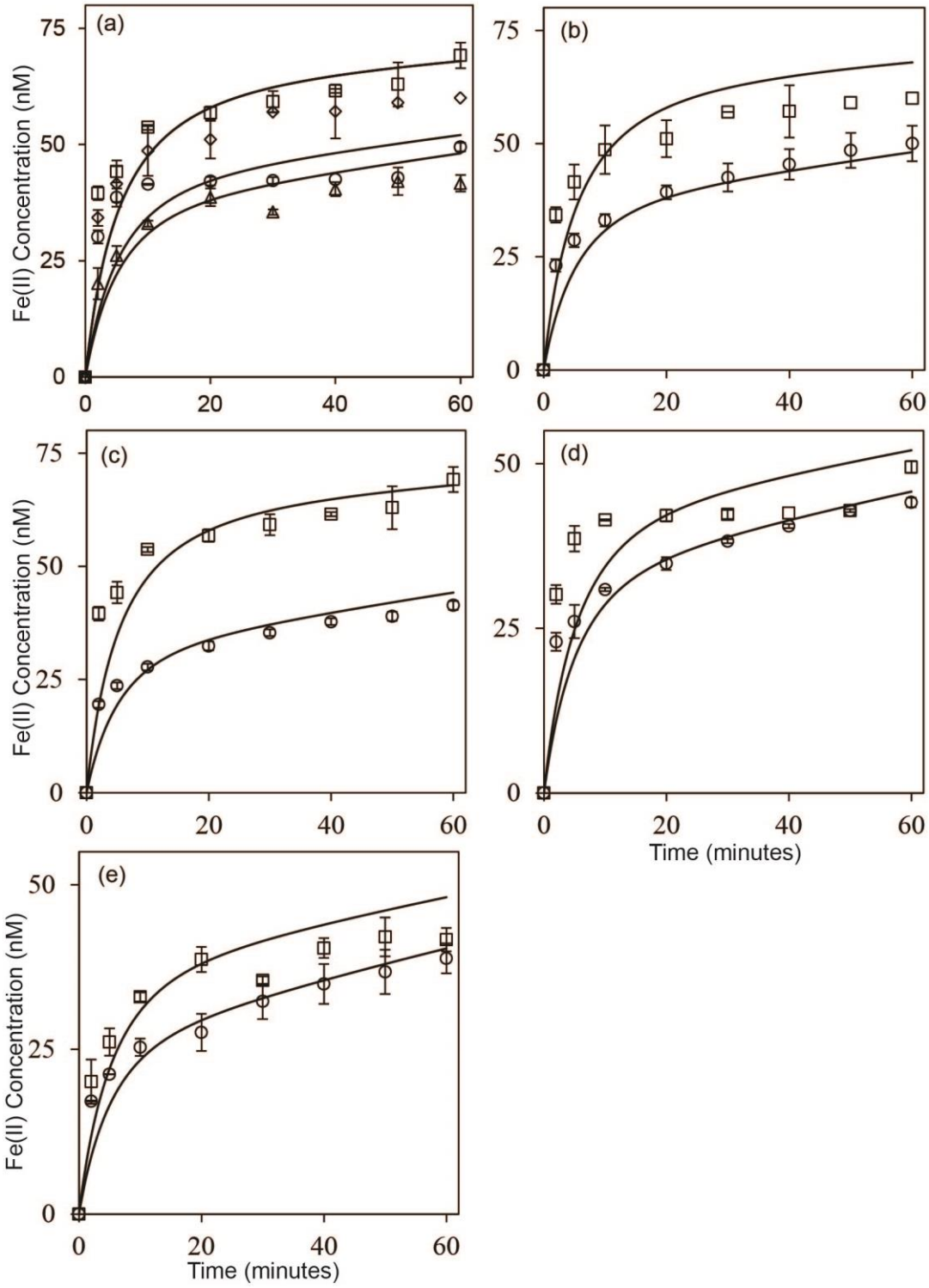

Figure 7.2: a) Generation of Fe(II) as a result of 100nM Fe(III) reduction in previously irradiated 10mg.L^{-1} SRFA solutions containing 1mM FZ at pH 6.8 (diamonds), 7.3 (squares), 8.3 (circles), and 8.7 (triangles). Generation of Fe(II) as a result of 100nM Fe(III) reduction in non-irradiated (circles) and previously irradiated (squares) 10mg.L^{-1} SRFA solutions containing 1mM FZ at pH 6.8 (panel b), 7.3 (panel c), 8.3 (panel d), and 8.7 (panel e). Symbols represent the average of duplicate measurements; lines represent model values.

When Fe(III) was added to SRFA solutions that were previously irradiated for 10 minutes, Fe(II) was generated due to Fe(III) reduction at all pH values (Figure 7.2a), in a manner similar to the observations in the non-irradiated solution (Figure 7.1). However, the Fe(III) reduction in previously irradiated SRFA solutions is pH dependent with Fe(II) concentration generated on Fe(III) reduction at pH 6.8 and 7.3 substantially higher than that at pH 8.3 and 8.7 (Figure 7.2a). In addition, Fe(II) generation in previously irradiated solution is higher than the Fe(II) generation in non-irradiated solution (Figure 7.2), especially at pH 6.8 (30% increase, Figure 7.2b) and pH 7.3 (45% increase, Figure 7.2c) as compared to 12% increase at pH 8.3 (Figure 7.2d) and 9% increase at pH 8.7 (Figure 7.2e) based on the Fe(II) generation at 60 min. This observation suggests that a reductant was generated in previously irradiated solution at pH 6.8-8.3 with this reductant playing a more significant role at lower pHs.

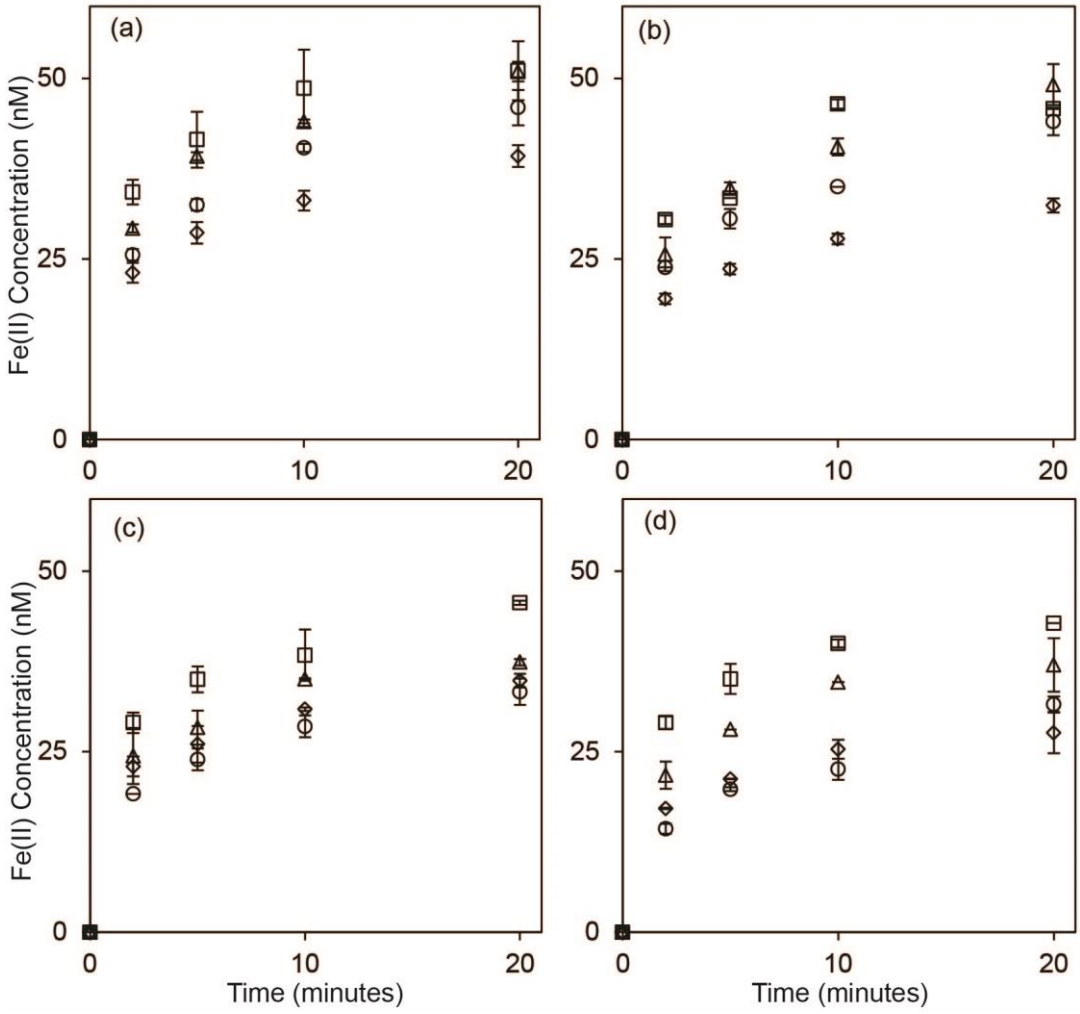

Figure 7.3: Generation of Fe(II) as a result of 100nM Fe(III) reduction in 10mg.L^{-1} SRFA solutions containing 1mM FZ that has been previously irradiated prior to 0 min (squares), 10 min (triangles), and 2 h (circles) storage in the dark, compared with non-irradiated solution (diamonds) at pH 6.8 (panel a), 7.3 (panel b), 8.3 (panel c), and 8.7 (panel d). Symbols represent the average of duplicate measurements; lines represent model values.

While the identity of this photo-generated Fe(III) reductant in unknown, we estimated the lifetime of this Fe(III) reductant experimentally. As shown in Figure 7.3, when Fe(III) was added to SRFA solutions that had been irradiated prior to storage in the dark, Fe(II) generation decreased as the duration of dark storage increased. In the previously irradiated solution stored in the dark for 2 hours, the Fe(II) generation is close to the Fe(II) generation in non-irradiated solution especially at pH 8.3 and 8.7, which suggests that the lifetime of Fe(III) reductant generated during irradiation $\leq$ 2 hours. Such a

longevity eliminates the possibility of $O_2^{\bullet-}$ ($t_{1/2}$ ~ 100 s) (Garg et al. 2011b) playing a role in Fe(III) reduction. Indeed, Fe(III) reduction in the presence and absence of 25 $kU.L^{-1}$ SOD (added either before and after irradiation) were essentially identical (data not shown; $p > 0.05$, calculated using one-way ANOVA), supporting the conclusion that superoxide does not participate in the Fe(III) reduction in previously irradiated SRFA solutions. The Fe(III) reducing organic moieties generated on irradiation could be semiquinone-like moieties that have been reported to be generated on irradiation of SRFA solution under acidic conditions (Chapter 3). By assuming a rapid Fe(III) reduction by R_s followed by a slower reduction by R_w, the concentration of R_{s0}, k_4, and pseudo first-order rate constant for eq.7.5 can be determined in the same manner as in non-irradiated solution (Table 7.1 and Table 7.2). As shown in Table 7.1, the increased Fe(II) generation in previously irradiated solution is mainly a result of an increased R_{s0} concentration with relatively invariant k_4 as compared to non-irradiated solution, leading to an increased Fe(II) generation in the initial stages (0-10 min). However, the change in Fe(III) reduction kinetics in the presence and absence of irradiation in later stages (pseudo first-order rate constants shown in Table 7.2) is relatively less important due to the small impact it has on Fe(II) generation. We thus hypothesize that the semiquinone-like moieties, acting as a stronger Fe(III) reductant, are responsible for the rapid generation of Fe(II) in the initial stages in non-irradiated and previously irradiated SRFA solutions. Concomitantly, hydroquinone-like moieties, are expected to reduce Fe(III) relatively slowly as reflected in the slower Fe(II) generation rate in later stages. This hypothesized mechanism will be further supported by kinetic modelling in a later section.

7.3.3. Fe(II) oxidation kinetics in non-irradiated SRFA solutions

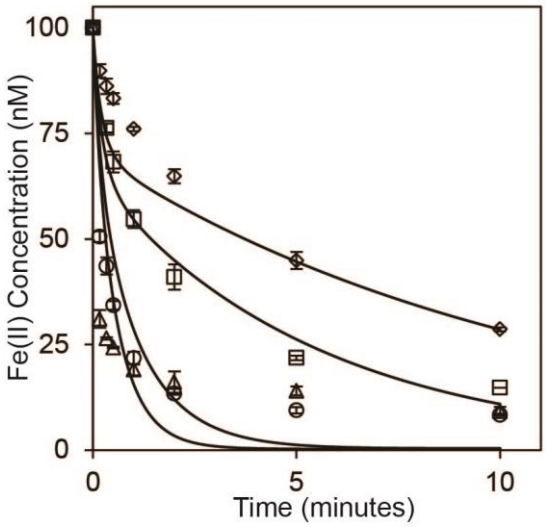

Figure 7.4: Concentration of Fe(II) remaining as a result of 100 nM Fe(II) oxidation in non-irradiated 10 $mg.L^{-1}$ SRFA solutions at pH 6.8 (diamonds), 7.3 (squares), 8.3 (circles), and 8.7 (triangles). Symbols represent the average of duplicate measurements; lines represent model values.

To fully understand the iron redox cycle, Fe(II) oxidation was studied by adding 100 nM Fe(II) in non-irradiated SRFA solutions and the decrease in Fe(II) concentration monitored. It should be noted that FZ was added here for Fe(II) measurement only, as opposed to Fe(III) reduction experiments which incorporated FZ as an Fe(II) scavenger to prevent Fe(II) oxidation. At all pH values (Figure 7.4), Fe(II) decays almost linearly in the initial stages due to rapid Fe(II) oxidation, while a relatively slower Fe(II) oxidation rate is observed in the later stages, presumably as a result an increasing Fe(III) reduction rate as Fe(III) is generated on Fe(II) oxidation. As shown in Figure 7.4, Fe(II) oxidation is strongly pH dependent in the pH range studied. For example, the half-life of Fe(II) is ~ 5 min at pH 6.8, and < 10 s at pH 8.7. The pH dependence of Fe(II) oxidation has been reported in many studies (Millero et al. 1987; Santana-Casiano et al. 2004) and it was mainly attributed to the changes in Fe(II) speciation with change in pH.

7.3.4. Fe(II) oxidation kinetics in previously irradiated SRFA solutions

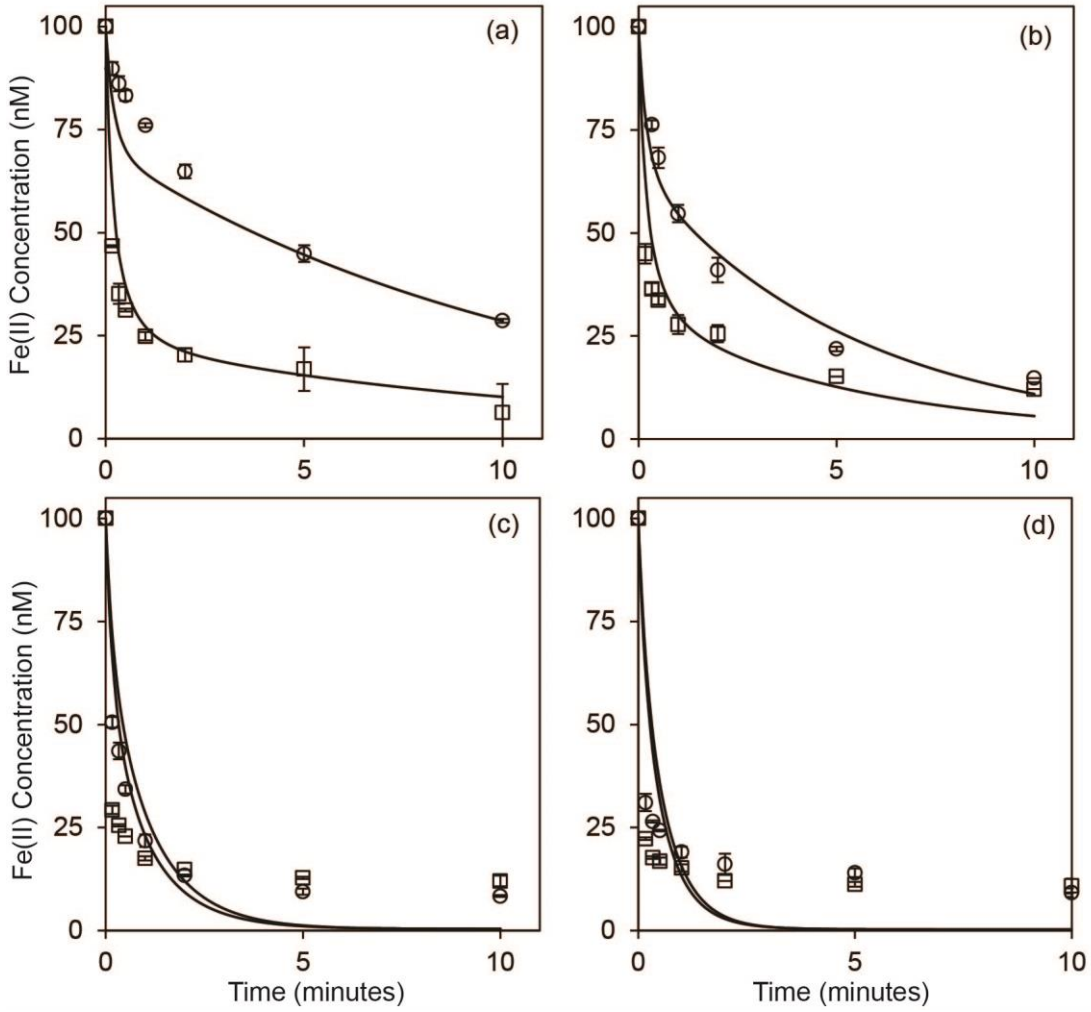

Figure 7.5: Concentration of Fe(II) remaining as a result of 100 nM Fe(II) oxidation in non-irradiated (circles) and previously irradiated (squares) 10 mg.L^{-1} SRFA solutions at pH 6.8 (panel a), 7.3 (panel b), 8.3 (panel c), and 8.7 (panel d). Symbols represent the average of duplicate measurements; lines represent model values.

As shown in Figure 7.5, Fe(II) decay rates in SRFA solutions that were previously irradiated for 10 min are higher than the Fe(II) decay rate in non-irradiated SRFA solutions, especially at pH 6.8 and 7.3. The effect of the increased Fe(II) oxidation rate is more dramatic in the initial stages when Fe(II) exists at relatively higher concentration, while this effect becomes negligible in later stages when Fe(II) was mostly oxidized. This increased Fe(II) oxidation rate in previously irradiated SRFA solutions suggests that an Fe(II) oxidant was generated on irradiation of SRFA solutions,

and the Fe(II) oxidation rate by this oxidant is comparable with the Fe(II) oxidation rate in non-irradiated solution. This observation is in agreement with the previous work at acidic conditions in Chapter 3, in which we reported that semiquinone-like moieties (A^-) were generated as a result of oxidation of hydroquinone-like moieties (A^{2-}) on irradiation with these semiquinone-like moieties the dominant Fe(II) oxidant in acidic environments where Fe(II) oxygenation is negligible. At circumneutral pH, it is likely that the same mechanism involving generation of semiquinone-like moieties on irradiation is responsible for the rapid oxidation of Fe(II) in previously irradiated solution, given that the semiquinone radicals tends to exist in higher concentration in fulvic acids as mentioned above.

It should be noted that we have observed both increased Fe(II) oxidation rate and increased Fe(III) reduction rate in previously irradiated SRFA solutions when compared with that observed in the non-irradiated SRFA solutions. One possibility is that both Fe(II) oxidant and Fe(III) reductant are generated on irradiation of SRFA, however the Fe(II) oxidation rate by the photo-generated oxidant is much faster than the reduction rate of Fe(III) by the photo-generated reductant, resulting in a net increase in Fe(II) oxidation when Fe(II) is added to previously irradiated SRFA solutions. Indeed, the Fe(II) oxidation rate by the photo-generated oxidant in previously irradiated solutions is expected to be very fast, as it is capable of exceeding the rapid Fe(II) oxidation rate by dioxygen. It is also likely that one entity (presumably semiquinone-like radicals) are generated during irradiation of SRFA and is responsible for both Fe(II) oxidation as well as Fe(III) reduction. This is supported by the similar lifetime of Fe(III) reductant and Fe(II) oxidant generated on irradiation of SRFA solutions (Figure 7.3 and Figure 7.6). This possibility will be further examined by the kinetic modelling in later section.

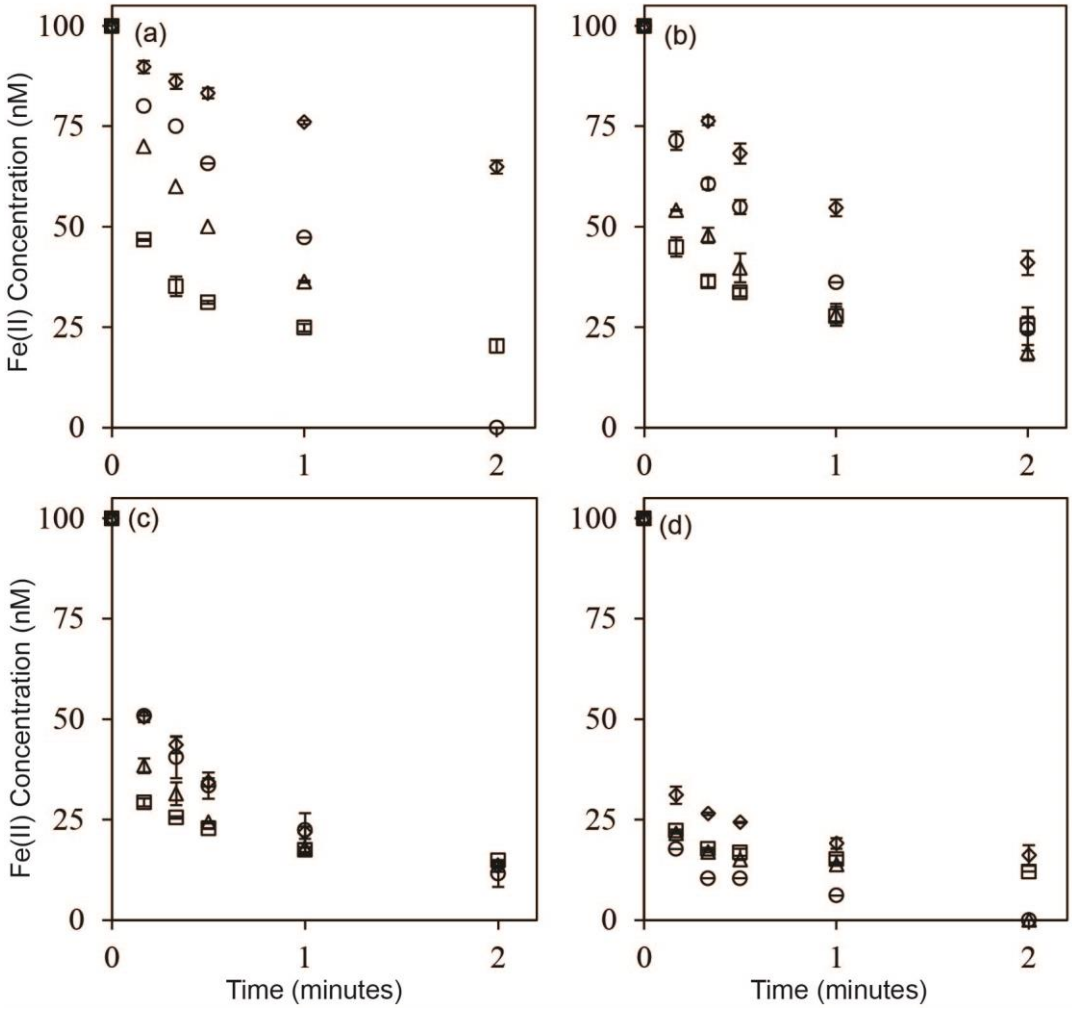

Figure 7.6: Concentration of Fe(II) as a result of 100 nM Fe(II) oxidation in 10 mg.L^{-1} SRFA solutions that has been previously irradiated prior to 0 min (squares), 10 min (triangles), and 2 h (circles) storage in the dark, compared with non-irradiated solution (diamonds) at pH 6.8 (panel a), 7.3 (panel b), 8.3 (panel c), and 8.7 (panel d). Symbols represent the average of duplicate measurements; lines represent model values.

7.3.5. Fe(III) reduction and Fe(II) oxidation kinetics in continuously irradiated SRFA solutions

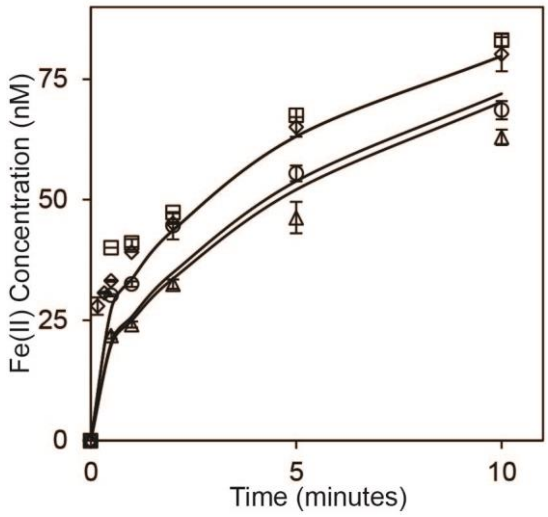

Figure 7.7: Generation of Fe(II) as a result of 100 nM Fe(III) reduction in continuously irradiated 10 mg.L^{-1} SRFA solutions at pH 6.8 (diamonds), 7.3 (squares), 8.3 (circles), and 8.7 (triangles). Symbols represent the average of duplicate measurements; lines represent model values.

When Fe(III) containing SRFA solutions were irradiated, the Fe(II) concentration increased as a result of Fe(III) reduction (Figure 7.7). The rates of Fe(II) generation in continuously irradiated solutions are significantly higher than those observed in non-irradiated (Figure 7.1) and previously irradiated SRFA solutions (Figure 7.2) at all pH values, suggesting that a reduction pathway other than those discussed in earlier sections plays an important role in continuously irradiated SRFA solutions. There are two potential pathways for the rapid photochemical Fe(III) reduction, namely LMCT and SMIR as discussed earlier. To probe the role of SMIR, the Fe(III) reduction kinetics was measured in the presence of 25 kU.L^{-1} SOD, and no significant impact (data not shown, $p > 0.05$, calculated using one-way ANOVA) of SOD addition is observed on the Fe(II) generation kinetics suggesting that superoxide does not play a role in Fe(III) reduction under the experimental conditions investigated here. This further supports the

important contention that Fe(III) is mainly reduced by an LMCT pathway in irradiated SRFA solutions.

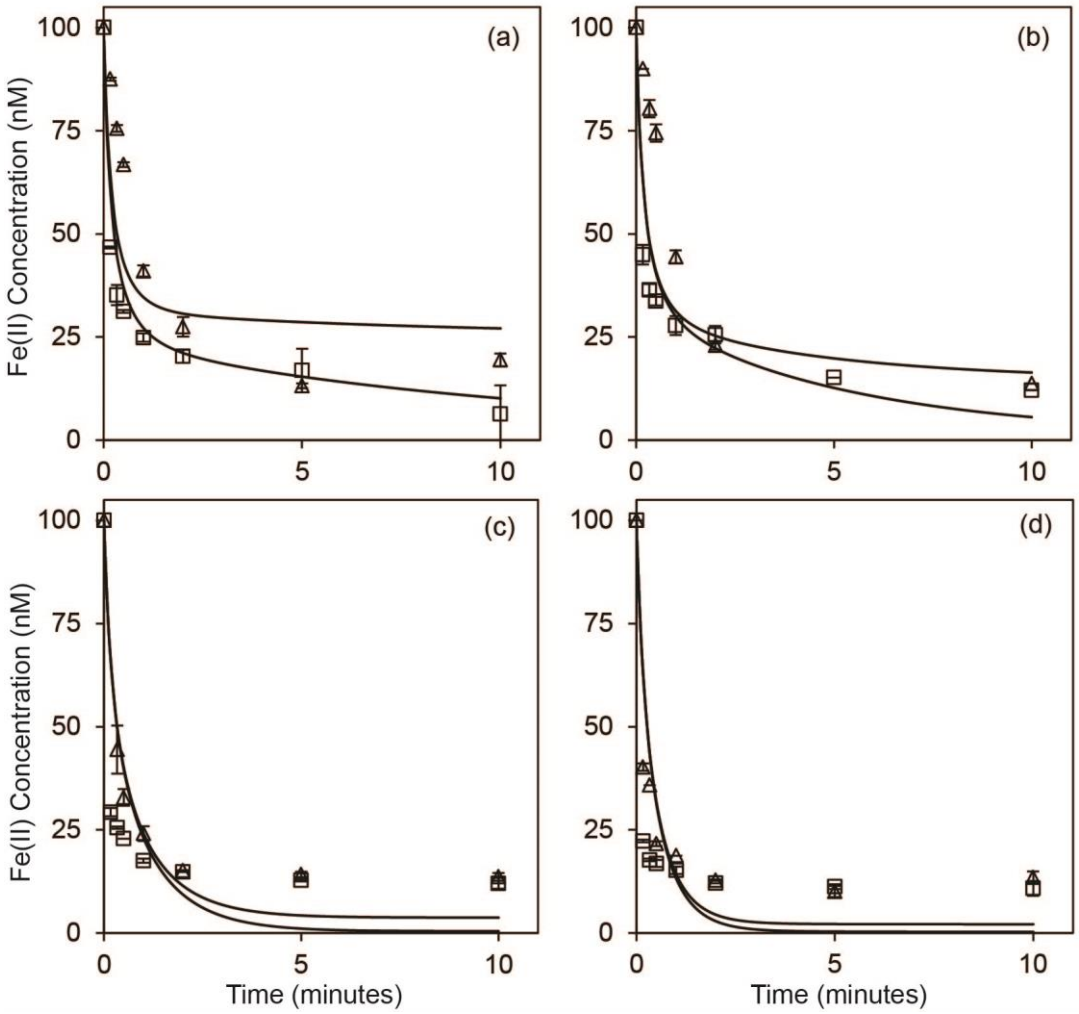

Figure 7.8: Concentration of Fe(II) remaining as a result of 100 nM Fe(II) oxidation in previously irradiated (squares) and continuously irradiated (triangles) 10 mg.L^{-1} SRFA solutions at pH 6.8 (panel a), 7.3 (panel b), 8.3 (panel c), and 8.7 (panel d). Symbols represent the average of duplicate measurements; lines represent model values.

Fe(II) oxidation in continuously irradiated SRFA solutions was also studied with the results (Figure 7.8) suggesting that Fe(II) oxidation rates in continuously irradiated solution are lower than that observed in previously irradiated SRFA solutions at all pH values investigated here due to the rapid reduction of any Fe(III) formed via Fe(II) oxidation in continuously irradiated SRFA solutions (Figure 7.7).

7.3.6. Role of superoxide

The role of superoxide on Fe transformations in previously and continuously irradiated solutions is negligible based on the observations presented above. This observation contradicts with the observations in other studies (Rose and Waite 2005; Rose and Waite 2006) in which an impact of SOD addition was reported with the conclusion reaches in those studies that superoxide played a significant role in photochemical Fe(III) reduction at circumneutral pH. A possible explanation for this discrepancy is the difference in iron: NOM ratios in this study and in the studies mentioned above. While most of the iron: NOM ratio was maintained at 0.56% - 7% in other studies (Rose and Waite 2005; Rose and Waite 2006), a significantly lower ratio (0.056%) was used here to avoid Fe(III) hydrolysis, as well as to maintain consistency with the ratios used under acidic conditions in Chapter 3, 5 and 6. The lower iron: NOM ratio results in creation of a stronger Fe-SRFA complex, which has a significant impact on the iron redox transformation rate and mechanism. The Fe(III) reduction rate via SMIR pathway is associated with Fe(III) complexation strength. Indeed, Rose and Waite (2005) reported that Fe(III) reduction rate by $O_2^{\bullet-}$ is generally faster with weakly organically complexed Fe(III) and inorganic Fe(III). Voelker and Sedlak (1995) also observed that inorganically complexed Fe(III) species are more readily reduced by $O_2^{\bullet-}$ than organically complexed Fe(III). The rate constant for inorganic Fe(III) reduction by $O_2^{\bullet-}$ was reported to be 1,500 times that for organically complexed Fe(III) at pH 8.1 (Garg et al. 2011a). Thus, with strong Fe-NOM complexation due to low iron: NOM ratio used in this study, the Fe(III) reduction occurs almost exclusively via LMCT rather than reduction by $O_2^{\bullet-}$ in continuously irradiated SRFA solutions.

7.3.7. Role of dioxygen

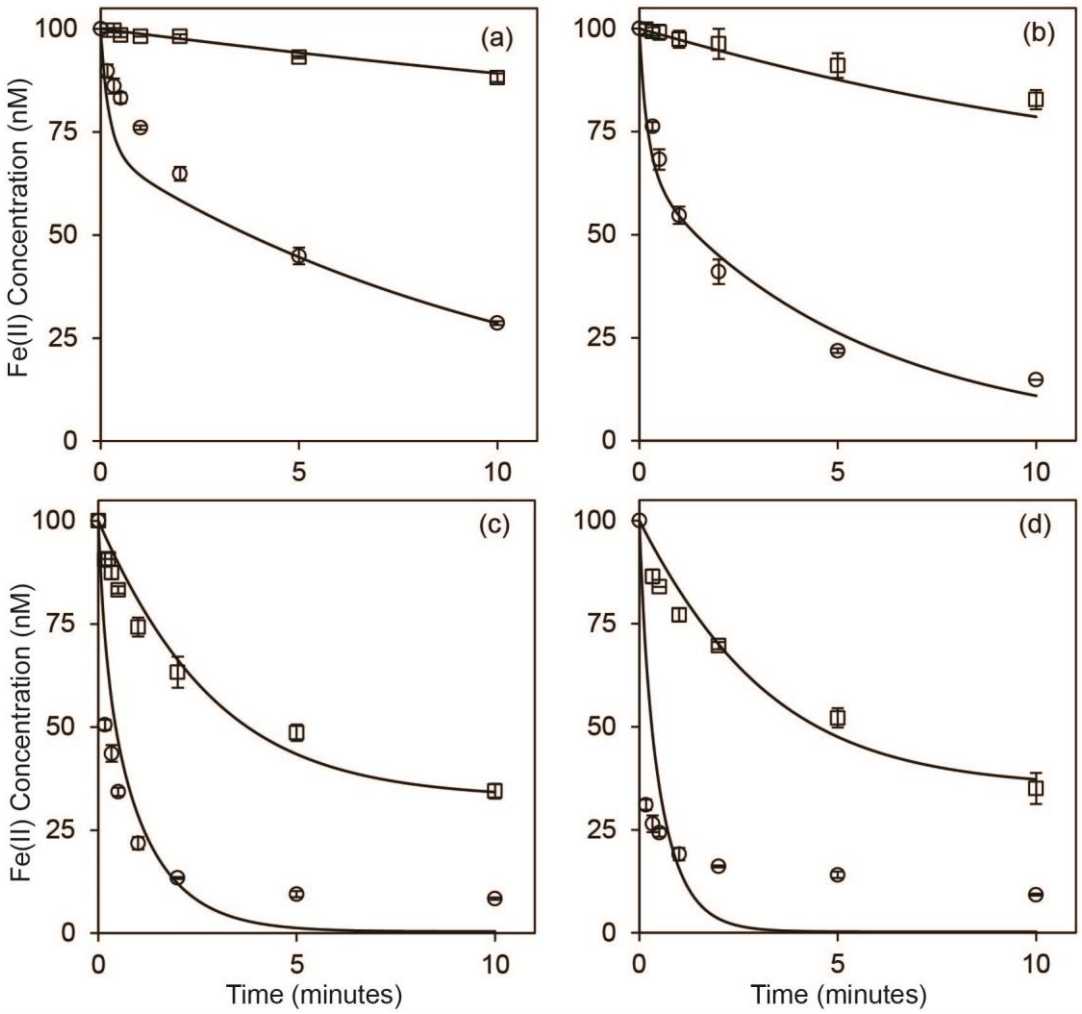

Figure 7.9: Concentration of Fe(II) remaining as a result of 100nM Fe(II) oxidation in non-irradiated air-saturated (circles) and partially deoxygenated(squares) 10mg.L^{-1} SRFA solutions at pH 6.8 (panel a), 7.3 (panel b), 8.3 (panel c), and 8.7 (panel d). Symbols represent the average of duplicate measurements; lines represent model values.

As shown in Figure 7.9, partial removal of oxygen (~ 95%) resulted in a significant decrease in Fe(II) decay rate at all pH values investigated here supporting the conclusion that Fe(II) oxidation mostly occurs as a result of its interaction with dioxygen in non-irradiated SRFA solutions. Since the pH of the solution was controlled by continuously sparging the 2 mM $NaHCO_3$ solution containing SRFA using pre-mixed synthetic air containing CO_2, intrusion of oxygen from ambient atmosphere cannot be completely prevented during the experiment. Furthermore, our results show

that the Fe(II) oxidation kinetics in partially deoxygenated solutions are strongly pH dependent, consistent with the observation in air saturated solution (Figure 7.4). At pH 6.8 and 7.3, Fe(II) oxidation was almost completely inhibited in partially deoxygenated solution; but occurs at a rapid rate at pH 8.3 and 8.7 even in partially deoxygenated solution.

7.3.8. Kinetics and mechanism of Fe redox transformations

The Fe redox transformations in the pH range 6.8-8.7 are significantly different from the Fe redox transformations under acidic conditions, mainly due to the rapid Fe(II) oxygenation rate at higher pH. However, there are a few similarities under the two pH conditions, (i) generation of relatively long-live Fe(II) oxidant on irradiation of SRFA and (ii) important role of LMCT in Fe(III) reduction in continuously irradiated SRFA solutions. A kinetic model (Table 7.3) is developed that given a good description of the experimental results. A brief summary of the key reactions and justification of rate constants is provided below.

Table 7.3: Kinetic model for Fe redox transformations in the pH range 6.8-8.7.

No	Reaction	Rate constant ($M^{-1}s^{-1}$)				Ref
	Fe redox transformations under non-irradiated condition					
1	$Fe(III)+A^{2-} \rightarrow Fe(II)+A^{-}$	1.0×10^{2} [a]				Chapter 3
2	$Fe(III)+A^{-} \rightarrow Fe(II)+A$	3.5×10^{4} [b]				This work
3	$Fe(II)+A^{-} \rightarrow Fe(III)+A^{2-}$	9.0×10^{5}				Chapter 3
4	$Fe(II)+O_2 \rightarrow Fe(III)+O_2^{\bullet-}$	pH 6.8	pH 7.3	pH 8.3	pH 8.7	This work
		6.0	12.0	55.0	100.0	
5	$Fe(III) \xrightarrow{h\upsilon} Fe(II)$	1.1×10^{-3} s^{-1}				Chapter 5

[a] $[A_0]$ = 35.4 µmol.g^{-1} SRFA as reported in Garg et al. (2013a).

[b] Concentrations of A^- are determined based on best-fit to experimental results. In non-irradiated solution, [A^-] are 35 nM, 35 nM, 32 nM, and 25 nM at pH 6.8, 7.3, 8.3, 8.7 respectively; in previously irradiated solution, [A^-] are 75 nM, 70 nM, 45 nM, and 35 nM at pH 6.8, 7.3, 8.3, 8.7 respectively

7.3.8.1. Fe(III) reduction by hydroquinone-like moieties

As reported under acidic conditions (Chapter 3), Fe(III) is reduced by hydroquinone (A^{2-}) that is present intrinsically in SRFA solutions. The total concentration of total reducing group A_0 is assumed to be 35.4 μmol.g^{-1} SRFA, the same as its concentration under acidic conditions (Chapter 3). Concentration of A^{2-} (determined by eq.7.8) at pH 6.8-8.7 here is slightly less than the total concentration of A_0 due to the presence of semiquinone-like moieties (A^-) at this pH range.

$$[A^{2-}] = [A_0] - [A^-] \quad (7.8)$$

The rate constant for reaction 1 (Table 7.3) is determined based on best-fit to the Fe(II) generation data in later stages (20-60 min). As shown in Table 7.1, the slower generation rate of Fe(II) generation due to Fe(III) reduction in 20-60 is invariant with pH. Thus, the rate constant k_1 is assumed to be pH-independent, consistent with that reported under acidic conditions in Chapter 3. The is mainly due to the invariant speciation/ reactivity of Fe(III) and hydroquinone (mostly doubly deprotonated form with pK_{a1} ~ 10 and pK_{a2} ~ 12) in the pH range 7.8-8.7.

7.3.8.2. Fe(III) reduction by semiquinone-like moieties

As hypothesized above, semiquinone-like moieties (A^-) are hypothesized to reduce Fe(III) rapidly under the conditions investigated here. These semiquinone-like moieties exist in non-irradiated SRFA solutions, and are also generated on irradiation of SRFA solutions. The concentration of A^- is determined based on best-fit to experimental

results assuming a 1:1 stoichiometry for Fe(III) reduction by A^- (reaction 2; Table 7.3), and the rapid Fe(III) reduction by A^- is terminated due to the consumption of A^-. The concentrations of A^- determined for various conditions and pH are provided in Table 7.3, with the concentration of A^- determined based on the measured initial Fe(III) reduction rate.

The rate constants for reaction 2 (Table 7.3) were determined based on best-fit to the Fe(II) generation data in the initial stages (0-10 min). The pH-independent k_2 suggest that the reactivity of Fe(III) and A^- is invariant, with A^- mainly present in deprotonated form (pK_a ~ 4) in the pH range studied here.

It should be noted that even though we can determine the generation of A^- based on the above mentioned assumption and can satisfactorily model experimental results, the mechanism by which this A^- is generated on irradiation is not clear. The mechanism developed in acidic pHs should not be applicable here, mainly because superoxide was shown to play a minimum role in Fe redox transformations as shown by SOD addition experiments. Thus, the A^- generation in acidic conditions via oxidation of A^{2-} by superoxide is not important under the experimental conditions here.

7.3.8.3. Fe(II) oxidation by semiquinone-like moieties

As reported in Chapter 3, semiquinone-like moieties are capable of oxidizing Fe(II) under acidic conditions. As the deprotonated semiquinone (A^-) is more reactive than the protonated form (HA), the reactivity of semiquinone in the pH range here is expected to be higher than that under acidic conditions. Thus, it is reasonable to include the Fe(II) oxidation by A^- (reaction 3; Table 7.3) in the model and attribute the increased Fe(II) oxidation in previously irradiated SRFA solutions to A^-. Using the concentration of A^- calculated above, the rate of Fe(II) oxidation by A^- is determined

to be 9.0 × 10^5 $M^{-1}s^{-1}$ at all pH values, approximately 10 fold higher than the rate constant reported under acidic conditions (Chapter 3). The model successfully predicts a more apparent increase in the Fe(II) oxidation in previously irradiated SRFA solutions at lower pH values (Figure 7.5). This is reasonable since the Fe(II) oxidation by oxygen (reaction 4; Table 7.3) is strongly pH dependent with the rate constant increasing with increase in pH. At pH 8.3 and pH 8.7, the oxygenation of Fe(II) occurs rapidly and hence increase in the Fe(II) oxidation by any photo-generated A^- (Figure 7.5) is not apparent.

7.3.8.4. Fe(II) oxidation by oxygen

The rate constant for Fe(II) oxidation by oxygen (reaction 4; Table 7.3) can be determined based on best-fit to experimental results, and is pH-dependent with increasing rate constant at higher pH, which is consistent with the results in other studies (Millero et al. 1987; Santana-Casiano et al. 2004).

7.3.8.5. Fe(III) reduction via LMCT

The rate constant for Fe(III) reduction via LMCT (k_5, reaction 5; Table 7.3) is determined on the basis of best-fit to the experimental data. The k_5 = 1.0 × 10^{-3} s^{-1} determined here is approximately 10% of the rate constant reported under acidic conditions (Chapter 5). Also, k_5 is determined to be pH-independent in the pH range investigated here, which is consistent with the invariant nature of Fe(III)-SRFA complex.

7.4. Conclusions

In this chapter, Fe redox transformations in SRFA solutions have been investigated in the pH range 6.8-8.7. The mechanism of Fe redox transformations observed here is

slightly different with that reported under acidic conditions, with the following key conclusions:

(1) Fe(II) oxygenation plays an increasingly important role in Fe(II) oxidation as pH increases. At pH 8.3 and 8.7, the role of Fe(II) oxygenation is significantly important than all other pathways.

(2) Semiquinone-like moieties are proposed to be capable of oxidizing Fe(II) and reducing Fe(III) at circumneutral pH. Semiquinone radicals can exist in non-irradiated SRFA solutions, and they are also generated when SRFA is irradiated. The presence of semiquinone radicals in non-irradiated SRFA solutions is likely due to the autoxidation of hydroquinone. The concentration of photo-generated semiquinone-like radicals (A^-) at pH 6.8 and 7.3 are more than the generation at pH 8.3 and pH 8.7. Although A^- was suggested to be generated via a superoxide-mediated pathway at acidic pH (Chapter 3), the role of superoxide is considered unimportant due to the insignificant effect of SOD addition. Thus, the pathway via which A^- is generated on irradiation is still unknown.

(3) LMCT is the dominant pathway of Fe(III) reduction in irradiated SRFA solutions. The discrepancy between this finding and others can be attributed to the much lower iron: NOM ratio used here, which is expected to create stronger Fe-SRFA complex that reacts with superoxide at a very slow rate.

Chapter 8. Conclusions

In this thesis, Fe redox transformation kinetics under the conditions present in natural waters are investigated. The experimental results show that Fe redox transformations are affected by the presence of NOM, calcium ions, light, and pH. A summary of the conclusions arising from these investigations is provided below.

In Chapter 3, Fe redox transformations were investigated in non-irradiated and previously irradiated SRFA solutions in the pH range 3-5. Our results show that hydroquinone-like groups present in SRFA solutions are capable of reducing Fe(III), forming Fe(II) and semiquinone-like moieties. These semiquinone-like moieties are long-lived (lifetime > 24 h) and can oxidize Fe(II) back to Fe(III) and hydroquinone. A dynamic equilibrium between hydroquinone/semiquinone and Fe(III)/Fe(II) redox couples controls the steady state Fe(II) concentration. On irradiation of SRFA solutions, hydroquinone-like moieties are partially oxidized to semiquinone-like moieties by photo-generated superoxide. These photo-generated semiquinone-like moieties are dominant Fe(II) oxidants in acidic environments where Fe(II) oxygenation is very slow. The Fe redox transformations in non-irradiated and previously irradiated SRFA solutions are pH dependent with Fe(II) oxidation rate increasing with increase in pH with this effect due principally to the formation of more reactive deprotonated semiquinone radicals at higher pHs.

In Chapter 4, Fe redox transformations were investigated in pure 1,4-hydroquinone solution in the pH range 3-5. In accord with the mechanisms proposed in SRFA solutions, pure 1,4-hydroquinone reduces Fe(III) to form Fe(II) and semiquinone radicals. The semiquinone radicals so formed are capable of oxidizing Fe(II), with the Fe(II) oxidation rate increasing with increase in pH due to the change in semiquinone radicals speciation, consistent with the Fe(II) oxidation kinetics in SRFA solutions. This process also overcomes the spin-restriction of autoxidation and facilitates the oxidation

of hydroquinone to form benzoquinone. However, there are significant differences between the Fe redox transformations in SRFA and pure hydroquinone solutions. Most importantly, the semiquinone radicals in SRFA solutions are more stable than the semiquinone radicals formed in pure hydroquinone solution with Fe turnover frequency in SRFA solutions calculated to be 10-20 fold higher than that in pure hydroquinone solution.

In Chapter 5, Fe redox transformations were investigated in continuously irradiated SRFA solutions in the pH range 3-5. Our results show that LMCT is the dominant Fe(III) reduction pathway while photo-generated superoxide and short-lived peroxyl radicals are the main Fe(II) oxidants in irradiated SRFA solutions. The generation of peroxyl radicals on irradiation of SRFA is pH dependent with increased concentration of peroxyl radicals generated at higher pHs. Irradiation of SRFA solutions creates a more dynamic Fe transformation, with Fe turnover frequency 10 fold higher than the TOF in non-irradiated SRFA solutions. The mechanism for Fe redox transformations developed here combined with that developed in Chapter 3 was used to predict diel variation in Fe redox transformations in acidic environments.

In Chapter 6, the effect of calcium ions on Fe redox transformations in SRFA solutions were investigated under acidic conditions. The presence of Ca^{2+} increases the Fe(III) reduction rate by forming a more photo-labile weakly complexed Fe(III) species while Fe(II) oxidation rates by dioxygen and semiquinone-like moieties decrease in the presence of Ca^{2+} due to the formation of weakly bound Fe(II) complexes. In the presence of Ca^{2+}, Fe TOF is enhanced by 25% in irradiated SRFA solutions, and decreased by 25% in non-irradiated SRFA solutions. The higher Fe(III) reduction rates and lower Fe(II) oxidation rates in the presence compared to the absence of calcium

maintain higher concentrations of Fe(II) thereby increasing the bioavailability of iron in calcium-containing waters.

In Chapter 7, Fe redox transformations in SRFA solutions were investigated in the pH range 6.8-8.7. Our results show that in the pH range studied, semiquinone-like radicals are intrinsically present in SRFA solutions. The concentration of these semiquinone-like moieties increases on irradiation due to oxidation of hydroquinone-like moieties as was observed to be the case under acidic conditions. These semiquinone radicals are capable of oxidizing Fe(II) and reducing Fe(III). Our results further show that Fe(II) oxidation by dioxygen plays an increasingly important role at higher pH with the Fe(II) oxygenation rate constant increasing with increase in pH due to changes in Fe(II) speciation. Under irradiated conditions, Fe(III) reduction mostly occurs via ligand-to-metal charge transfer. Even though significant concentrations of superoxide are generated on irradiation of SRFA (~ 30-100 nM), no reduction of Fe(III)-SRFA by superoxide is observed under the experimental conditions investigated here possibly due to the formation of a strong Fe(III)-SRFA complex that is less prone to reduction by superoxide.

We consider that the work presented in this thesis has considerable scientific and environmental merit as the findings extend markedly our understanding of Fe redox transformations. Stable semiquinone-like moieties have been shown to play a significant role in Fe redox transformations in NOM solution as well as in pure hydroquinone solutions at all pH values examined. The effect of semiquinone-like moieties are especially important at acidic pH where Fe(II) oxygenation is negligible. Light is a critical factor controlling Fe redox transformations, by directly reducing Fe(III) via LMCT process, and indirectly generating ROS such as $O_2^{\bullet -}$ that reduces Fe(III), as well

as altering the composition of quinone moieties in NOM. Thus, significant diel variation of Fe redox transformations is expected. During the daytime, dynamic cycling rate between Fe(II) and Fe(III) is expected due to the light induced Fe(II) oxidation and Fe(III) reduction processes; at night, stable quinone moieties play a dominant role in Fe redox transformations, and the iron cycling rate is expected to be much slower. This thesis also shows that pH plays a key role in determining dominant pathways mediating Fe(II) oxidation and Fe(III) reduction. At acidic pH, quinone-like moieties play a dominant role; while oxygenation of Fe(II) becomes increasingly important as pH increases, suppressing the role of all other pathways.

While the work reported in this thesis provides new insights into Fe redox transformations in terrestrial systems, it also has implications to waters on the coastal environment that receive NOM from terrigenous sources. However, caution is needed when extrapolating the results obtained in this study to the open oceans that have remarkably different composition compared to terrestrial and coastal waters. In addition, the results of this work can be extended to iron rich environments with micromolar Fe concentrations, since the mechanism of Fe redox transformations is expected to be similar to that reported here at nanomolar Fe concentrations. However, suitable adjustment must be made for the fact that the proportion of Fe present in the form of iron (oxy)hydroxides is certain to be higher at these higher total Fe concentrations.

Overall, the various factors affecting Fe redox transformations mediated by SRFA have been examined in this thesis. However, there are still knowledge gaps remaining that require further investigation. Although the results support the involvement in Fe redox transformations of quinone-like moieties present in SRFA, no direct measurement of quinone-like moieties is included. Further work on measurement of these entities will be

useful. In addition, future work can be extended to natural environments to explore the importance of the proposed mechanisms in a much more complex but realistic setting.

References

Aeschbacher, M., C. Graf, R. P. Schwarzenbach and M. Sander (2012) 'Antioxidant properties of humic substances', *Environmental Science and Technology*, 46(9): 4916-4925.

Aeschbacher, M., M. Sander and R. P. Schwarzenbach (2010) 'Novel electrochemical approach to assess the redox properties of humic substances.', *Environmental Science and Technology*, 44: 87-93.

Alegría, A. E., P. Sanchez-Cruz and L. Rivas (2004) 'Alkaline-earth cations enhance *ortho*-quinone-catalyzed ascorbate oxidation', *Free Radical Biology and Medicine*, 37: 1631-1639.

Arment, A. R. and W. W. Carmichael (1996) 'Evidence that microcystin is a thio-template product', *Journal of Phycology*, 32(4): 591-597.

Bakajová, B. and W. R. Von (2011) 'Radical stabilization in dissolved humates', *Open Journal of Physical Chemistry*, 01: 55-60.

Barbeau, K., E. L. Rue, C. G. Trick, K. T. Bruland and A. Butler (2003) 'Photochemical reactivity of siderophores produced by marine heterotrophic bacteria and cyanobacteria based on characteristic Fe(III) binding groups', *Limnology and Oceanography*, 48(3): 1069-1078.

Batchelli, S., F. L. L. Muller, K. C. Chang and C. L. Lee (2010) 'Evidence for strong but dynamic iron-humic colloidal associations in humic-rich coastal waters', *Environmental Science and Technology*, 44(22): 8485-8490.

Bielski, B., D. Cabelli, R. Arudi and A. Ross (1985) 'Reactivity of HO_2/O_2^- radicals in aqueous solution', *Journal of Physical and Chemical Reference Data*, 14: 1041-1100.

Blesa, M. A., E. B. Borghi, A. J. G. Maroto and A. E. Regazzoni (1984) 'Adsorption of EDTA and iron-EDTA complexes on magnetite and the mechanism of dissolution of magnetite by EDTA', *Journal of Colloid and Interface Science*, 98(2): 295-305.

Blesa, M. A., H. A. Marinovich, E. C. Baumgartner and A. J. G. Maroto (1987) 'Mechanism of dissolution of magnetite by oxalic acid-ferrous ion solutions', *Inorganic Chemistry*, 26(22): 3713-3717.

Borer, P., S. M. Kraemer, B. Sulzberger, S. J. Hug and R. Kretzschmar (2009) 'Photodissolution of lepidocrocite (γ-FeOOH) in the presence of desferrioxamine B and aerobactin', *Geochimica et Cosmochimica Acta*, 73: 4673-4687.

Borghi, E. B., A. E. Regazzoni, A. J. G. Maroto and M. A. Blesa (1989) 'Reductive dissolution of magnetite by solutions containing EDTA and Fe-II', *Journal of Colloid and Interface Science*, 130(2): 299-310.

Borman, C. J., B. P. Sullivan, C. M. Eggleston and P. J. S. Colberg (2010) 'Is iron redox cycling in a high altitude watershed photochemically or thermally driven?', *Chemical Geology*, 269(1-2): 33-39.

Browning, T. J., E. P. Achterberg, J. C. Yong, I. Rapp, C. Utermann, A. Engel and C. M. Moore (2017) 'Iron limitation of microbial phosphorus acquisition in the tropical North Atlantic', *Nature Communications*, 8.

Burton, E. D., R. T. Bush and L. A. Sullivan (2006) 'Acid-volatile sulfide oxidation in coastal flood plain drains: Iron-sulfur cycling and effects on water quality', *Environmental Science and Technology*, 40(4): 1217-1222.

Buxton, G. V., C. L. Greenstock, W. P. Helman and A. B. Ross (1988) 'Critical review of rate constants for reactions of hydrated electrons, hydrogen atoms and hydroxyl radicals ($^{\bullet}OH/ ^{\bullet}O^{-}$) in aqueous solution', *Journal of Physical and Chemical Reference Data*, 17(2): 513-886.

Byrne, R. H. and D. R. Kester (1976) 'Solubility of hydrous ferric oxide and iron speciation in seawater', *Marine Chemistry*, 4(3): 255-274.

Chen, J., B. Gu, R. Royer and W. Burgos (2003) 'The roles of natural organic matter in chemical and microbial reduction of ferric iron', *The Science of The Total Environment*, 307(1-3): 167-178.

Chevallier, E., R. D. Joliboisa, N. Meuniera, P. Carliera and A. Monodb (2004) 'Fenton-like'' reactions of methylhydroperoxide and ethylhydroperoxide with $Fe2^{+}$ in liquid aerosols under tropospheric conditions', *Atmospheric Environment*, 38: 921-933.

Chuang, P. Y., R. M. Duvall, M. M. Shafer and J. J. Schauer (2005) 'The origin of water soluble particulate iron in the Asian atmospheric outflow', *Geophysical Research Letters*, 32(7).

Coale, K. H., K. S. Johnson, S. E. Fitzwater, R. M. Gordon, S. Tanner, F. P. Chavez, L. Ferioli, et al. (1996) 'A massive phytoplankton bloom induced by an ecosystem-scale iron fertilization experiment in the equatorial Pacific Ocean', *Nature*, 383(6600): 495-501.

Cooper, W. J., R. G. Zika, R. G. Petasne and A. M. Fischer (1989) 'Sunlight-induced photochemistry of humic substances in natural waters: major reactive species', *ACS Symposium Series*, 219: 333-362.

Cornell, R. M. and P. W. Schindler (1987) 'Photochemical dissolution of goethite in acid oxalate solution', *Clays and Clay Minerals*, 35(5): 347-352.

Cory, R. M. and D. M. McKnight (2005) 'Fluorescence spectroscopy reveals ubiquitous presence of oxidized and reduced quinones in dissolved organic matter', *Environmental Science and Technology*, 39: 8142-8149.

Crichton, R. R. and J. R. Boelaert (2001) *Inorganic biochemistry of iron metabolism : from molecular mechanisms to clinical consequences*. Chichester ; New York: Wiley.

Dalrymple, R. M., A. K. Carfagno and C. M. Sharpless (2010) 'Correlations between dissolved organic matter optical properties and quantum yields of singlet oxygen and hydrogen peroxide.', *Environmental Science and Technology*, 44: 5824-5829.

Dent, D. (1986) *Acid sulphate soils: a baseline for research and development*. Wageningen, Netherlands: International Institute for Land Reclamation and Improvement/ILRI.

Diaz, J. M., C. M. Hansel, B. M. Voelker, C. M. Mendes, P. F. Andeer and T. Zhang (2013) 'Widespread production of extracellular superoxide by heterotrophic bacteria', *Science*, 340(6137): 1223-1226.

Duesterberg, C. K., S. E. Mylon and T. D. Waite (2008) 'pH effects on iron-catalyzed oxidation using Fenton's reagent', *Environmental Science and Technology*, 42: 8522-8527.

Eaton, D. R. (1964) 'Complexing of metal ions with semiquinones. an electron spin resonance study', *Inorganic Chemistry*, 3: 1268-1271.

Emmenegger, L., D. W. King, L. Sigg and B. Sulzberger (1998) 'Oxidation kinetics of Fe(II) in a eutrophic swiss lake', *Environmental Science and Technology*, 32(19): 2990-2996.

Faust, B. C. and R. G. Zepp (1993) 'Photochemistry of aqueous iron(III)-polycarboxylate complexes: Roles in the chemistry of atmospheric and surface waters', *Environmental Science and Technology*, 27: 2517-2522.

Fimmen, R. L., R. M. Cory, Y. P. Chin, T. D. Trouts and D. M. McKnight (2007) 'Probing the oxidation-reduction properties of terrestrially and microbially derived dissolved organic matter', *Geochimica et Cosmochimica Acta*, 71: 3003-3015.

Finden, D. A. S., E. Tipping, G. H. M. Jaworski and C. S. Reynolds (1984) 'Light-induced reduction of natural iron(III) oxide and its relevance to phytoplankton', *Nature*, 309(5971): 783-784.

Fujii, M., A. Imaoka, C. Yoshimura and T. D. Waite (2014) 'Effects of molecular composition of natural organic matter on ferric iron complexation at circumneutral pH', *Environmental Science and Technology*, 48(8): 4414-4424.

Fujii, M., A. L. Rose, T. D. Waite and T. Omura (2008) 'Effect of divalent cations on the kinetics of Fe(III) complexation by organic ligands in natural waters', *Geochimica et Cosmochimica Acta*, 72: 1335-1349.

Fujii, M., A. C. Yeung and T. D. Waite (2015) 'Competitive effects of calcium and magnesium ions on the photochemical transformation and associated cellular uptake of iron by the freshwater cyanobacterial phytoplankton microcystis aeruginosa', *Environmental Science and Technology*, 49(15): 9133-9142.

Fukushima, M. and K. Tatsumi (2001) 'Degradation pathways of pentachlorophenol by photo-fenton systems in the presence of iron(III), humic acid, and hydrogen peroxide', *Environmental Science and Technology*, 35(9): 1771-1778.

Garg, S., H. Ito, A. L. Rose and T. D. Waite (2013a) 'Mechanism and kinetics of dark iron redox transformations in previously photolyzed acidic natural organic matter solutions', *Environmental Science and Technology*, 47(4): 1861-1869.

Garg, S., C. Jiang, C. J. Miller, A. L. Rose and T. D. Waite (2013b) 'Iron redox transformations in continuously photolyzed acidic solutions containing natural organic matter: Kinetic and mechanistic insights', *Environmental Science and Technology*, 47: 9190-9197.

Garg, S., C. Jiang and T. D. Waite (2015) 'Mechanistic insights into iron redox transformations in the presence of natural organic matter: Impact of pH and light', *Geochimica et Cosmochimica Acta*, 165: 14-34.

Garg, S., A. L. Rose and T. D. Waite (2007a) 'Superoxide-mediated reduction of organically complexed iron(III): Impact of pH and competing cations (Ca^{2+})', *Geochimica et Cosmochimica Acta*, 71(23): 5620-5634.

Garg, S., A. L. Rose and T. D. Waite (2007b) 'Superoxide mediated reduction of organically complexed iron(III): comparison of non-dissociative and dissociative reduction pathways', *Environmental Science and Technology*, 41(9): 3205-3212.

Garg, S., A. L. Rose and T. D. Waite (2011a) 'Pathways contributing to the formation and decay of ferrous iron in sunlit natural waters' In *Aquatic Redox Chemistry*(ed.): ACS symposium series: 153-176.

Garg, S., A. L. Rose and T. D. Waite (2011b) 'Photochemical production of superoxide and hydrogen peroxide from natural organic matter', *Geochimica et Cosmochimica Acta*, 75: 4310-4320.

Ginn, H. P., L. A. Pearson and B. A. Neilan (2010) 'NtcA from Microcystis aeruginosa PCC 7806 is autoregulatory and binds to the microcystin promoter', *Applied and Environment Microbiology*, 76(13): 4362-4368.

Glover, F., K. L. Whitworth, P. Kappen, D. S. Baldwin, G. N. Rees, J. A. Webb and E. Silvester (2011) 'Acidification and Buffering Mechanisms in Acid Sulfate Soil

Wetlands of the Murray-Darling Basin, Australia', *Environmental Science and Technology*, 45(7): 2591-2597.
Goldstone, J. V., M. J. Pullin, S. Bertilsson and B. M. Voelker (2002) 'Reactions of hydroxyl radical with humic substances: bleaching, mineralization, and production of bioavailable carbon substrates', *Environmental Science and Technology*, 36(3): 364-372.
Hering, J. G. and F. M. Morel (1988) 'Humic acid complexation of calcium and copper.', *Environmental Science and Technology*, 22: 1234-1237.
Hong, S. K. and M. Elimelech (1997) 'Chemical and physical aspects of natural organic matter (NOM) fouling of nanofiltration membranes', *Journal of Membrane Science*, 132: 159-181.
Hutchins, D. A. and P. W. Boyd (2016) 'Marine phytoplankton and the changing ocean iron cycle', *Nature Climate Change*, 6(12): 1072-1079.
Hutchins, D. A., C. E. Hare, R. S. Weaver, Y. Zhang, G. F. Firme, G. R. DiTullio, M. B. Alm, et al. (2002) 'Phytoplankton iron limitation in the Humboldt Current and Peru Upwelling', *Limnology and Oceanography*, 47(4): 997-1011.
Ianni, J. C. (2003) 'A comparison of the Bader-Deuflhard and the Cash-Karp Runge - Kutta integrators for the GRI-MECH 3.0 model based on the chemical kinetics code Kintecus', *Combustion*, 1: 1368-1372.
Jerzykiewicz, M., A. Jezierski, F. Czechowski and J. Drozd (2002) 'Influence of metal ions binding on free radical concentration in humic acids . A quantitative electron paramagnetic resonance study', *Organic Geochemistry*, 33: 265-268.
Jezierski, A., F. Czechowski, M. Jerzykiewicz and J. Drozd (2000) 'EPR investigations of structure of humic acids from compost, soil, peat and soft brown coal upon oxidation and metal uptake', *Applied Magnetic Resonance*, 18: 127-136.
Johnson, K. A., Z. B. Simpson and T. Blom (2009) 'Global Kinetic Explorer: A new computer program for dynamic simulation and fitting of kinetic data', *Analytical Biochemistry*, 387(1): 20-29.
Johnston, S. G., P. G. Slavich and P. Hirst (2005) 'The impact of controlled tidal exchange on drainage water quality in acid sulphate soil backswamps', *Agricultural Water Management*, 73(2): 87-111.
Khaikin, G. I., Z. B. Alfassi, R. E. Huie and P. Neta (1996) 'Oxidation of ferrous and ferrocyanide ions by peroxyl radicals', *Journal of Physical Chemistry*, 100(17): 7072-7077.
Kochany, J. and E. Lipczynska-Kochany (2007) 'Fenton reaction in the presence of humates. Treatment of highly contaminated wastewater at neutral pH', *Environmental Technology*, 28(9): 1007-1013.
Krishnamurthy, A., J. K. Moore, N. Mahowald, C. Luo, S. C. Doney, K. Lindsay and C. S. Zender (2009) 'Impacts of increasing anthropogenic soluble iron and nitrogen deposition on ocean biogeochemistry', *Global Biogeochemical Cycles*, 23(3): n/a-n/a.
Kuma, K., A. Katsumoto, H. Kawakami, F. Takatori and K. Matsunaga (1998) 'Spatial variability of Fe(III) hydroxide solubility in the water column of the northern North Pacific Ocean', *Deep-Sea Research Part I-Oceanographic Research Papers*, 45(1): 91-113.
Kuma, K. and K. Matsunaga (1995) 'Availability of colloidal ferric oxides to coastal marine-phytoplankton', *Marine Biology*, 122(1): 1-11.
Kustka, A. B., Y. Shaked, A. J. Milligan, D. W. King and F. M. M. Morel (2005) 'Extracellular production of superoxide by marine diatoms: Contrasting effects

on iron redox chemistry and bioavailability', *Limnology and Oceanography*, 50(4): 1172-1180.
Latch, D. E. and K. McNeill (2006) 'Microheterogeneity of singlet oxygen distributions in irradiated humic acid solutions', *Science*, 311(5768): 1743-1747.
Lebedev, A. V., M. V. Ivanova and E. K. Ruuge (2003) 'How do calcium ions induce free radical oxidation of hydroxy-1,4-naphthoquinone? Ca^{2+} stabilizes the naphthosemiquinone anion-radical of echinochrome A', *Archives of Biochemistry and Biophysics*, 413: 191-198.
Lee, Y. P., M. Fujii, K. Terao, T. Kikuchi and C. Yoshimura (2016) 'Effect of dissolved organic matter on Fe(II) oxidation in natural and engineered waters', *Water Research*, 103: 160-169.
Li, W. J., L. Xu, X. H. Liu, J. C. Zhang, Y. T. Lin, X. H. Yao, H. W. Gao, et al. (2017) 'Air pollution-aerosol interactions produce more bioavailable iron for ocean ecosystems', *Science Advances*, 3(3).
Liu, X. W. and F. J. Millero (1999) 'The solubility of iron hydroxide in sodium chloride solutions', *Geochimica et Cosmochimica Acta*, 63(19-20): 3487-3497.
Liu, X. W. and F. J. Millero (2002) 'The solubility of iron in seawater', *Marine Chemistry*, 77(1): 43-54.
Livingstone, D. A. (1963) 'Chemical composition of rivers and lakes' In *U.S. Geological Survey Professional Paper 440-G*(ed.), Washington: United State Govrnment Printing Office.
Lottermoser, B. G. (2007) *Mine Wastes : Characterization, Treatment, Environmental Impacts*. Berlin, Heidelberg: Springer Berlin Heidelberg.
Macalady, D. L. and K. Walton-Day (2011) 'Redox chemistry and natural organic matter (NOM): Geochemists' dream, analytical chemists' nightmare', *ACS Symposium Series*, 1071: 85-111.
Mahowald, N. M. and C. Luo (2003) 'A less dusty future?', *Geophysical Research Letters*, 30(17).
Martin, J. H., K. H. Coale, K. S. Johnson, S. E. Fitzwater, R. M. Gordon, S. J. Tanner, C. N. Hunter, et al. (1994) 'Testing the Iron Hypothesis in Ecosystems of the Equatorial Pacific-Ocean', *Nature*, 371(6493): 123-129.
Martin, J. H. and S. E. Fitzwater (1988) 'Iron deficiency limits phytoplankton growth in the north-east Pacific subarctic', *Nature*, 331(6154): 341-343.
Martin, J. H., S. E. Fitzwater and R. M. Gordon (1990a) 'Iron deficiency limits phytoplankton growth in Antarctic waters', *Global Biogeochemical Cycles*, 4(1): 5-12.
Martin, J. H., R. M. Gordon and S. E. Fitzwater (1990b) 'Iron in Antarctic waters', *Nature*, 345(6271): 156-158.
McCarthy, B., A. Conallin, P. D'Santos and D. Baldwin (2006) 'Acidification, salinization and fish kills at an inland wetland in south-eastern Australia following partial drying', *Ecological Management & Restoration*, 7(3): 218-223.
Meisel, D. (1975) 'Free energy correlation of rate constants for electron transfer between organic systems in aqueous solutions', *Chemical Physics Letters*, 34: 263-266.
Menzel, D. W., E. M. Hulburt and J. H. Ryther (1963) 'The effects of enriching Sargasso sea water on the production and species composition of the phytoplankton', *Deep-Sea Research*, 10(3): 209-219.
Miller, C. J., S. M. V. Lee, A. L. Rose and T. D. Waite (2012) 'Impact of natural organic matter on H_2O_2-mediated oxidation of Fe(II) in coastal seawaters', *Environental Science and Technology*, 46: 11078-11085.

Miller, C. J., A. L. Rose and T. D. Waite (2009) 'Impact of natural organic matter on H_2O_2-mediated oxidation of Fe (II) in a simulated freshwater system', *Geochimica et Cosmochimica Acta*, 73: 2758-2768.

Miller, D. M., G. R. Buettner and S. D. Aust (1990) 'Transition metals as catalysts of 'autoxidation' reactions', *Free Radical Biology and Medicine*, 8: 95-108.

Millero, F. J. and S. Sotolongo (1989) 'The Oxidation of Fe(II) with H_2O_2 in Seawater', *Geochimica et Cosmochimica Acta*, 53(8): 1867-1873.

Millero, F. J., S. Sotolongo and M. Izaguirre (1987) 'The oxidation-kinetics of Fe(II) in seawater', *Geochimica et Cosmochimica Acta*, 51(4): 793-801.

Moonshine, M., Y. Rudich, S. Katsman and E. R. Graber (2008) 'Atmospheric HULIS enhance pollutant degradation by promoting the dark Fenton reaction', *Geophysical Research Letters*, 35(20).

Morel, F. and J. G. Hering (1993) *Principles and Applications of Aquatic Chemistry*. New York: John Wiley & Sons, Inc.

Morel, F. M. M., A. B. Kustka and Y. Shaked (2008) 'The role of unchelated Fe in the iron nutrition of phytoplankton', *Limnology and Oceanography*, 53(1): 400-404.

Morton, S. D. and T. H. Lee (1974) 'Algal blooms - possible effects of iron', *Environmental Science and Technology*, 8(7): 673-674.

Murphy, T. P., D. R. S. Lean and C. Nalewajko (1976) 'Blue-green-algae: their excretion of iron-selective chelators enables them to dominate other algae', *Science*, 192(4242): 900-902.

Nagai, T., A. Imai, K. Matsushige, K. Yokoi and T. Fukushima (2007) 'Dissolved iron and its speciation in a shallow eutrophic lake and its inflowing rivers', *Water Research*, 41(4): 775-784.

Neta, P., R. E. Huie and A. B. Ross (1990) 'Rate constants for reactions of peroxyl radicals in fluid solutions', *Journal of Physical and Chemical Reference Data*, 19(2): 413.

Nurmi, J. T. and P. G. Tratnyek (2002) 'Electrochemical properties of natural organic matter (NOM), fractions of NOM, and model biogeochemical electron shuttles', *Environmental Science and Technology*, 36: 617-624.

Palmer, N. and R. von Wandruszka (2001) 'Dynamic light scattering measurements of particle size development in aqueous humic materials', *Fresenius' Journal of Analytical Chemistry*, 371(7): 951-954.

Paul, A., S. Hackbarth, R. D. Vogt, B. Röder, B. K. Burnison and C. E. W. Steinberg (2004) 'Photogeneration of singlet oxygen by humic substances: comparison of humic substances of aquatic and terrestrial origin.', *Photochemical & photobiological sciences*, 3: 273-280.

Paul, A., R. Stosser, A. Zehl, E. Zwirnmann, R. D. Vogt and C. E. Steinberg (2006) 'Nature and abundance of organic radicals in natural organic matter: effect of pH and irradiation', *Environmental Science and Technology*, 40(19): 5897-5903.

Peiffer, S., K. Walton-Day and D. L. Macalady (1999) 'The interaction of natural organic matter with iron in a wetland (Tennessee Park, Colorado) receiving acid mine drainage', *Aquatic Geochemistry*, 5(2): 207-223.

Pham, A. N. and T. D. Waite (2008a) 'Modeling the kinetics of Fe(II) oxidation in the presence of citrate and salicylate in aqueous solutions at pH 6.0−8.0 and 25 °C', *Journal of Physical Chemistry A*, 112(24): 5395-5405.

Pham, a. N. and T. D. Waite (2008b) 'Oxygenation of Fe(II) in natural waters revisited: Kinetic modeling approaches, rate constant estimation and the importance of various reaction pathways', *Geochimica et Cosmochimica Acta*, 72: 3616-3630.

Pullin, M. J. and S. E. Cabaniss (2003) 'The effects of pH, ionic strength, and iron–fulvic acid interactions on the kinetics of non-photochemical iron transformations. II. The kinetics of thermal reduction', *Geochimica et Cosmochimica Acta*, 67(21): 4079-4089.

Quigg, A., Z. V. Finkel, A. J. Irwin, Y. Rosenthal, T. Y. Ho, J. R. Reinfelder, O. Schofield, F. M. M. Morel and P. G. Falkowski (2003) 'The evolutionary inheritance of elemental stoichiometry in marine phytoplankton', *Nature*, 425(6955): 291-294.

Ratasuk, N. and M. A. Nanny (2007) 'Characterization and quantification of reversible redox sites in humic substances', *Environmental Science and Technology*, 41(22): 7844-7850.

Remucal, C. K. and D. L. Sedlak (2011) 'The role of iron coordination in the production of reactive oxidants from rerrous iron oxidation by xxygen and hydrogen peroxide.' In *Aquatic Redox Chemistry*, 177-197.

Rich, P. R. and D. S. Bendall (1980) 'The kinetics and thermodynamics of the reduction of cytochrome c by substituted p-benzoquinols in solution', *Biochimica et Biophysica Acta*, 592: 506-518.

Roginsky, V. and T. Barsukova (2000) 'Kinetics of oxidation of hydroquinones by molecular oxygen. Effect of superoxide dismutase', *Journal of the Chemical Society, Perkin Transactions 2*: 1575-1582.

Roginsky, V. a., L. M. Pisarenko, W. Bors and C. Michel (1999) 'The kinetics and thermodynamics of quinone-semiquinone-hydroquinone systems under physiological conditions', *Journal of the Chemical Society, Perkin Transactions 2*: 871-876.

Rose, A. L., A. Godrant, M. Furnas and T. D. Waite (2010) 'Dynamics of nonphotochemical superoxide production and decay in the Great Barrier Reef lagoon', *Limnology and Oceanography*, 55(4): 1521-1536.

Rose, A. L. and T. D. Waite (2002) 'Kinetic model for Fe(II) oxiadtion in seawater in the absence and presence of natural organic matter', *Environmental Science and Technology*, 36: 433-444.

Rose, A. L. and T. D. Waite (2003) 'Kinetics of iron complexation by dissolved natural organic matter in coastal waters', *Marine Chemistry*, 84(1-2): 85-103.

Rose, A. L. and T. D. Waite (2005) 'Reduction of organically complexed ferric iron by superoxide in a simulated natural water', *Environmental Science and Technology*, 39(8): 2645-2650.

Rose, A. L. and T. D. Waite (2006) 'Role of superoxide in the photochemical reduction of iron in seawater', *Geochimica et Cosmochimica Acta*, 70: 3869-3882.

Rush, J. D. and B. H. J. Bielski (1985) 'Pulse radiolytic studies of the reaction of HO_2/O_2^- with iron(II)/iron(III) ions. The reactivity of HO_2/O_2^- with ferric ions and its implication on the occurrence of the Haber-Weiss reaction', *Journal of Physical Chemistry*, 89: 5062-5066.

Santana-Casiano, J. M., M. Gonzaalez-Davila and F. J. Millero (2005) 'Oxidation of nanomolar levels of Fe(II) with oxygen in natural waters', *Environmental Science and Technology*, 39(7): 2073-2079.

Santana-Casiano, J. M., M. González-Dávila, a. G. González and F. J. Millero (2010) 'Fe(III) reduction in the presence of Catechol in seawater', *Aquatic Geochemistry*, 16: 467-482.

Santana-Casiano, J. M., M. González-Dávila, A. G. González, M. Rico, A. López and A. Martel (2014) 'Characterization of phenolic exudates from Phaeodactylum

tricornutum and their effects on the chemistry of Fe(II)–Fe(III)', *Marine Chemistry*, 158: 10-16.
Santana-Casiano, J. M., M. González-Dávila and F. J. Millero (2004) 'The oxidation of Fe(II) in NaCl–$HCO3^{-}$ and seawater solutions in the presence of phthalate and salicylate ions: a kinetic model', *Marine Chemistry*, 85(1-2): 27-40.
Scott, D. T., D. M. Mcknight, E. L. Blunt-Harris, S. E. Kolesar and D. R. Lovley (1998) 'Quinone moieties act as electron acceptors in the reduction of humic substances by humics-reducing microorganisms', *Environmental Science and Technology*, 32: 2984-2989.
Sedwick, P. N., E. R. Sholkovitz and T. M. Church (2007) 'Impact of anthropogenic combustion emissions on the fractional solubility of aerosol iron: Evidence from the Sargasso Sea', *Geochemistry Geophysics Geosystems*, 8.
Senesi, N. (1990a) 'Molecular and quantitative aspects of the chemistry of fulvic acid and its interactions with metal ions and organic chemicals. Part I. The electron spin resonance approach', *Analytica Chimica Acta*, 232: 51-75.
Senesi, N. (1990b) 'Molecular and quantitative aspects of the chemistry of fulvic acid and its interactions with metal ions and organic chemicals. Part II. The fluorescence spectroscopy approach', 232: 77-106.
Sholkovitz, E. R., P. N. Sedwick and T. M. Church (2009) 'Influence of anthropogenic combustion emissions on the deposition of soluble aerosol iron to the ocean: Empirical estimates for island sites in the North Atlantic', *Geochimica et Cosmochimica Acta*, 73(14): 3981-4003.
Sima, J. and J. Makaiiova (1997) 'Photochemistry of iron (III) complexes', *Coordination Chemistry Reviews*, 160: 161-189.
Skogerboe, R. K. and S. A. Wilson (1981) 'Reduction of Ionic Species by Fulvic-Acid', *Analytical Chemistry*, 53(2): 228-232.
Smetacek, V., C. Klaas, V. H. Strass, P. Assmy, M. Montresor, B. Cisewski, N. Savoye, et al. (2012) 'Deep carbon export from a Southern Ocean iron-fertilized diatom bloom', *Nature*, 487(7407): 313-319.
Song, Y. and G. R. Buettner (2010) 'Thermodynamic and kinetic considerations for the reaction of semiquinone radicals to form superoxide and hydrogen peroxide', *Free Radical Biology and Medicine*, 49: 919-962.
Southworth, B. A. and B. M. Voelker (2003) 'Hydroxyl radical production via the photo-Fenton reaction in the presence of fulvic acid', *Environmental Science and Technology*, 37(6): 1130-1136.
Stevenson, F. J. (1994) *Humus chemistry : genesis, composition, reactions*. New York, N.Y.: John Wiley.
Stewart, B. D., R. T. Amos, P. S. Nico and S. Fendorf (2011) 'Influence of uranyl speciation and iron oxides on uranium biogeochemical redox reactions', *Geomicrobiology Journal*, 28: 444-456.
Stookey, L. L. (1970) 'Ferrozine---a new spectrophotometric reagent for iron', *Analytical Chemistry*, 42: 779-781.
Strathmann, T. J. (2011) 'Redox reactivity of organically complexed iron(II) species with aquatic contaminants', *ACS Symposium Series*, 1071: 283-313.
Strzepek, R. F. and P. J. Harrison (2004) 'Photosynthetic architecture differs in coastal and oceanic diatoms', *Nature*, 431(7009): 689-692.
Stumm, W. and B. Sulzberger (1992) 'The cycling of iron in natural environments - considerations based on laboratory studies of heterogeneous redox processes', *Geochimica et Cosmochimica Acta*, 56(8): 3233-3257.

Sunda, W. G. and S. a. Huntsman (1995) 'Iron uptake and growth limitation in oceanic and coastal phytoplankton', *Marine Chemistry*, 50: 189-206.

Szilagyi, M. (1971) 'Reduction of Fe^{3+} ion by humic acid preparations', *Soil Science*, 111(4): 233-235.

Thorn, K. A., J. B. Arterburn and M. A. Mikita (1992) '^{15}N and ^{13}C NMR investigation of hydroxylamine-derivatized humic substances', *Environmental Science and Technology*, 26: 107-116.

Tipping, E. (2002) *Cation binding by humic substances*. New York: Cambridge University Press.

Uchimiya, M. and A. T. Stone (2006) 'Redox reactions between iron and quinones: Thermodynamic constraints', *Geochimica et Cosmochimica Acta*, 70: 1388-1401.

Vajda, S., P. Valko and T. Turányi (1985) 'Principal component analysis of kinetic models', *International Journal of Chemical Kinetics*, 17: 55-81.

Vermilyea, A. W., S. P. Hansard and B. M. Voelker (2010) 'Dark production of hydrogen peroxide in the Gulf of Alaska', *Limnology and Oceanography*, 55(2): 580-588.

Vione, D., F. Merlo, V. Maurino and C. Minero (2004) 'Effect of humic acids on the Fenton degradation of phenol', *Environmental Chemistry Letters*, 2(3): 129-133.

Voelker, B. M. and D. L. Sedlak (1995) 'Iron reduction by photoproduced superoxide in seawater', *Marine Chemistry*, 50(1-4): 93-102.

Voelker, B. M., D. L. Sedlak and O. C. Zafiriou (2000) 'Chemistry of superoxide radical in seawater: Reactions with organic Cu complexes', *Environmental Science and Technology*, 34(6): 1036-1042.

Voelker, B. M. and B. Sulzberger (1996) 'Effects of fulvic acid on Fe(II) oxidation by hydrogen peroxide', *Environmental Science and Technology*, 30(4): 1106-1114.

von Sonntag, C., P. Dowideit, X. Fang, R. Mertens, X. Pan, M. N. Schuchmann and H.-P. Schuchmann (1997) 'The fate of peroxyl radicals in aqueous solution', *Water Science and Technology*, 35(4): 9-15.

von Sonntag, C. and H.-P. Schuchmann (1991) 'The elucidation of peroxyl radical reactions in aqueous solution with the help of radiation-chemical methods', *Angewandte Chimie International Edition English*, 30: 1229-1253.

Wilcoxen, J., B. Zhang and R. Hille (2011) 'Reaction of the molybdenum- and copper-containing carbon monoxide dehydrogenase from oligotropha carboxydovorans with quinones', *Biochemistry*, 50: 1910-1916.

Wilson, T. R. S. (1975) 'Salinity and the major elements of sea water' In *Chemical Oceanography*, in Riley, J. P. and G. Skirrow (ed.), London: Academic Press: 364-413.

Yamazaki, I. and T. Ohnishi (1966) 'One-electron-transfer reactions in biochemical systems I. Kinetic analysis of the oxidation-reduction equilibrium between quinol-quinone and ferro-ferricytochrome c', *Biochimica et Biophysica Acta*, 112: 469-481.

Yates, L. M. and R. von Wandruszka (1999) 'Effects of pH and metals on the surface tension of aqueous humic materials', *Soil Science Society of America Journal*, 63(6): 1645-1649.

Yuan, X., C. J. Miller, a. N. Pham and T. D. Waite (2014) 'Kinetics and mechanism of auto- and copper-catalyzed oxidation of 1,4-naphthohydroquinone', *Free Radical Biology and Medicine*, 71: 291-302.

Yuan, X., a. N. Pham, C. J. Miller and T. D. Waite (2013) 'Copper-catalyzed hydroquinone oxidation and associated redox cycling of copper under conditions

typical of natural saline waters', *Environmental Science and Technology*, 47: 8355-8364.

Zhang, Y., R. Del Vecchio and N. V. Blough (2012) 'Investigating the mechanism of hydrogen peroxide photoproduction by humic substances', *Environmental Science and Technology*, 46: 11836-11843.

Zika, R. G., J. W. Moffett, R. G. Petasne, W. J. Cooper and E. S. Saltzman (1985) 'Spatial and temporal variations of hydrogen peroxide in Gulf of Mexico waters', *Geochimica et Cosmochimica Acta*, 49(5): 1173-1184.